Tribological and mechanical properties of compliant bearings for total joint replacements.

Ian C. Burgess

Tribological and Mechanical Properties of Compliant bearings for Total Joint Replacements.

Ian C. Burgess. M.Eng. (Loughborough University).

A Thesis submitted for the Degree of Doctor of Philosophy at the University of Durham.

January 1997.

To Kate, for all your love and support.

Acknowledgements.

Thesis writing is a lonely business, but this was made less so by my family, friends and colleagues who have supported me during my research at Durham. I have received academic encouragement, practical assistance, and also financial support from a number of individuals and organisations. I would like to thank all of them.

- Professor Tony Unsworth and Dr Jimmy Cunningham, my joint supervisors, for the discussion and critical comment, and for proof reading this thesis.
- Dr Richard Hall for his assistance with the statistics, and practical help when I first arrived at Durham.
- Mr Milos Kolar whose microprocessor expertise was essential in the use of the friction and knee simulators.
- Technical support staff at Durham especially Mr Neil Heron, Mr Tony McFarlane and Mr George Turnbull.
- Mr Jim Swift for discussions regarding the computer modelling of the servo hydraulic systems.
- Dr Nigel Smith, Dr Eric Jones and Dr Christina Doyle of Howmedica whose enthusiasm, and hard work in the production of samples, have contributed greatly to the advances made during this research.
- Whilst at Durham, I have been funded by Howmedica Europe, Staines, UK for which I am grateful.

Whilst working on this thesis Alice was born. She interspersed the grind of writing up with real joy and laughter, and was an inspiration for it's completion.

Abstract.

The tribology of a wide range of designs of compliant layer acetabular cups has been evaluated using a simulator. The simulator applied a dynamic load of 2 kN and a sinusoidal motion of ±25°, and measured the frictional resistance directly. In general the friction developed in these joints was extremely low, with friction factors typically below 0.01. When the experimental results were compared with theoretical estimates of friction a poor correlation was found. Further analysis suggested that the design of compliant layer acetabular cups was insensitive to many of the parameters suggested by theory. In particular, the radial clearance and femoral head size were not found to be critical. In addition, methods were proposed and their effectiveness demonstrated to measure friction at the on-set of motion (start-up friction), and the steady state friction in realistic compliant layer knees.

The adhesion between compliant layers and a rigid backing have been investigated, with the aim of developing a good bond between them. The peel test was used to demonstrate an excellent diffusion bond between a low modulus medical grade polyurethane, and a similar high modulus grade of polyurethane. The processing conditions used to manufacture the test piece were optimised to maximise the bond strength. The bond was found to be stable after immersion in Ringers solution at 37°C for 52 weeks, and after acetabular cups were subjected to 14 million 4 kN loading cycles.

A six station knee wear simulator was designed and commissioned. The simulator applied a dynamic load and an anterior-posterior translation individually to each station, as well as a flexion-extension motion common to all six stations. The simulator was computer controlled entirely using servo hydraulics. Wear rates were obtained from tests lasting up to 8 million cycles conducted on UHMWPE joints.

Contents.

Nomenclature.

For convenience the nomenclature has been split it to two sections; symbols used in the lubrication, contact, adhesion and wear analyses, and symbols used in the computer simulation of the hydraulic control systems in Chapter 7.

Nomenclature for lubrication, contact, adhesion and wear analyses.

a, a_h Circular or major elliptical contact radius, Hertzian case (m).

a_b Blister test debond radius (m).

A, A_i Angle of extension-flexion, at point i (°).

A_f, A_{fi} Angle of extension-flexion from a forward loading cycle, at point i (°).

A_r, A_{ri} Angle of extension-flexion from a reverse loading cycle, at point i (°).

b, b_h Minor elliptical contact half radius, Hertzian case (m).

b_p Sample width (m).

c Increment of crack growth (m).

E Elastic modulus (Pa).

E_1 Elastic modulus of the femoral component (Pa).

E_2 Elastic modulus of the acetabular or tibial compliant layer (Pa).

E_{adj} Adjusted modulus $= \frac{4LRh_t}{\pi a^4}\left\{\frac{(1+\nu_2)(1-2\nu_2)}{1-\nu_2}\right\}$, where ν_2=0.4 (Pa).

E' Modulus term $\frac{1}{E'} = \frac{1-\nu_2^2}{E_{adj}}$, where ν_2=0.4 (Pa).

E'' Modulus term $\frac{1}{E''} = \frac{(1+\nu_2)(1-2\nu_2)}{(1-\nu_2)E_{adj}}$, where ν_2=0.4 (Pa).

f, f_i Friction factor, at point i, $= \frac{T}{R_1 L}$.

$f(h_t/a_b)$ Function determined by Bennett *et al.* (1977).

F, F_i, Peel force, at data point i (N).

F_{max} Maximum peel force (N).

F_{mean} Mean peel force (N).

G_c Adhesive fracture energy (Jm^{-2}).

h_{cen} Central lubricant film thickness (EHL) (m).

h_{min} Minimum lubricant film thickness (EHL) (m).

$h_{r,min}$ Minimum lubricant film thickness (μ-EHL) (m).

h_t Thickness of compliant layer (m).

H Blister height (m).

i Point in the simulator cycle (i=0 to 128).

k Ellipticity ratio =a/b or Wear factor (mm^3/Nm).

k_p Factor effecting the peel stress.

l Gauge length (m).

N Number of cycles.

L, L_i Applied load, at point i (N).

L_f, L_{fi} Applied simulator load from a forward loading cycle, at point i (N).

L_r, L_{ri} Applied simulator load from a reverse loading cycle, at point i (N).

P_p Peel strength =F/b (Nm^{-1}).

P, P_{cr} Blister test pressure, critical pressure (Pa).

R Equivalent radius $= \frac{R_1 R_2}{R_2 - R_1}$ (m).

R_1 Radius of the femoral component (hips) (m).

R_2 Radius of the acetabular component (m).

r_1 Radius of the femoral component in the anterior-posterior plain (knees) (m).

r_1' Radius of the femoral component in the medial-lateral plain (knees) (m).

r_2 Radius of the tibial component in the anterior-posterior plain (m).

r_2' Radius of the tibial component in the medial-lateral plain (m).

S_t Stroke ratio $= \frac{\pi \alpha R_1}{180 a}$ for hips.

T, T_i True frictional torque, at point i (Nm).

T_e Frictional torque due to eccentric loading (Nm).

T_f, T_{fi} Frictional torque from a forward loading cycle, at point i (Nm).

T_r, T_{ri} Frictional torque from a reverse loading cycle, at point i (Nm).

u, u_i Entraining velocity, at point i (ms^{-1}).

U Strain energy density (Jm^{-3}).

U_e Elastic energy (J).

V Volume (mm^3).

W_d Work done (J).

x_m, x_i Extension at F_{mean}, at point i (m).

Z, Z_i Sommerfeld number, at point i, $= \frac{\eta u R_1}{L}$.

α Flexion-extension amplitude (°).

α_o Angular offset (°).

β Peel angle (°).

λ Surface separation ratio.

λ_2, λ_2^* Wave length, correlated wave length of acetabular/tibial surface roughness (m).

Λ Extension ratio.

η Viscosity (Pa s).

υ Pendulum frequency (Hz).

μ Coefficient of friction.

σ_1 Amplitude of asperity roughness of femoral surface roughness (m).

σ_2 Amplitude of asperity roughness of acetabular/tibial surface roughness (m).

σ_p Stress in the adhesive layer at the peel front (Nm^{-2}).

ν Poisson's ratio, ν_1 and ν_2 the femoral and tibial components.

τ_{max} Maximum shear stress (Nm^{-2}).

γ_{max} Maximum shear strain.

γ_m Surface free energy (Jm^{-2}).

ψ Angle between major and minor axes (rads).

Nomenclature for computer simulation (Chapter 7).

Pressure (Nm^{-2}).

P,ΔP pressure, pressure difference.

P_1 pressure in cylinder 1.

P_2 pressure in cylinder 2.

ΔP_A pressure difference across surface A, cylinder 1 exhaust port.

ΔP_B pressure difference across surface B, cylinder 1 supply port.

ΔP_C pressure difference across surface C, cylinder 2 supply port.

ΔP_D pressure difference across surface D, cylinder 2 exhaust port.

a exhaust or atmospheric pressure (1×10^5).

P_s supply pressure (140×10^5).

Oil Flow (m^3s^{-1}).

Q oil flow.

Q_t total oil flow supplied.

Q_1 net flow in to cylinder 1.

Q_2 net flow in to cylinder 2.

Q_A oil flow over surface A, cylinder 1 exhaust port.

Fluid flow constants.

K_d decay coefficient for capillary flow (A^{-1}).

K_o orifice flow constant ($m^3s^{-1}A^{-1}Pa^{-0.5}$).

K_c capillary flow constant ($m^3s^{-1}Pa^{-1}$).

K isentropic tangent bulk modulus for Shell tellus 37 oil at 140 bar ($1.7\times10^9Nm^{-2}$).

Servo valve data.

Q_v maximum flow capacity of a valve at pressure P_v (m^3s^{-1}).

P_V pressure at which the valve size data is specified (Nm^{-2}).
i_r maximum valve current (A).
Q_l oil leakage at the null point at pressure P_l (m^3s^{-1}).
P_l pressure at which the valve leakage is specified (Nm^{-2}).
τ frequency response characteristic (s^{-1}).
Ω armature coil resistance (Ω).

Cylinder data.

V cylinder volume (m^3).
A_1 area of piston in cylinder 1.
A_2 area of piston in cylinder 2.
d_1 bore diameter (m).
d_2 rod diameter (m).
L actuator stroke length (m).
x piston position (m).
$\dot{x}$ piston velocity (ms^{-1}).
$\ddot{x}$ piston acceleration (ms^{-2}).

Mechanical system variables.

M load mass (kg).
F actuator force (N).

Control variables.

t time (s).
i armature or spool positioning current (A).
v input or request signal (V).
v_{fb} feedback or transducer signal (V).
v_{sp} armature or spool positioning voltage (V).
g summing amplifier gain.

Abbreviations.

AA Acrylic acid.
ADC Analogue to digital converter.
BDO 1,4 butanediol.
BW Body weight.

C80A	Corethane 80A.
C75D	Corethane 75D.
Ch80A	ChronoFlex AL-80A.
CMC	Carboxylmethyl cellulose.
CMM	Co-ordinate measuring machine
CSIRO	PU material supplied by CSIRO, Victoria, Australia.
DAC	Digital to analogue converter.
DLC	Diamond like coating.
DPPC	Dipalmitoyl phosphatidylcholine.
EDA	Ethylene diamine.
EHL	Elastohydrodynamic lubrication.
ESC	Environmental stress cracking.
HEMA	2-hydroxyethylmethacrylate.
HMDI	Hydrogenated MDI.
LDT	Linear displacement transducer.
MDA	4,4 methylenedianline.
MDI	4,4 diphenyl methane diisocyanate.
MIO	Metal ion oxidation.
NOP	Noncontacting Optical Profiler.
P80A	Pellethane 2363 80A.
PC	Proprietary polycarbonate macrodiol or Personal computer.
PCB	Printed circuit board.
PHECD	Poly-1,6-hexyl 1,2-ethyl carbonate diol.
PnMEG	Longer chain PTMEG.
PTMEG	Poly-tetramethylene ether glycol.
PU(s)	Polyurethane(s).
PUU(s)	Polyurethane urea(s).
s.d.	Standard deviation.
TJR(s)	Total joint replacement(s).
TKR(s)	Total knee replacement(s).
T80A	Tecoflex EG 80A.
TT80A/93A	Tecothane 1080A/1093A.
TT75D	Tecothane 1075D.
UHMWPE	Ultra high molecular weight polyethylene.
UTS	Ultimate tensile strength.
μ-EHL	Microelastohydrodynamic lubrication.

List of Tables.

List of Figures.

Chapter 1. Introduction.

Most of us know someone who has an artificial joint; typically an elderly relative or neighbour with an artificial hip. For these people, who suffered with diseased or traumatically damaged joints, total joint replacement (TJR) restores pain free function, and is undoubtedly one of the most successful major surgical operations currently undertaken in medicine.

Arthroplasty of the hip or knee is common. Williams *et al.* (1992) estimated that in the UK some 30,000 primary hip replacements, and 10,000 primary knee replacements were conducted in 1989/90; and in the USA 120,000 hips and an equal number of knees were being replaced annually. In the UK 5.6% of all over 65's undergo elective hip replacement (Williams *et al.*, 1994) and the number is increasing. Although the cost of primary hip or knee replacement was estimated at £4000, it was considered to be one of the best value major medical interventions (Cavanagh *et al.*, 1992).

The pioneer of the modern total hip replacement (THR) was Professor Sir John Charnley, who developed a stainless steel femoral component articulating in an ultra high molecular weight polyethylene (UHMWPE) acetabular component based on a head diameter of 7/8" (22.2 mm). The prosthesis was fixed to bone using acrylic bone cement, and was designed to exhibit low wear and low frictional torque. Charnley's design is still one of the best selling prostheses today with excellent follow up results of 84% survival at 20 years (Kavanagh *et al.*, 1994), which begs the question 'are new designs of artificial joints really necessary?'

Artificial joints do fail, and subsequently require a revision procedure to replace the ineffective and painful joint. In the UK in 1991 13% of all THR procedures were revisions, and this figure is known to be increasing (Williams *et al.*, 1992). It is expected

to increase further as the overall prevalence of THR increases. The cost of a revision procedure is generally higher than a primary procedure and so, in addition to patient suffering, failure of artificial joints is clearly a drain on health care resources. Also younger patents would benefit if artificial joints could be designed to last longer, so avoiding the need for a revision procedure. There is therefore a clear need to improve the lifetime of TJRs in a cost effective way.

The objective of this work was to design, develop and evaluate a new generation of artificial joints which would last longer than conventional currently available prostheses. The design of these new prostheses draws on the arrangement found in the natural synovial joint, that is a bearing consisting of a hard substrate lined with a layer of low modulus material. Such a bearing has been shown to be lubricated in a similar way to the natural joint, and so extremely low friction and wear, and hence a long component life, could be expected. Several groups (Unsworth *et al.*, 1981, Dowson *et al.*, 1991) have already demonstrated the concept, however some major technical issues must be overcome before such a device could be implanted. For example, the device must be designed to operate with a film of lubricant separating the two articulating surfaces, the low modulus layer must be firmly bonded to a rigid backing, and the materials used must be both biocompatible and able to withstand many millions of gait cycles. This thesis concerns itself with the application of engineering principles, in particular tribology and materials science, to some of these problems, with the aim of producing a joint capable of commercial use.

Part A of this thesis concerns the advancement of compliant bearing technology. The concept of the compliant bearing joint was not new, and so in Chapter 2 the relevant theoretical and experimental work is reviewed. In addition, important work in the development of biocompatible elastomers, particularly polyurethanes, is also reviewed, as are methods of evaluating layer adhesion. In Chapter 3 the methods and materials used in the experimental studies are outlined. Two main experimental studies were conducted;

the first using the Durham friction simulator to study the tribological performance of compliant layer hips and knees; and the second to evaluate the adhesion and mechanical performance of the bonded layer system. The results from these two studies are presented and discussed in Chapters 4 and 5 respectively.

Clearly, if such a concept is ever to undergo clinical trials then extensive long term simulator based wear testing will be required. Although multi-station hip simulator machines exist world wide, there are considerably fewer knee simulator stations to support the development of compliant bearing knee joints. Hence Part B of this thesis reports on a six station knee wear simulator which was designed and commissioned as part of this research. In Chapter 6 the literature pertinent to the development of a knee simulator is reviewed, with the aim of drawing up a design specification. The design and development of first a single station prototype, and then a six station machine is outlined in Chapter 7. In particular the computer simulation used in the design of the servo hydraulic systems which applied the complex load and motion profiles is discussed. Finally, in order to validate the machine, several multi-million cycle wear tests were conducted using conventional prostheses, and the results are presented in Chapter 8. With the introduction of CE marking in Europe for implantable devices by 1998 and the implications for standards and product testing, it was hoped that the knee simulator work would also make a timely contribution to the current debate regarding the wear testing of conventional knee prostheses.

There have been many developments in the field of TJRs, some with questionable benefits in terms of performance and value for money (Bulstrode *et al.*, 1993). Sound and extensive research and development is required if compliant bearings are to become the next generation of TJRs, and not just a 'designer' joint doomed to failure. In Chapter 9 the work presented in this thesis is reviewed, and conclusions from this drawn.

Chapter 2. Literature Review.

2.0 Introduction.

The concept of using low modulus layers on the bearing surface of a total joint replacements (TJRs) is based on the natural synovial joint which has such a compliant layer, the articular cartilage. A combination of lubrication mechanisms has been proposed for the synovial joint which results in fluid film lubrication (Unsworth *et al.*, 1974), which explains the long life and low friction associated with the natural joint. Currently most TJRs consist of a rigid femoral component articulating on an ultra high molecular weight polyethylene (UHMWPE) component. This bearing is far less compliant than the natural joint, resulting in a mixed lubrication regime (Unsworth, 1978) with partial contact of the two articulating surfaces, which in turn leads to wear and higher friction. The overall objective of this research is to develop acetabular and tibial components incorporating a compliant polyurethane (PU) surface layer.

The relevant literature is presented in four broad sections. First an overview of the lubrication of natural and conventional artificial joints is presented. This is important as it illustrates the basic principles of tribology on which compliant bearing TJRs are based. Next the literature relating directly to compliant bearings is discussed. A wealth of experimental evidence demonstrating fluid film lubrication has been presented, and in addition theoretical analyses have been conducted which consider both the tribology and the mechanics of such devices; a good correlation has been demonstrated between theory and experiment. Biomedical grade PU is the candidate material for the compliant layer,

however degradation of this material has been reported *in vivo*. Thus thirdly, an overview of the literature relating to the biocompatibility of suitable grades of PU is presented. Finally, methods of promoting and evaluating adhesion of the compliant PU layer to a rigid backing are considered. This is particularly important if a long life in excess of current conventional joints is to be assured.

2.1 Lubrication of natural and artificial joints.

Natural Joints.

The mode of lubrication of the natural synovial joint has been extensively studied, particularly over the last forty years, using many different experimental configurations and analytical techniques. Several useful reviews of the extensive literature have been published, including Higginson (1978), Medley *et al.* (1984), Dowson (1990), and Unsworth (1993). From these reviews it is clear that fluid film lubrication is predominant in natural healthy joints, and that several different mechanisms are important in maintaining the load carrying capacity of the film of fluid which separates the joint surfaces.

Elastohydrodynamic lubrication (EHL) and squeeze film action are the two main lubrication mechanisms, and much has been published in support of these two mechanisms. During EHL, pressure is generated in the lubricant by an entraining motion between the two inclined joint surfaces. During squeeze film action the two joint surfaces move towards each other and the fluid is squeezed out of the joint space over a finite time. Both EHL and squeeze film action are enhanced by elastic deformation of the joint

surfaces and increases in fluid viscosity. It is for this reason that the mechanical (elastic) properties of articular cartilage, together with the viscosity and constituents of synovial fluid, have been shown to be important in the lubrication of synovial joints. During the walking cycle, squeeze film action is predominant at heel strike, when the load is high but there is no entraining motion between the joint surfaces. During the stance phase EHL maintains the fluid film integrity as the entraining motion increases. During the swing phase the joint is lightly loaded with high entraining velocities and hence hydrodynamic action increases the film thickness to a maximum, ready for the next heel strike.

During periods of sustained heavy loading the film of fluid may be completely squeezed out, as may be expected when standing for long periods without entraining motion. When a film of fluid is not separating the joint surfaces, intimate contact and adhesion between surface asperities is prevented by a strongly adhering boundary lubricant. Experiments have shown (Linn and Radin, 1968) that it is the protein component of synovial fluid which acts as an efficient boundary lubricant, protecting the joint surfaces during periods when EHL is ineffective.

The thickness of the fluid film has been calculated using various analytical techniques of increasing sophistication to model EHL (see Section 2.2.2). The values reported for hip and knee joints are remarkably similar, of the order of 1 μm (Dowson, 1981). However articular cartilage was found to have a surface roughness of between 2 and 6 μm (see Sayles *et al.*, 1979) which suggested that EHL was not sufficient to maintain fluid film lubrication. However, Dowson and Jin (1986, 1992) showed that pressure perturbations in the lubricant would develop due to the entraining action of surface roughness. The pressure perturbations could effectively smooth the surface asperities, and sustain film

thicknesses of less than 1 μm, a mechanism known as microelastohydrodynamic lubrication (μ-EHL). However Dowson and Jin based their analysis on surface roughness with a wavelength greater than that found in practise, and so Yao and Unsworth (1993) extended the argument to include surface roughness of various forms more typical of articular cartilage. They demonstrated that short wave length tertiary undulations observed on the surface of cartilage would only sustain fluid film lubrication under dynamic loading conditions.

Artificial Joints.

Artificial replacement joints are formed from hard material couples, typically metallic materials on UHMWPE, ceramic on UHMWPE, and metal on metal. They differ fundamentally from the natural synovial joint in that the load bearing surfaces are several orders of magnitude more rigid than articular cartilage. This is illustrated by considering the elastic modulus of cartilage which is typically 20 MPa [1], and comparing it to the harder artificial joint materials, which have elastic moduli of 200 GPa for metallic materials, 450 GPa for ceramic, and 1.4 GPa for UHMWPE (Dowson *et al.*, 1991). It was clear from the literature that the EHL and squeeze film action were enhanced by the compliance of the bearing surfaces and thus, since the bearing surfaces of artificial joints are less compliant, one would expect a less effective lubrication regime to operate. This was demonstrated experimentally by Unsworth (1978) and O'Kelly *et al.* (1979), when they showed that artificial joints operated in a mixed lubrication regime. During mixed lubrication the load is carried partly by the pressure developed in the lubricant through EHL and squeeze mechanisms, and partially by asperity contact between the two

[1]The value of elastic modulus is very dependent on the test method used. Johnson *et al.*, (1975) tested unconstrained samples in dynamic compression and reported values of 12-45 MPa, whereas Higginson and Snaith (1979) who tested constrained samples reported values of 50-500 MPa.

articulating surfaces. This asperity contact leads to the generation of wear particles, which have been implicated in bone resorption and the loosening of prosthetic components (Howie *et al.*, 1993), resulting in failure.

Natural joints enjoy fluid film lubrication, whereas artificial joints operate in the mixed lubrication regime. The wear of current artificial joints can be minimised, through the use of different bearing materials and coatings, but not eliminated. Since the bearing surfaces are rigid asperity contact is expected, leading to wear related problems. Artificial joints based on compliant bearing surfaces are designed to operate with fluid film lubrication like the natural joint. Hence it is the lubrication of this new generation of artificial joints which is the key to negligible wear and an extended service life.

2.2 Compliant bearing total joint replacements.

The development of compliant bearing TJRs at the University of Durham started when Unsworth *et al.* (1981) used a joint simulator to show that an acetabular cup lined with silicone rubber exhibited friction factors as low as 0.003, indicative of fluid film lubrication. Subsequently, Unsworth *et al.* (1987, 1988) replaced the silicone rubber with more suitable PU elastomers, and experimentally determined that an optimum layer thickness and compliance existed which gave rise to optimum lubrication characteristics. In addition, Pearcy (1988) conducted experiments which showed that the PU layers were not damaged if third body particles such as bone cement were introduced, or the joint ran dry for short periods. The group at Durham then turned their attention to some of the problems associated with developing compliant bearing TJRs into a product available for

implantation. Blamey *et al.* (1991) considered the issue of degradation of the PU layer. They considered several different types of commercially available nominally 'biocompatible' PUs, and assessed the effect of 120 days immersion in Ringers solution on mechanical properties and friction. They concluded that aliphatic polyether-urethanes were most resistant to degradation and maintained low friction, and hence were the most suitable for use in this application. However, this type of PU has subsequently been shown to degrade *in vivo* under certain conditions (Stokes, 1987) illustrating that, in retrospect, immersion in Ringers solution is an unsuitable *in vitro* model to assess biocompatibility. Blamey *et al.* (1993) also considered the problem of bonding the complaint layer to the rigid backing, and advocated the use of a mechanically bonded PU layer to a UHMWPE backing using compression moulding techniques.

Throughout the last decade or so, relevant experimental and theoretical work has also been conducted in a number of other research centres, most notably at the University of Leeds, where Dowson (1989) introduced the term 'cushion form bearings' to describe compliant bearing joints. Experimental work has concentrated on the evaluation of the lubrication regime, either by measuring friction or by direct measurement of the lubricant film thickness. Theoretical analyses have been conducted to evaluate the contact area and the lubricant film thickness in the prosthesis during physiological loading conditions. Initially, a degree of uncertainty existed between experimental and theoretical approaches, although recently useful correlations between the two have been demonstrated.

2.2.1 Experimental evaluation of compliant bearing tribology.

Frictional measurement has been extensively used as an indirect assessment of the lubrication in loaded contacts through Stribeck analysis, described for example by Unsworth *et al.* (1987). If the coefficient of friction μ is plotted against the Sommerfeld parameter **Z**, then the shape of the resulting Stribeck curve is indicative of the lubrication regime, Figure 2.1. A falling curve indicates a mixed lubrication regime, where the load is carried by partial asperity contact and partly by the pressure developed in the lubricant. A slightly rising curve with overall low friction indicates fluid film lubrication, where the load is carried entirely by pressure developed in the lubricant with no asperity contact. The Stribeck curve is thus a simple lubrication chart, and has been used extensively by a number of groups (*i.e.* Unsworth *et al.*, 1987 and Auger *et al.*, 1993b) to evaluate the lubrication of compliant bearing joints.

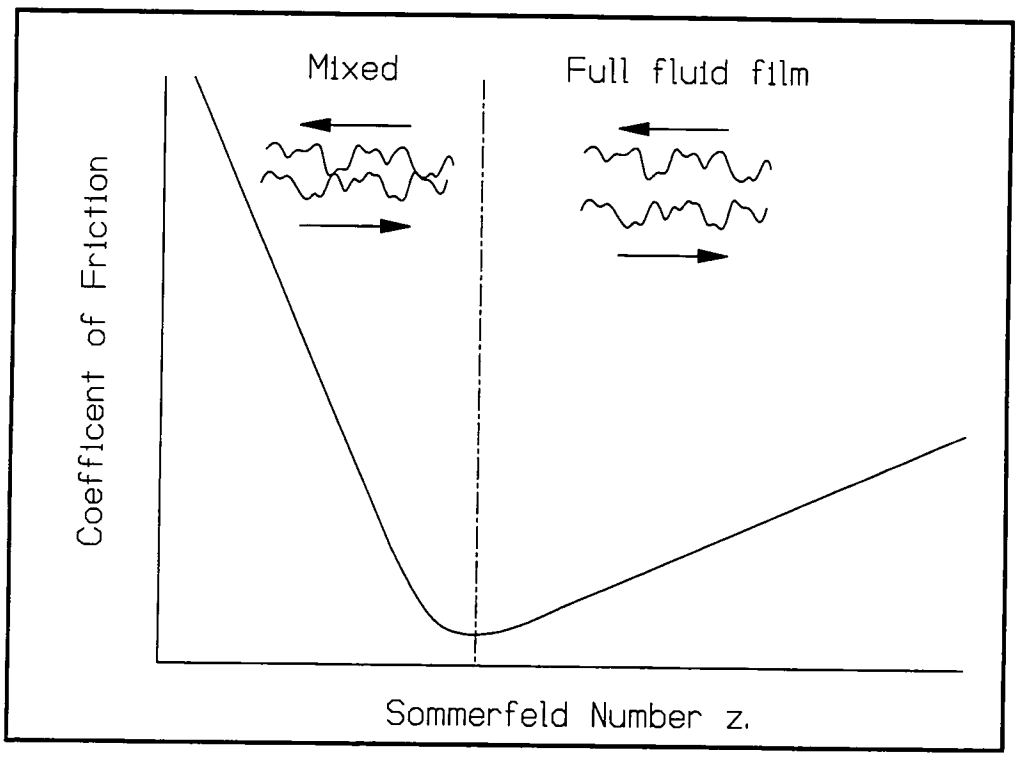

Figure 2.1 Idealised Stribeck plot. The falling curve indicates mixed lubrication (partial asperity contact) and the rising curve indicates fluid film lubrication (no asperity contact).

Gladstone and Medley (1990) measured friction under conditions of constant load and sinusoidal velocity applied to a compliant bearing line contact using pin-on-plate apparatus. They used Stribeck analysis to demonstrate experimentally that fluid film lubrication occurred in the contact, which they then compared with a simple inclined plane model of elastohydrodynamic lubrication (Medley *et al.*, 1984) and demonstrated good agreement with theory. They went on to suggest that the durability of compliant lubricated contacts could be adequately evaluated using simple constant load pin-on-plate apparatus, so long as the experiment was designed to operate in the fluid film regime. Such an approach was used a decade earlier by Medley *et al.* (1980) when they demonstrated low wear in fluid film lubricated polyurethane contacts. However, this simple model had two main disadvantages; the simplified geometry resulted in unrepresentative stresses in the material and at the interface; and it did not have a dynamically applied load, which was shown by Unsworth (1993) to be a fundamental factor in the lubrication of natural and hence compliant bearing joints.

Unsworth *et al.* (1987, 1988) measured friction under conditions of dynamic load and sinusoidal motion applied using a joint simulator. They used Stribeck analysis to demonstrate that while conventional hip replacements operated in the mixed lubrication regime, cups with a compliant bearing surface enjoyed fluid film lubrication. Auger *et al.* (1990) at the University of Leeds, also used Stribeck analysis and a joint simulator (first reported by O'Kelly *et al.*, 1977) when they measured the frictional torque developed in compliant line contacts. They reported extremely low coefficients of friction and confirmed the presence of fluid film lubrication experimentally, but did not demonstrate good agreement with the theory proposed by Medley *et al.* (1984). Importantly, they concluded that the theoretically predicted coefficients of friction were below the

measurement threshold of the simulator which, together with measurement uncertainties associated with misalignment torque and vibrations, rendered a comparison between theory and experiment extremely difficult. In a later study using the same apparatus, a better agreement with theory was demonstrated for both compliant line contacts (Auger *et al.*, 1993a and 1995a) and compliant layer acetabular cups (Auger *et al.*, 1993b). It was suggested that this improvement was due to an improved experimental protocol, and in particular the use of a procedure (discussed latter in Section 3.2.2) which eliminated torque due to misalignment of the components in the test apparatus. They concluded from their comparison between a conventional UHMWPE cup and a compliant bearing cup both of which were designed to operate with the same elastohydrodynamic film thickness (termed elastohydrodynamic equivalence) that μ-EHL was a particularly important lubricating mechanism in this application.

Direct measurement of the lubricant film thickness is the other experimental approach which has been used to evaluate the tribology of compliant layered contacts. Jin *et al.* (1994a and b) reviewed the use of interferometry techniques to assess film thickness. They extended previous work to conditions more relevant to the contact found in compliant layer acetabular cups. They conducted film thickness measurements under conditions of static load and constant velocity, and obtained fair agreement with EHL theory. They also conducted experiments under conditions of a suddenly applied load and zero entraining velocity, and obtained a fair agreement with squeeze film theory. These results enable the theoretical film thickness equations discussed in the next section to be applied with increasing confidence to the design of compliant layered TJRs.

However, the use of interferometry to measure film thickness in real compliant layered TJRs under physiological conditions of dynamic loads and variable velocity would be extremely difficult and has not yet been reported. Ikeuchi *et al.* (1993) observed the contact and lubrication regime under these conditions in a compliant hip cup using a transparent femoral head, and reported that small pools of fluid were trapped in the contact by the extremely compliant layer which they used. Murakami and Ohtsuki (1987) and Murakami *et al.* (1993) used electrical resistance methods to evaluate the lubrication regime developed in both conventional and compliant layered knee prosthesis on a knee joint simulator. The method did not enable an absolute value of film thickness to be evaluated, only that high values of resistance indicated the relative separation of the two bearing surfaces due to fluid film lubrication. Partial contact and hence mixed lubrication was indicated by low resistance between the surfaces. They demonstrated for the first time that the application of a compliant layer to the tibial component of a realistic knee prosthesis could result in fluid film lubrication.

The experimental evidence reviewed so far suggests that fluid film lubrication exists in compliant layer joints, and hence there would be a likely increase in the life of the prosthesis. However the work of Caravia *et al.* (1993a, 1993b, 1995) has shown that at the start of relative motion between preloaded compliant layer contacts, fluid film lubrication does not occur and contact between the surfaces results. They used a simple pin on plate configuration to assess the start up friction at the onset of motion after loading the contact for up to 400 s. Such conditions may occur in a TJR at the start of a walking cycle after standing for long periods without entraining motion. They measured the coefficient of friction at start up between a metallic indenter and a PU layer (Caravia *et al.*, 1993a) and reported values >1, which is several orders of magnitude greater than

the values reported here for fully lubricated contacts (<0.01). The start up friction increased as the preloading time increased, nearing a maximum value after approximately 100 s. The start up friction was shown to reduce with increasing roughness of the indenter, an observation which is at odds with the need for a smooth surface for fluid film lubrication during normal operation. The same technique was used to assess the start up friction between an indenter and a hydrogel layer (Caravia *et al.*, 1993b) and they reported values of between 0.1 and 0.5 depending on the type of hydrogel. Hydrogels offered both improved start up and steady state mixed lubrication performance when compared with PU. This was thought to be due to the release of water from the hydrogel polymer network when loaded, coupled with lower surface energy interactions when contact did occur. However, the mechanical properties of the hydrogels were considerably lower than those of PU, making the use of hydrogels for this demanding application questionable. To complete the study, the start up friction between two PU layers was measured (Caravia *et al.*, 1995) and found to be extremely high, with values of coefficient of friction up to 4 reported. They suggested that since both surfaces were compliant, asperity deformation would result in an increase in the real area of contact, and also adhesive forces between two PU asperities may be greater than those between metal and PU. Clearly, exact replication of the natural joint with both bearing surfaces having a compliant surface was undesirable. High values of start up friction may have implications on the performance of the compliant layer TJRs, since asperity interaction at start up would result in wear, and high start up frictional torque may contribute to cup loosening through either fatigue or shear failure of the fixation. Thus start up friction in a real prosthesis under conditions of dynamic physiological loading would merit further investigation. Such an investigation is reported in Section 4.2.7.

Considering the great interest shown in compliant bearing TJRs, little work has been reported concerning the long term performance and wear of these joints. Medley *et al.* (1980) demonstrated low wear in fluid film lubricated PU contacts when tested in a simple pin on plate wear screening device. Jin *et al.* (1993a) conducted similar experiments and confirmed this observation. They also concluded that if the contact operated under mixed lubrication conditions the wear factor significantly increased to a level two orders of magnitude greater than UHMWPE operating under similar conditions. However, it is generally considered that these simple pin on plate models have little relevance to the tribological conditions occurring physiologically and that only simulator studies and ultimately clinical trials will give a real indication of the long term performance. Auger *et al.* (1995b) evaluated the wear and durability of simple plane compliant layer tibial components on a knee simulator, and identified several different failure modes. They observed fatigue failure of low modulus ($\mathbf{E_2}$=6 MPa) compliant layered components known to operate under fluid film lubrication after only 0.2×10^6 cycles, demonstrating that the mechanical performance of the prosthesis is equally as important as is its mode of lubrication. However they observed no wear debris or structural failure when a higher modulus ($\mathbf{E_2}$=20 MPa) compliant layered tibial component was tested to 5×10^6 cycles; although deformation, creep and some debonding of the layer were noted. There can be little doubt that extensive and successful *in vitro* durability testing will be required before compliant bearing TJRs can progress to clinical trials.

2.2.2 Theoretical evaluation of compliant bearing tribology.

Theoretical analysis of the lubricant film thickness in compliant layered contacts requires that both the Reynolds' equation (which describes the flow of lubricant) and the elasticity

equations (which describe the deformation of the contact) are solved simultaneously. This requires massive computational power and hence simplification of the problem to various degrees. Initially, solutions were developed for the case of an infinitely long rigid cylinder in contact with a compliant layered plane. Line contact reduces the problem to one of two dimensional fluid flow and plane strain. Subsequently three dimensional solutions have become available for point contacts which are more suitable for both natural hip and knees joints, and compliant layer TJRs. These solutions were initially considered for lubrication of the natural joint, which has a Poisson's ratio (ν) for cartilage of about 0.4 (Hayes *et al.*, 1972). However, from the perspective of compliant TJR design, a simply applied formula which is valid for an incompressible material with ν =0.5 and for point contacts would be of most use.

Hooke and O'Donoghue (1972) considered compliant layered line contacts under conditions of constant velocity and load. They reported film thickness results for ν=0.5 and for a large range of $\mathbf{a/h_t}$ values (0.01 to 32). Medley *et al.* (1984) conducted a transient analysis of a line contact representing a human ankle joint using a dynamic load and sinusoidal varying velocity. They included both EHL and squeeze terms, and used either the constrained column model (see Higginson, 1966) or the inclined plane model (which they found more efficient in terms of computing time) for the deformation of the contact. Importantly, they demonstrated that the film thickness remained fairly constant during the dynamic walking cycle, with a value of about 0.7 μm.

A full numerical solution for the elastic deformation of a layered line contact (Meijers, 1968) was compared with the constrained column model by Dowson and Jin (1990). They concluded that provided ν<0.45 and $\mathbf{a/h_t}$>2 then the column model could be used to

predict film thickness with fair accuracy, and with considerable reductions in computing time. Jin *et al.* (1993b) used a simplified equation to represent the elastic deformation of a line contact, valid only when $\mathbf{a>>h_t}$, which enabled them to derive an analytical solution for the steady state lubricated line contact problem due to entraining action for both incompressible and compressible layers. For compressible layers, their results were very similar to the numerical constrained column model solution, presented by Smith and Medley (1987) for ν=0.4.

Dowson and Yao (1990) presented a numerical solution to the EHL film thickness prediction problem for point contacts under steady state conditions of constant load and velocity. Their solution was only valid for ν<0.4, and $\mathbf{a/h_t}$>10 since they used the constrained column model. They presented 3-D film thickness profiles for both circular and elliptical contacts which indicated a gradually tapering film thickness in the entraining direction, with the minimum film thickness being very near to the outlet edge of the lubricated contact. They showed that the film thickness for layered compliant contacts were larger than the those for rigid contacts, but not as large as those for semi infinite compliant contacts. However the numerical methods used were complex, and results were presented for only one circular and one elliptical contact. Dowson and Yao (1994) extended their analysis to give results for 21 cases, and curve fitted the results to give useful empirical formulae for the steady state film thickness for both circular and elliptical contacts. However, the column model on which the solutions were based was only applicable for ν<0.4, and so Dowson *et al.* (1991) proposed a simple method which adjusted the elastic modulus value and enabled incompressible layer contact problems (ν=0.5) representative of compliant replacement joints to be assessed. The method is discribed by Auger *et al.* (1993b), and later in Section 2.2.4.

Jin *et al.* (1993c) used the results of Dowson and Yao (1990) to simplify the point contact problem to one of two dimensions, which they then solved for the case of steady state entraining action. They then used the principle of superposition to combine the EHL and dynamic squeeze film action, and conducted transient film thickness analysis for a natural hip joint subjected to a dynamically applied load and variable entraining velocity. They showed that the squeeze film thickness decayed slowly over the duration of the stance phase of the dynamic cycle, and was subsequently replenished by the entraining EHL action during the swing phase. This result was particularly important, and agreed with transient film thickness results for line contacts (Medley *et al.*, 1984). Since the film thickness remained essentially constant throughout the cycle and was determined predominantly by EHL, application of the steady state EHL formula would lead to a good estimate of the film thickness.

2.2.3 Contact mechanics.

The magnitude of the stresses and strains developed in the compliant layer will influence the long term mechanical performance of the joint. In particular they will indicate the susceptibility of both the layer to fatigue failure, and layer/backing interface to debonding. Hence an understanding of the mechanical behaviour of compliant bearings is important .

Hayes *et al.* (1972), McCormick (1978), Matthewson (1981) and Jaffar (1988) have all considered the contact problem of a plane compliant layer indented by a rigid sphere, essentially representative of compliant layer hip or knee joints. Numerical methods were used to solve elasticity equations for various ratios of $\mathbf{a/h_t}$ and values of ν up to 0.5, to

give the radius of the contact area. In addition, McCormick (1978) considers a general solution for elliptical contacts, and several of the authors consider the stresses in the layer and at the interface. However, in all cases the numerical procedures used were complex making them inconvenient to apply to different joint designs. The relationship between various dimensionless groups were presented graphically, and although these results were more accessible, the application to specific design cases was still long-winded.

Ihara *et al.* (1986) and Jin *et al.* (1991) have used finite element analysis to predict the stresses in the layer and at the interface for a plane compliant layer indented by a rigid sphere. They also considered the effect of friction at the contact. The maximum shear stress was found at the layer/backing interface for the case of zero friction, but as the friction increased so did the maximum shear stress which was located on the surface of the layer. Although Ihara *et al.* (1986) presented design charts, these were only applicable for values of $\mathbf{a/h_t}<2$, untypical of the bearings considered here. Strozzi and Unsworth (1994) used finite element analysis to consider the true curved geometry of the problem, that of a sphere in a cup. Both Jin *et al.* (1991) and Strozzi and Unsworth (1994) presented results for a limited number of design cases, and so although they illustrated trends in mechanical behaviour, their results were not easily applicable for the analysis of other specific design cases.

Yao (1994) used a 'semi-analytical' approach to analyse the contact between a rigid sphere and a compliant layer bonded to a rigid substrate, for a range of aspect ratios ($0<\mathbf{a/h_t}<100$), and values of ν up to 0.5. Design charts were presented for the dimensionless contact radius, contact pressure and the full stress field within the layer. The results for contact area were shown to compare well with the more complex

numerical solutions due to Hayes *et al.* (1972), McCormick (1978), Jaffar (1988) and Jin *et al.* (1991). The results were used by Yao *et al.* (1994) to develop simple power law formulae to predict the contact area, maximum Tresca shear stress and the maximum shear strain for compliant layer joints with aspect ratios in the range $0<a/h_t<20$. The results are thus easily accessible and useful in the design of compliant bearing TJRs.

2.2.4 Design of compliant bearing TJRs.

The design of a compliant bearing hip prosthesis was discussed by Dowson *et al.* (1991). They advocated the use of certain equations to predict the film thickness and contact area, and investigated the effect of changing layer thickness, layer modulus and radial clearance on the lubricant film thickness, contact area, and normal contact stress. Their parameteric study clearly showed that it was beneficial to maximise the contact area to promote fluid film lubrication, and they suggested that an optimum layer thickness and elastic modulus existed. They identified that although a reduction in elastic modulus would improve the effectiveness of both EHL (through increased contact area) and μ-EHL (through increased asperity deformation), it would also lead to larger strains in the layer and an increased likelihood of fatigue failure. They did not consider shear stress at the layer/backing interface.

Yao *et al.* (1994) considered the design only from a contact mechanics perspective, but extend the analysis conducted by Dowson *et al.* (1991) to include simple power law formula for the maximum shear stress and strain within the layer, and contact area. They showed how similar contact radii could be achieved with various combinations of layer thickness, layer modulus and joint conformity. However they proposed that it was more desirable to achieve the desired contact radius with a thick stiff layer in a more

conforming joint, as this represented a good compromise in reducing both the shear stress and shear strain.

Both analysis of lubrication and contact mechanics have been employed to evaluate the design of compliant bearing TJRs, and these have been reviewed in the previous two sections. Although the methodology discussed by Dowson *et al.* (1991) is not greatly changed, slightly different design equations are advocated here. Refinements in the models and numerical techniques, coupled with the development of power law design equations, mean that the equations used here represent the analyses most easily applicable to lubricated point contacts for incompressible layers.

Hip Joints.

Firstly considering the circular contacts representing the hip joint. The film thickness can be calculated using Equation 2.1 and 2.2 (Dowson and Yao, 1994).

$$h_{cen} = 1.68R\left(\frac{\eta u}{E'R}\right)^{0.54}\left(\frac{h_t E'}{E''R}\right)^{0.37}\left(\frac{L}{E'R^2}\right)^{-0.18} \qquad 2.1$$

$$h_{\min} = 1.59R\left(\frac{\eta u}{E'R}\right)^{0.56}\left(\frac{h_t E'}{E''R}\right)^{0.36}\left(\frac{L}{E'R^2}\right)^{-0.20} \qquad 2.2$$

Care must be taken to use the correct modulus terms. The constrained column model, used to derive Equations 2.1 and 2.2 required $\nu_2 \leq 0.4$. In order to accommodate a layer with $\nu_2=0.5$ Dowson *et al.* (1991) indicated that an adjusted modulus $\mathbf{E_{adj}}$ should be used in place of $\mathbf{E_2}$, as described by Auger *et al.* (1993b). The full elasticity solution was used to calculate the dry contact half width **a**, and $\mathbf{E_{adj}}$ determined from the constrained column model using $\nu_2=0.4$ in order to give the same contact area as that given by the

full elasticity solution, Equation 2.3. This allows the film thickness equations based on the constrained column model to be applied to incompressible layers.

$$E_{adj} = \frac{4LRh_t}{\pi a^4}\left\{\frac{(1+\nu_2)(1-2\nu_2)}{1-\nu_2}\right\} \qquad 2.3$$

where ν_2=0.4.

The modulus terms can now be written for the single layer case, Equations 2.4 and 2.5.

$$\frac{1}{E'} = \frac{1-\nu_2^2}{E_{adj}} \qquad 2.4$$

where ν_2=0.4.

$$\frac{1}{E''} = \frac{(1+\nu_2)(1-2\nu_2)}{(1-\nu_2)E_{adj}} \qquad 2.5$$

where ν_2=0.4, since the above equation is derived directly from the constrained column model, as outlined in Yao and Dowson (1994). The contact radius, maximum shear stress and maximum shear strain for circular point contacts are found using Equations 2.6 to 2.8 (Yao *et al.*, 1994).

$$a = 0.94 h_t^{0.38}\left(\frac{LR}{E_2}\right)^{0.21} \qquad 2.6$$

$$\tau_{max} = 0.22\left(\frac{L^{0.52}E_2^{\,0.48}}{h_t^{0.56}R^{0.48}}\right) \qquad 2.7$$

$$\gamma_{max} = 0.72\left(\frac{L}{E_2 h_t R}\right)^{0.5} \qquad 2.8$$

Knee joints.

Secondly, considering the case of elliptical contacts more representative of the knee joint. The film thickness can be calculated from Equations 2.9 and 2.10 (Dowson and Yao, 1994) so long as the entraining action is along the minor axis, and remembering that the

load is distributed between two condyles, and using the adjusted modulus scheme discussed for hips.

$$h_{cen} = 3.66R\left(\frac{\eta u}{E'R}\right)^{0.54}\left(\frac{h_t E'}{E''R}\right)^{0.37}\left(\frac{L}{E'R^2}\right)^{-0.18}\left(1 - 0.61e^{-0.12k}\right) \qquad 2.9$$

$$h_{\min} = 3.54R\left(\frac{\eta u}{E'R}\right)^{0.56}\left(\frac{h_t E'}{E''R}\right)^{0.36}\left(\frac{L}{E'R^2}\right)^{-0.20}\left(1 - 0.64e^{-0.15k}\right) \qquad 2.10$$

Considering the contact mechanics, the elliptical contact half widths **a** and **b** for the semi-infinite Hertzian case are given by Timoshenko and Goodier (1970), Equations 2.11 to 2.17.

$$a = m\sqrt[3]{\frac{3\pi L(k_1 + k_2)}{4(A + B)}} \qquad 2.11$$

$$b = n\sqrt[3]{\frac{3\pi L(k_1 + k_2)}{4(A + B)}} \qquad 2.12$$

$$\text{where } k_1 = \frac{1 - \nu_1^2}{\pi E_1},\ k_2 = \frac{1 - \nu_2^2}{\pi E_2} \qquad 2.13$$

$$A + B = \frac{1}{2}\left(\frac{1}{r_1} + \frac{1}{r_1'} + \frac{1}{r_2} + \frac{1}{r_2'}\right) \qquad 2.14$$

$$B - A = \frac{1}{2}\left[\left(\frac{1}{r_1} - \frac{1}{r_1'}\right)^2 + \left(\frac{1}{r_2} - \frac{1}{r_2'}\right)^2 + 2\left(\frac{1}{r_1} - \frac{1}{r_1'}\right)\left(\frac{1}{r_2} - \frac{1}{r_2'}\right)\cos 2\psi\right]^{\frac{1}{2}} \qquad 2.15$$

The coefficients m and n depend on the ratio of (B-A):(A+B), such that

$$\cos\theta = \frac{B - A}{A + B} \qquad 2.16$$

where

$$m = 1.84 \times 10^{-4}\theta^2 - 0.0436\theta + 3.44 \text{ and } n = 9.36 \times 10^{-3}\theta + 0.15 \qquad 2.17$$

where θ is in degrees. (Equations 2.17 are empirical formulae fitted to the data given by Timoshenko and Goodier, 1970). The Hertzian contact half widths can then be used to obtain results for the layered case using the graphical results given in McCormick (1978).

2.3 Medical grade polyurethane.

The objective here is to identify suitable elastomeric materials which allow compliant bearing TJRs to be developed with reasonable confidence of a successful out come. The choice of elastomeric material for the compliant layer of the bearing is an important one, since its properties will influence both the bearing's mechanical and tribological performance. The material's chemistry will determine the stability of the elastomer in the harsh physiological environment. Clearly the research was started with a suitable group of materials in mind, but it is interesting to review the issue of material selection. In his review of elastomers for biomedical applications, McMillin (1994) identified silicone rubbers, olefin based elastomers and hydrogels together with polyurethanes as potentially suitable for long term implant applications. Typical mechanical properties of these materials are given in Table 2.1

	Articular cartilage	Silicone rubber	Poly(olefin) elastomer	Hydrogel	Polyurethane
Tensile strength (MPa)	10-30	3-12	10-16	0.5-10	20-60
Tensile modulus (MPa)	10-100	-	-	0.5-90	10-100
Elongation (%)	80	300-1000	250-520	100-200	250-600

Table 2.1. Typical mechanical properties of biomedical elastomers suitable for long term implant, compared with articular cartilage. After Corkhill *et al.* (1990) and Pinchuk (1994).

Silicone rubbers have been used extensively in biomedical applications since 1962; including breast implants, finger prostheses, and tubing. However they tended to be used in low stress applications due to low tensile strengths. Extensive testing and *in vivo* implant experience indicated that silicones could be considered generally inert and

biocompatible (Pinchuk, 1994). However, in the early 1990's reports associating silicone breast implants with autoimmune diseases resulted in many product liability suits filed in the USA. As a result the materials manufacturer (Dow Corning, MI, USA) withdrew all its silicone products from the long term implant market. Silicone rubbers are also extremely hydrophobic which is undesirable in this application since the natural lubricant is water based. For these reasons silicone rubbers were discarded as potential compliant layer materials.

There are a range of olefin based rubbers and elastomers, some of which were discussed by McMillin (1994), in various stages of development. Since they are based on simple straight chain hydrocarbons suitable biostable performance should be assured. They typically possess superior mechanical properties compared with silicones. However these materials have no long term *in vivo* track record and for this reason they were not considered here.

Hydrogels are "cross linked hydrophilic polymer networks which are water swollen but do not dissolve in water" (Corkhill *et al.*, 1990). They are based on a range of biocompatible polymer networks, and are used extensively for soft contact lenses. They are similar to natural cartilage in their high water content (typically 30-80 %) and hence are particularly attractive for compliant layer TJR. The bioengineering group at the University of Leeds conducted collaborative research with Tighe's group at Aston University (Birmingham, UK) to demonstrate the tribological advantages of high water content hydrogels in this application (Caravia *et al.*, 1993b). Although recent work (Corkhill *et al.*, 1990, Aronhime *et al.*, 1994) developed hydrogels with tensile strengths

as high as 20 MPa their mechanical properties, particularly in fatigue, are still considered too low for this application.

Polyurethane (PU) has superior mechanical properties for this demanding high stress application compared with the other implant elastomers considered above. Catheters, pacemaker leads, vascular prostheses, flexible artificial heart valves and the housings of artificial hearts and ventricular assist devices have been made from medical grade thermoplastic PUs. Hence there is considerable experience in the use of PU for long term implants, particularly for pacemaker lead insulation where some degradation and failure has been reported. McMillin (1994), Pinchuk (1994) and Stokes *et al.* (1995) recently reviewed PU history, chemistry, commercial availability, degradation mechanisms and the development of new 'biostable' PUs for long term implants in some detail. In addition, the papers published in the *Journal of Biomaterials Applications*, **3**(2), 1988 represented the consensus of scientific opinion in the late 1980's.

The term polyurethane refers to polymers made by the addition of an isocyanate with a hydroxyl, and covers a huge range of materials with different properties. Thermoplastic PU elastomers for biomedical applications have quite specific chemistry, and can be considered as block copolymers comprising either polyester or polyether 'soft' segments linked together by urethane or urethane urea 'hard' segments. The hard domains are crystalline with hydrogen bonding between the molecules, whereas the soft domains remain amorphous. This molecular structure gives rise to unique mechanical properties which can be fine tuned by varying the ratios of 'hard' and 'soft' segments. It is important to appreciate the chemistry of the various commercially available PUs as this will influence their biocompatibility. There are three main monomers which are reacted

together to produce these PUs; the diisocyanate, macrodiol and chain extender. The abbreviations subsequently used are defined in the Nomenclature, and Table 3.1.

There are two classes of diisocyanates which form the hard segment; aromatic (MDI) and aliphatic (HMDI), and much debate has ensued as to which is preferable. Recently Hergenrother *et al.* (1993) conclusively demonstrated that aliphatic based PUs were more susceptible to degradation than aromatic PUs. The disadvantage of aromatic MDI based PU is the risk of leaching out small amounts of potential carcinogen MDA (4,4 methylenedianiline) after steam sterilisation or processing the polymer with a high moisture content. In fact Hirata *et al.* (1995) detected MDA after sterilising both aromatic **and** aliphatic PUs using γ-irradiation, autoclave and ethylene oxide, although the amounts were so small in all cases that they concluded the increased risk was practically negligible. In addition Pinchuk (1994) argued at great length that no conclusive evidence existed which implicates MDA as a carcinogen. This seems to be the consensus opinion since commercial medical grade PUs are currently predominantly based on aromatic diisocyanate chemistry.

The macrodiols form the soft segments of the PU, and polyether or polyester monomers are most commonly used. Polyester PUs make up the bulk of industrial use, but are subject to hydrolytic degradation and are not used in implantable devices (Stokes *et al.* 1995). Polyether urethanes, typically based on PTMEG, have found the most wide spread application for long term implants, of which Pellathane 2363 was one of the most widely used commercial grades. However the softer grades of polyether PUs, used as pacemaker leads, were liable to degrade under certain conditions and although excellent results were obtained in some devices (Stokes *et al.*, 1995) the litigious environment in the USA

resulted in the withdrawal of some polyether PUs from the market; *e.g.* Pellathane, and Biomer (Eithicon, NJ, USA) (McMillin, 1994). New 'biostable' PUs based on different macrodiol soft segment chemistry are currently being developed and will be discussed later.

Chain extenders link together the pre-polymer formed from the macrodiol and diisocyanate. BDO is most commonly used and yields a thermoplastic PU which is easily processed. Amine chain extenders such as ethylene diamine (EDA) are also used, although these yield a polyurethane urea (PUU), *e.g.* Biomer. The advantage of the urea linkage is its excellent flexural strength, resulting in the use of Biomer for heart diaphragms before its withdrawal. However PUUs can not be thermally processed, limiting applications to thin section solvent cast components. In addition Hergenrother *et al.* (1993) showed that BDO chain extended PU retained its mechanical properties better than EDA chain extended PUU after implantation.

2.3.1 Polyurethane biostability.

Having reviewed the elastomers available for implant devices and concluded that PU was the most suitable, the stability of PU in a bioenvironment will be discussed and related back to the polymer chemistry. PU absorbs water (up to 3%) which interferes with the hydrogen bonding resulting in reversible plasticization and up to a 30% reduction in tensile strength (Pinchuk, 1994, Zdrahala and McGary, 1986). In addition to plasticization, the main degradation mechanisms are due to hydrolysis and oxidation of the polymer which causes cracking and loss of mechanical properties. Hydrolysis (degradation due to water) of ester linkages in polyester PU is well understood and this has generally precluded their use in implant applications, whereas the ether linkages in

polyether PUs are hydrolytically stable resulting in use *in vivo*. Ether linkages however, are subject to autoxidation when in direct contact with tissue (Stokes *et al.*, 1995). In most cases the interface between the device and the body is a layer of foreign body giant cells and/or macrophages. These cells release numerous enzymes and oxidants such as H_2O_2, $O_2^{-}\cdot$, and $HO\cdot$ which interact with the polymer promoting a chain reaction which oxidises the ether soft segments and can lead to eventual chain cleavage. Surface cracks only a few microns deep have been observed *in vivo,* with an increased incidence in the softer grade (higher ether content) polyether PUs. Since the half life of these free radicals is very short they act only in the surface of the device and cannot diffuse through the polymer bulk, making autoxidation a surface phenomenon.

Autoxidation can be augmented by other parameters to cause severe degradation in the polymer bulk. Two mechanisms popularised by Stokes (1987) were environmental stress cracking (ESC) and metal ion oxidation (MIO). ESC was thought to require the action of oxidants, residual stress, and proteins such as α_2-macroglobobin for degradation of ether linkages (Stokes *et al.* 1995), resulting in deep crazed cracks. MIO was observed in devices containing metallic components such as insulated cardiac pacing leads. The metallic corrosion products, typically Co in the case of pacing lead alloys, were shown to accelerate autoxidation in the presence of H_2O_2, although MIO could also occur anaerobically when no oxidant producing foreign body response occurred (Stokes *et al.* 1995). In contrast to ESC which proceeded from the device surface, MIO occurred from the PU/metallic interface outwards. Complete reviews of the many *in vitro* and *in vivo* studies which have investigated ESC and MIO were given by Pinchuk (1994) and Stokes *et al.* (1995).

ESC could not be reproduced *in vitro* until recently when Zhao *et al.* (1995) reported ESC type failures both in human plasma-$H_2O_2/CoCl_2$ and glass wool -$H_2O_2/CoCl_2$ systems. Accelerated *in vivo* testing (Stokes *et al.* 1987) involved subcutaneous implant of PU strained up to 400%. These *in vitro* and *in vivo* test methods were important tools in understanding the degradation mechanisms, and the subsequent development of new biostable PU.

2.3.2 New biostable polyurethanes.

The market for a thermoplastic PU suitable for long term implantation is huge (Szycher, 1987), and as a result much effort has been made to improve the biostability of PUs. Since the ether linkage is implicated in the oxidative degradation of current PU, several groups have developed new biostable grades based on novel macrodiol chemistry.

Corvita Co. (FL, USA) has developed a polycarbonate PU based on PHECD soft segments called Corethane, while retaining the stable hard segment chemistry used in Pellathane and some other polyether PUs (Corethane product literature 1993, Pinchuk 1994). Corethane demonstrated a greatly improved resistance to ESC both *in vitro* (Zhao *et al.*, 1995) and *in vivo* (Pinchuk, 1994), when compared with both hard and soft grades of Pellathane. These results were confirmed in a severe *in vivo* test when Corethane microfilament vascular grafts (extremely large surface area) implanted under 400% stress showed little degradation after 2 years implantation. Corethane was also shown to be less prone to promote cell growth on its surface (Tanzi *et al.* 1994) which may reduce the exposure to cell produced oxidants and in part explain its improved stability.

PolyMedica Ind. (MA, USA) also developed a new polycarbonate PU (although the exact macrodiol chemistry is unavailable) called Chronoflex. Although the hard segment chemistry was based on the potentially less stable aliphatic diisocyanate, encouraging *in vitro* and *in vivo* results were reported (Stokes *et al.*, 1995). The group based at CSIRO[2] and the University of South Wales (NSW, Australia) used a different approach, by developing longer chain polyester macrodiols, with 6, 8 and 10 carbons between the ether linkages (rather than the 4 carbons of PTMEG) (Gunatillake *et al.* 1992). These materials tended to be stiffer than the equivalent PTMEG based PU, but demonstrated improved *in vivo* biostability (Pinchuk 1994) possibly as a result of the reduced number of ether linkages.

Two conclusions can be drawn from this section of the literature; firstly that PU was the best choice of implant grade elastomer for this demanding application; and secondly that new PU technology was being developed independantly which resulted in considerable improvements in biostablity. Clearly both encourage the development of PU compliant layer joints.

2.4 Evaluation of compliant layer adhesion.

In order to understand the interface between the compliant layer and the rigid backing, an appreciation of the science of adhesion is required. Mechanisms which result in a good interfacial bond, and methods of testing the bond are particularly important. These two topics have been extensively reviewed by Kinloch (1987), which serves as a excellent

[2] CSIRO Division of Chemicals and Polymers, Private Bag 10, Clayton Victoria 3168, Autralia.

reference text, and Packham (1992), who edited a useful quick reference handbook. In order to place the evaluation of compliant layer adhesion in context, a review of the literature concerning adhesion mechanisms in general, and a more detailed review of test methods applicable to the compliant layer configuration, is given here. The small amount of published literature concerning the adhesion of thermoplastic PU to rigid substrates is also reviewed.

2.4.1 Mechanisms of adhesion.

To attain good adhesion there is an initial requirement that the bonding surfaces must attain intimate molecular contact, which is governed by the surface free energies of the adherend and substrate. Given that contact occurs between the two surfaces, the nature and strength of the bonding forces are termed the mechanisms of adhesion. Four mechanisms have been proposed; mechanical interlocking, diffusion theory, electronic theory and adsorption theory.

Mechanical interlocking is important on two scales. On a macro scale the bonding of porous structures such as wood and fibre relies on interpenetration of an adhesive into a substrate's surface to form a mechanically interlocked structure. On a micro scale chemical pretreatment methods for some plastics and metals can remove certain material phases from the surface forming a rough, often dendritic, structure with many opportunities for mechanical interlocking. In contrast, mechanically roughening a surface generally results in a cleaner larger bonding area which increases bond strength; mechanical roughening rarely results in sites for mechanical interlocking. In the only study to examine methods of producing compliant layer joints with improved layer adhesion, Blamey *et al.* (1993) based their work on improved mechanical interlocking.

However this is not considered to be a significant mechanism for the PU/UHMWPE or PU/PU interfaces considered here.

Diffusion theory concerns the interdiffusion of polymer chains across the polymer/polymer interface, and requires the polymers to be mutually soluble and the macromolecules or chain segments to be sufficiently mobile. The theory is due to Voyutskii (1963) who examined the adhesion of polymers to themselves (autohesion). Mixing of polymer chains is facilitated if the polymers are amorphous, not crosslinked and above their glass transition temperature. This is likely to be an important mechanism in the adhesion between grades of polyurethane from the same family since a degree of mutual solubility is assured, especially at elevated temperatures.

If two surfaces which have different electronic band structures are brought together then some electron transfer may occur, resulting in a double layer of electronic charge at the interface. *Electronic theory* treats the interface like a capacitor, and suggests that if two charged surfaces are separated then energy will be required to break the electrostatic forces. There is little doubt that electrostatic attraction between surfaces does contribute to adhesive bonding, but in most typical systems its contribution is insignificant (Kinloch, 1987), and hence it is not considered to be an important mechanism here.

Adsorption theory states that, provided intimate contact between the two surfaces occurs, bonding as a result of interatomic or intermolecular forces will be achieved. This is the most widely applicable adhesion mechanism. Three categories of bond exist: secondary bonds including van der Waals and hydrogen bonds are the most common with bond energies of 0.1 to 40 kJ/mol; donor-acceptor bonds which fall between hydrogen and

primary ionic bonds with a large range of bond energies; and primary chemical bonds which include ionic, covalent and metallic bonding with bond energies of 60-1100 kJ/mol. Intimate contact requires atoms to be close on an atomic scale (say <1 nm), which necessitates surface wetting of a liquid component on to a substrate, and will be dependent on surface energy considerations. London dispersion forces (a subset of van der Waals forces) occur between all neutral atoms and alone can give rise to high bond strengths. In addition, if it is energetically favourable for the atoms to undergo any combination of the other bonding types this may further enhance the bond strength.

Having outlined the four mechanisms of adhesion which are generally considered important in high strength adhesive bonds; methods of evaluating the adhesion between a compliant layer and a rigid backing are considered.

2.4.2 Test methods.

In order to evaluate the bond between a flexible adherend and a stiffer substrate, two experimental methods are most applicable: the peel and blister tests. Fracture mechanics have been applied to an analysis of both these tests. There are two classical approaches to fracture mechanics. The first was an energy balance approach due to Griffith (1920), who stated that fracture occurred when sufficient energy was released from the strain field around the crack to create new fracture surfaces. The second was due to Irwin (1973), who found that for a linear elastic material the stress around a crack could be uniquely defined by a stress intensity factor **K**, and that when this factor exceeded a critical value $\mathbf{K_c}$ fracture occurred. An energy balance approach is most suited to the analysis of these test geometries since the flexible component generally does not exhibit linear elastic behaviour, and hence the stress intensity factor approach is invalid. In addition to the

basic analysis, factors affecting the results such as testing rate, geometry, viscoelasticity and plastic effects can be more easily incorporated by considering an energy balance approach.

The objective of previous workers in this area was to develop an expression for bond energy which was independent of test geometry. The Griffith hypothesis can be expressed as:

$$\frac{1}{b_p}\frac{\delta(W_d - U_e)}{\delta c} \geq 2\gamma_m \qquad 2.18$$

where the difference between the work done $\mathbf{W_d}$ and the elastic energy of the bulk material $\mathbf{U_e}$ is converted to surface free energy $\gamma_\mathbf{m}$ by an increment of crack growth $\delta\mathbf{c}$ though a material of width $\mathbf{b_p}$. There is much evidence to suggest that the energy required to cause crack growth is far greater than $2\gamma_\mathbf{m}$. $\gamma_\mathbf{m}$ reflects the energy required to fracture only secondary bonds whereas stronger primary bonds may contribute to the strength of a bonded interface. Hence $2\gamma_\mathbf{m}$ can be replaced by the intrinsic fracture energy $\mathbf{G_0}$, the energy required solely to fracture all types of intrinsic bond. However fracture in real materials will involve some localised viscoelastic and plastic energy dissipation around the crack tip. Hence for this real situation, the adhesive fracture energy $\mathbf{G_c}$, which encompasses all the energy losses required to extend a crack by unit length in a sample of unit width, replaces $2\gamma_\mathbf{m}$ in Equation 2.18. The objective of solving 2.18 for $\mathbf{G_c}$ is to identify a measure of adhesion dependent only on the material system being evaluated, and independent of test geometry and protocol. The evaluation of $\mathbf{G_c}$ has formed the basis of much discussion regarding the peel and blister test methods, which are reviewed in the next sections

2.4.2.1 Peel test.

The peel test is the most common method of testing flexible joints, and involves stripping a flexible layer away from a rigid substrate, Figure 2.2. Several peel test geometries exist which were illustrated by Packham (1992) and are embodied in a range of international standards. In its simplest form the test yields the force required to peel the adherend from the substrate, which is suitable for comparison purposes. However, a measure of $\mathbf{G_c}$ would aid comparison with other material systems and adhesion tests.

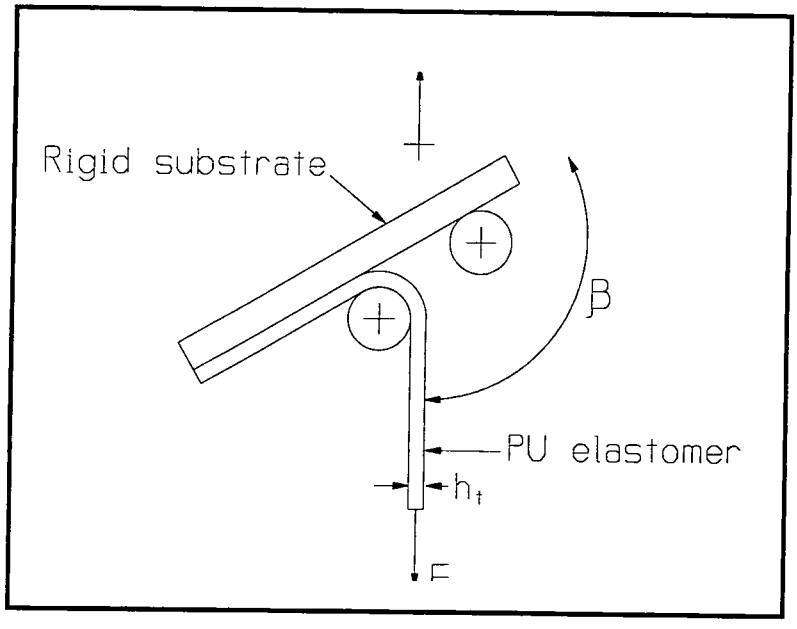

Figure 2.2. Diagram of the peel test arrangment.

By considering the energy balance for the peel test an expression for $\mathbf{G_c}$ can be derived, and since this fracture mechanics based approach avoids the need to develop complex stress analysis it has been far more widely applied than the stress analysis approach discussed latter. Lindley (1971) considered the energy balance in peeling an elastic, but not necessarily linear elastic, material an amount **c**. He assumed that the stress field at the crack tip was independent of **c**, and that as the length **c** was peeled and transferred from the unstressed to the stressed state,

1. The point of application of the force moved by a distance Λc, and hence the energy input was $F\Lambda c$.
2. The peeled adherend gained strain energy $cb_p h_t U$.
3. Equilibrium of the sample was maintained by a force $F\cos\beta$ which moved by a distance c, and hence required an energy $Fc\cos\beta$.
4. As a result a bond of length c will have fractured requiring an energy $G_c b_p c$.

He showed that equating the input energy (1) against the energy terms (2), (3) and (4), dividing by c, and rearranging gave an expression for G_c, Equation 2.19.

$$G_c = \frac{F\Lambda}{b_p} - \frac{F\cos\beta}{b_p} - h_t U \qquad 2.19$$

Unlike the measured peel strength P_c, fracture mechanics suggests that G_c is independent of test geometry for a given test rate and temperature. However, several groups (*e.g.* Gent and Hamed, 1977a&b, Kinloch *et al.*, 1994) have reported that G_c varied with flexible layer thickness and peel angle. This apparent dependence of G_c on test geometry, and the discrepancy with classical fracture mechanics has been explained in terms of additional energy dissipating mechanisms associated with the advancing peel front. Appropriate energy terms may include plastic and viscoelastic deformation due to bending of the flexible layer as it is bent through the peel angle and then straightened, local to the crack front. These additional energy terms form the basis of the subsequent discussion, with the objective of identifying factors which will dictate the experimental protocol, and influence the magnitude of the results.

Gent and Hamed (1977a,b) observed experimentally that the peel strength increased and then decreased with increasing layer thickness h_t. They suggested that as a thin layer is peeled the energy dissipated during bending would be small, but that more energy would

be dissipated as $\mathbf{h_t}$ increased, resulting in higher peel forces. However as $\mathbf{h_t}$ increased still further the bending stresses would no longer be sufficient to cause plastic deformations, resulting in a reduction in peel strength.

The importance of plastic deformation due to bending of the flexible layer and the resulting energy dissipation is further reinforced if the dependence of $\mathbf{P_c}$ and $\mathbf{G_c}$ on peel angle is considered. Kinloch (1987) concluded that there was much experimental evidence to confirm both the fracture mechanics and stress analysis approaches (Equation 2.20), namely that $\mathbf{P_c}$ was inversely proportional to (1-cosβ), while $\mathbf{G_c}$ was independent of peel angle. However experimental discrepancies to these relationships exist in the literature (e.g. Kinloch *et al.*, 1994), and are again explained by considering the full energy balance including plastic bending of the peel arm. Gent and Hamed (1977b) argued that at high peel angles the contribution from plastic yielding would be relatively high resulting in $\mathbf{P_c}$ values generally larger than expected, while at low peel angles the increased contribution of mode II loading would result in a larger value of $\mathbf{G_c}$.

In order to quantify these additional energy dissipating mechanisms, Kinloch *et al.* (1994) proposed a general scheme to assess the energy dissipated due to local bending of the peeling arm using a model proposed by Kim and Kim (1988), but with the additional feature of root rotation of the peel front. For the adhesive system they considered, Kinloch *et al.* (1994) showed that if their scheme were applied, then the true value of $\mathbf{G_c}$ was indeed independent of β and $\mathbf{h_t}$. The draw back of Kinloch's approach for this application is that they used a bilinear work-hardening material model, which does not accurately represent the PU used in this work.

Intuitively, pure mode I loading when β is 0°, and pure mode II loading when β is 180°, would be expected for the peel test. Anderson *et al.* (1974) suggested that variation of the loading mode ratio from mode I to mode II may have some effect on the measured value of $\mathbf{G_c}$. However, Kinloch *et al.* (1994) made the distinction between the applied peel angle and actual local peel angle at the crack front. They found for a particular test, that while the applied β was varied from 60-150° the measured local β only varied from 25-50 °, and that this small range of local β meant that a mixed mode analysis of the peel test was not necessary. This observation was reinforced by the work of Crocombe and Adams (1981) who found that the amount of mode II loading was ≈30% and essentially independent of peel angle, except when the flexible adherend was incompressible when the value dropped to ≈10%.

Irrespective of loading mode, one of the main criticisms of the peel test geometry is that plane strain (a triaxial stress field) exists in the centre of the specimen whereas plane stress (a biaxial stress field) exists at the edge of the specimen. Since fracture generally occurs more easily in a triaxial stress field the measured value of $\mathbf{G_c}$ will sometimes vary with the ratio of plane stress to plane strain, and hence specimen width.

The value of $\mathbf{G_c}$ is highly dependent on test rate and temperature; the results of Kinloch *et al.* (1994) and Gent and Lai (1994) typified this effect. This reflects the nature of $\mathbf{G_c}$ which is a measure of the energy associated with the fracture process and as such includes viscoelastic energy dissipated locally in the plastic zone ahead of the crack tip. Kinloch (1987) suggested that viscoelastic hysterisis dissipated energy as the material was subjected to a stress strain cycle as the crack approached and then receded. As might be expected, a decrease in temperature or an increase in crack velocity both resulted in an

increase in the measured value of $\mathbf{G_c}$ through an decrease in viscoelastic energy dissipated locally.

A different approach to the analysis of a peeling bond is now discussed, as characterised by the work of Kaelble (1960), who considered the tensile stresses in an adhesive layer supported on a rigid substrate as the flexible adherend is peeled. He assumed linear elasticity and the theory of small bending deformations, and derived an expression which related peel force **F** to peel angle β and stress in the adhesive layer at the peel front σ_p, Equation 2.20, where $\mathbf{k_p}$ depends upon material properties and test geometry.

$$\frac{F}{b_p} = k_p \frac{\sigma_p^2}{(1 - \cos\beta)} \qquad 2.20$$

Although the stresses developed at the peel front would be useful for comparison, for example, with results from stress analyses for compliant layer bearings (*e.g.* Yao *et al.*, 1994), Kaelble's approach is difficult to apply in this application since PU is not a linear elastic material, and no adhesive layer exists since the flexible adherend is bonded directly to the rigid substrate. In addition, Gent and Hamed (1975) argued that the stress analysis approach was only valid for small bending deformations of the peeled strip, and showed that this only held when certain geometric test conditions were met. Niesiolowski and Aubrey (1981) showed that the filaments which sometimes form behind the peel front may also effect the measured peel strength and stress distribution, and proposed modifications to Kaelble's analysis to take account of this feature. Crocombe and Adams (1981) used a large displacement finite element analysis to investigate stresses developed during peeling, but only elastic materials were considered. Importantly, they showed that a small increase in bond strength resulted in a large disproportionate increase in the peel strength.

The peel test is a well researched and understood test, routinely used to assess the adhesion between flexible layers and a rigid backing. It is the test best suited to evaluation of compliant layer adhesion and the factors effecting it. However, special test pieces of a particular geometry were required. From the literature it was clearly important to control all aspects of test geometry, together with test rate and temperature.

2.4.2.2 Blister test.

The blister test, Figure 2.3, consists of a flexible adherend of thickness $\mathbf{h_t}$ bonded to a rigid substrate, except for a circular unbonded area of radius $\mathbf{a_b}$. When the unbonded area is pressurised with a fluid a blister is formed, which maintains the initial radius until a critical pressure $\mathbf{P_{cr}}$ is reached and a crack propagates. The development of the blister test was review by Kinloch (1987), much of which was due to Williams and his co-workers at University of Salt Lake City (*i.e.* Williams, 1969, Anderson *et al.*, 1977). Williams (1969) conducted an analysis of the blister test using a fracture mechanics energy balance approach and developed an expression for the adhesive fracture energy $\mathbf{G_c}$, which can be expressed in its general form (Andrews and Stevenson, 1978) as Equation 2.21.

$$G_c = \frac{P_{cr}^2 . a_b}{E . f\left(h_t / a_b\right)} \qquad 2.21$$

Several solutions exist for $\mathbf{f(h_t/a_b)}$ which were usefully reviewed by Briscoe and Panesar (1991). Two closed form analytical solutions for the displacement of the flexible layer under pressure are available; that of a thin plate at low values of $(\mathbf{h_t/a_b})$, and that of an infinitely thick medium when $(\mathbf{h_t/a_b})>5$. To enable samples with intermediate values of $(\mathbf{h_t/a_b})$ to be tested Bennett *et al.* (1977) used finite element analysis to establish $\mathbf{f(h_t/a_b)}$

for a full range of values, and Chang and Peng (1992) extended this analysis for non-linear elastic materials. In contrast, Andrews and Stevenson (1978) considered the relative contributions of the strain energy due to bending from the 'near field' (stress around the crack tip for the infinitely thick case) and the 'far field' (the energy due to the deflection of the thin plate) to give expressions for $\mathbf{f(h_t/a_b)}$ over a range of $(\mathbf{h_t/a_b})$ values. An approach arguably more applicable to thin elastic membranes with high bond strengths and hence large deformations is that conducted by Gent and Lewandowski (1987) and separately by Briscoe and Panesar (1991), who considered the strain energy due to stretching and proposed different forms of an expression for $\mathbf{G_c}$. Note that Briscoe and Panesar (1991) point out that selection of the most appropriate solution for $\mathbf{f(h_t/a_b)}$ often presents a major source of potential error when conducting blister test experiments. For the preliminary experiments conducted here the results of Bennett *et al.* (1977) were used to determine $\mathbf{f(h_t/a_b)}$.

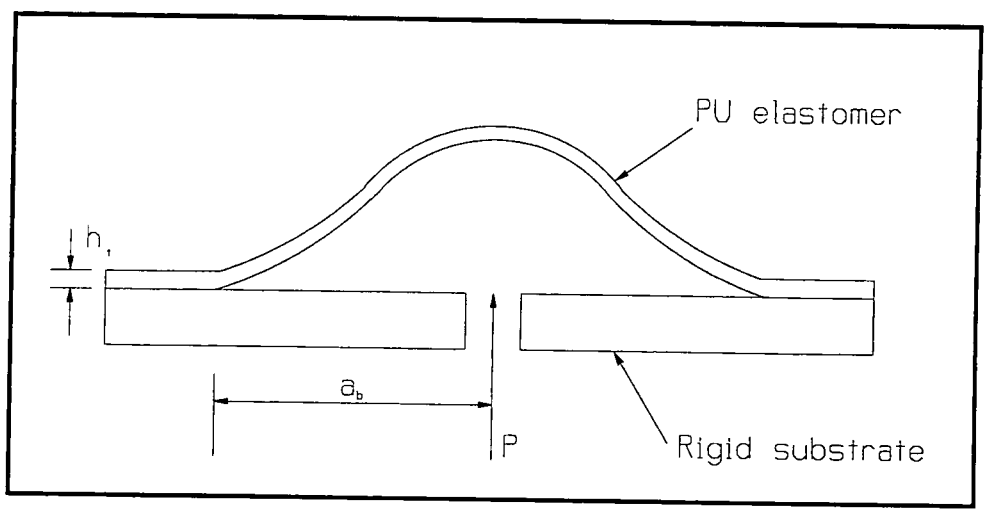

Figure 2.3 Diagram of the blister test arrangment.

There are several advantages offered by the blister test. Since the crack front does not intersect a free surface, the stress field is entirely plane strain, and the axisymmetric geometry of the sample simplifies the theoretical analysis. In addition Anderson *et al.* (1977) suggested that if environmental elements are incorporated in the pressure medium

then their effect on the bond strength could be studied. The major draw back with the test is the formation of an initial debond radius which has a naturally sharp crack. Anderson *et al.* (1977), Briscoe and Panesar (1991), Chu and Durning (1992) and Parry and Wronski (1992) have all observed that $\mathbf{G_c}$, determined from the initial debond area, was significantly higher than that determined if the sample was subsequently retested with the naturally sharp cracked debond area. They all suggested that this was a result of the initially less than naturally sharp crack, and advocated precracking before $\mathbf{G_c}$ measurements were conducted.

Anderson *et al.* (1974) has shown that the measured value of $\mathbf{G_c}$ is not independent of test geometry and cites loading mode changes, from mixed mode I/II loading to predominantly mode I loading as $(\mathbf{h_t/a_b})$ is increased, as an explanation of his findings. Kinloch (1987) suggests that for pure mode I loading $(\mathbf{h_t/a_b})$ must be greater than 4, whereas Anderson seems to suggest a value of $\approx$1. From a theoretical stand point Jensen (1991) confirms Anderson's experimental findings in that his analysis proposes a strong dependence on mode mixity for $\mathbf{G_c}$. However, Briscoe and Panesar (1991) suggest that Anderson's observations may not be a result of loading mode changes, but due to the use of an unsuitable model for the experimental conditions he used.

When conducting the test in its simplest form, $\mathbf{G_c}$ is determined by measuring the critical pressure $\mathbf{P_{cr}}$ and debond radius $\mathbf{a_b}$ (Equation 2.21) at the onset of fast crack propagation. However, Briscoe and Panesar (1991) observed slow crack growth (an increase in $\mathbf{a_b}$) before $\mathbf{P_{cr}}$ was reached. They suggested that difficulty in measuring $\mathbf{a_b}$ and $\mathbf{P_{cr}}$ at the onset of fast crack growth was a possible source of experimental error. In a more sophisticated application of the test, some workers have measured blister geometry with

respect to time during testing. Andrews and Stevenson (1978) used high speed photography to investigate the dependence of G_c on crack velocity, as did Briscoe and Panesar (1991) who also studied the variation of blister height **H** during the test. Chu and Durning (1992) measured **P**, and also a_b and **H** using a video camera, all with respect to time during quasi-steady state crack propagation after initial debonding. They proposed and demonstrated that P^{-3}, a_b^3 and H^3 were linear with time, and that G_c could be found independently from the gradient of any of these three relationships.

G_c is highly dependent on crack velocity, as demonstrated by both Andrews and Stevenson (1978) and Briscoe and Panesar (1991). Andrews discussed evidence for this dependence, and concluded that variations in the viscoelastic energy dissipated locally in the plastic zone ahead of the crack tip was responsible, at least in part, for his experimental observations.

The blister test clearly had some potential, particularly because of its possible application to real engineering components (unlike the peel test). Although no analysis had been conducted on curved surfaces, it could be a useful tool for measurement of layer adhesion in acetabular cups, forming the basis of a quality control test. However the problems of creating a controlled sharp cracked debond area must be over come. Never the less, preliminary investigations were considered worth while.

2.4.3 The adhesion of polyurethane to rigid substrates.

Only limited information regarding the adhesion of polyurethane to rigid substrates is available in the literature. Recently several groups have investigated the adhesion of polyurethane elastomers to metallic substrates. Briscoe and Panesar (1992) reported $\mathbf{G_c}$ values between 18/8 stainless steel and a polyurethane elastomer of <1 kJm^{-2}. Gahde *et al.* (1992) discussed a number surface treatment methods for improving the bond between PU and an unalloyed steel, and observed maximum shear strength values of 30 MPa, but did not report $\mathbf{G_c}$ values. Morris and Shanahan (1994) assessed the bond between PU and sintered stainless steel, and reported that interpenetration of the polymer into the porous metal matrix increased $\mathbf{G_c}$ through improved mechanical interlocking, although absolute values were not given.

PU has also been bonded to other polymers. Sanchez-Adsuar *et al.* (1994) examined the adhesion of solvent based thermoplastic PU to synthetic rubber and found that the ratio of hard/soft segments affected adhesion strength. They suggested that this was due to an adsorption bonding mechanism, through polar interactions between the rubber and polyester and/or urethane groups. T-peel strengths of <5 kNm^{-1}, but not $\mathbf{G_c}$ values, were reported.

Chapter 3. Materials and Methods.

3.0 Introduction.

Both fluid film lubrication and good adhesion of the low modulus elastomeric layer are fundamental to the successful performance of compliant layer prostheses. Hence, the effects of bearing design and manufacturing route on these two properties was evaluated, with the aim of improving the understanding of the factors which govern them. Three types of samples were manufactured; acetabular cups, tibial components, and peel test samples. The lubrication regime was investigated using the Durham friction simulator, and the adhesion between the layer and different backing materials was determined using both peel and blister tests. The surface topography was evaluated using a non contacting optical profiler. The materials and methods used for preparation of samples, and the experimental protocol used to evaluate them are discussed here.

3.1 Materials.

Several groups (Murakami *et al.*, 1993, Unsworth *et al.*, 1981) conducted their early work using metal backed silicone rubber bearings, since the bearings were easily moulded in the laboratory. Medical grade thermoplastic PU was first used to make prototype acetabular cups by Unsworth *et al.* (1987, 1988), who noted that it could be manufactured with a range of compliance, by varying the ratios of the hard to soft segments, and that it potentially had suitable biostability and structural properties. The polymer was heated to

its melting point in a metal backed cup and the bearing surface was formed around a hemispherical pin. The layer was held in place for the duration of short term friction tests by four PU lugs in the metal cup. Blamey *et al.* (1993) used a similar method of manufacturing acetabular cups, but noted that the design was still not suitable for *in vivo* use. They proposed and demonstrated a good mechanical interlock between a UHMWPE backing and PU compliant layer by using a multi-step compression moulding manufacturing route. Auger *et al.* (1993a,1993b) also used PU, but favoured polyethersulphone as the hard backing material. They solvent-cast a thin PU layer on to the surface of the polyethersulphone, and subsequently injection moulded the PU layer. This resulted in a well bonded layer of the required thickness. However, none of these manufacturing routes or backing material combinations offered a product which had the potential to perform for several decades *in vivo* without failure of the interface.

Two approaches have been used in this study. Initially UHMWPE was considered as the backing material, incorporating a surface enhancing treatment which would improve the adhesion of an injection moulded PU layer. Subsequently, PU was proposed as both the backing and bearing material. A high modulus medical grade thermoplastic PU was specified for the backing material and a lower modulus PU of the same type for the compliant layer. The PU/PU design could be manufactured by a two stage injection moulding route, and an improved bond between the two was expected.

3.1.1 Choice of medical grade polyurethane.

Based on an understanding of PU technology (discussed in Section 2.3) an informed choice had to be made regarding which of the commercially available medical grade PUs

would be most suitable for this application. The PUs considered during this study are given in Table 3.1.

Material	Nominal Shore Hardness	Urethane Type	Monomers	Manufacturer.
Pellathane 2363	80A	Aromatic Polyether urethane	MDI PTMEG BDO	Dow Chemicals MI, USA
Tecoflex	80A, 93A	Aliphatic Polyether urethane	HMDI PTMEG BDO	Thermedics Inc. MA, USA
Tecothane	80A, 93A, 75D	Aromatic Polyether urethane	MDI PTMEG BDO	Thermedics Inc. MA, USA
Corethane	80A, 75D	Aromatic Polycarbonate urethane	MDI PHECD BDO	Corvita Corp. FL, USA
Chronoflex AL	80A	Aliphatic Polycarbonate urethane	HMDI PC BDO	PolyMedica Ind. MA. USA.
CSIRO	85A	Aromatic Polyether urethane	MDI PnMEG BDO	CSIRO, Victoria, Australia.

Table 3.1. Classification of polyurethane used during this study. Monomers: **Diisocyanates**; MDI: 4,4 diphenyl methane diisocyanate, HMDI: Hydrogenated MDI. **Macrodiols**; PTMEG: Poly-tetramethylene ether glycol, PHECD: poly-1,6-hexyl 1,2-ethyl carbonate diol. PC: Proprietary polycarbonate macrodiol, PnMEG: longer chain PTMEG. **Chain extenders**; BDO: 1,4 butanediol.

The materials based on PTMEG soft segments represent old polyether urethane technology, and they are known to degrade in the body. The polymers which use either different macrodiols (i.e. Corethane and ChronoFlex) or more hydrophilic PTMEG (i.e.

CSIRO) represent new technology, and a potential improvement in biostability. Although all the above were considered, Corethane 75D and 80A were selected as the preferred materials for the backing and compliant layer respectively, mainly as a result of impressive results from early biocompatibility tests (subsequently published by Pinchuk, 1994). However, although Corethane was used predominantly, all the PUs in Table 3.1 were used occasionally, either to investigate the effect of modulus on lubrication or to assess their effect on layer adhesion.

3.1.2 The UHMWPE / PU concept.

The orthopaedic community has much experience of UHMWPE. The advantage of using UHMWPE backed compliant layer prostheses was that they could easily be incorporated in to existing designs *i.e.* snap fit metal backed tibial or acetabular components. In order to assess the bond integrity, UHMWPE / PU peel test samples were manufactured. UHMWPE blocks 100×20×8 mm were machined and cleaned in refluxing/boiling cyclohexane for 30 minutes and then refluxing/boiling ethanol for a further 30 minutes. The surface was then characterised and surface treatment conducted in the Interdisciplinary Research Centre in Polymer Science and Technology (University of Durham). The blocks were then shipped to Howmedica (Limerick, Eire) for injection moulding. The UHMWPE blocks were heated to 120 °C for between 15 - 75 minutes before moulding to ensure the mobility of any grafting agent present. Each block was placed in the cavity of a mould and a PU layer 150×20×3 mm was injection moulded on to the surface. The moulding conditions were varied depending upon the polymer being moulded. No UHMWPE / PU acetabular or tibial components were manufactured.

3.1.3 The PU / PU concept.

The potential advantage of using an all PU compliant bearing was an improvement in bond integrity between the soft layer and hard backing. In order to assess the bond integrity PU / PU peel test samples (Figure 3.1) were manufactured. High modulus PU blocks 100×20×8 mm were initially injection moulded. These were then ejected from the mould and allowed to cool. Subsequently, these blocks were replaced into the cavity of the mould and a low modulus PU layer 150×20×3 mm was injection moulded on to the surface. The manufacturing process is shown schematically in Figure 3.2

Acetabular cups (Figure 3.3) were made in much the same way. Initially a high modulus PU shell was injection moulded. The internal shell diameter was equal to the femoral head diameter plus twice the layer thickness and any clearance, and was formed around a removable core. The shell was ejected from the mould, allowed to cool, and a hole was then drilled in its pole. The shell was then replaced in the cavity of the mould, and the initial core replaced with one of diameter equal to the femoral head diameter plus the required clearance. The low modulus PU was then injection moulded through the hole in the shell to form the compliant lining. The acetabular cup manufacturing process is shown schematically in Figure 3.4.

Realistic tibial components are complex in shape, and hence tooling development costs were high. Therefore, to manufacture a pre-prototype tibial component for initial evaluation and to establish test protocols, existing tooling was used. When conducting a knee replacement procedure a surgeon will commonly use trial tibial bearings in order to establish the component thickness to give the required tension in the ligaments. After slight modification, a trial mould was found to be suitable. Due to moulding difficulties,

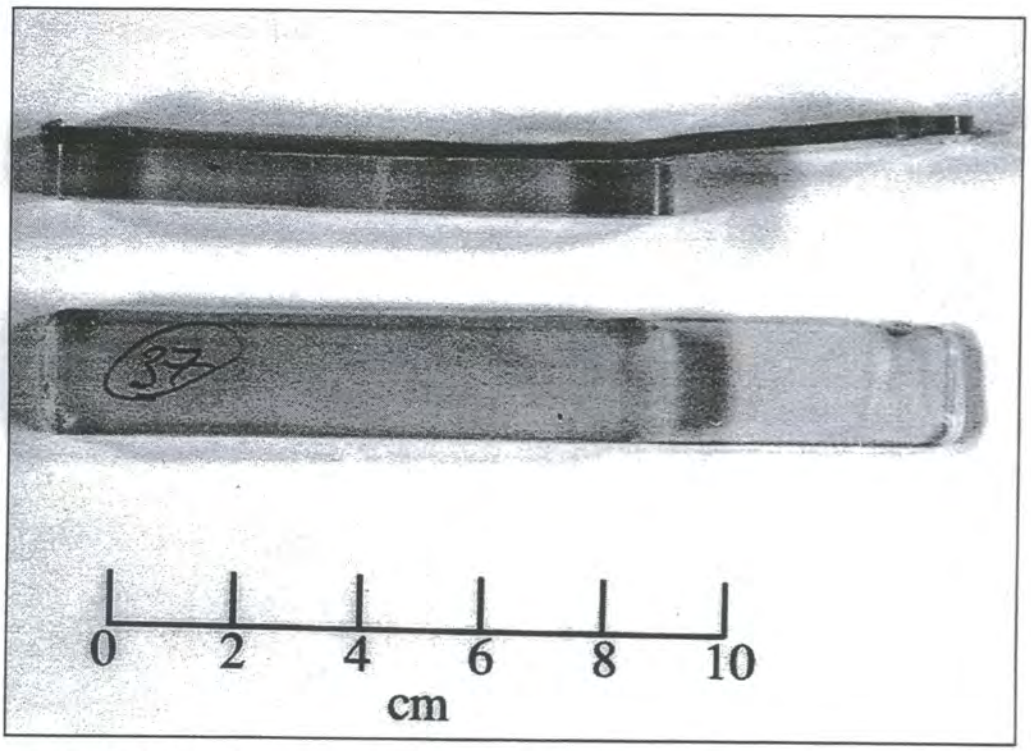

Figure 3.1 PU / PU peel test sample, for layer adhesion evaluation.

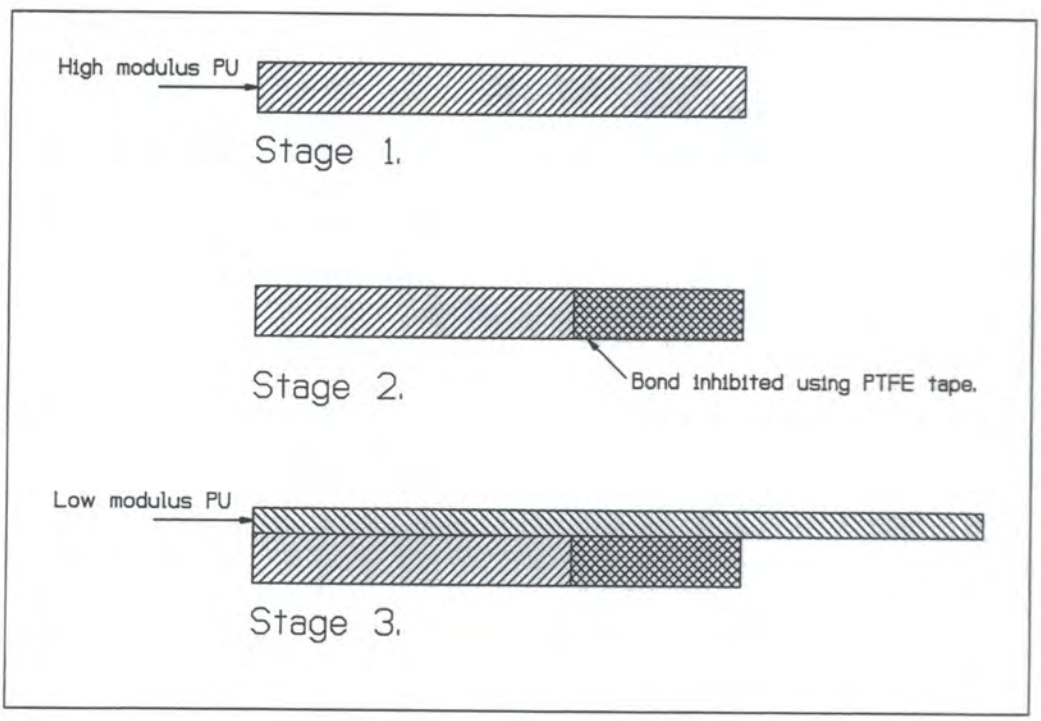

Figure 3.2 The injection moulding route for PU/PU peel test samples. Initially the high modulus PU backing is made. The lower modulus PU is then moulded on to the surface.

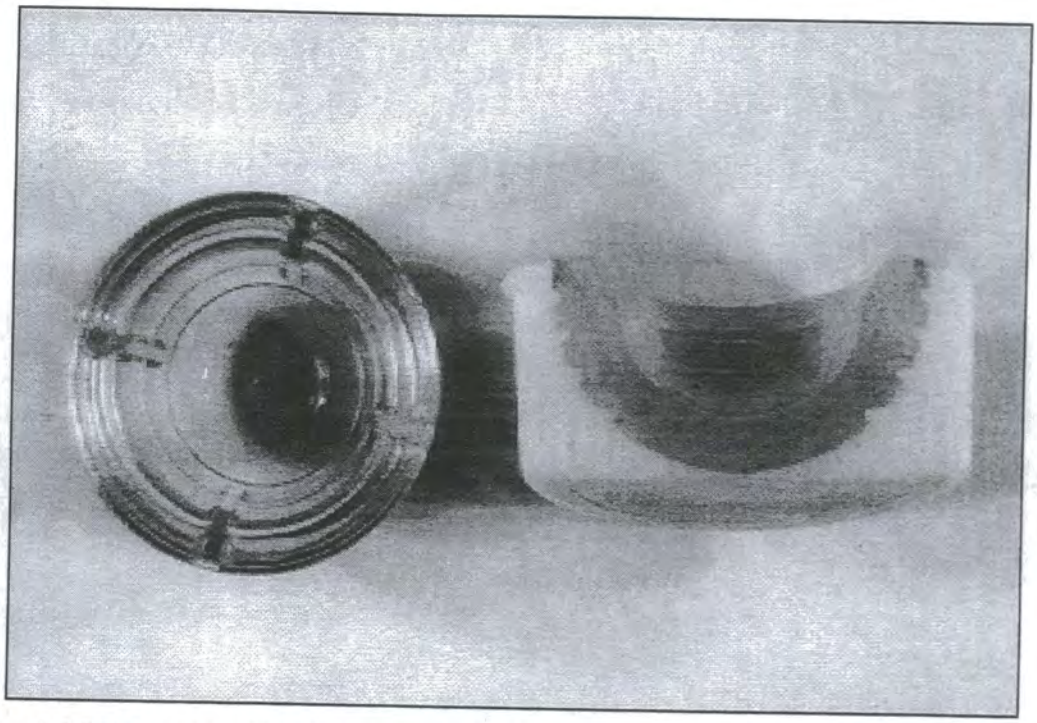

Figure 3.3 PU/PU compliant bearing acetabular cups.

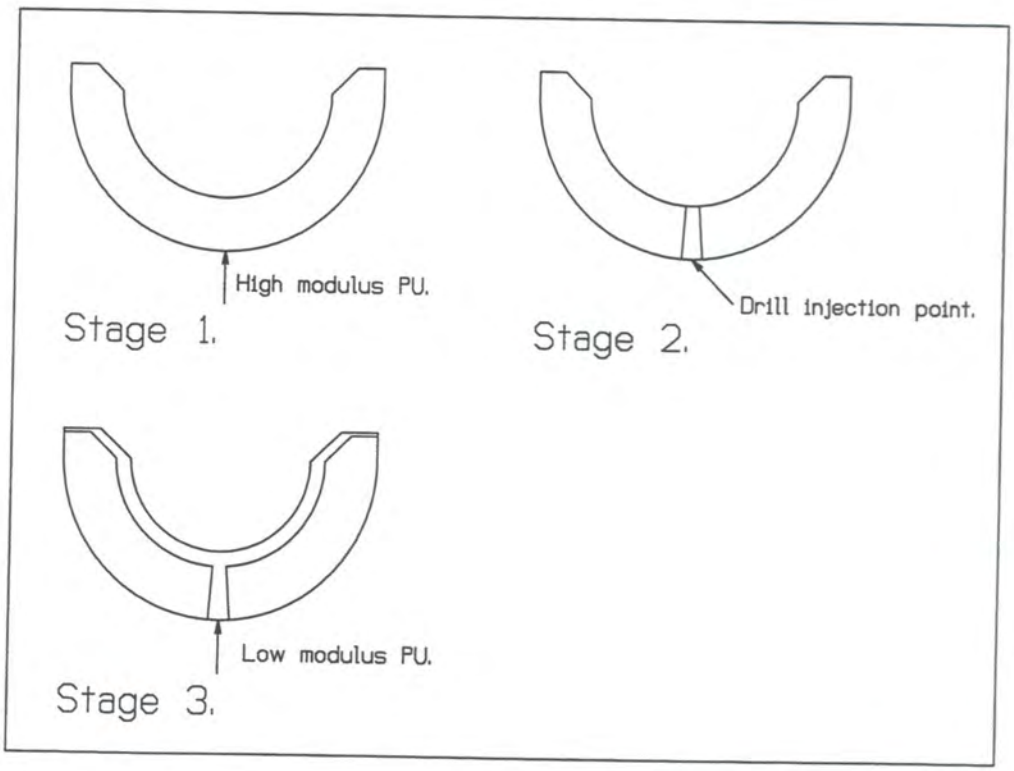

Figure 3.4 The injection moulding route for PU / PU acetabular cups. Initially a high modulus PU shell is moulded. A hole is drilled in the pole, and a low modulus compliant layer is moulded through it.

the high modulus PU was replaced with acrylic in the initial pre-prototypes. Tibial bearings were made in much the same way as acetabular cups and peel test specimens, with 2 or 3 mm thick PU layers (Figure 3.5).

This two part injection moulding process to manufacture peel test samples, acetabular cups and tibial components was conducted by Howmedica (Limerick, Eire), and hence the tooling and process development are not considered here.

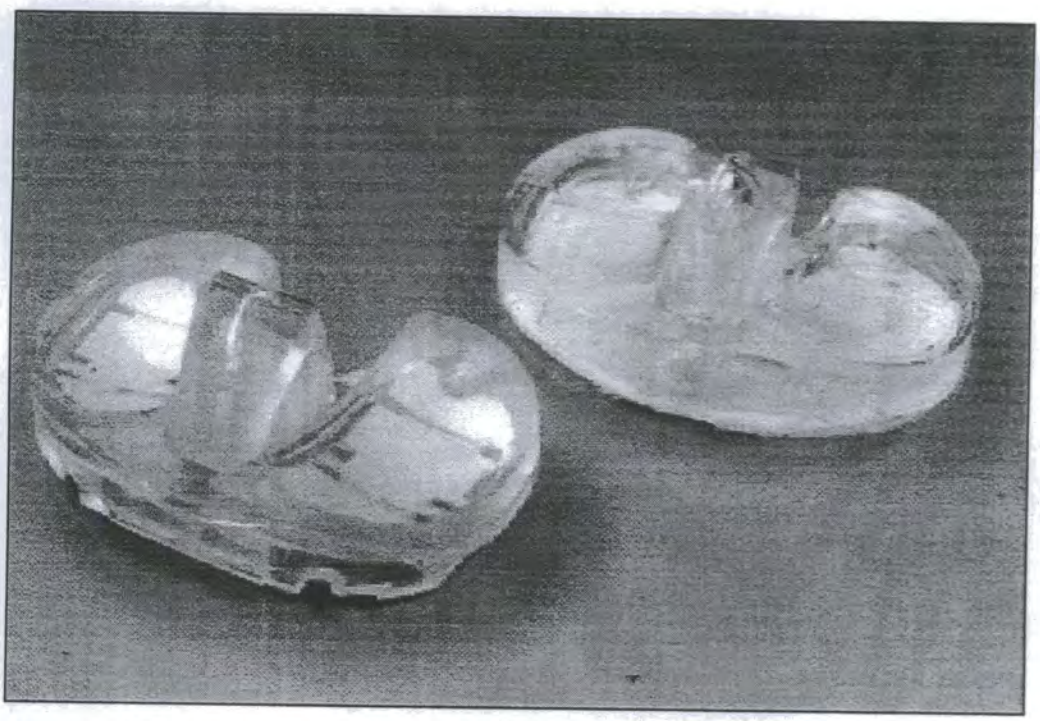

Figure 3.5 Pre-prototype acrylic / PU tibial compliant bearings.

3.2 Friction measurement.

It was clear from a review of the literature that compliant layer bearings would only give longer joint implant times if they were carefully designed to promote fluid film lubrication. Experimental verification of the design was important since the existing theoretical analyses are still largely unproven. Pioneering work on the tribology of natural and artificial joints was conducted using friction measuring joint simulators, and in much the same way, the compliant bearings have been assessed and the design refined. All the experimental work presented here was conducted on the second Durham Friction Simulator.

3.2.1 Apparatus.

The second Durham Friction Simulator was commissioned by Blamey (1993), and has subsequently been refined as part of this study (Hall *et al.*, 1994). It is similar to the Leeds friction simulator which was described by O'Kelly *et al.* (1977) and updated by Auger *et al.* (1990), and to the original Durham friction simulator described by Unsworth *et al.* (1981, 1987 and 1988). The simulator was described in detail by Blamey (1993), and so only a brief description and details of the modifications will be given here. The apparatus, shown in Figure 3.6, consisted of three main systems, one applied the joint load, another provided the extension-flexion motion, and a third measured the frictional torque. The test joint was mounted with its centre of rotation co-incident with the centre of rotation of the simulator. The femoral component was mounted uppermost, i.e. hips were anatomically inverted, whereas knees were placed in the anatomically correct position, Figures 3.7 and 3.8.

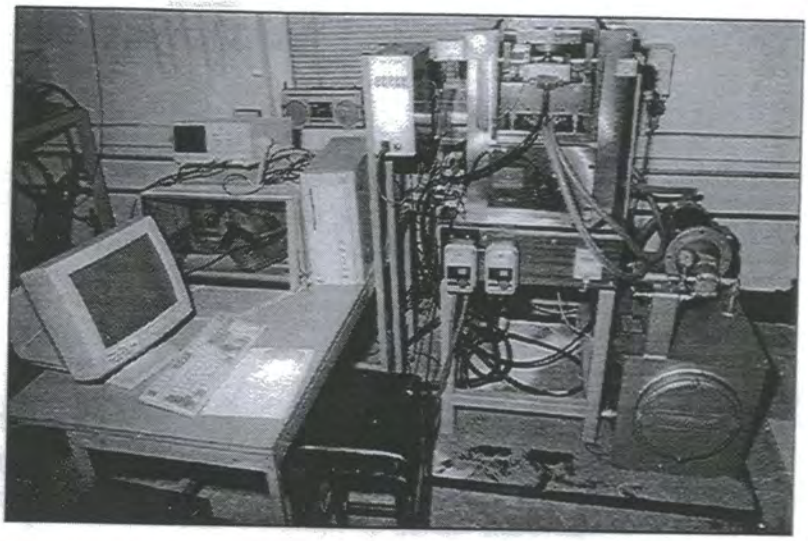

Figure 3.6 The second Durham Friction Simulator.

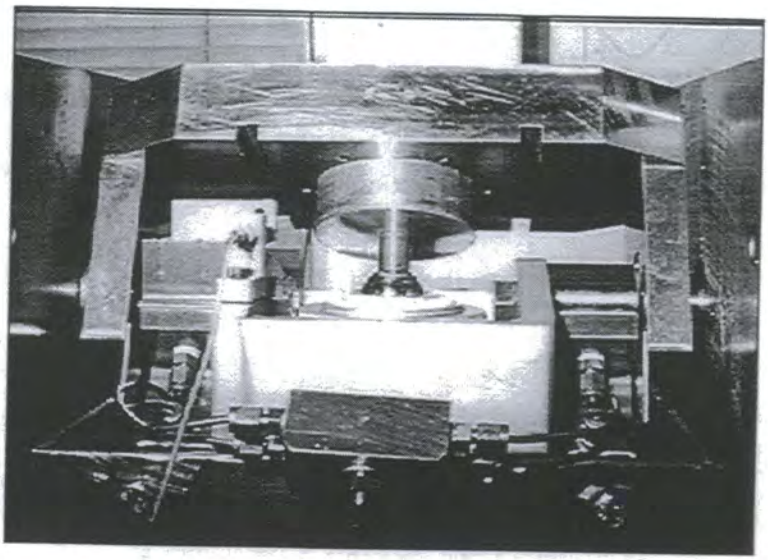

Figure 3.7 A view of the friction carriage in the hip mode.

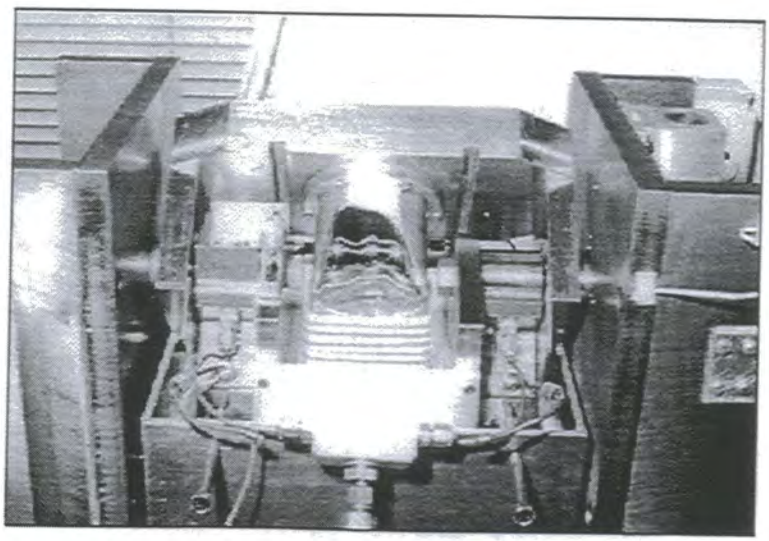

Figure 3.8 A view of the friction carriage in the knee mode.

3.2.1.1 Load system.

The load was applied by a servo-hydraulic system, using four miniature load cells to measure the applied load, and to provide closed loop feedback control. Blamey (1993) designed the apparatus using a proportional valve to control fluid flow to the hydraulic cylinder. This was to save on capital cost and power. In addition, he used two strain gauged support bars as the load transducer. However, the electrical noise resulting from the modulation of the proportional valve control current caused noise problems in the strain gauge bridge. The strain gauge bridge also exhibited non linearity and hysteresis, resulting in unsatisfactory control of the system. In contrast, the updated system incorporating a servo valve and load cells provided excellent control and load measurement characteristics.

All the experiments reported here used a simple load profile comprising a low load swing phase and a higher load stance phase. This was done in order to promote constant conditions over which any lubricating regime may stabilise. Both Unsworth *et al.* (1987, 1988) and Auger *et al.* (1990, 1993a and 1993b) used a similar simplified profile. Figure 3.9 compares this with the normalised results presented by Paul (1967), who used force plate data and a biomechanical model to predict joint reaction forces in the natural hip, and Seireg and Arvikar (1975) who conducted a similar analysis for the knee joint. The magnitude of the peak loads of a normal healthy person reported in the literature vary considerably, with Paul (1967) reporting 3.9×body weight (*BW*) for the hip joint, Morrison (1970) reporting 4.0×*BW* for the knee joint, and Seireg and Arvikar (1975) reporting 5.4 and 7.1×*BW* for hips and knees respectively. In practise, the maximum loads applied by recipients of TJR's will also vary. Older less active patients will tend to

apply lower loads than the peak loads reported in the literature. During the experiments reported here, peak loads of nominally 2 kN or 2.7×*BW* have been applied.

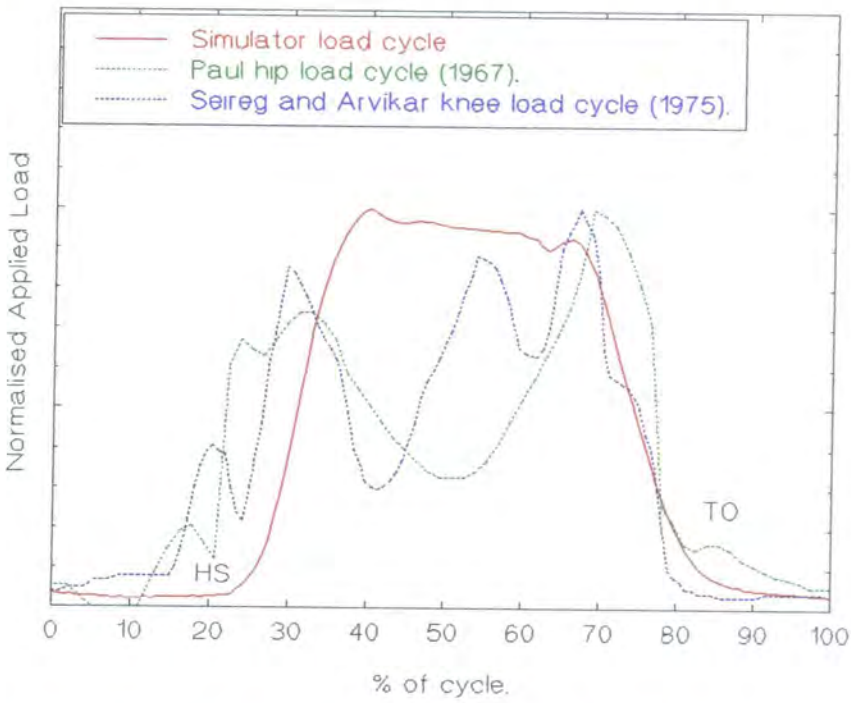

Figure 3.9 Load performance of the second Durham friction simulator, compared with the natural healthy hip and knee.

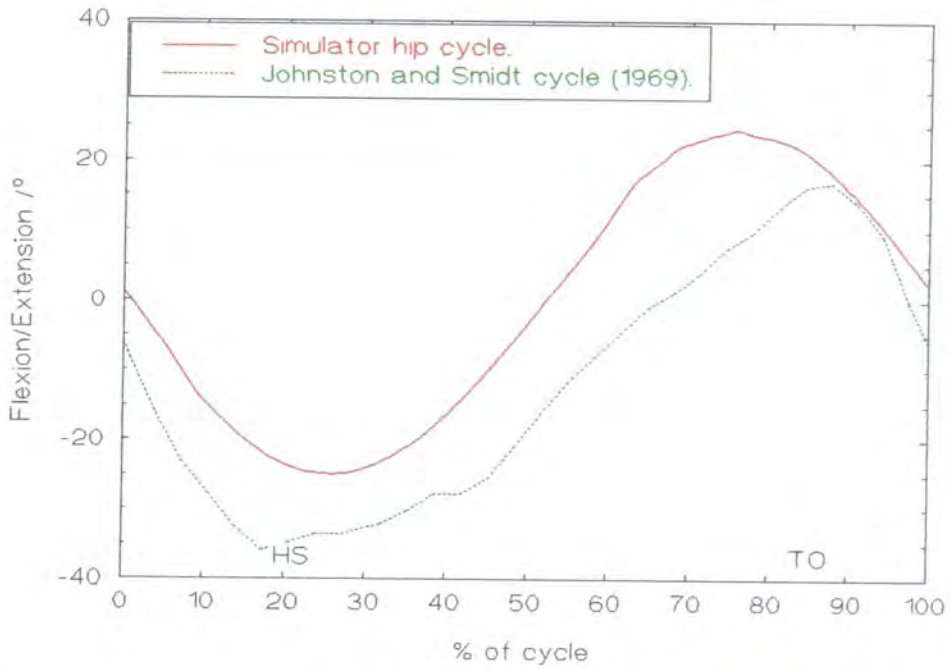

Figure 3.10. Motion performance of the second Durham friction simulator, compared with the natural healthy hip.

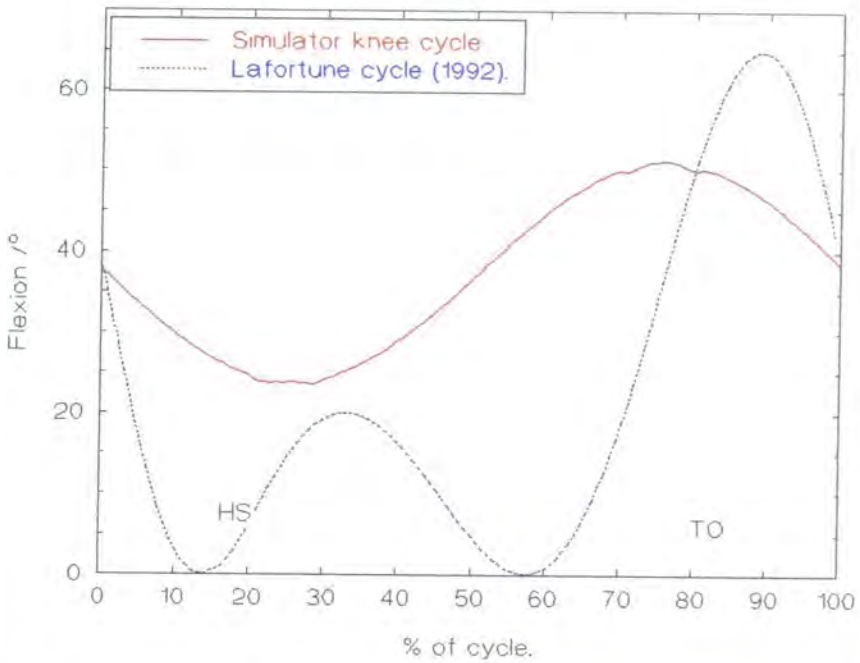

Figure 3.11. Motion performance of the second Durham friction simulator, compared with the natural healthy knee.

3.2.1.2 Motion system.

In order to measure friction directly, only motion in the sagittal plane was applied. An electric motor drove a rack and pinion through a scotch yoke mechanism, resulting in approximately sinusoidal motion of the femoral component, with a frequency of 0.8 Hz. The amplitude of oscillation was set by adjusting the scotch yoke. In an additional modification to Blamey's design, the angular offset was fixed by adjustment of the rack length. For the experiments on hip joints, ±24° motion was used, with no angular offset from vertical. For knee joints, ±14° motion was used, with 36° angular offset from vertical. The applied motion compares well with flexion extension motion for the normal hip (Johnston and Smidt, 1969) Figure 3.10, but is a poor approximation of that for the knee (Lafortune *et al.*, 1992) Figure 3.11. Although detailed simulation of physiological loads and motions was not achieved, since motion synchronised with a dynamic load are the main components of physiological gait, it was assumed that the basic lubrication mechanisms will be very similar to those occurring under physiological conditions.

3.2.1.3 Friction system.

Friction was measured directly using a method first used by Unsworth *et al.* (1974). The acetabular or tibial component was mounted on a carriage supported on two hydrostatic journal bearings, which allowed rotation in the sagittal plane. The articulation of the femoral component resulted in a frictional torque which tended to rotate the carriage. The carriage was restrained by a piezoelectric quartz force transducer, which measured frictional force directly. An analysis of the hydrostatic bearing operation (Appendix A) showed that the coefficient of friction of these bearings was several orders of magnitude less than 0.01, the coefficient of friction typical of compliant bearing prosthesis. The friction carriage and hydrostatic journal bearings assembly was mounted on two low friction linear hydrostatic bearings, which allowed small anterior-posterior translations resulting from small mounting misalignments of the test prosthesis.

3.2.1.4 Instrumentation and control.

The simulator was controlled using a 68020 microprocessor (Motorola), schematically shown in Figure 3.12. An incremental encoder (Holmer), driven by the motion system, provided a clock pulse which synchronised the motion with the servo-hydraulically controlled load and the measurement systems. The cycle was divided into 128 pulses. On each clock pulse, the digital to analogue converter (DAC) was updated with the correct load profile signal, and the three analogue to digital converters (ADC's) were read and the results written to a file. The three ADC's were connected to the load, position and friction transducers. The applied load was measured by miniature load cells (Model 13E, RDP) situated under the four corners of the linear hydrostatic bearings. The angular position was measured using a rotary potentiometer. The frictional torque was measured using a piezoelectric force transducer (9203, Kistler) and charge amplifier (5039A, Kistler). All

68020 control software was written by members of the Microprocessor Centre (University of Durham).

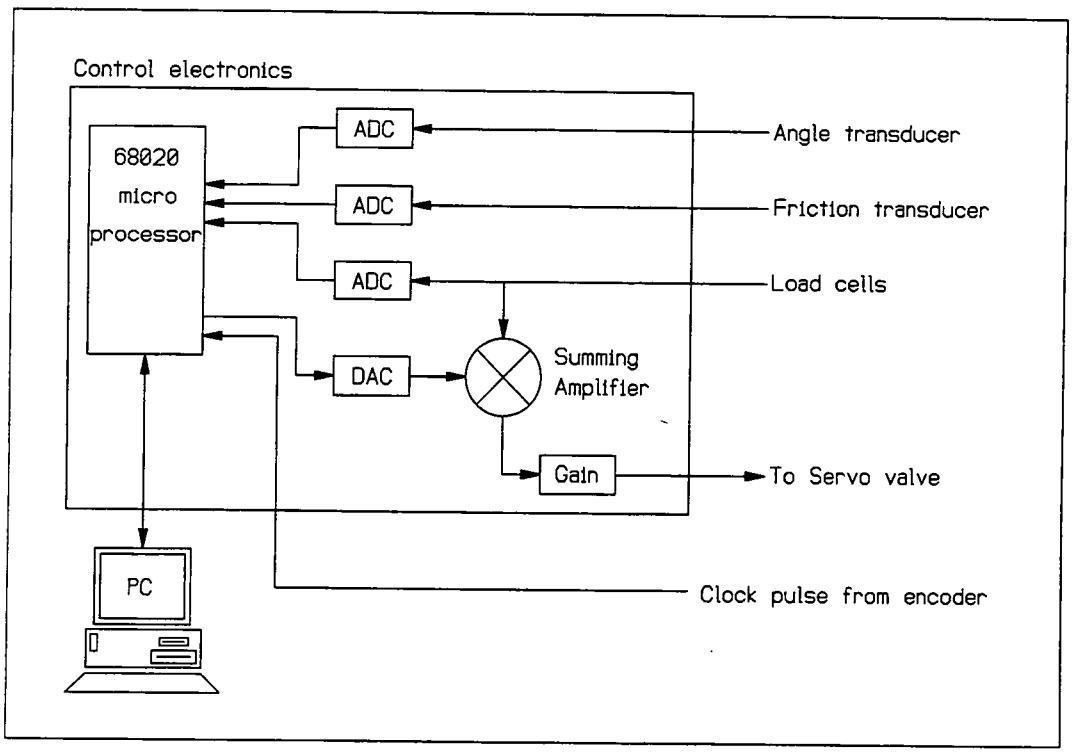

Figure 3.12 Schematic representation of the control microprocessor and electronics, and PC for data capture.

3.2.1.5 Calibration and error analysis.

To ensure correct and reliable operation of the simulator, the measurement transducers were calibrated approximately every two months. The ADC digital output results were converted to real physical units by applying calibration coefficients of the general form

$$\textit{Physical units} = \boldsymbol{m} \times \textit{digital units} + \boldsymbol{c}$$

The load DAC and ADC were calibrated against an external load cell, the position ADC against an angular spirit level, and the friction ADC against a known applied torque. The resolution of the measuring systems were 3.3 N/bit, 0.03 °/bit and 1.8 Nmm/bit for the load, angle and friction ADC's respectively.

A detailed assessment of the precision of the simulator is given in Appendix B. For the case of an applied load of 2 kN, a femoral head of radius 16 mm and friction factor values of 0.1, 0.01 and 0.001, the maximum error in the friction factor result was estimated to be 4.5%, 12% and 98% respectively. Although this was an estimate of the *maximum* error, the results were indicative of the trend in relative precision of the machine. For friction factors between 0.1 to 0.01 (the range of conventional joints) the experiment had an acceptable relative precision, better than ≈10%. However, for friction factor values below 0.01 (typical of compliant bearing joints) the relative precision decreased drastically, and although the simulator demonstrated low friction factor values, these results indicated that discerning trends in this region would be difficult.

3.2.2 Experimental Protocol.

Both Auger *et al.* (1993b) and Saikko (1992) discussed the importance of eliminating frictional torque errors due to misalignment of the components within in the apparatus. An experimental protocol has been developed which both minimised the physical misalignment of the components when mounting them in the apparatus, and eliminated the effect of any remaining misalignment torque through a new experimental procedure.

3.2.2.1 Elimination of misalignment errors: Hip joint mode.

For correct operation of the simulator several sets of centres had to be aligned. Firstly, the centre of the femoral head had to be aligned with the centre of rotation of the motion mechanism. Secondly, the centre of the acetabular cup had to be aligned with the centre of rotation of the journal hydrostatic bearings. Finally, these two sets of centres had to be co-incident. Misalignments of only 0.15 mm would result in a torque of the same order of magnitude as the true frictional torque developed in compliant bearing joints.

If the stem on which the femoral head was mounted was too long or too short its centre would move relative to the apparatus. This motion could be measured using a dial gauge, and by adjusting the stem length this motion could be minimised. As a result, the femoral head could be mounted to within ±0.05 mm of the centre of rotation of the pendulum. Any remaining slight motion of the head centre was accommodated by fore-aft motion of the linear hydrostatic bearings. To minimise misalignment of the acetabular component, a jig was used when mounting the cup, Figure 3.13. The jig was adjusted so as to hold the acetabular cup in position in the mounting medium, so that its centre was aligned with the centre of rotation of the hydrostatic journal bearing. The two sets of centres (femoral head/motion mechanism and acetabular cup/journal bearings) were aligned by fore-aft motion of the linear hydrostatic bearing, which could be checked for alignment by passing a straight 5 mm diameter mandrel through holes machined through the centres of the motion mechanism and hydrostatic journal bearing.

Misalignment of the centre of the acetabular cup with respect to the hydrostatic journal bearings was not accommodated by the system, and yet such misalignment would result in an offset force and a torque acting on the friction carriage as a load was applied. However carefully the cup was mounted, small misalignments up to 0.25 mm were considered likely, resulting in a torque applied to the friction carriage potentially larger than the frictional torque being measured. This was observed experimentally, as in certain cases cups were seen to rotate counter to the direction to the applied frictional torque, since the torque resulting from misalignment was larger in magnitude and acting in the opposite direction. In order to eliminate this misalignment torque a new experimental procedure was required.

Elimination of misalignment torque was achieved by measuring the frictional torque with the stance phase applied first during clockwise rotation, and then during counter-clockwise rotation. These two tests were referred to as forward loading and reverse loading, and are illustrated in Figure 3.14. It was assumed that the true frictional torque **T** would be the same magnitude but opposite in sign during forward and reverse loading. Also, that the misalignment torque $\mathbf{T_e}$ would have the same magnitude and sign irrespective of loading direction. Thus the torque measured during the forward and reverse loading directions $\mathbf{T_f}$ and $\mathbf{T_r}$ would be the sum of the frictional torque and the misalignment.

$$T_f = T_e + T \qquad 3.1$$

$$T_r = T_e - T \qquad 3.2$$

Subtracting 3.2 from 3.1 and rearranging

$$T=(T_f - T_r)/2 \qquad 3.3$$

Thus to determine the true frictional torque both a forward and reverse loading test were conducted, and the results combined to give the true frictional torque, Equation 3.3.

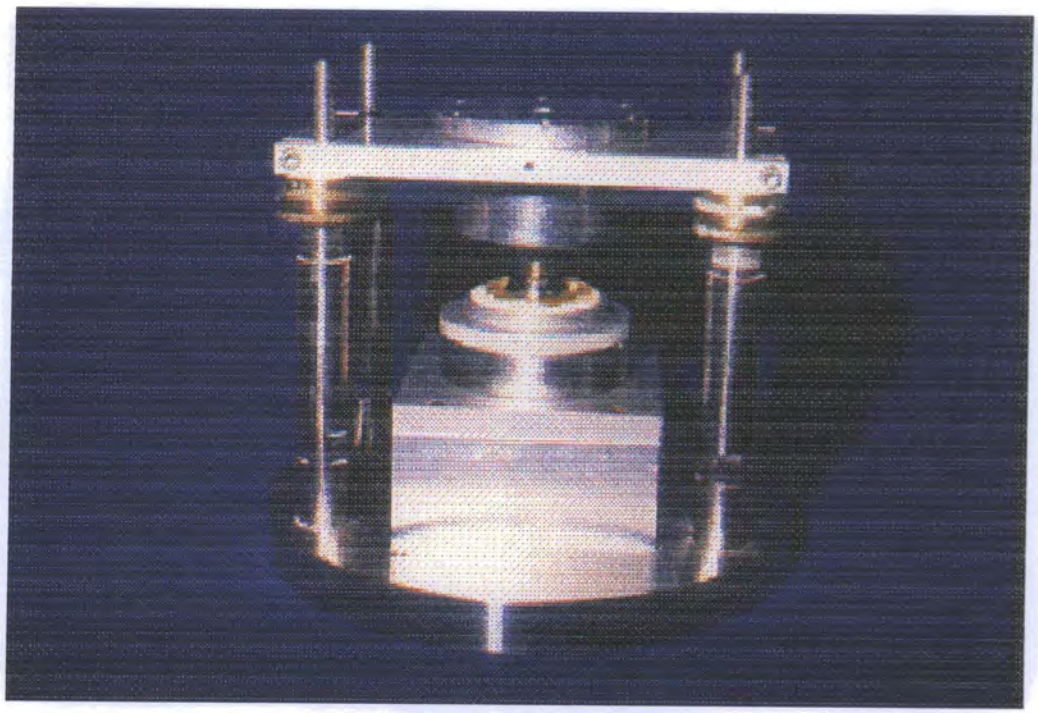

Figure 3.13 Acetabular cup centralising and mounting rig.

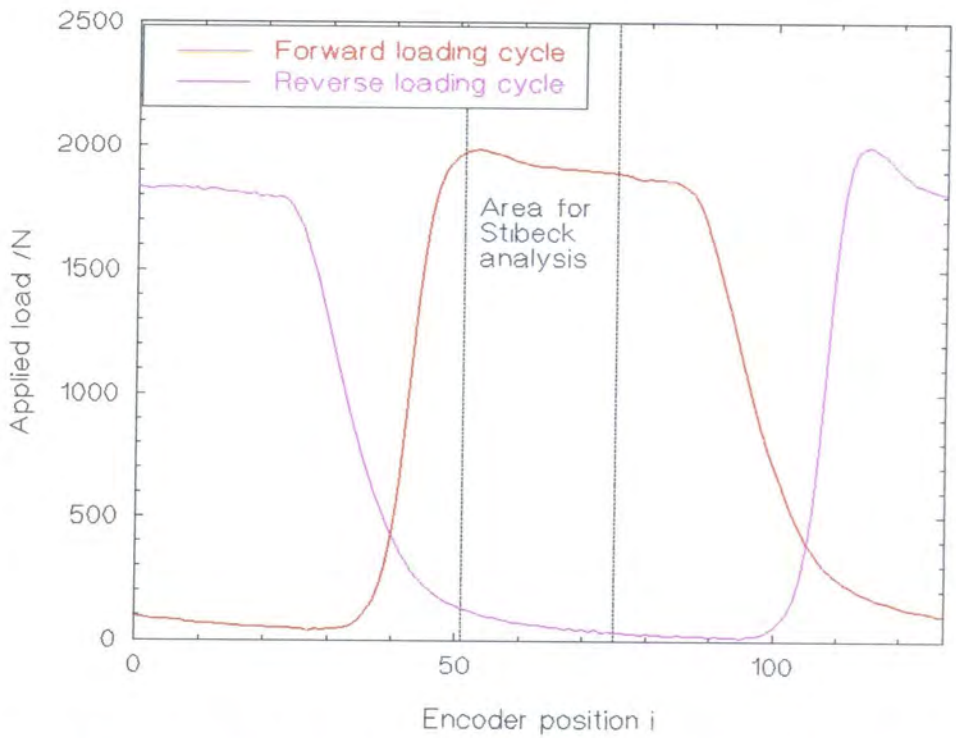

Figure 3.14 Forward and reverse loading cycles, which are similar but out of phase by 64 encoder pulses. Stribeck analysis is conducted at i=51, 57, 63, 69, and 75, in the area indicated.

3.2.2.2 Elimination of misalignment errors: Knee joint mode.

The friction in prosthetic knee joints has been measured for the first time here, however there were some limitations in the model used. A knee joint is considerably less conforming than a hip joint, and so the anterior-posterior hydrostatic bearings were disabled to avoid excessive fore-aft motion. Since no anterior-posterior translation was possible, the contact area was fixed at one position on the tibial component. This is contrary to the situation found when the joints are implanted (see Chapter 6). The prosthetic knee joint has a variable centre of rotation, unlike the simulator which had a fixed centre of rotation. Hence, in order to minimise anterior-posterior translation of the loaded contact across the surface of the tibial component, the femoral component was mounted with the centre of rotation of the posterior condyles aligned with the centre of rotation of the motion mechanism. In order to avoid fouling of the femoral mount an amplitude of only ±14° was used.

Similar arguments to those applied when testing hips were applied to minimise misalignment errors when conducting the experiment with knees. However, due to the changed geometry certain differences existed. Once the femoral component was mounted no adjustment to align its centre of rotation with that of the motion mechanism was possible, and an uncorrectable misalignment error of ±0.2 mm was measured using a dial gauge. A deeper friction carriage was designed to accommodate the larger radii of the posterior condyles. Although the linear hydrostatic bearings were disabled, anterior-posterior alignment was still critical, and so four bolts were added to the loading stage which allowed accurate positioning of the carriage to minimise misalignment torques. Forward and reverse loading tests were conducted and analysed in a similar manner to the hip experiments.

3.2.2.3 Test protocol

A test protocol has been developed which reflects the need to eliminate misalignment errors. The components were carefully mounted and a forward and reverse loading test conducted. In addition, it was considered important to clean the components under test thoroughly since small third body debris would disrupt the expected thin lubricating film. An outline of the test protocol is given in Table 3.2.

1. Check alignment of femoral component.
2. Mount acetabular component in bone cement, using correctly adjusted jig.
3. Align scratches (if any) with direction of motion.
4. Warm up the simulator by conducting a 400 cycle test.
5. Clean metallic and UHMWPE components with acetone, and polyurethane components with water or soap solution. Dry using a soft lint free cloth.
6. Select (in software) the required minimum and maximum loads (normally 50N and 2000N), a forward or reverse loading profile, and the cycles required to be recorded (normally the 1^{st}, 21^{st} and 41^{st}). The joint ID and lubricant viscosity are also noted.
7. Conduct a 'forward loading' test.
8. Conduct a 'reverse loading' test.
9. Repeat 5 to 8 for the required ranges of lubricant viscosity, cleaning thoroughly when changing lubricants, and using a random order of lubricants. Discard the first result of each run.
10. On completion of the required tests, process the results.

Table 3.2 Outline of the experimental protocol used during simulator experiments.

3.2.2.4 The results.

Having conducted a set of experiments the results were processed. The overall objective was to conduct a Stribeck analysis of the results, which required the friction factor and Sommerfeld number to be evaluated. During the nominated cycles of interest, at each

encoder position **i**, the applied load $\mathbf{L_i}$, resulting frictional torque $\mathbf{T_i}$, and angle of the pendulum $\mathbf{A_i}$ were recorded in digital form. These were then converted to real physical units using the calibration coefficients. To enable the forward and reverse loading results to be combined as outlined in Equation 3.3, the phase discrepancy between the forward and reverse loading had to be accommodated. For each of the 128 points in each cycle recorded, the mean load $\mathbf{L_i}$ and angle $\mathbf{A_i}$ were given by Equations 3.4 and 3.5. The true frictional torque $\mathbf{T_i}$ was given by Equation 3.6. Position **i** in the forward loading test was equivalent to position **i+64** during the reverse loading cycle.

$$L_i = \frac{L_{fi} + L_{r(i+64)}}{2} \qquad 3.4$$

$$A_i = \frac{A_{fi} + A_{r(i+64)}}{2} \qquad 3.5$$

$$T_i = \frac{\left|T_{fi} - T_{r(i+64)}\right|}{2} \qquad 3.6$$

Throughout the results presented here the coefficient of friction is approximated by the friction factor **f**, a quantity defined by Unsworth (1978). The case of a femoral head articulating in an acetabular socket was discussed by Gore *et al.* (1981) who pointed out that since the pressure distribution of the normal load is unknown, the true coefficient of friction cannot be determined. Friction factor is used by most authors, even though they may refer to the quantity as the coefficient of friction. The friction factor approaches the coefficient of friction as the loading regime becomes a point contact in the pole of the cup. The friction factor at each point in the cycle $\mathbf{f_i}$ is given by Equation 3.7.

$$f_i = \frac{T_i}{R_1 L_i} \qquad 3.7$$

The simple harmonic flexion-extension motion was driven with a frequency υ, an amplitude α, and an angular offset of α_0. The entraining velocity $\mathbf{u_i}$ was given by Equation 3.8, since the velocity of the acetabular or tibial component was zero.

$$u_i = \frac{1}{2}\left(2\pi \frac{\alpha 2\pi}{360} \upsilon \cos\left(2\pi \frac{i}{128} + 2\pi \frac{\alpha_0}{360}\right)\right)R_1 \qquad 3.8$$

The Sommerfeld number $\mathbf{Z_i}$, defined in Equation 3.9, was then calculated.

$$Z_i = \frac{\eta u_i R_1}{L_i} \qquad 3.9$$

For each of the 128 points in the cycle, the load, angle, frictional torque, friction factor and Sommerfeld number were calculated. Auger *et al.* (1993b) noted that during the swing phase of the walking cycle the applied loads are very small, and hence the errors associated with calculating the friction factor are very large. Of considerably more interest was the friction factor during the high load stance phase of the cycle. Auger *et al.* (1993b) conducted their Stribeck analysis at a single point in the cycle corresponding to maximum load and sliding velocity. Throughout the results presented here the Stribeck analysis was conducted using results from five points during the high load stance phase, corresponding to **i**=51, 57, 63, 69 and 75 of the forward cycle, Figure 3.14. These five points were treated as five independent results, which were used to calculate simple statistics, such as mean and standard deviation. The mean friction factor was plotted against the Sommerfeld number and the results used to determine the lubrication regime in operation in the contact.

3.2.3 Lubricant and femoral components.

Two lubricant types were used during friction measurement; silicone fluid (Dow Corning 200 Fluid) and carboxymethyl cellulose sodium salt (BDH, UK). The silicone fluid was

available in a range of viscosities, from 0.0008 to 30 Pa s. The CMC fluids were made by mixing various proportions of the powder with distilled water to create fluids with viscosities which varied from 0.001 to 0.150 Pa s. The viscosity of a lubricant was measured on a Ferranti Shirley cone on plate viscometer using a shear rate of 3000 s^{-1} (as used by Cooke *et al.*, 1978 and Unsworth *et al.*, 1987). The properties of silicone fluid are essentially Newtonian over this range of shear rates, whereas both synovial fluid and CMC fluid are markedly non-Newtonian in nature with similar rheological properties (Cooke *et al.*, 1978). For this reason the majority of measurements were made using CMC fluids. Silicone fluids were used to evaluate the agreement of theory with experiment for higher viscosity lubricants. A range of femoral components were used during the hip and knee friction measurement experiments, details of which are given in Table 3.3.

Femoral component	Material	Dimensions /mm	Surface Characteristics.	
			R_a /μm	R_q /μm
Ball bearing	Cr plated Steel.	31.74	0.067	0.100
Exeter 32 mm (Howmedica, UK)	CoCrMo	31.92	0.008	0.010
Biolux 32 mm (Sulzer, Swiss)	Al_2O_3	31.96	0.003	0.005
DLC coated 32 mm (Howmedica, UK)	DLC on CoCrMo	31.96	0.038	0.054
Exeter 28 mm (Howmedica, UK)	CoCrMo	27.96	0.010	0.100
Exeter 22 mm (Howmedica, UK)	CoCrMo	22.20	0.010	0.100
Interax midi 500 knee (Howmedica, UK)	CoCrMo	see Table 4.9	0.031	0.043

Table 3.3. Details of the femoral components used during the friction experiments.

3.3 Adhesion measurement.

The integrity of the bond between the soft layer and the stiff backing is crucial to the long term performance of the bearing. Yao (1994) demonstrated that in a lubricated contact, the maximum shear stress occurred at the interface between the layer and backing, and hence debonding of the compliant layer would be a probable failure mode. In order to assess the bond integrity two test protocols have been developed, the peel test and blister test; both commonly used to assess the bond strength between a flexible material and a rigid backing. The peel test apparatus and geometry were simple and well understood, allowing the performance of different material combinations and process conditions to be easily assessed. However, the flat peel test could not be applied to compliant layer acetabular cups or tibial components, and so the blister test protocol was developed. This allowed comparison between peel test data, and blister test results from real components.

3.3.1 The Peel Test.

The objective of the test was to assess the integrity of the bond between a flexible elastomeric layer and a rigid substrate. The force required to peel the flexible layer from the rigid backing of a specially prepared specimen was measured. The adhesive fracture energy $\mathbf{G_c}$, could then be calculated from the peel force and the test geometry. Peel test samples consisted of a stiff backing block 100×20×8 mm, over moulded with a flexible layer 150×20×3 mm, as described in Section 3.1.3, Figures 3.1 and 3.2. The initial 35 mm of the interface was debonded, either by manually peeling the interface apart using pliers, or by using PTFE tape to block those areas during moulding

The floating roller peel test was conducted as outlined in BS 5350:Part C9 (1990), using a Lloyd R6000 universal material testing machine. Figure 3.15 shows the test equipment. A cross head separation speed of 200 mm min^{-1} and a peel angle of 60° were used. It was important to use cam action grips to hold the flexible layer so that as the applied load stretched and thinned the sample, a firm grip was maintained. The components were arranged so that at the start of the test the grip and roller mechanism were almost touching. This resulted in an initial unpeeled length of 43±1 mm. On completion of each test the force extension curve was saved. The maximum peel force $\mathbf{F_{max}}$, the mean peel force $\mathbf{F_{mean}}$ and the adhesive fracture energy $\mathbf{G_c}$ were calculated and reported for each peel test. In order to calculate $\mathbf{G_c}$ a separate tensile test of the flexible material was conducted, and the extension ratio Λ and strain energy density **U** at the mean peel force calculated.

The mean force was calculated by first comparing the force/extension curve for a flexible layer tested in tension with an initial gauge length of 43 mm, to the force/extension curve for the peel test, shown in Figure 3.16. Where the two curves deviate was defined to be the start of the peeling process. The mean peel force was defined as the sum of the force data points once peeling had commenced, divided by the number of data points.

The extension ratio was defined as the extension of the flexible material divided by the original gauge length, under the application of the mean peel force. This could be calculated from the separate tensile test data, since the extension ratio in the peeled material would be the same as that for the flexible layer in tension under the same force. A tensile test was conducted on a 43 mm gauge length, and the extension ratio

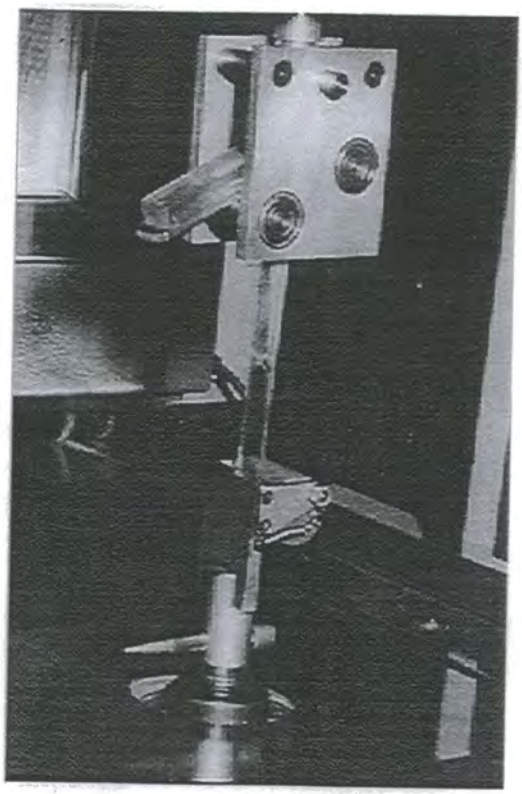

Figure 3.15 View of peel test equipment, mid way through a test.

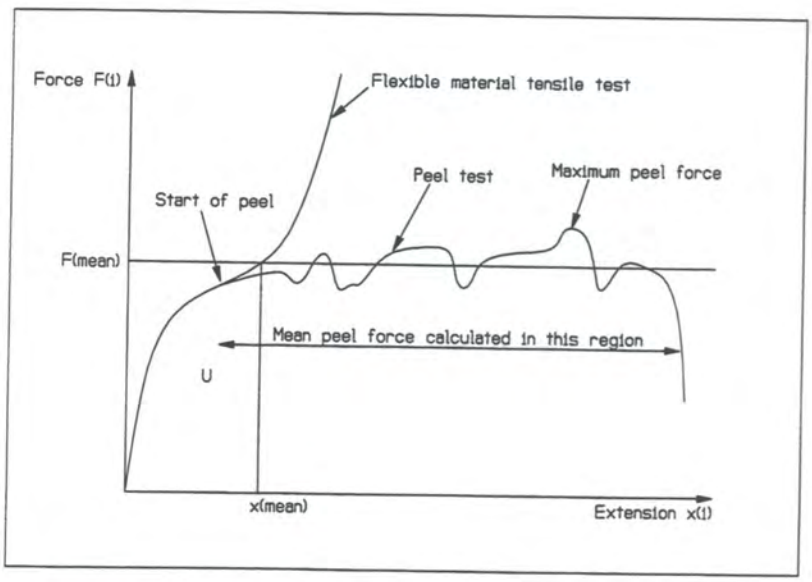

Figure 3.16 Force extension curves for a typical peel test, compared to a normal tensile test of the flexible layer.

calculated for an applied force equal to the mean peel force, Equation 3.10.

$$\Lambda = \frac{l + x_m}{l} \qquad 3.10$$

The strain energy density **U** in the peeled length of flexible material due to application of the mean peel force was equal to that in the flexible layer in tension under the same force. It was determined by calculating the area under the force/extension curve from the tensile test of the flexible material, at an applied force equal to the mean peel force, and dividing by the volume of the strained material, Equation 3.11.

$$U = \frac{\sum_{i=0}^{i=m} \frac{(x_i - x_{i-1})(F_i + F_{i-1})}{2}}{l h_t b_p} \qquad 3.11$$

The adhesive fracture energy $\mathbf{G_c}$ was then calculated from Equation 3.12.

$$G_c = \frac{F_{mean}\Lambda}{b_p} - \frac{F_{mean}\cos\beta}{b_p} - h_t U \qquad 3.12$$

3.3.2 The Blister Test.

This test was used to assess the integrity of the bond between the compliant layer and stiff backing of a prototype acetabular cup. The cups were mounted on the equipment, and oil was forced in to an initial small circular debonded area. The oil pressure required to propagate a crack was measured. From the critical pressure $\mathbf{P_{cr}}$ and geometry of the sample, the system parameter adhesive fracture energy $\mathbf{G_c}$ could be calculated.

A mounting hole and initial debonded area was machined in the pole of the acetabular cups using a CNC lathe. A 8.75 mm flat bottomed cutter rotating at 400 revs/min was used to cut the hole in the pole of the cup. The cup was mounted on to the apparatus by

tapping 1/8 BSP threads 2/3 of the length of the hole, and then screwing the cup on to the apparatus.

The blister test rig (Figure 3.17) consisted of a piston operated via a stepper motor and screw thread. The stepper motor motion was controlled using a PC. Movement of the piston forced oil at a controlled rate through a mounting block to the specimen. The oil pressure was measured using a 100 bar pressure transducer (Intersonde DAX 22), amplifier, and chart recorder. The piston and pipe work were evacuated using a vacuum pump before filling with oil. The cup was screwed on to the mounting block, and oil was forced in to the debonded area. The critical pressure required to propagate the crack (the peak pressure) was recorded (Figure 3.18). Each test took approximately 20 s. On completion of each test the adhesive fracture energy was estimated from Equation 3.13.

$$G_c = \frac{P_{cr}^2 . a_b}{E_2 . f\left(h_1 / a_a\right)} \qquad 3.13$$

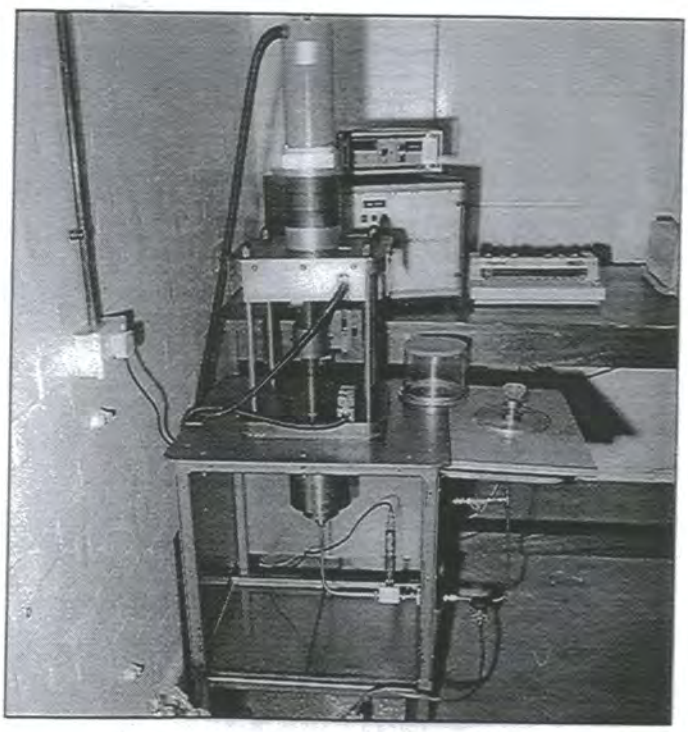

Figure 3.17 View of blister test equipment.

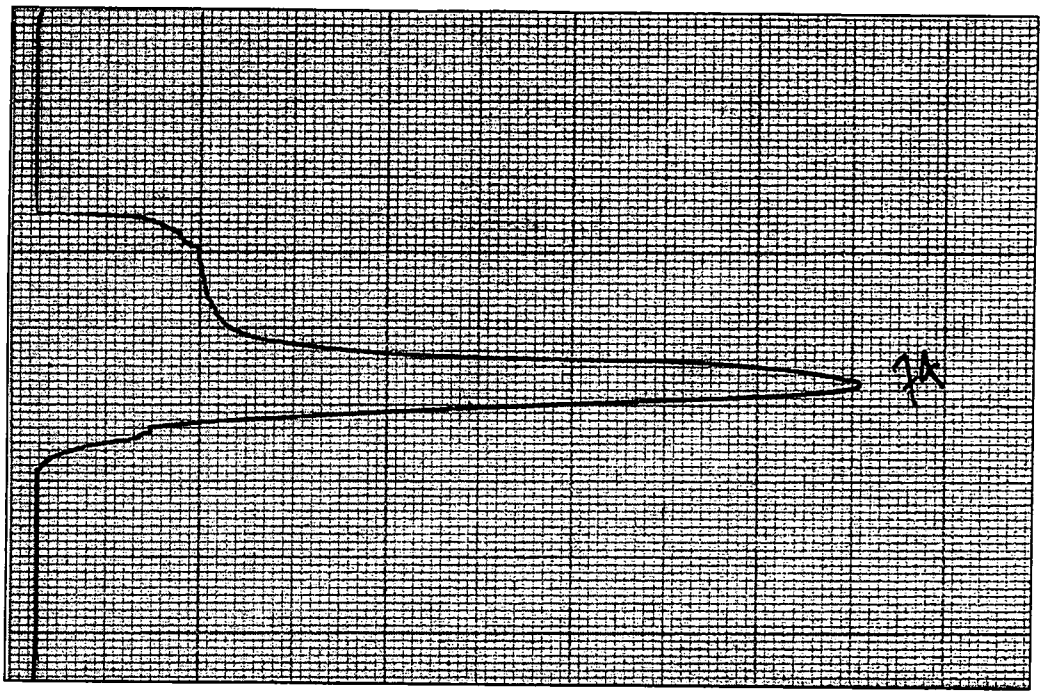

Figure 3.18 Pressure-Time curve for a typical blister test (pressure on the X-axis, time on the Y axis). The critical pressure P_{cr} is the maximum pressure reached.

3.4 Non-contacting optical profilometry.

In order to evaluate the bearing surfaces a Micromap 512 non-contacting optical profiler (NOP) (Micromap Corp., AZ) at the Department of Materials, University of Newcastle, was used. The machine used Phase Shifting Interferometry, where by a white light beam was split, half falling on a reference surface, and half on the sample. The phase shift was achieved using a piezo electric drive which moved the reference beam, and the interference pattern was recorded using a CCD camera and analysed using PC based software. The result was a 3D profile, with a vertical resolution of 1 Å, and a horizontal resolution (depending on the magnification) of 2.5 μm for the ×10 objective used throughout this study. An area 0.5×0.5 mm^2 was measured.

NOP was used in preference to a conventional stylus profiler for a number of reasons. The NOP gave a 3D profile which was easily manipulated to examine the surface in a number of ways. These included oblique views and contour maps which enabled the surface to be visualised very easily, conventional 2D profiles, bearing area curves, autocovariance data in both 2D and 3D, and 3D slope plots; together with a range of surface statistics. It was trivial to remove spherical form from the 3D profile in software, hence measurement of cups and heads was very simple. In addition, surface deformation might be expected on a micro scale when measuring a compliant surface using a stylus profiler.

However, some differences do exist between surface parameter data derived from NOP and conventional stylus instruments (Williams and Statham, 1993). The difference in probe types (stylus verses light beam) and sampling size leads to, in effect, different filtering for the two methods; it is well understood that the choice of waviness filter greatly effects the numerical roughness and waviness results. Hence, just as the choice of cut-off length is one of the principal measurements conditions for a stylus instrument, the choice of optical objective and form filter is fundamental in NOP measurement. Although differences do exist between machines, and the stylus method is more 'standardised', the ease of obtaining extensive 3D data using NOP made it an invaluable technique for this application, and will ensure its greater use in tribology in the future. The 'standard' experimental settings used here are given in Appendix C.

3.5 Measurement of bearing dimensions.

Bearing dimensions were one of the most significant design parameters thought to influence the lubrication regime. In addition, creep of the compliant layer after a period under load and the resulting change in bearing dimensions was also considered important, as this may change the lubrication regime and hence the joint's long term performance. Several methods of assessing bearing dimensions and creep in acetabular cups using Co-ordinate Measuring Machines (CMMs) were used; at Howmedica (Limerick, Eire) and at the National Gear Metrology Centre (University of Newcastle upon Tyne).

Howmedica CMM. Ten data points were taken on the bearing surface (Figure 3.19), using a Mututoyo CMM. A sphere was then fitted to these points. The diameter of the sphere, and the maximum deviation of the measured data from this sphere, were reported. Typically, this method gave a range of ±0.04 mm for sphere diameter, and a range of ± 0.1 mm for values of maximum deviation. This method was used to determine the cup dimensions used in the lubrication analyses.

Newcastle CMM. A Hofler EMZ 632 CNC gear measuring machine with 4-axis measurement (X, Y, Z and rotary) was used. Initially three datum surfaces were defined (Figure 3.20a); followed by the measurement of two circles (361 points per circle), four X-sections (230 points per section) and a sphere (31 points) in the pole of the cup (Figure 3.20b). The results were presented both in graphical form, and as least-squares-fit diameters and form errors. The accuracy was estimated to be ±0.035 mm for the scanned circles, ±0.01 mm for the X-sections, ±0.02 mm for the sphere, and typically ±0.005 mm

for the form errors. (The main source of non-repeatability was the definition of datum B). This method was used only for the creep experiment (Section 5.4)

Indirect CMM. In addition to direct measurement of the cup itself, indirect measurement using replicas was used. The objective was to develop a technique which could be used to assess the dimensional changes of compliant bearings after removal of the load but before any recovery remote from the CMM apparatus. Provil (Bayer, UK), a polyvinylsiloxane used in dentistry as a replica material was chosen. It was dimensionally stable and cures in under 60 seconds with linear shrinkage of 0.04%. Replicas made on different days by different operators were measured using the Howmedica CMM method, and the results compared with the direct CMM measurement of the same cups. The method gave a range of only ±0.01 mm for the sphere diameter, and hence could be used to demonstrate relative differences in bearing dimensions. However the analysis showed that there was a significant difference (P=0.011) between the direct and replica methods. A systematic error was identified, of approximately 0.2 %, leading to an under estimate of the diameter by the replica method, compared with the direct CMM method. This could be attributed to a combination of replica material shrinkage, and slight deformation of the replica by the CMM probe. This method was also used in the creep experiment (Section 5.4).

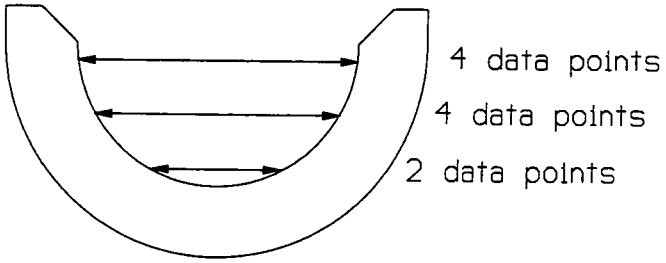

Figure 3.19. Howmedica CMM measurement protocol. Ten data points were taken in the positions shown, and a least squares fit sphere and form errors were reported.

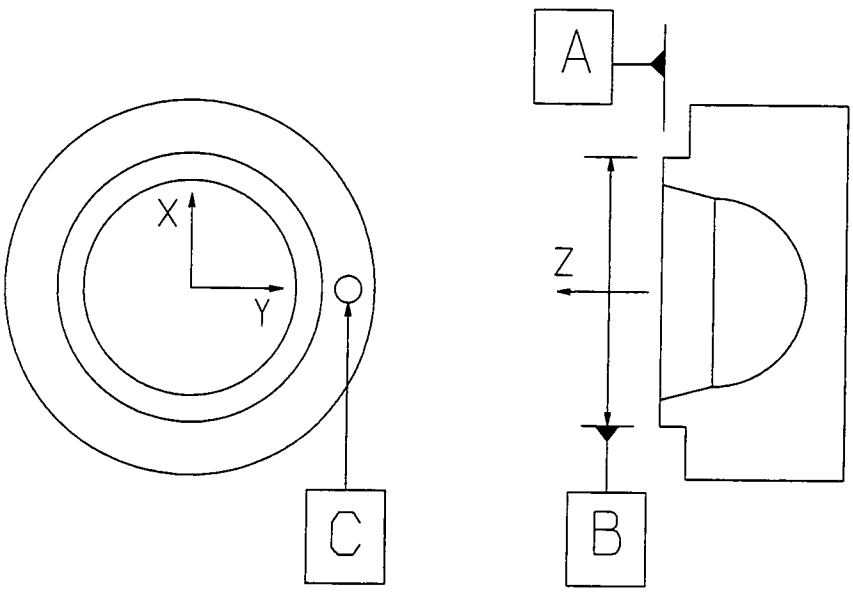

Figure 3.20a. Newcastle CMM measurement protocol. Definition of the axis datum (surface A, diameter B, and reference hole C) and axis orientation.

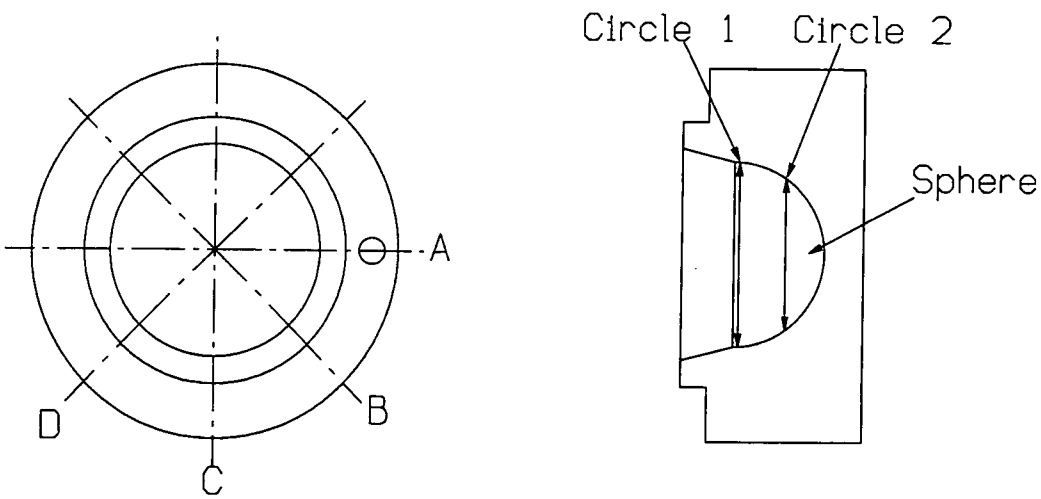

Figure 3.20b. Newcastle CMM measurement protocol. Definition of the scanned circles 1 and 2, X-sections A to D, and sphere in the pole of the cup.

Chapter 4. Friction: Results and Discussion.

4.0 Introduction.

The objective of these experiments was to investigate the design parameters which influence the tribological performance of compliant bearings. This was done using the Durham friction simulator as described in Section 3.3. Stribeck analyses were conducted for a range of compliant bearing acetabular cups and, for the first time, realistic compliant bearing tibial components. These experimental results were then compared with both EHL and μ-EHL theory, thus enabling an experimental verification of the design equations cited in the literature. In addition, the start-up frictional torque was assessed for the first time under physiological gait conditions in acetabular cups. The conclusions of this series of experiments were recommendations on the design of compliant bearing TJRs.

4.1 Comparison of theory with experiment.

Experimental values of friction factor were compared with both EHL and μ-EHL theory. A good agreement would validate the use of the theory for compliant bearing design.

EHL theory.

Using the same scheme as Auger *et al.* (1993b) the theoretical coefficient of friction was determined from the shear stress relationship for a Newtonian fluid, Equation 4.1, and

EHL film thickness Equation 2.1 for $\mathbf{h_{cen}}$. This assumes that the film of lubricant is the same shape as the dry contact area, which is given by Equation 2.6. The coefficient of friction was estimated for a range of viscosities and plotted against Sommerfeld number, and compared with the experimental results.

$$\mu = \frac{\pi a^2 \eta \frac{u}{h_{cen}}}{L} \qquad 4.1$$

Micro EHL theory.

Two approaches have been used when comparing μ-EHL theory with experimental results; a simple surface separation parameter approach used by Auger *et al.* (1993b), and an asperity lubrication model proposed by Yao and Unsworth (1993). Auger used a surface separation parameter, defined in Equation 4.2, which for hard bearing surfaces normally predicts the initiation of film breakdown when $\lambda<3$. He argued that if low friction and near fluid film lubrication were maintained when $\lambda<3$ this was evidence of μ-EHL.

$$\lambda = \frac{h_{cen}}{\sqrt{\sigma_1^2 + \sigma_2^2}} \qquad 4.2$$

The asperity lubrication model proposed by Yao and Unsworth predicts a revised film thickness based on the surface topography and the smooth EHL theoretical film thickness. They considered several types of surface topography, of which the most relevant is isotropic waviness, given in Equation 4.3. The μ-EHL film thickness $\mathbf{h_{r,min}}$ was then used to estimate the theoretical friction in the same way as for the smooth EHL case (by substituting $\mathbf{h_{r,min}}$ for $\mathbf{h_{cen}}$ in Equation 4.1), and comparing it with experimental friction factors as before.

$$h_{r,\min} = 1.94\left\{\frac{\eta u\left(1-\nu_2^2\right)}{E_2}\right\}^{0.65}\left\{\frac{\lambda^2}{4\pi^2\sigma_2}\right\}^{0.77}\lambda\left(\sigma_2 - h_{\min} - h_{r,\min}\right)^{-0.21} \qquad 4.3$$

It should be noted that the asperity lubrication model becomes more accurate as the wave length shortens and roughness increases. In addition, careful examination of Equation 4.3 shows it has no real roots when $\mathbf{h_{min}}>\sigma_2$, *i.e.* when the predicted EHL film thickness is larger than the amplitude of the surface roughness. Even though fluid film lubrication is assured in this situation, pressure perturbations would still smooth the surface asperities to some degree and hence modify the film thickness and the theoretical estimate of friction. Since compliant bearings are manufactured with σ_2 values typically <0.3 μm, which is smaller than the typical EHL film thickness predictions for viscosities above 0.01 Pa s, the theory is generally only valid for low viscosity lubricants.

4.2 Friction measurements -hips.

4.2.1 Conventional joints.

The frictional resistance of conventional joints, both new and explanted, was measured using the Durham friction simulator. These experiments were, in part, conducted by the author and are published elsewhere (Hall *et al.*, 1994, Unsworth *et al.*, 1995). The results are an important benchmark against which to compare compliant bearings. Conventional joints were shown to operate with a mixed lubrication regime synonymous with asperity contact and wear; with friction factors ranging typically from 0.05 for 0.001 Pa s

lubricant, to 0.02 for 0.1 Pa s lubricant. In addition, friction factors for the dry contacts were typically 0.1.

4.2.2 Dry Friction Measurements.

In order to establish the frictional resistance developed in a compliant layer dry contact, frictional measurements were made in the usual way but no lubricant was used. A reduced maximum load of 1000 N was used to avoid overloading the friction transducer. Acetabular cups made from four different bearing materials were used (discussed later in Section 4.2.6), in conjunction with Exeter and Biolux femoral heads. The results are given in Table 4.1.

The dry friction factors in all cases were extremely high, with a range of approximately 0.8 to 1.0. Clearly dry contact in compliant layer joints would result in high shear forces at the bearing surface, undoubtedly leading to rapid wear or structural failure of the joint. In addition, the resulting frictional torque of approximately 30 Nm (with a 32 mm head) is approaching the level of 100 Nm required to dislodge a well fixed cemented prostheses measured by Anderson *et al.* (1972). From all perspectives, a compliant bearing running dry would be vastly inferior to current conventional prostheses.

Bearing Material	Dry Friction Factor Exeter Head		Dry Friction Factor Biolox Head	
	mean	s.d	mean	s.d
Chronoflex	0.98	0.08	0.95	0.12
Tecothane	0.77	0.30	0.93	0.17
Corethane	1.01	0.18	1.02	0.13
CSIRO	1.07	0.12	0.83	0.17

Table 4.1. Dry friction factor results.

4.2.3 Fluid film lubrication of compliant layer cups.

Several groups have already established that, when well lubricated, compliant bearings operate with very low friction, typically <0.01. One of the first objectives in this study was to demonstrate that the new injection moulded PU/PU acetabular compliant bearings would also operate with low friction and fluid film lubrication. A C80A/C75D cup was manufactured and tested in conjunction with a 31.74 mm Cr plated ball bearing head. The cup, soft2, was tested using both CMC fluids (0.001 to 0.1 Pa s) and silicone fluids (0.8 to 30 Pa s), and Stribeck analyses conducted. The experiment was then repeated with a 31.92 mm Exeter head with the CMC fluids only. The design parameters for the cup/head combinations are given in Table 4.2, and the results are shown in Figures 4.1 and 4.2.

Clearly the joint operates with extremely low friction with either of the heads. The friction factors for the CMC fluids were all below 0.01, considerably lower than conventional joints. This result confirms the earlier results of Unsworth *et al.* (1987,1988), Blamey *et al.* (1991) and Auger *et al.* (1993b). The shape of the Stribeck curves from the ball bearing results for the CMC and silicone fluids are very similar when compared over similar viscosity ranges. The curves show a minimum at approximately 10^{-9} which corresponds to a viscosity of approximately 0.01 Pa s, that of synovial fluid (Cooke *et al.*, 1978).

A slightly falling Stribeck curve was observed over the lubricant viscosity range 0.001 to 0.01 Pa s, indicative of mixed lubrication. If the frictional resistance in this mixed lubrication regime is considered as simply the sum of the contributions from asperity contact on one hand, and shearing of the lubricating film on the other, then the degree of

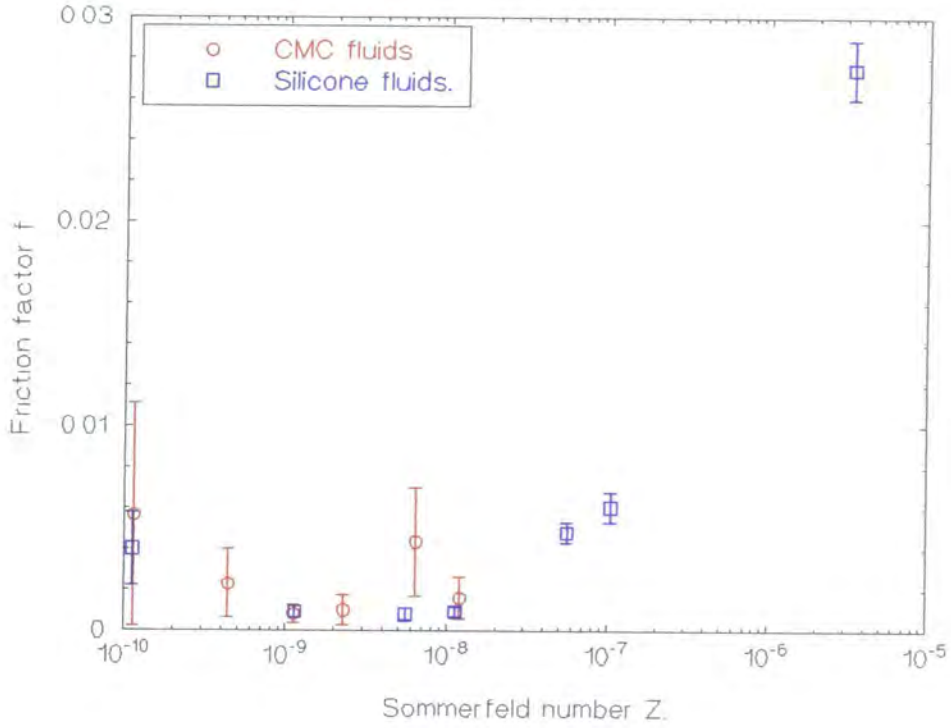

Figure 4.1. Stribeck analysis; Cup soft2 and ball bearing head. Three runs for each result.

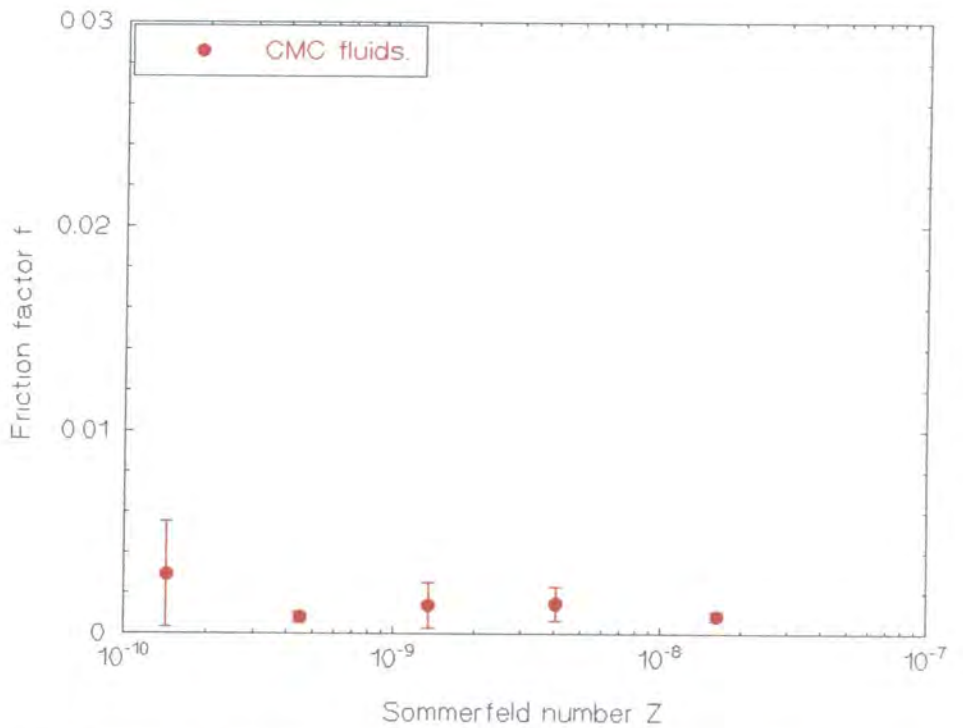

Figure 4.2. Stribeck analysis; Cup soft2 and Exeter head. Three runs for each result.

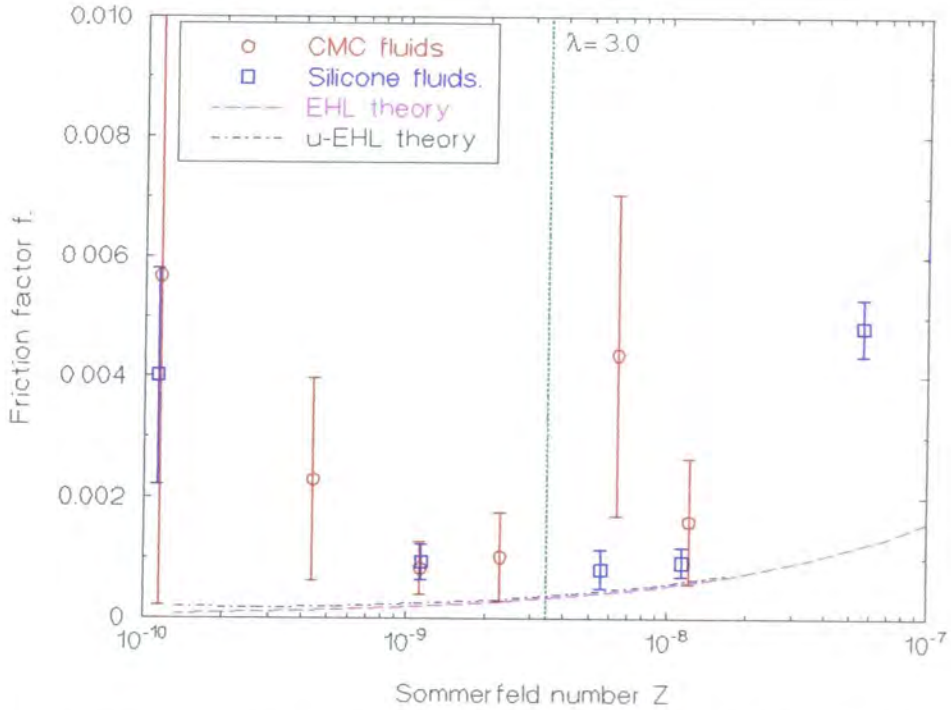

Figure 4.3. Comparison of theory with experiment; Cup soft2 and ball bearing head.

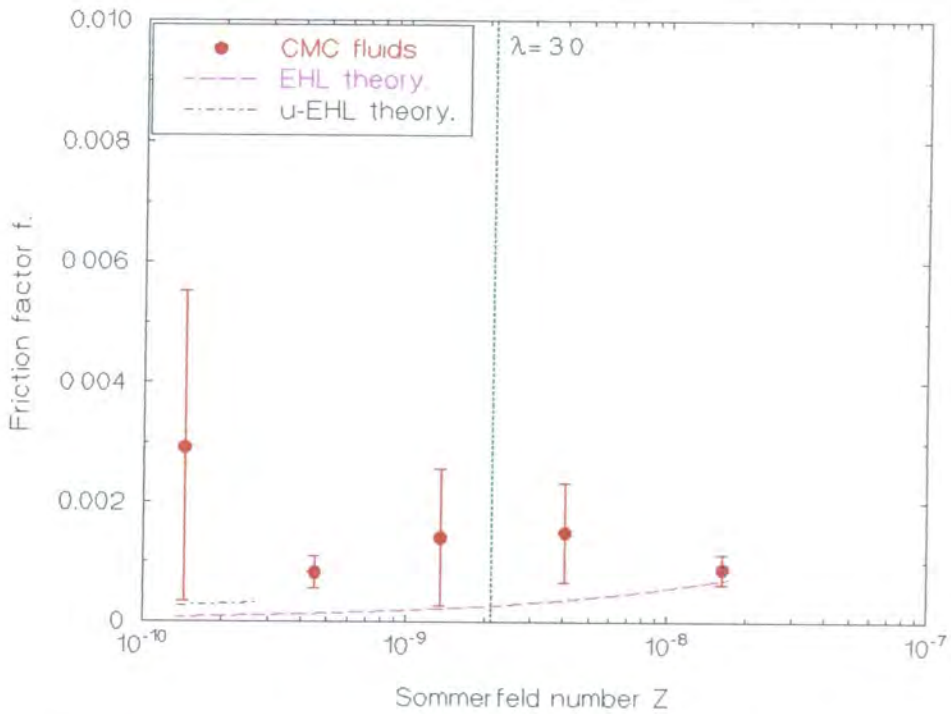

Figure 4.4. Comparison of theory with experiment; Cup soft2 and Exeter head.

Design Parameters.	soft2/Ball bearing.	soft2/Exeter head.
Head radius: R_1 /mm	15.87	15.96
Cup radius: R_2 /mm	16.13	16.13
Head modulus: E_1 /GPa	200	200
Head Poissons ratio: ν_1	0.3	0.3
Layer modulus: E_2 /MPa	19.2	19.2
Layer Poissons ratio: ν_2	0.5	0.5
Entraining velocity: u /mms^{-1}	16.95	17.05
Applied load : L /N	2000	2000
Layer thickness: h_t /mm	1.94	1.94
RMS femoral: σ_1 /μm	0.100	0.010
RMS layer: σ_2 /μm	0.216	0.216
Wave length: λ_2^* /μm	140	140
Equivalent radius: R /m	0.736	1.514
Contact half width: a /mm	11.13	14.43
Stroke ratio: S_t	0.42	0.46
Max. Shear stress: τ_{max} /MPa	1.53	0.92
Max. Shear strain: γ_{max}	0.21	0.13
EHL film thickness: h_{min} /μm *	0.053	0.104
μ-EHL film thickness: $h_{r,min}$ /μm *	0.014	0.038

Table 4.2 Design parameters for the 32 mm C80A/C75D acetabular cup soft2. (* when η =0.001 Pa s).

asperity contact can be estimated.

$$\mu_{mixed} = \frac{\%\,contact}{100}\mu_{dry} + \frac{1 - \%\,contact}{100}\mu_{EHL}$$

For both compliant and conventional bearings the EHL theoretical fluid film friction is less than 0.001; whereas dry friction is approximately 1.0 for compliant bearings, and 0.1 for conventional joints. Since the measured friction factors for compliant bearings are

typically less than 0.01 this indicates less than 1% asperity contact. In contrast, the same argument indicates in the order of 50% asperity contact for conventional joints. Thus the compliant bearing was judged to operate with negligible asperity contact, over the range of viscosities considered.

Comparing the soft2/ball bearing head results with theory, Figure 4.3, clearly the experimental friction factors are slightly higher than those predicted theoretically, which is in agreement with the observations made by Auger *et al.* (1993b). In his study, Auger observed "reasonably close" agreement between theory and experiment for only one of the lubricants used (a mineral oil of viscosity 0.256 Pa s), but went on to conclude that "the agreement achieved gives greater confidence in the use of EHL theory for ... design of cushion form bearings". It is worth noting that no agreement was found for viscosities representative of physiological lubricants, *circa* 0.01 Pa s. He suggested that the ratio of stroke length to contact width, which was shown to be critical by Hirano and Murakami (1975) was smaller than optimum which reduced the film thickness and hence increased the measured friction. When considering both the theoretical and experimental results one must recognise, firstly the difficulty of measuring such small frictional torque values, and secondly the difficulty of modelling the behaviour of the lubricant in such a thin film. Although EHL theory does predict the trends observed experimentally, its use in the design of compliant bearings is not proven here, nor by Auger. However Figure 4.3 does confirm the importance of μ-EHL, as indicated by the low friction when $\lambda<3$. Although the asperity lubrication model predicts thinner film thicknesses and hence higher estimates of theoretical friction resulting in closer agreement between theory and experiment over its limited range of applicability, neither this model nor the EHL model accurately predict these experimental results.

The soft2/ball bearing experimental results are noteworthy because of the far from optimum nature of the contact. The use of the 31.74 mm ball bearing results in a relatively low conformity contact with a relatively rough femoral surface. Contrast this with the more optimum contact of the soft2/Exeter head combination, which has higher conformity and a significantly smoother femoral surface, but gives very similar experimental results, Figure 4.2. The more optimum soft2/Exeter head combination compares more favourably with the theoretical estimates, Figure 4.4, especially for the 0.1 Pa s result. Once again the position of the λ=3.0 line indicates the importance of μ-EHL, but the usefulness of either the EHL or μ-EHL theory in predicting the experimental results is still not proven. Indeed the experimental results thus far seem to indicate that the design of compliant bearing acetabular cups is not particularly sensitive to some of the parameters suggested by the theory.

4.2.4 Effect of bearing conformity.

The results from the previous section indicated that bearing conformity may not be critical, as EHL theory predicts. Hence C75D/C80A acetabular cups were manufactured with different clearances and tested in the normal way with an Exeter head and CMC fluids. Two sets of experiments were conducted; the first using cups manufactured with a moderate radial clearance (C1, C2, and C3), and the second using cups made with a larger radial clearance (R1, R3, and R4), as indicated in Table 4.3. The larger clearance set of cups were subsequently found to have been produced with typically 100 μm lobes on the bearing surface[1] (measured by Rank Taylor Hobson using a Talyrond 73, illustrated in Figure 4.5).

[1]During the manufacture of these cups the C75D backing shell was poorly supported in the mould, and deformed under the pressure as the C80A compliant layer was injected (Stage 3, Figure 3.4) resulting in the four leaf clover effect, Figure 4.5.

	C1	C2	C3	R1	R3	R4
Core diameter /mm	32.35	32.70	32.42	33.00	32.70	32.42
R_2 /mm	16.08	16.23	16.11	16.47	16.50	16.20
h_t /mm	1.92	1.77	1.90	1.54	1.76	1.80
R /m	2.139	0.959	1.773	0.520	0.910	1.077
a /mm	14.9	12.2	14.3	10.2	12.1	12.6
S_t	0.90	1.09	0.94	1.31	1.11	1.06
τ_{max} /MPa	0.83	1.27	0.91	1.84	1.31	1.19
γ_{max}	0.12	0.18	0.13	0.26	0.18	0.17
h_{min} /μm *	0.113	0.077	0.104	0.055	0.075	0.082

Table 4.3 Design parameters and minimum film thickness results for the series of cups used to assess the effect of conformity. (* when η=0.001 Pa s.) (Those parameters not detailed here are the same as for the Exeter head case in Table 4.2., with the exception of the cup surface roughness which was not measured.)

The frictional results for the two sets of cups are presented in Figures 4.6 and 4.7. For C series cups there is no perceivable difference between the different clearances, indicating that in this range at least, conformity is not critical (Figure 4.6). However, for the R series cups conformity seems to be more important (Figure 4.7), but interestingly not with the trend suggested by EHL theory. The fact that none of the R series cups performs as well as the C series, and that the largest clearance cup gaves the lowest friction factors can be explained by considering the contact area and the relative interaction with the lobes. If the contact area is small and predominantly confined to the pole of the cup then interaction with the lobes will be minimal, whereas if the contact area is large and extends up the cup sides, the interaction with the lobe high spots will become more marked. These results show clearly that sphericity of the bearing surface is important, and that small out of roundness will be better accommodated by lower conformity bearings.

The R1 result is particularly noteworthy, as it suggests that large clearance cups with significant out of roundness can still perform with fairly low friction.

Comparisons between EHL theory and experimental results were conducted for the C series cups (Figures 4.8 to 4.10), with similar levels of agreement as the previous section. The EHL comparison was not made for the R series cups, since the lobes clearly resulted in a degree of bearing surface contact. The surface topography of neither of these sets of cups was measured, and hence μ-EHL was not quantitatively assessed.

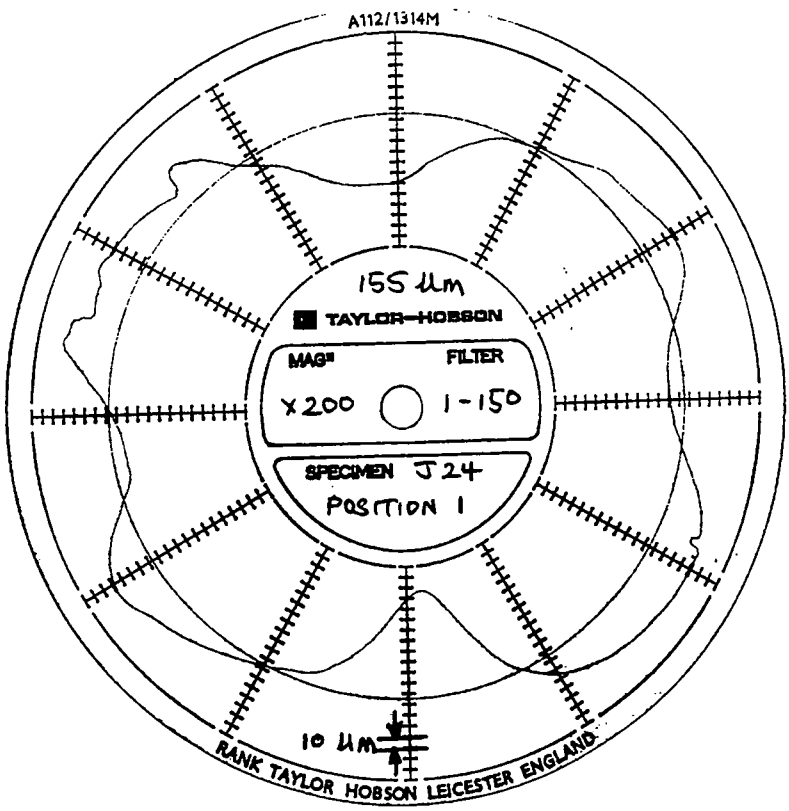

Figure 4.5 Talyrond result for lobed cups.

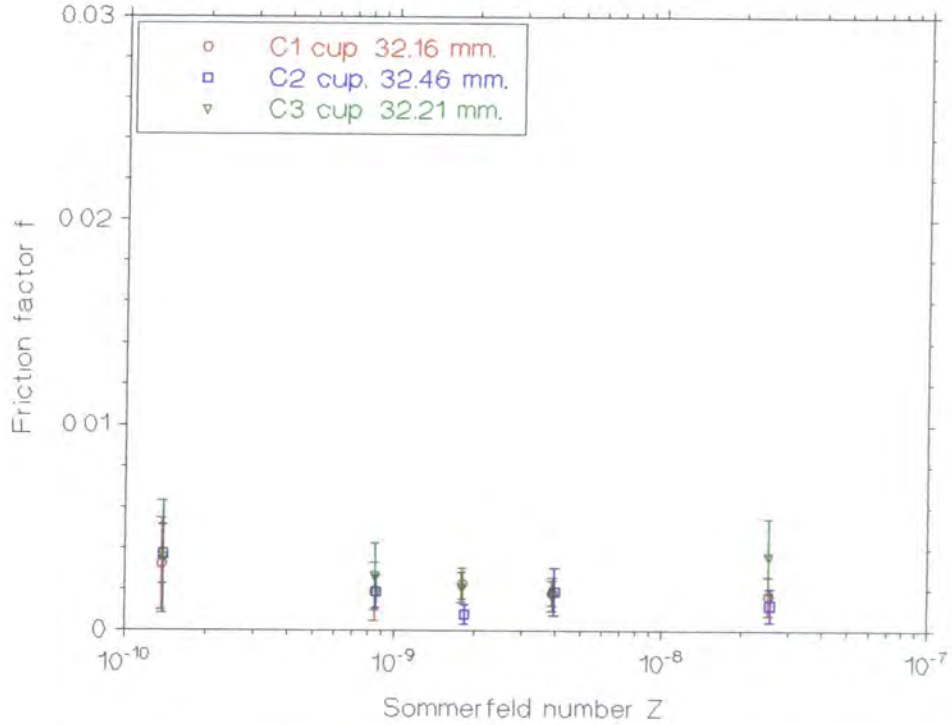

Figure 4.6 Stribeck analysis; C series cups and Exeter head. One run on each of three cups for each result.

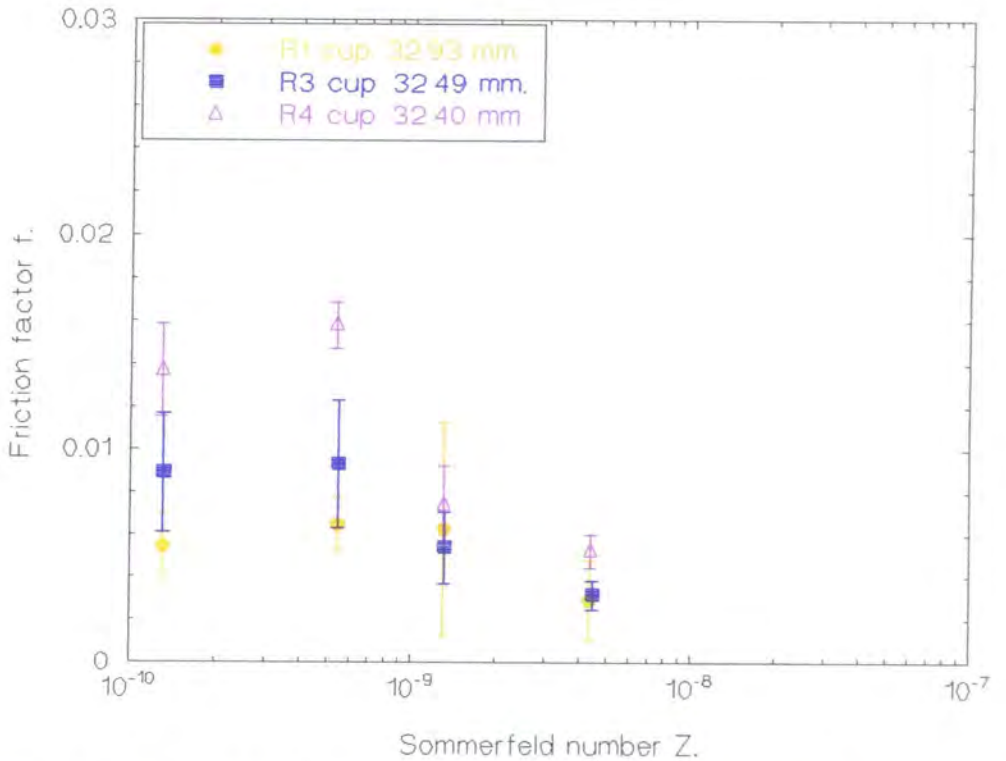

Figure 4.7 Stribeck analysis; R series cups and Exeter head. Two runs for each result.

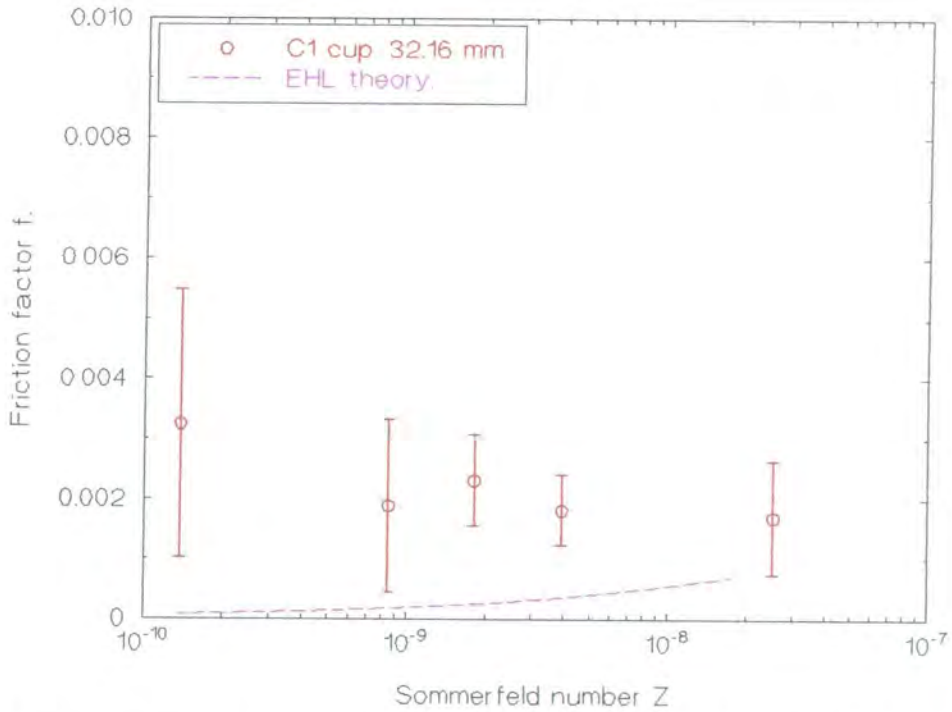

Figure 4.8 Comparison of theory with experiment; Cup C1 with Exeter head. One run on each of three cups for each result.

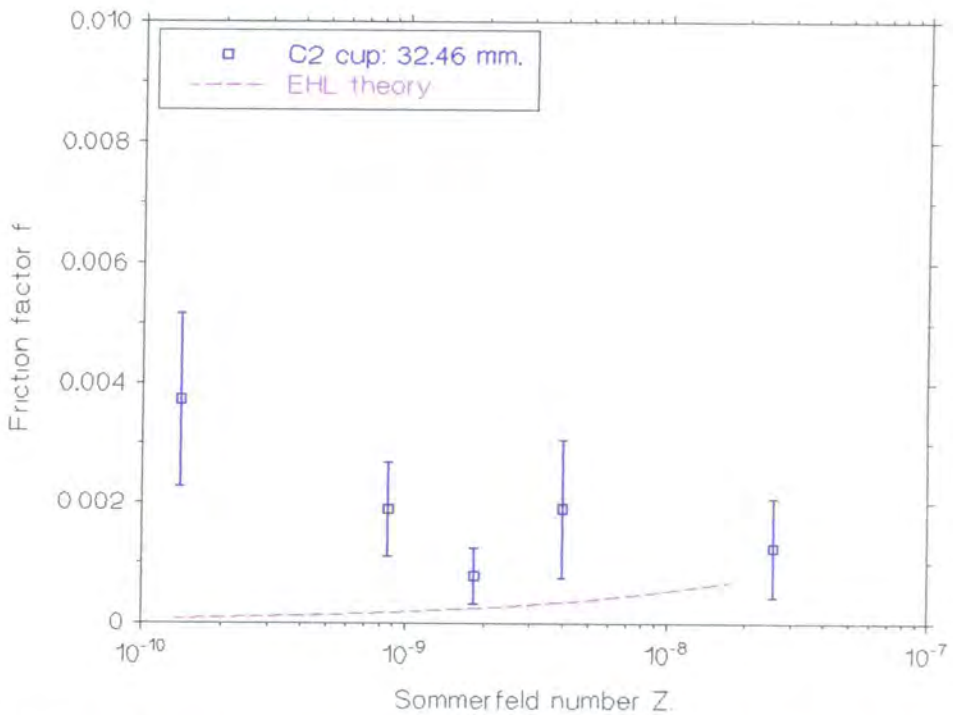

Figure 4.9 Comparison of theory with experiment; Cup C2 with Exeter head. One run on each of three cups for each result.

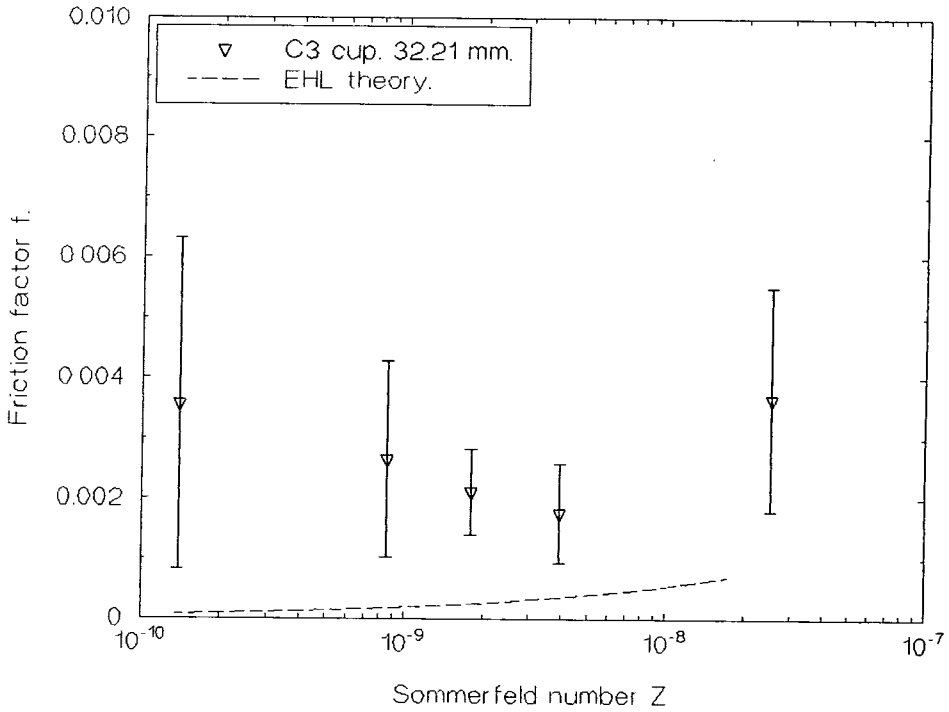

Figure 4.10 Comparison of theory with experiment; Cup C3 with Exeter head. One run on each of three cups for each result.

4.2.5 Effect of femoral head size.

For conventional joints, femoral head sizes typically vary from 32 mm to 22 mm in diameter. Whereas 22 mm joints have advantages such as lower wear volumes and reduced frictional torques; 32 mm joints have reduced penetration rates and lower contact stresses. Twenty eight mm joints are popular as they represent a compromise between the two. Equation 2.1 indicates that entraining velocity, which is directly related to head size, is the most important parameter affecting film thickness in compliant layer bearings. Although the need to maximise velocity and hence head size suggests a 32 mm head should be used, there are several reasons why smaller head sizes should also be considered. Compliant layer bearings are unlikely to be used in humans until extensive animal studies have been conducted and likely animal models, such as sheep or dogs, will not accommodate 32 mm heads. In addition, surgeons have developed techniques and preferences suited to 28 mm

and 22 mm joints. Hence from animal trial, surgical and commercial perspectives, compliant bearings based on a range of head sizes would be desirable.

Acetabular cups were manufactured from C75D/C80A with nominal head sizes of 22 mm and 28 mm and tested in the normal way. The results were plotted on the same axis as the 32 mm joint discussed in Section 4.2.3 (Figure 4.11). Clearly the 32 mm and 22 mm joint perform with extremely low friction indicative of near fluid film lubrication. However, the 28 mm joint operates with higher friction and mixed lubrication.

Design Parameters.	22 mm cup (S4)	28 mm cup (BG64)	32 mm cup (soft2)
R_1 /mm	11.10	13.98	15.96
R_2 /mm	11.27	14.46	16.13
u /mms^{-1}	11.85	14.95	17.05
h_t /mm	1.60	2.15	1.94
σ_1/μm	0.010	0.010	0.010
σ_2 /μm	0.287	0.202	0.216
λ_2^* /μm	98	88	140
R /m	0.736	1.195	1.514
a /mm	11.13	13.79	14.43
S_t	0.42	0.43	0.46
τ_{max} /MPa	1.53	1.03	0.92
γ_{max}	0.21	0.15	0.13
h_{min} /μm *	0.053	0.088	0.104
$h_{r,min}$ /μm *	0.014	0.020	0.038

Table 4.4 Design parameters and minimum film thickness results for the cups used to assess the effect of head size. (* when η=0.001 Pa s.) (Those parameters not detailed here are the same as for the 32 mm Exeter head case, Table 4.2.)

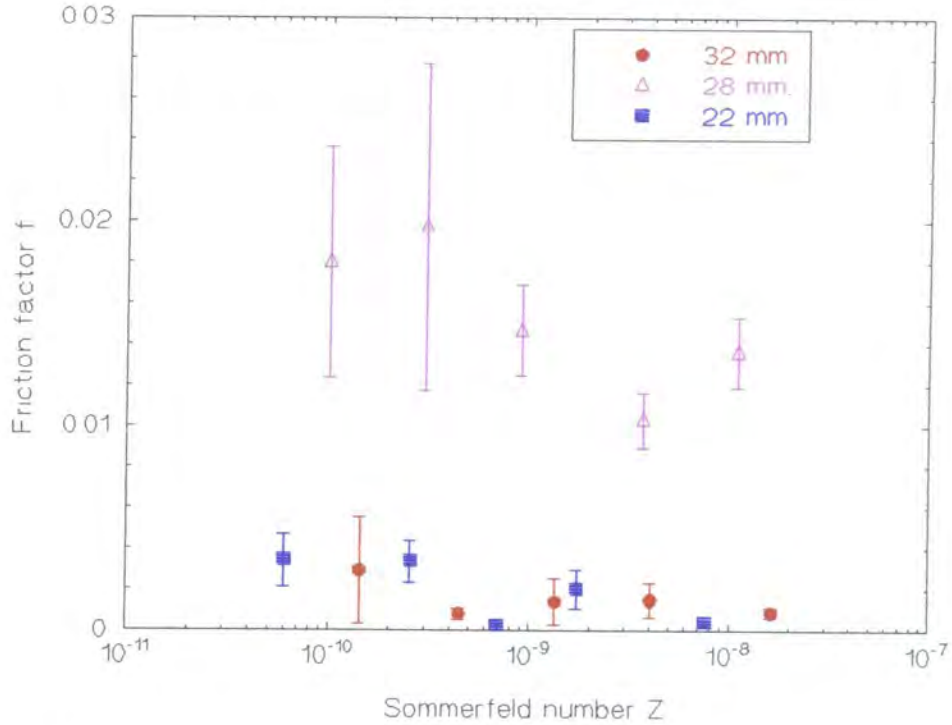

Figure 4.11 Stribeck analysis; 22 mm, 28 mm and 32 mm cups with Exeter heads.

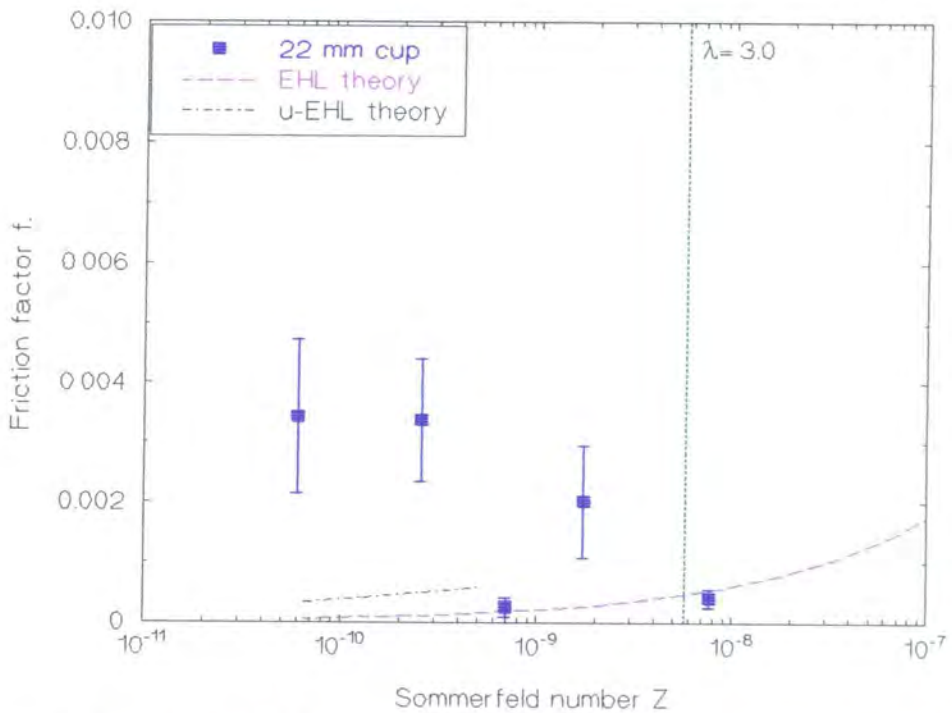

Figure 4.12 Comparison of theory with experiment; Conditioned 22 mm cup with an Exeter head. Three runs for each result.

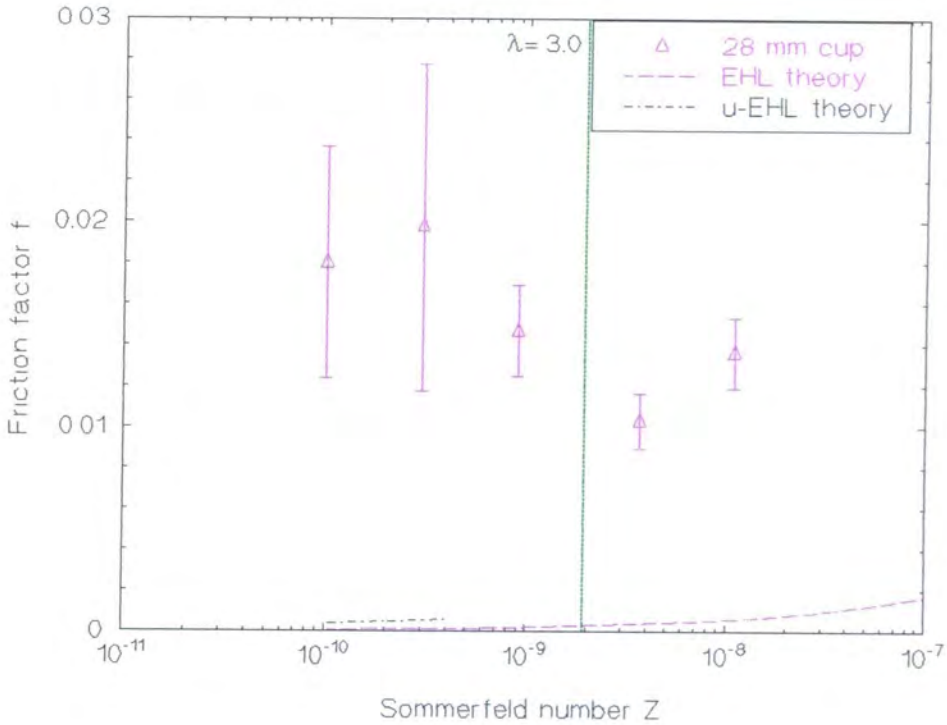

Figure 4.13 Comparison of theory with experiment; Conditioned 28 mm cup with an Exeter head. Three runs per result.

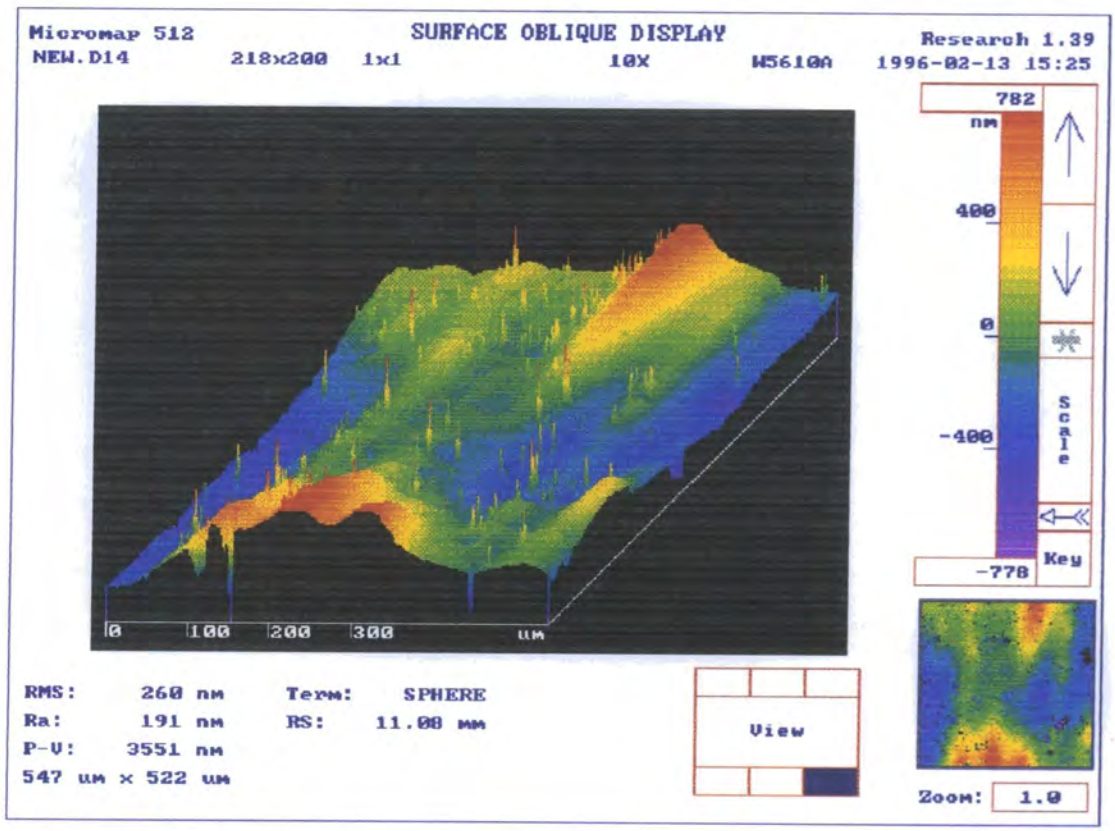

Figure 4.14 NOP oblique view of the 22 mm acetabular cup.

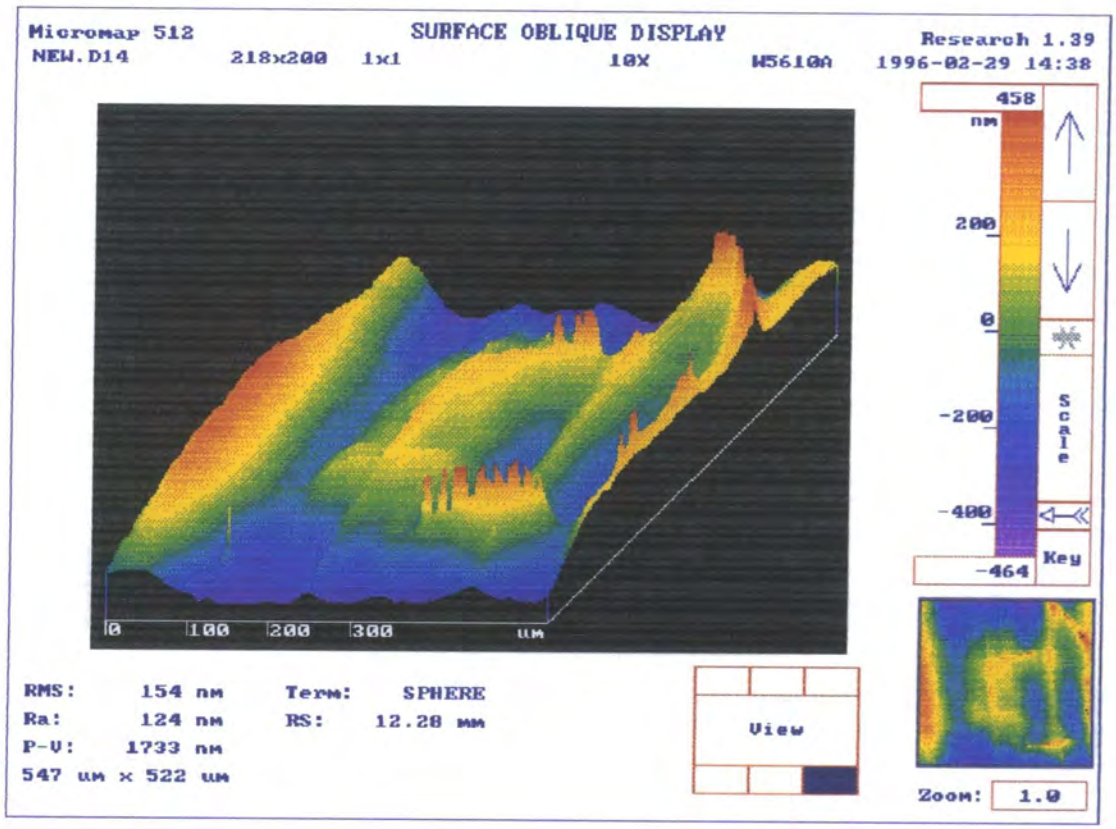

Figure 4.15 NOP oblique view of the 28 mm acetabular cup.

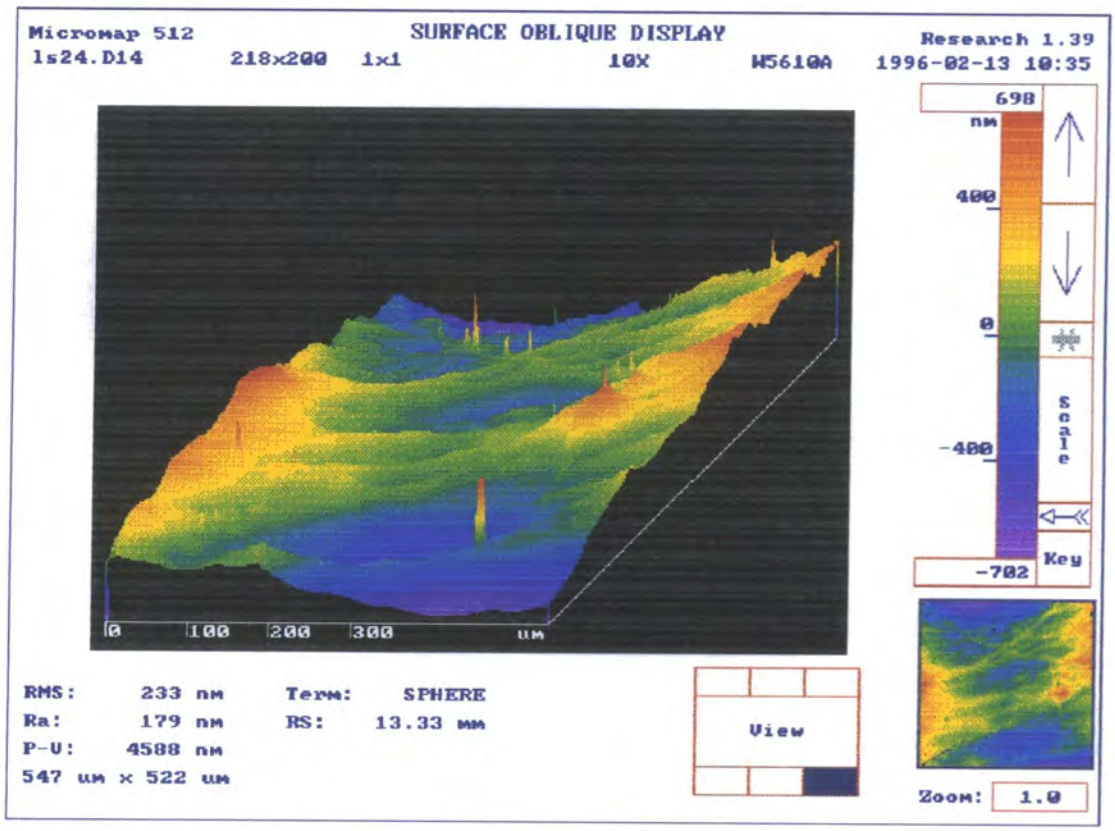

Figures 4.16. NOP oblique view of the 32 mm acetabular cup.

Comparing EHL estimates of film thickness and friction with the experimental results does not explain why the 28 mm joint is significantly different to the 22 mm or 32 mm joints (Table 4.4, Figures 4.12, 4.13 and 4.4). The surfaces of the bearings were examined in detail in an effort to establish a difference between the bearing sizes. Oblique views of each bearing surface are given in Figures 4.14, 4.15, and 4.16. The R_a and σ_2 values were all comparable. None of the autocorrelation functions demonstrated periodicity of the surface, and λ_2^* values were comparable in all cases. The skewness of the bearing surfaces was also assessed, but was subject to large random statistical variations in the data, with no apparent differences between cups, and values of typically ± 0.5. The surface roughness data was used in the normal way to estimate μ-EHL film thickness and friction, but did not explain the poor performance of the 28 mm cup, which remains unresolved. However the experimental results from the 22 mm cup showed some agreement with theory, and based on the surface separation parameter approach, confirmed once again the importance of μ-EHL, especially when the EHL performance is less than optimum.

4.2.6 Effect of layer modulus.

Unsworth *et al.* (1987) assessed the effects of layer compliance. They used 32 mm compliant layer cups with a hardness range of 2.5 to 8 N/mm^2, and demonstrated an optimum hardness of 4 N/mm^2 (equivalent to an elastic modulus of ≈12 MPa) resulted in the lowest friction factor results. Although theoretical analysis suggests E_2 is one of the least important design parameters, the literature suggests that it is significant. The objective of this series of experiments was to assess the effect of layer compliance using the new generation of biostable PUs.

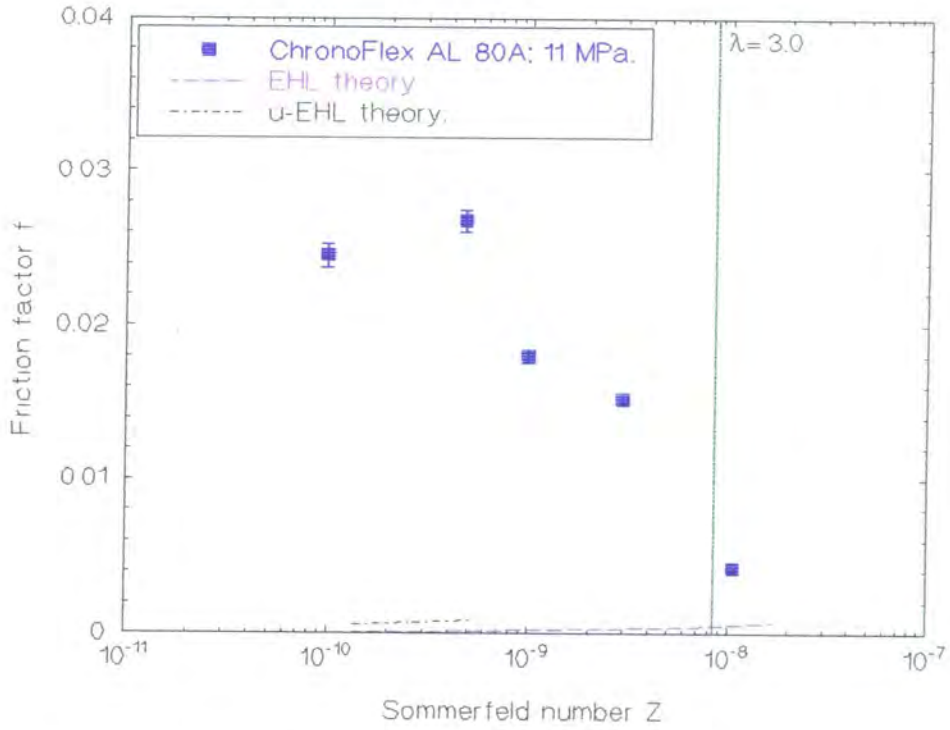

Figure 4.17 Comparison of theory with experiment; Chronoflex cup with ball bearing head. One run on one cup for each result.

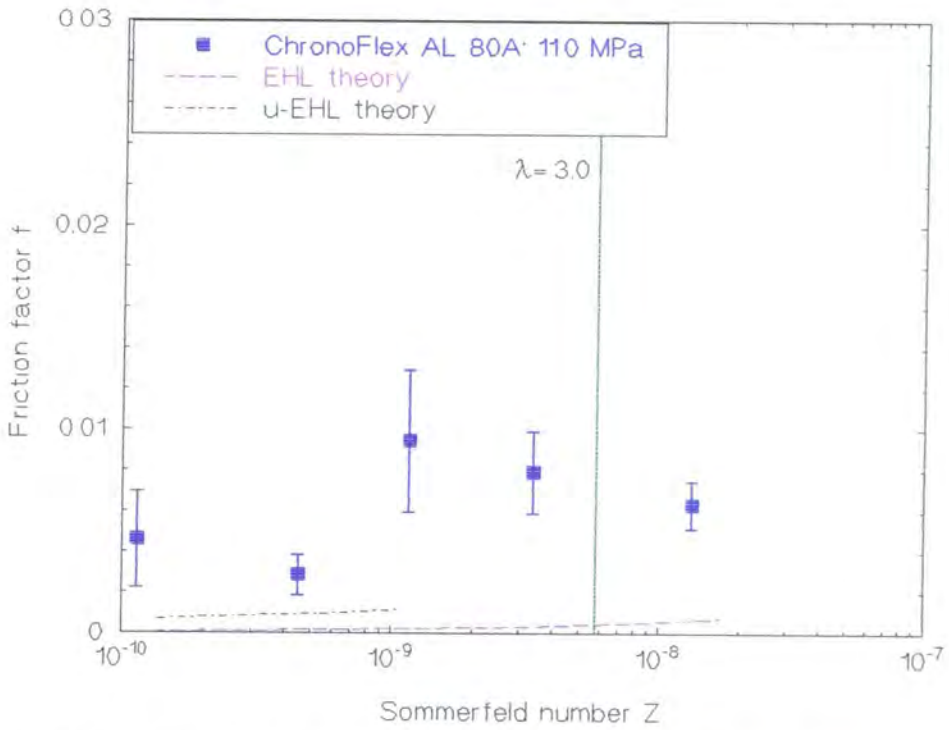

Figure 4.18 Comparison of theory with experiment; Chronoflex cup with Exeter head. Three runs on one cup for each result.

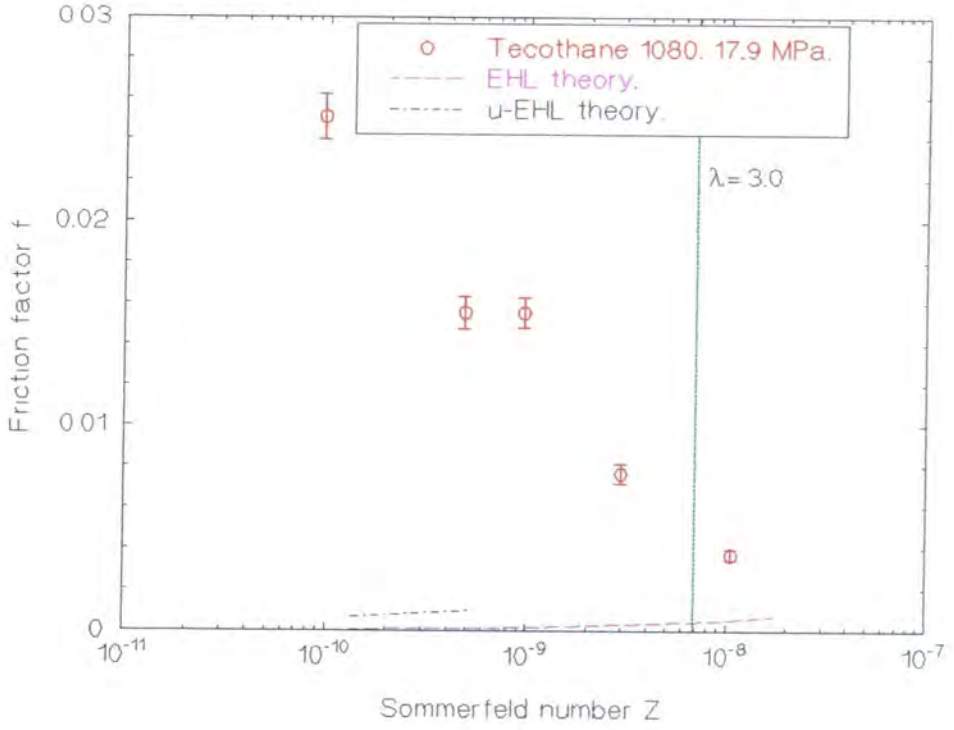

Figure 4.19 Comparison of theory with experiment; Tecothane cup with ball bearing head. One run on one cup for each result.

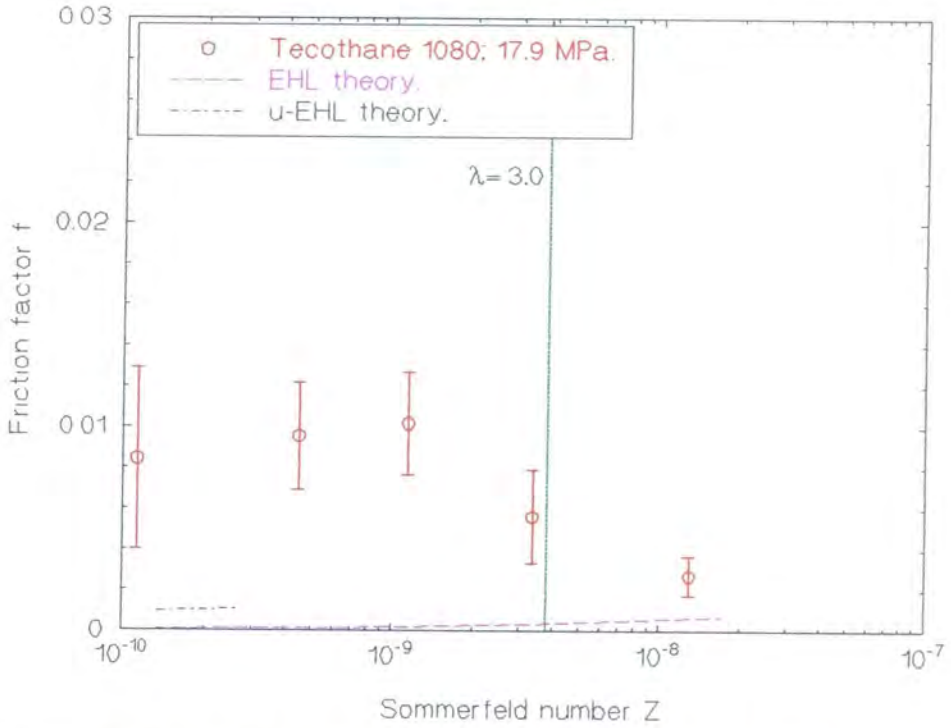

Figure 4.20 Comparison of theory with experiment; Tecothane cup with Exeter head. Three runs on one cup for each result.

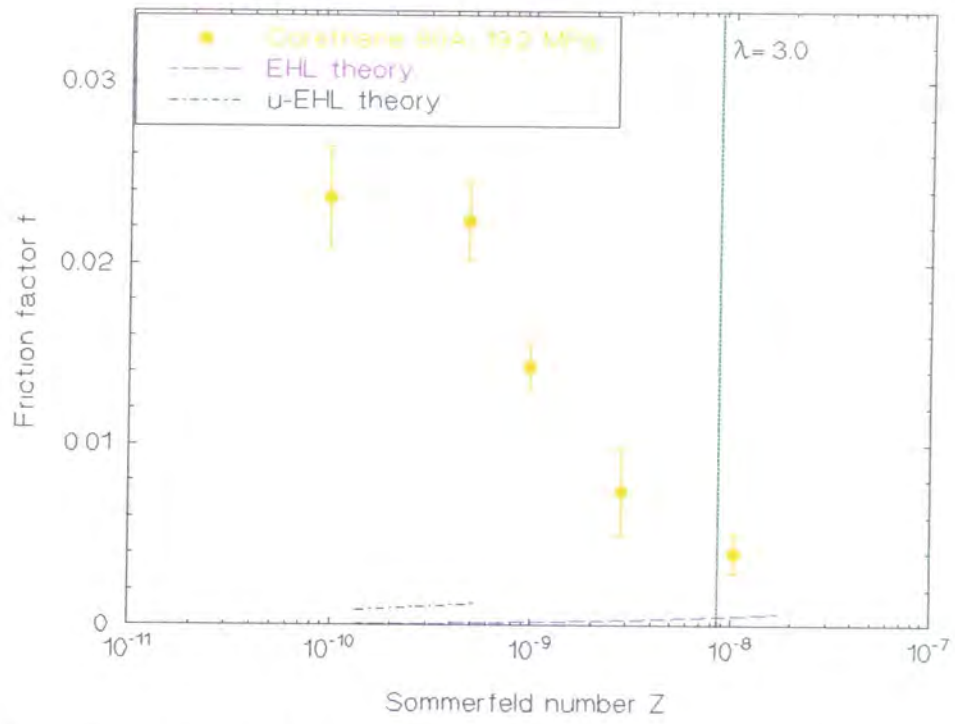

Figure 4.21 Comparison of theory with experiment; Corethane cups with ball bearing head. Two runs on each of two cups for each result.

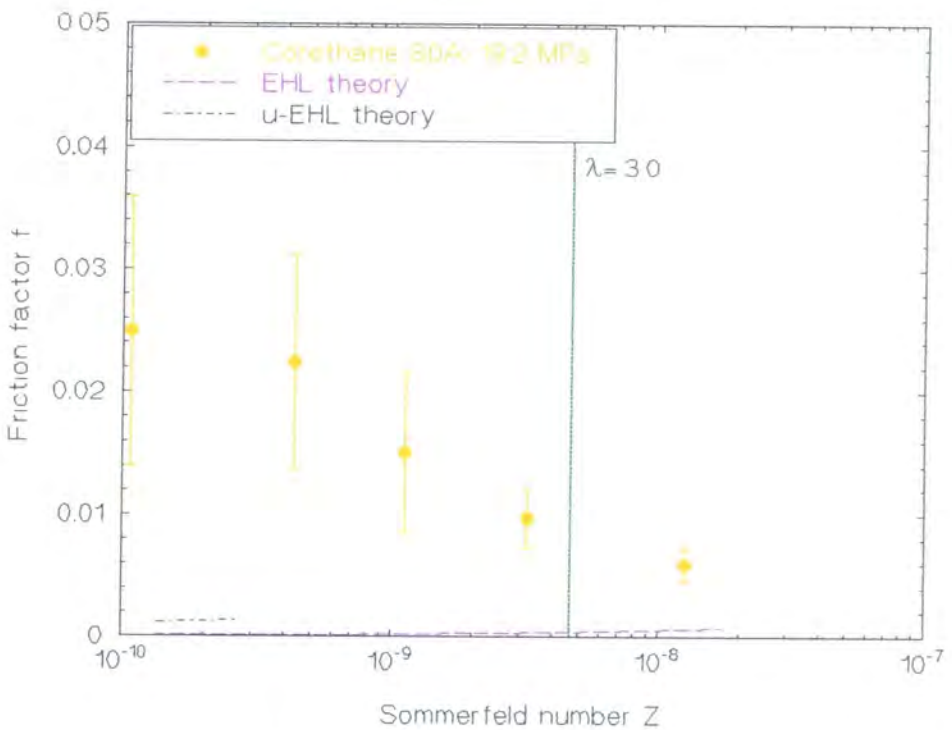

Figure 4.22 Comparison of theory with experiment; Corethane cups with Exeter head. Three runs on each of two cups for each result.

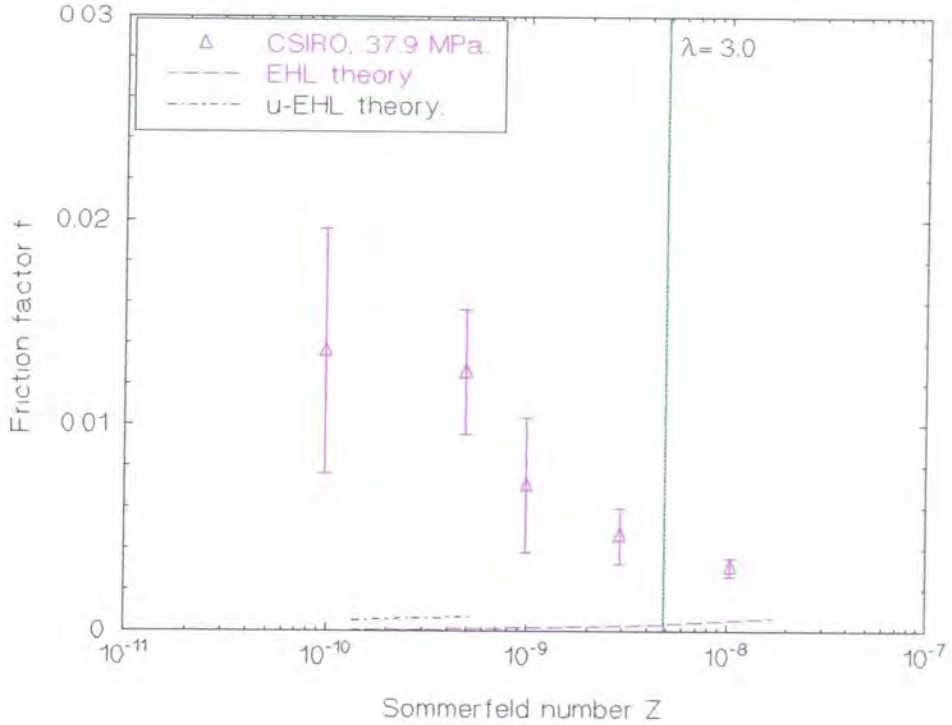

Figure 4.23 Comparison of theory with experiment; CSIRO cups with ball bearing head. One run on each of two cups for each result.

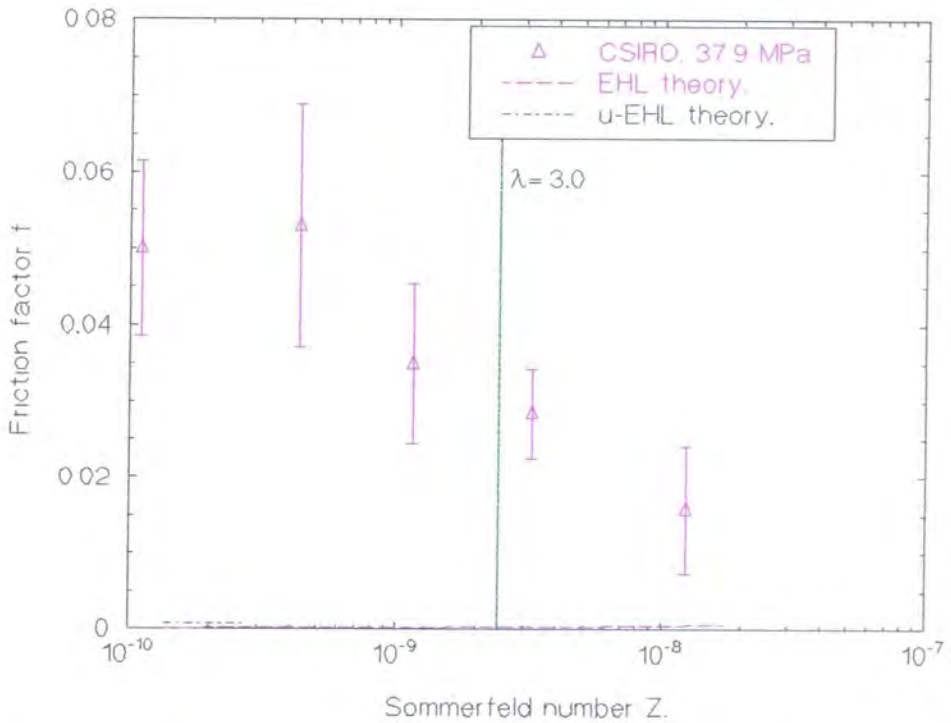

Figure 4.24 Comparison of theory with experiment; CSIRO cups with Exeter head. Two runs on each of two cups for each result.

Four PUs were used, as detailed in Table 4.5. These cups were tested using both the Exeter and ball bearing heads, and the experimental results compared with theory in the normal way (Figures 4.17 to 4.24). These Stribeck plots show the cups generally performed poorly with mixed lubrication, hence with little or no agreement with theory.

	Chronoflex E_2: 11.0 MPa		Tecothane E_2: 17.9 MPa		Corethane 80A E_2: 19.2 MPa		CSIRO E_2: 37.9 MPa	
R_2 /mm	16.12		16.05		16.04		16.04	
h_t /mm	1.88		1.95		1.96		1.96	
σ_2 /μm	419		380		430		242	
λ_2 /μm	100		100		100		100	
Head used:	BB	EX	BB	EX	BB	EX	BB	EX
R /m	1.02	1.60	1.47	3.09	1.53	3.35	1.51	3.24
a /mm	14.2	15.6	14.1	16.5	14.0	16.5	12.1	14.2
S_t	0.93	0.85	0.94	0.81	0.95	0.81	1.10	0.94
τ_{max} /MPa	0.91	0.74	0.95	0.66	0.96	0.66	1.34	0.93
γ_{max}	0.22	0.18	0.14	0.10	0.13	0.09	0.10	0.07
h_{min} /μm *	0.097	0.117	0.100	0.137	0.100	0.139	0.081	0.111
$h_{r,min}$ /μm *	0.018	0.018	0.014	0.015	0.012	0.012	0.014	0.015

Table 4.5 Design parameters and minimum film thickness results for the cups used to assess the effect of layer modulus. Heads used: BB -31.74 mm ball bearing; EX -31.92 mm Exeter head. * when η=0.001 Pa s. (Those parameters not detailed here are the same as for the Exeter head case, Table 4.2.)

If all the Exeter head results are plotted on the same axis then an interesting trend is observed (Figure 4.25). The most compliant Chronoflex cup performs well (the only low friction result from this series of experiments), whereas the other cups perform with higher friction, which increases with increasing layer modulus. Clearly asperity contact and mixed lubrication is predominant. Increasing modulus will lead to a decrease in the effectiveness of EHL and μ-EHL mechanisms, a reduction in lubricant film thickness,

and hence an increase in asperity contact. The theory predicts only small variations in film thickness between these cups, especially μ-EHL film thickness predictions (see Table 4.5). Only a small increase in the number of asperity interactions is required for large increases in friction factor. However, the film thickness estimates do not correctly predict the experimental ranking of these cups, whereas layer conformity does. Note that, with the exception of the Chronoflex cup, all the other cup /Exeter head combinations are highly conforming with small radial clearances of typically 0.08 mm. Although highly conforming contacts favour the generation of thick films, they will be far more susceptible to imperfections in the bearing form. Thus it seems there is a practical limit to increasing conformity, beyond which mixed lubrication predominates.

The combined experimental results using the ball bearing head shows a less distinct but intriguing trend (Figure 4.26) Using the ball bearing rather than the Exeter head the conformity of the contact is considerably reduced and the bearing surface is an order of magnitude rougher. The softer Chronoflex cup significantly worsens and the harder CSIRO cup significantly improves (relative to their respective Exeter head results). The net result is a less distinct but opposite trend, compared with the Exeter head. The softest cup now performs with the highest friction, whereas the hardest cup performs with the lowest friction. Once again the theory, which takes in to account all design factors including conformity, roughness and compliance can not predict the experimental results. A possible explanation for this trend reversal is that the clearance of the soft Chronoflex cup has become too large and the effectiveness of the EHL mechanism has decreased. In contrast the conformity of the other cups is more optimal with the ball bearing head, but the harder CSIRO cups out perform the others by virtue of their smoother surfaces.

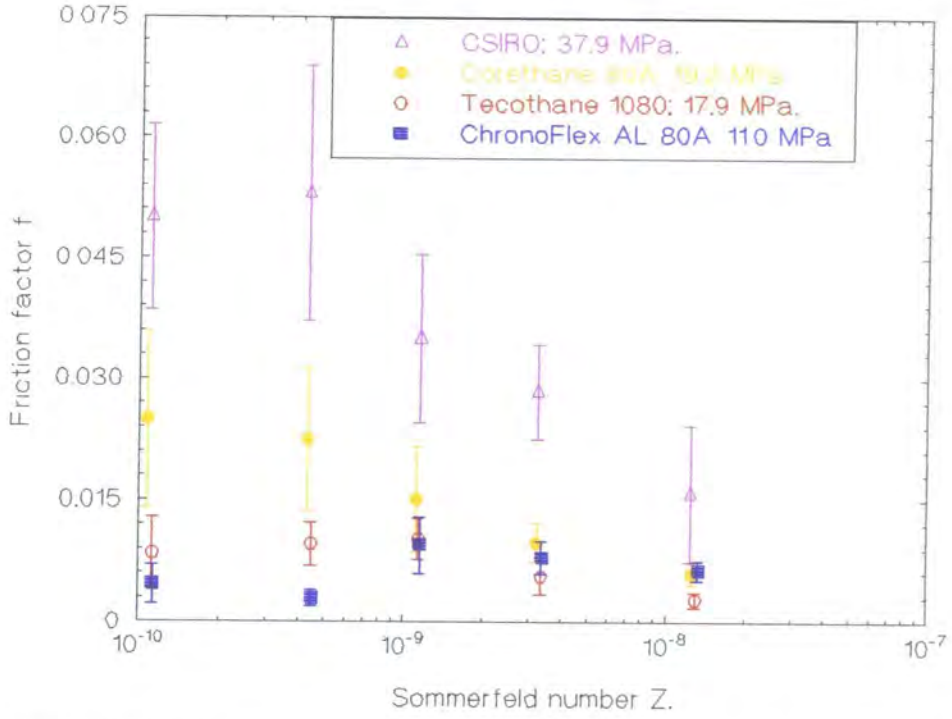

Figure 4.25. Effect of layer compliance; four cups of different modulus with the 31.92 mm Exeter head. See Figures 4.17 to 4.24 for the number of test runs for each result.

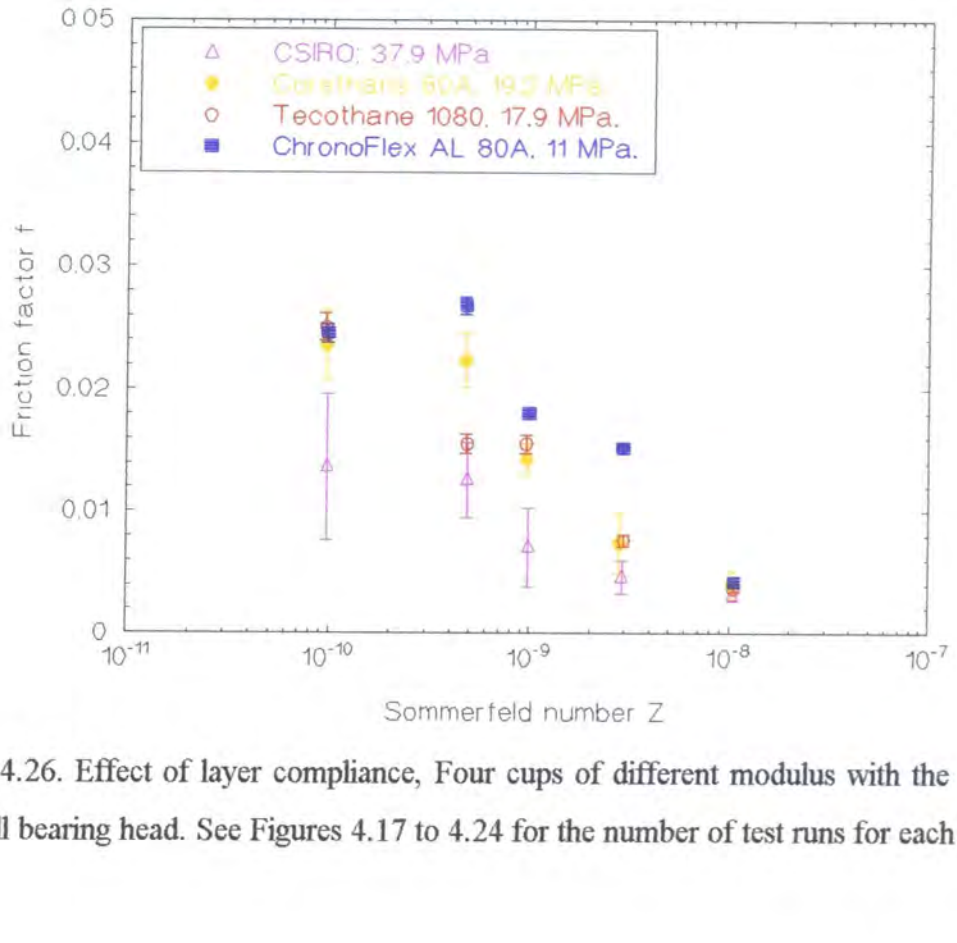

Figure 4.26. Effect of layer compliance, Four cups of different modulus with the 31.74 mm ball bearing head. See Figures 4.17 to 4.24 for the number of test runs for each result.

In any event, the CSIRO/ball bearing result is particularly notable. For the first time low friction has been demonstrated experimentally with an elastic modulus of 37.2 MPa, which is a significantly harder PU than used by previous researchers. Reference to Table 4.5 and the design literature (Dowson *et al.*, 1991 and Yao *et al.*, 1994) confirms that increasing $\mathbf{E_2}$ decreases the shear stresses and shear strains in the layer, making it less susceptible to debonding and fatigue failure.

4.2.7 Start-up friction.

Caravia *et al.* (1993) indicated that start up friction in a compliant layer contact could be very high, and that this may lead to early failure of the joint. Thus the objective of this set of experiments was to assess the extent of the problem in a real compliant hip under physiological conditions. During the normal operation of the Durham friction simulator, at the start of each run the load is applied to the test component, and the computer then waits for the operator to start the extension motion before the data capture commences. Since the 'reverse cycle' starts during the high load stance phase of the cycle (see Figure 3.14) this gives the opportunity to evaluate the effects of preloading the test cup. This is achieved by delaying the start of the motor for the required preload time. Only reverse frictional torque $\mathbf{T_{ri}}$ can be measured in this way, not forward frictional torque $\mathbf{T_{fi}}$. Since high friction at start up after preloading was expected, the contribution from eccentric loading was considered to be relatively small and thus the error in using only $\mathbf{T_{ri}}$ to calculate friction factor was negligible.

The head/cup combinations used are given in Table 4.6. The first four complete cycles for each combination were recorded, although in all cases $\mathbf{T_{ri}}$ data from only the first two cycles are presented (Figures 4.27 to 4.30) since the 2^{nd}, 3^{rd}, and 4^{th} cycles were all

similar. The friction factors, found from the first frictional torque data point $\mathbf{T_{r1}}$ of the first cycle, are plotted against preload time in Figure 4.31.

Acetabular cup	Femoral head.	Start-up friction factor. at t mins of 2000 N preload.				
		t=1	2	5	10	20
Unconditioned cup **N246** (R_2=16.2 mm)	Exeter head (R_1=15.94 mm)	0.34	0.48	0.52	0.52	0.55
Unconditioned cup **N246** (R_2=16.2 mm)	DLC Exeter head (R_1=15.98 mm)	0.07	0.09	0.22	0.34	0.43
Conditioned cup **soft2*** (R_2=16.13 mm)	Exeter head (R_1=15.94 mm)	0.06	0.16	0.20	0.23	0.43
Conditioned cup **soft2*** (R_2=16.13 mm)	DLC Exeter head (R_1=15.98 mm)	0.08	0.17	0.20	0.30	0.29

Table 4.6. Start-up friction results. (*Refers to cups immersed in Ringers solution at 37° C for several months. The effect of 'conditioning' or moisture absorption is discussed in the next section.)

In general the results show that as relative motion starts the frictional torque is high, but that this quickly reduces within one cycle, to the extremely low values expected from compliant cups. Two characteristics have been used to differentiate between the material couples, the initial friction factors, and the rate at which the frictional torque decreases during the loading phase.

The unconditioned cup / Exeter head develops very high frictional torque which remains high throughout the period of loading, Figure 4.27. If a DLC coated head is used with the unconditioned cup then the initial frictional torque is lower (especially with small preload times) Figure 4.28, and it reduces still further as fluid is entrained during the lower load swing phase.

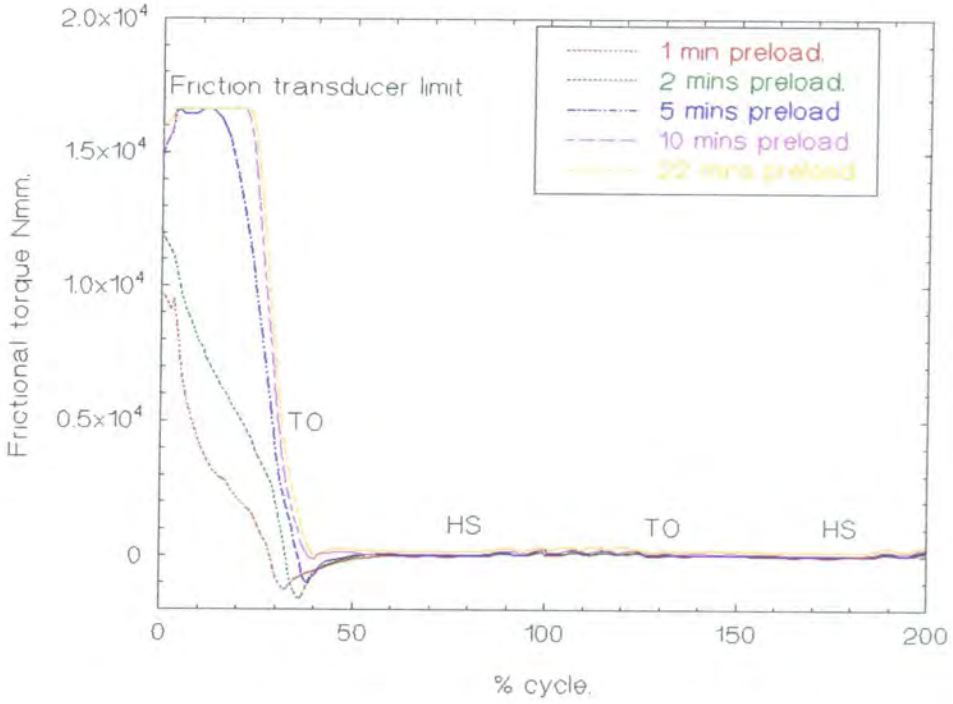

Figures 4.27 Start-up friction results; unconditioned cup N246 with the Exeter head.

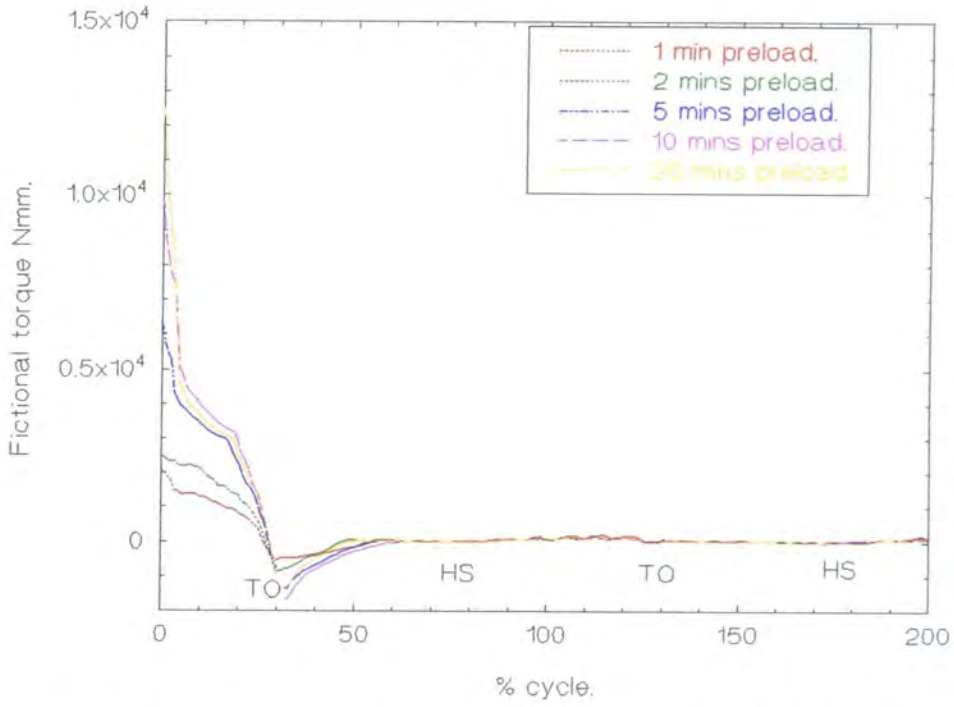

Figures 4.28 Start-up friction results; unconditioned cup N246 with the DLC coated head.

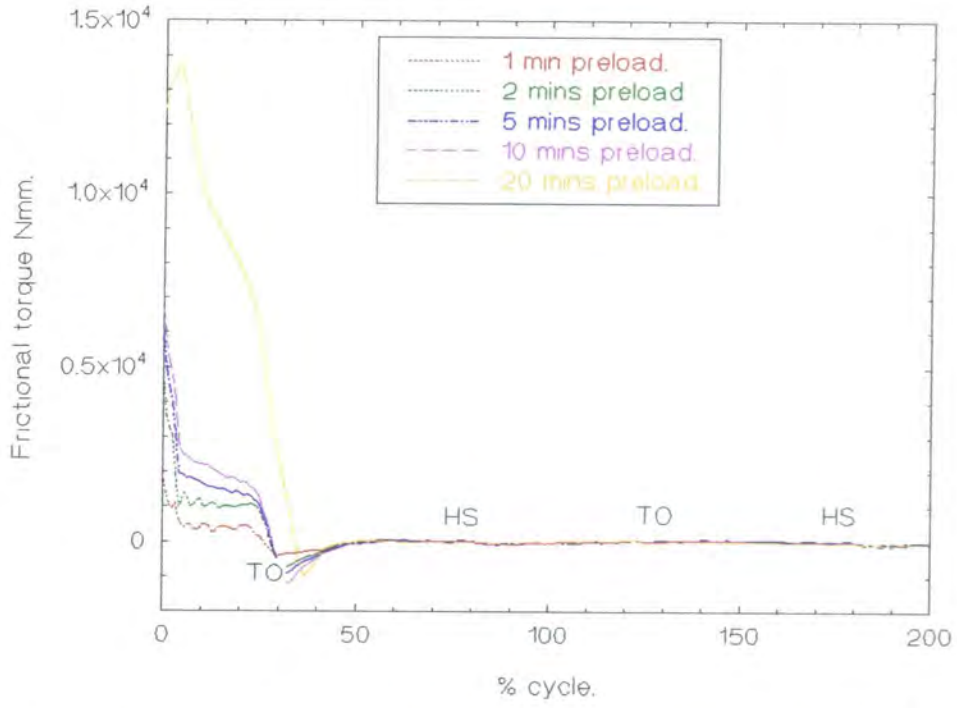

Figures 4.29 Start-up friction results; conditioned cup soft2 with the Exeter head.

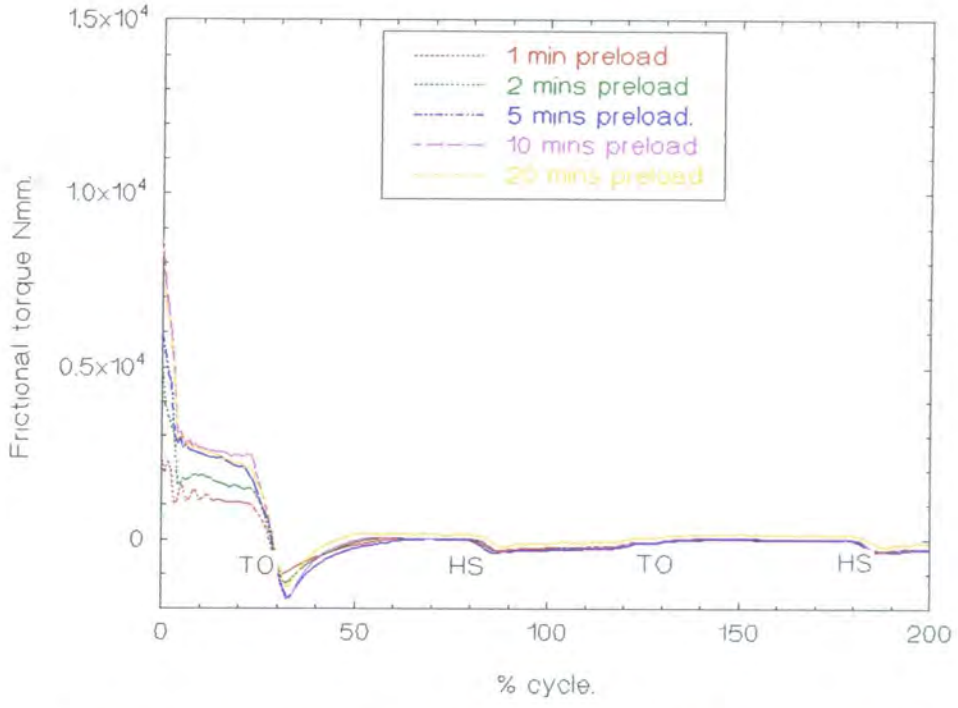

Figures 4.30 Start-up friction results; conditioned cup soft2 with the DLC head.

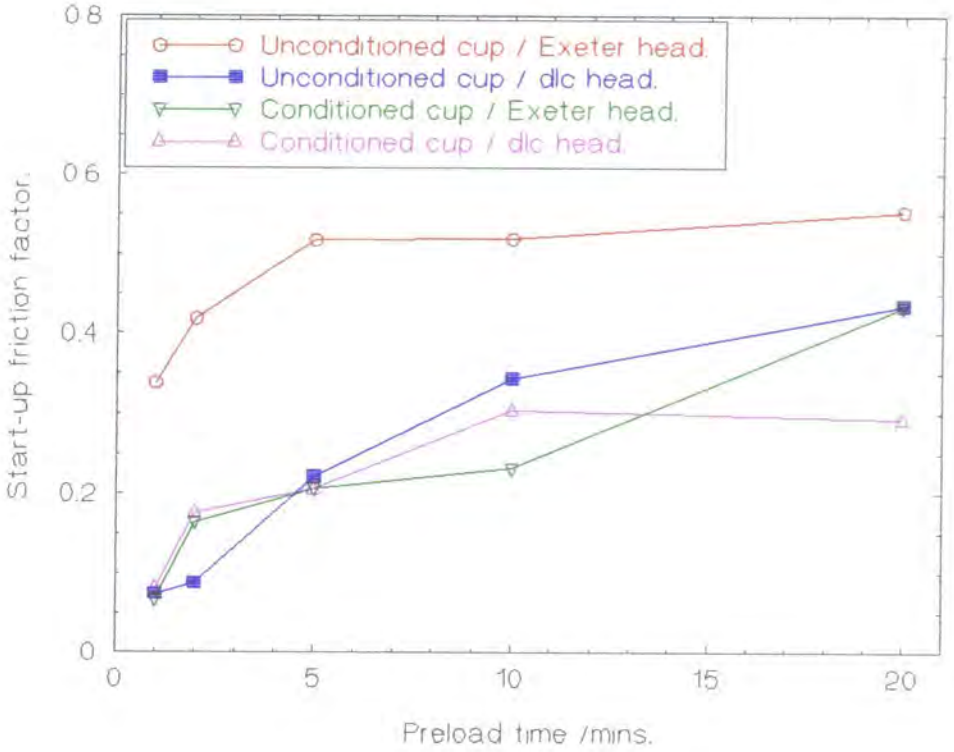

Figure 4.31 Effect of preload time on the start-up friction for different cup/head combinations.

The conditioned cup, Figures 4.29 and 4.30, develops similar initial frictional torque values to the unconditioned cup / DLC head combination. However the frictional torque quickly reduces to a lower near constant value for the remainder of the stance phase. The exception to these observations is the 20 mins preload result with the Exeter head. There is little to differentiate between head types with the conditioned cup.

4.2.8 Effect of Moisture Absorption.

PU absorbs approximately 3% moisture when immersed in an aqueous environment, which modifies the material properties (see Section 2.3.1 and 5.3). Some of the latter experiments were conducted using cups which were 'conditioned', by immersion in Ringers solution for more than 96 hours at 37°C. These included the start-up experiments, which demonstrated reduced friction for conditioned cups when compared

with cups which were not conditioned. Since surface contact is predominant it seems conditioning modifies the asperity interaction. The objective of this set of experiments was to compare the effect of conditioning on a cup known to perform with low friction and near fluid film lubrication, with a cup which was shown to operate with higher friction and mixed lubrication during steady state testing. Two C75D/C80A cups were considered; soft2 (used unconditioned in Section 4.2.3) and coreA (used unconditioned in section 4.2.6). These cups were conditioned and Stribeck analyses conducted in the normal way (Figures 4.32 and 4.33).

Conditioning had no measurable effect on the performance of soft2 (which already enjoyed near full fluid film lubrication), but a reduction in friction was observed after conditioning coreA. It seems probable that conditioning has modified either the surface energy, or contributed in some way to an enhanced boundary lubrication mechanism, leading to reduced adhesion between surface asperities. It is unlikely that the absorbed moisture would become available for lubrication in a mechanism similar to that thought to be important in cartilage (Mow *et al.*, 1990). This is a very significant result, as it illustrates the potential for improvements in boundary lubrication of PU surfaces.

4.3 Discussion of the friction results -hips.

4.3.1 Discussion of steady state friction results.

During this study, more steady state friction experiments have been conducted than have been previously reported in the literature. Not only was friction measured, but also a range of other parameters, enabling a comparison with the current EHL and μ-EHL

theory for a large number of joints. Although a good agreement between theory and experiment is found in some cases, in others little correlation is observed. Most of these joints performed with very low friction, far lower than conventional joints, although it is clear that some asperity contact is occurring especially with low viscosity lubricants. Thus the lubrication regime may be between fluid film and mixed in some cases, and in others predominantly mixed. The use of the theory implicitly assumes full fluid film lubrication, which may not be occurring. However, the fluid film theory may still be of some use, since in mixed lubrication a decreasing film thickness will increase the incidence of asperity contact. Hence comparison of film thickness estimates should reliably rank the designs and predict the observed experimental trends.

Considering only results for the cups lubricated with water, and excluding the R-series cups due to out of roundness, the experimental friction factor is plotted against EHL and, where evaluated, μ-EHL film thickness predictions (Figure 4.34). Neither comparison ranks the experimental results correctly, nor do they indicate a film thickness below which significant asperity contact and high friction occurs. Clearly comparing experiment with theory based on fluid film lubrication is not useful in this case.

Spikes (1996) points out in his recent review of mixed lubrication, that modelling the transition between the established EHL and boundary mechanisms is still in its infancy. For example, μ-EHL modelling does not take in to account the possibility of film breakdown and load sharing by asperity contact. Bearing surface topography will influence both fluid film formation and asperity load carrying, and as such is a particularly important parameter. Although the NOP techniques used here give easy visualisation of the surfaces and extensive data, obtaining useful parameters to feed in to

the models requires careful consideration. For example the μ-EHL film thickness is sensitive to λ_2, but in the absence of any obvious periodicity defining λ_2 is a source of inaccuracy.

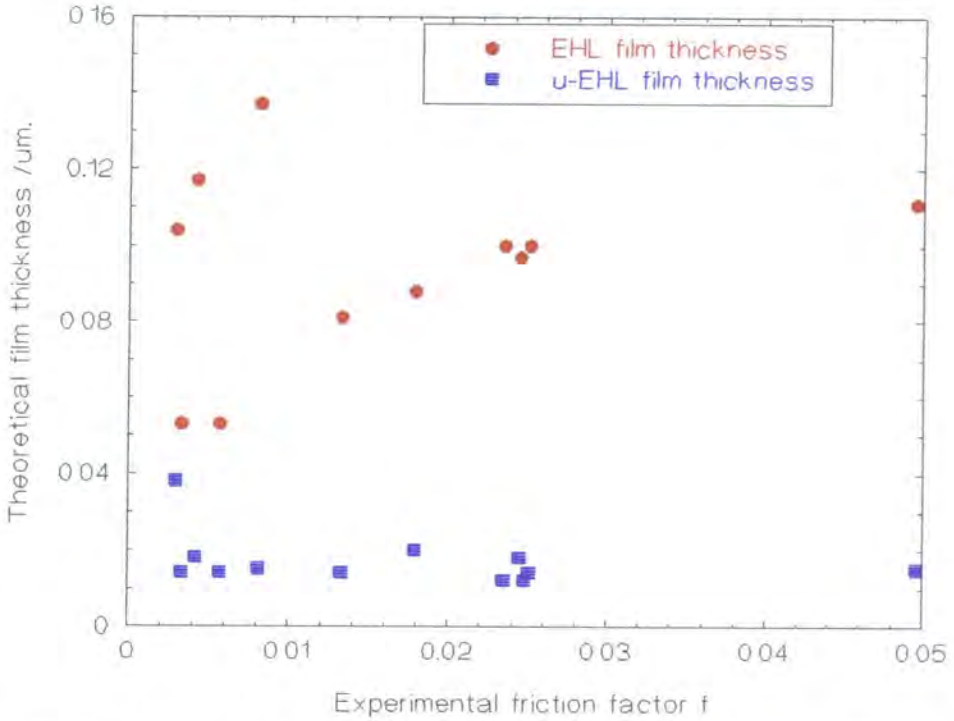

Figure 4.34. Comparison of theory with experiment. Film thickness estimates do not correctly rank the experimental results, nor do they indicate a critical film thickness below which asperity contact and higher friction occurs.

Another source of error is the measurement of the internal dimensions of the cups. This affects the equivalent radius and thus the EHL film thickness estimate. The error in the measurement protocol, discussed in Section 3.5, depends largely on the out of roundness of the cup, and although ±0.04 mm is typical it can be as much as ±0.1 mm.

No matter how accurately the bearing is characterised before it is tested, a third source of error is introduced as the bearing is loaded. A cup may be manufactured with perfect sphericity, but as soon as load is applied the bearing surface will creep, probably on both a micro and macro scale. This will change the effective equivalent radius, layer thickness,

and may also affect surface topography. For example, after loading a 2 mm thick layer cup for 1 million cycles the layer thickness was found to reduce by ≈0.6 mm, and the cup radius change in the contact area (Section 5.4). No account of this creep behaviour has been taken in the theoretical estimates of film thickness.

Comparisons with EHL and μ-EHL theory are not worthwhile for this application, since the lubrication regime falls between fluid film and mixed lubrication, and small errors in the bearing characterisation lead to large errors in film thickness estimates. However, several important design recommendations can be made from an evaluation of the experimental results.

Clearance between head and cup is not critical, so long as it isn't so small that significant contact occurs, due either to a grabbing type mechanism or an inability to tolerate out of roundness of the bearing surface. For 32 mm cups a radial clearance of 0.08 mm is too tight, whereas a radial clearance of between 0.10 and 0.25 performs well so long as other design criteria are met. Bearing form is important, as out of roundness can lead to asperity contact. Significant out of roundness can be tolerated better by large clearance bearings, although there is a trade off with increased contact stress (with the associated problems of increased susceptibility to creep and mechanical failure).

Head size and surface topography are also considered. The results indicate that head size may not be critical, contrary to theory. Both 32 mm and 22 mm cups perform with very low friction and near fluid film lubrication (although 28 mm cups give unexplained high friction results). In general, bearing roughness should be minimised. From the limited

results σ_2 values below 0.25 μm (R_a values typically below 0.20 μm) give the best results.

Layer modulus is more important than alluded to by theory. However it is difficult to recommend an optimum layer modulus since the experiments were conducted on cups with clearances which were too small and with rough bearing surfaces. Corethane 80A has generally performed well and thus still remains the preferred material. Significantly, a harder material with an elastic modulus of almost 40 MPa also performed well under certain circumstances.

In conclusion although a poor correlation between fluid film lubrication theory and experimental results is reported, useful design information has been evaluated. The design of compliant bearings is less critical than previously thought (Dowson *et al.*, 1991, Yao *et al.* , 1994), particularly with respect to design clearance. However small radial clearances below 0.1 mm, out of roundness, and bearing roughness above 0.25 μm should be avoided. PU with a modulus of 20 MPa will perform well, but harder grades may also be considered.

4.4.2 Discussion of start-up friction and conditioning results.

Caravia *et al.* (1993a) assessed start-up friction developed between a thin polyurethane layer and several types of indenter using a pin on plate rig. They used a constant contact stress of 2 MPa and a sliding velocity of 8 mms^{-1}. The indenter was loaded for between 5 s and 400 s and the peak friction measured using water as a lubricant. In contrast, this simulator experiment used a dynamically applied load with a maximum contact stress of

7.3 MPa, a sinusoidal sliding velocity of maximum 34 mms^{-1}, and a preload applied for between 60 s and 1200 s.

This experiment is more physiologically accurate than those conducted by Caravia. However, loads of 2 kN are unlikely to be applied for durations exceeding 60 s when the joint is perfectly still. In normal joint use, any loads applied to the joint at rest will be small, and in addition when the joint is loaded and nominally not in motion (*i.e.* standing in a queue) the natural tendency for small joint motions may be enough to maintain some degree of lubrication.

Caravia *et al.* (1993a) showed that the start-up friction increased with decreasing indenter roughness and increasing layer modulus. The start-up friction increased with increasing preload time up to 80 s, after which they suggested the squeeze film action reached equilibrium and the friction increased no further. They reported higher values of start-up friction than this study, i.e. coefficients of friction between 0.6 and 1.1 for similar modulus material at 160 s preload. Indenter roughness was found to be particularly important. This was thought to be a result of the rougher indenter trapping pools of lubricant between the asperities, resulting in less asperity contact on initiation of sliding, and in addition a reduced real area of contact.

Unlike Caravia, this experiment has shown a steady increase in start-up friction with increasing preload time throughout the range considered. The squeeze film effect will be negligible beyond one minute of preload. However creep of the compliant layer, resulting in an increase in contact area and even grabbing of the femoral head may explain these

experimental results. The surface roughness of the two heads and two cups used have not been assessed, but little variation between samples would be expected.

In this experiment the conditioned cup gives lower start-up friction than the unconditioned cup, and the DLC coated head gives slightly lower start-up friction than the uncoated head. On conditioning, PUs absorb moisture and this will result in a more hydrophilic surface, which will tend to maintain a more lubricious surface during preloading. In addition the energy of adhesion between surface asperities may be reduced. Clearly, conditioning the compliant layer cup reduces the start-up frictional torque. The slightly improved performance of the DLC coated head may also be explained by a change in surface energy compared with the Exeter head.

This work has shown that friction factors below those suggested by Caravia *et al.* (1993), and below those expected for dry contact, occur when assessed in a worst case physiological simulation. Friction factors of ≈0.1 indicate that some contact between bearing surfaces is occurring. The importance of an effective boundary lubrication mechanism to protect natural cartilage during high load low velocity conditions is widely acknowledged. Such a mechanism is also required for PU compliant layer TJRs, if they are to perform without wear under a variety of load and motion conditions. Both the start-up friction and moisture absorption studies do suggest that preconditioning the joints improves their boundary lubrication mechanism. Recent work by Williams *et al.* (1995) suggests that boundary lubrication may be further enhanced by attracting DPPC (a naturally occurring boundary lubricant) to the bearing surface. Pre-conditioning the prosthesis may be desirable before implantation, although moisture absorption and attraction of naturally occurring boundary lubricants may occur in the body during the

convalescence period after the operation. Understanding and improving the boundary lubrication mechanisms for compliant layer TJRs is an important area which warrants further investigations, using the tools and protocol developed here.

4.5 Friction measurement -knees.

In this preliminary study, the friction has been measured in four compliant layer tibial components using the Durham friction simulator, and the results compared to theory in much the same way as the hip experiments, but using the experimental protocol detailed in Section 3.3.2.2. The objective of this set of experiments was to conduct more physiologically accurate evaluations of compliant layer knees than have been reported in the literature. Tibial components were manufactured as detailed in Section 3.1.3, using two different materials, each with layer thicknesses of 2 mm and 3 mm. The tibial components were conditioned in distilled water at 20°C for more than 96 hours before testing. In addition, a conventional UHMWPE tibial component of the same geometry was tested. Table 4.7 summarises the common design parameters used throughout the experiments. The results are given in Figures 4.35 to 4.39.

The UHMWPE conventional bearing friction results were indicative of mixed lubrication, Figure 4.35. The results were repeatable, and comparable with those of UHMWPE hip prostheses (Unsworth *et al.,* 1995), which gave confidence in the new experimental protocol. A comparison with theory confirmed the experimental observations, that neither EHL nor μ-EHL effects resulted in fluid film lubrication.

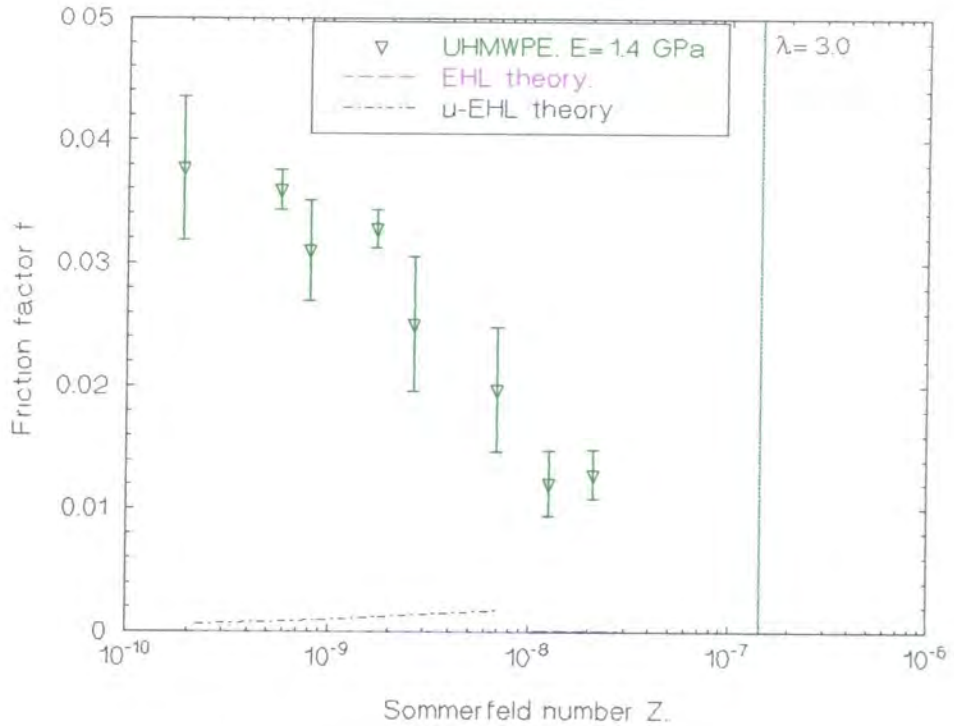

Figure 4.35. Knee friction experiments; Stribeck analysis for conventional UHMWPE tibial bearing. Six runs on one bearing for each result.

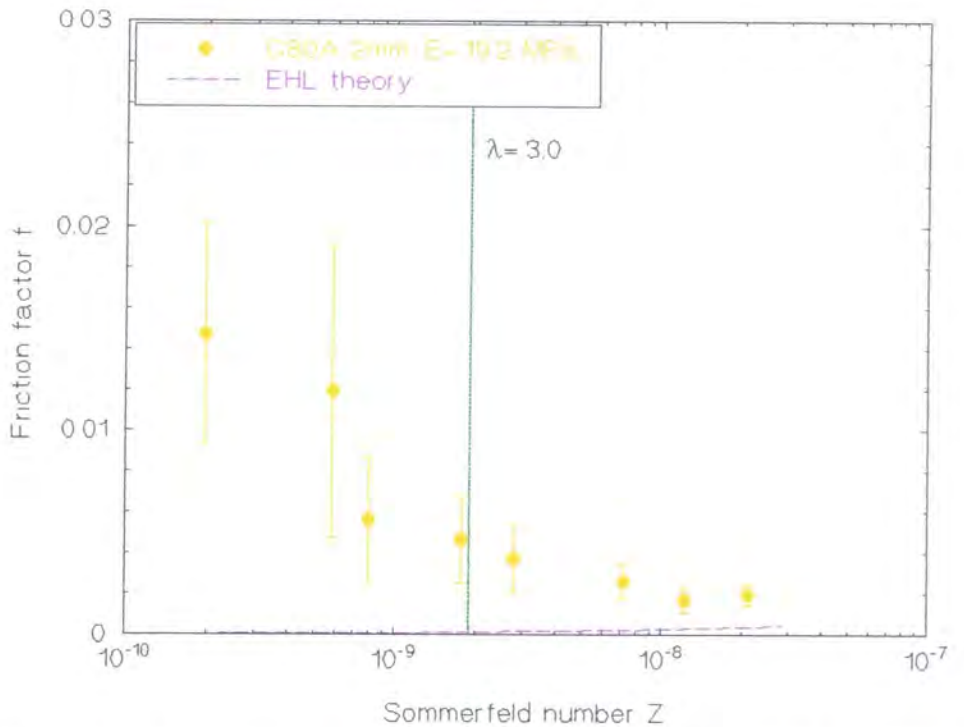

Figure 4.36 Knee friction experiments; Stribeck analysis for Corethane 80A 2 mm compliant layer tibial bearing. Six runs on one bearing for each result.

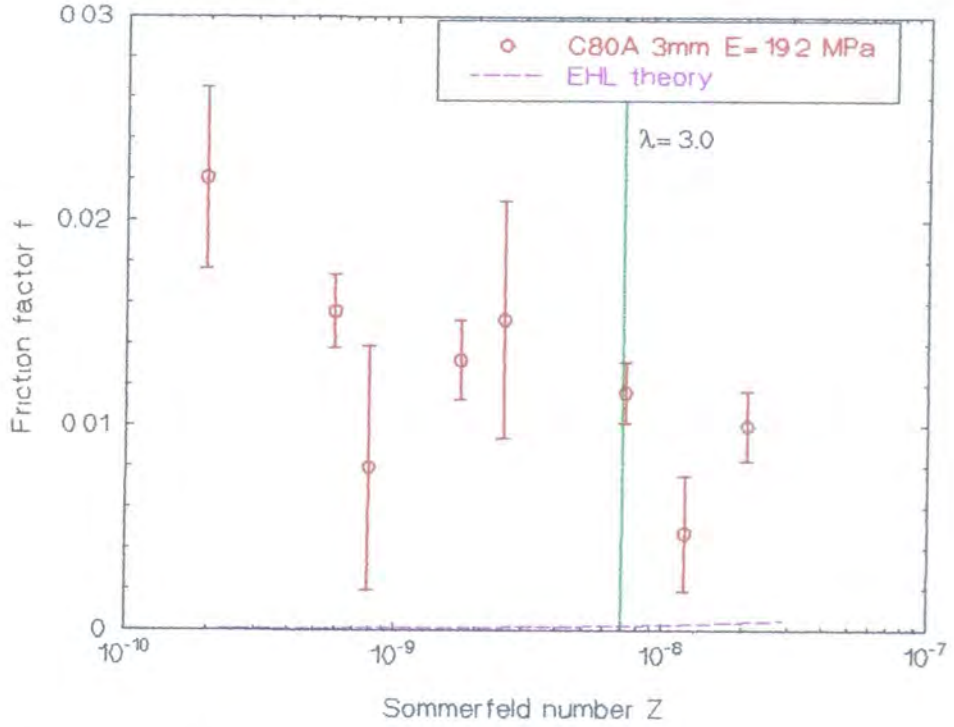

Figure 4.37. Knee friction experiments; Stribeck analysis for Corethane 80A 3 mm compliant layer tibial bearing. Six runs on one bearing for each result.

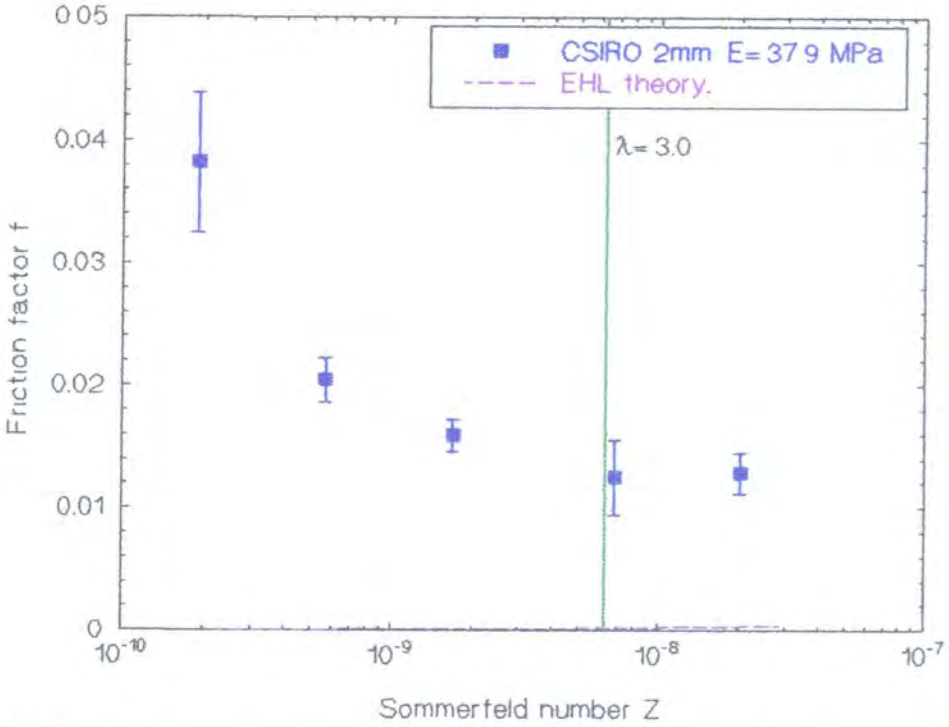

Figure 4.38. Knee friction experiments; Stribeck analysis for CSIRO 2 mm compliant layer tibial bearing. Three runs on one bearing for each result.

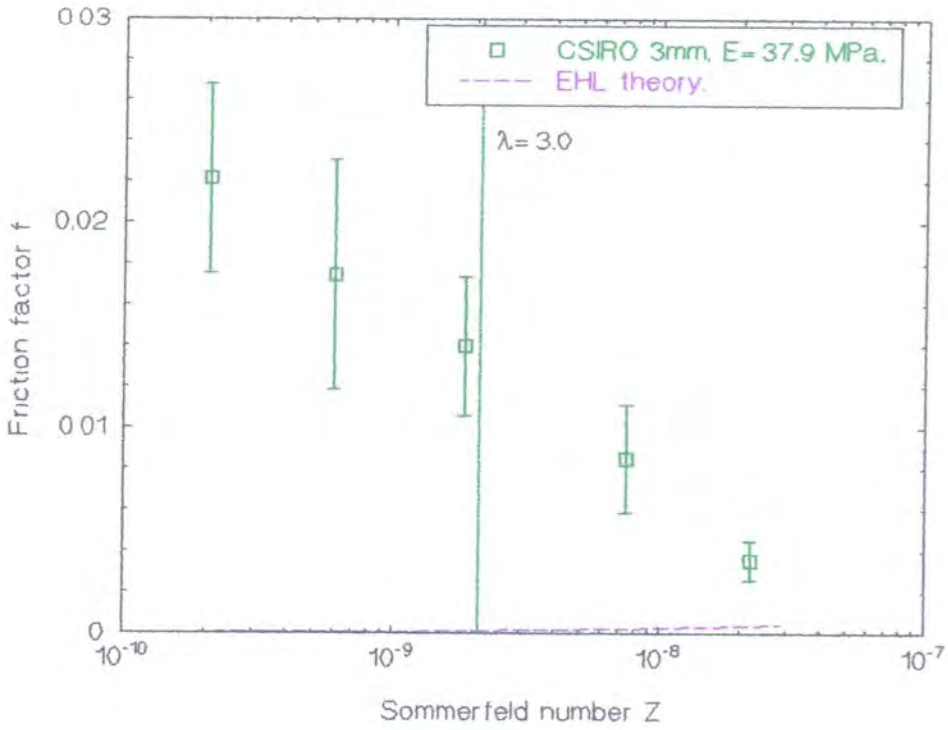

Figure 4.39. Knee friction experiments; Stribeck analysis for CSIRO 3 mm compliant layer tibial bearing. Three runs on one bearing for each result.

Design Parameters.	Knee experiments.
Femoral radius a-p: r_1 /mm	19.6
Femoral radius m-l: r_1' /mm	38.4
Tibial radius a-p: r_2 /mm	-53.4
Tibial radius m-l: r_2' /mm	-50.0
Equivalent Radius a-p: R_x /m	0.031
Equivalent Radius m-l: R_y /m	0.165
Femoral modulus: E_1 /GPa	200
Femoral Poissons ratio: v_1	0.3
Femoral surface RMS: σ_1 /μm	0.040
Entraining velocity: u /mms^{-1}	23.0
Applied load : L /N *	2000

Table 4.7 Common design parameters used in all the knee friction experiments. (* The load is nominally divided equally between each condyle.)

The results from the compliant layer knee bearings were encouraging, with all but one showing lower friction than the conventional joint, Figures 4.36 to 4.39. However in all cases some degree of mixed lubrication predominated. The experimental results were compared with EHL theory but not μ-EHL theory, since in most cases $\mathbf{h_{cen} > \sigma 2}$ or $\mathbf{h_{cen} \approx \sigma 2}$ and thus Equation 4.3 had no real roots or was very inaccurate. To summarise the experimental results, they were ranked in the order of increasing measured friction:

C80A 2 mm < C80A 3 mm ≈ CSIRO 3 mm < CSIRO 2 mm.

None of the experimental results compared well with the EHL theory. However, given that some asperity interaction occurred, thicker lubricant films would result in less contact and lower friction factors. Thus considering the EHL prediction of $\mathbf{h_{min}}$ (Table 4.8) the theory does suggest the ranking observed experimentally, with the exception of the C80A 3 mm bearing. Although the C80A 3 mm bearing has the largest contact area and hence should develop the thickest lubricant film, its poorer performance compared with C80A 2 mm bearing may be explained by its significantly rougher bearing surface.

Design Parameters.	UHMWPE	C80A 2 mm	C80A 3 mm	CSIRO 2 mm	CSIRO 3 mm
E_2 /MPa	1400	19.2	19.2	37.9	37.9
h_t /mm	∞	2.0	3.0	2.0	3.0
σ2 /μm	0.500	0.034	0.123	0.060	0.032
λ_2^* /μm	80	80	80	80	80
a /mm	1.8	4.8	5.7	3.8	4.9
b /mm	4.8	12.5	13.5	10.3	11.6
S_t	1.99	0.76	0.71	0.93	0.82
h_{min} /μm *	0.028	0.031	0.036	0.023	0.029

Table 4.8. Design parameters and theoretical results for the knee friction experiments. (* when η=0.001 Pa s.)

4.6 Discussion of the friction results -knees.

There is little in the literature regarding experimental evaluation of compliant layer knees. Murakami *et al* (1987, 1993) demonstrated fluid film lubrication with a compliant layer tibial bearing with realistic geometry, but did not measure friction. Conversely, Auger *et al* (1993a, 1995a) used a less realistic cylinder on flat line contact model of the knee, but measured friction and conducted Stribeck analyses. They used the Leeds hip function simulator to measure friction under conditions of a dynamically applied load, and sinusoidal motion untypical of the knee joint. Their results showed extremely low friction was attainable. In addition, Auger *et al* (1995b) also reported that a flat tibial component manufactured from a 20 MPa 5 mm layer of Tecoflex 93A showed no visible wear debris after 5 million cycles on a knee simulator, although some delamination and smearing of the bearing surface was observed.

The results reported here are compared with the results presented by Auger *et al.* (1993a, 1995a) for 20 MPa and 6 MPa layers, Figures 4.40 and 4.41. Auger used lower loads and higher velocities and higher viscosity lubricants than the present study, coupled with generally larger contact areas, Table 4.9. The results for the 6 MPa layers were all extremely low, indicating that most of the load was carried by the lubricant. The results for the 20 MPa layer differed between papers (probably due to a slightly different surface roughness characteristics of the cylinder, with the smoother finish improving the results for the 2.5 mm layer, and worsening the results for the 5.0 mm layer) but were higher than the 6 MPa layer, and indicative of mixed lubrication. Comparing the best results (lowest friction) achieved in each study for 20 MPa layers (the C80A 2 mm layer with the

2.5 mm 20 MPa layer in Auger's 1995 study) clearly the results are very similar, Figure 4.42. The Sommerfeld number accounts for the differing velocities and makes for a fair comparison. These results are encouraging, as they demonstrate both general agreement with the literature, and that fairly low friction is possible under low velocity sub-optimal test conditions. Thus if loads, velocities and contact conditions were used which more closely matched those expected *in vivo*, extremely low friction may be obtained experimentally with lubricants of near physiological viscosity. The evaluation of compliant layer knees using more refined and physiologically relevant test conditions would be interesting.

	This Study	**Auger *et al.* (1993a, 1995a)**
Applied Load.	2000 N	1380 N
Applied motion.	±14°	±27°
Maximum velocity.	23.4 mm/s	67 mm/s
Lubricant range.	0.001-0.1 Pa s	0.001-0.49 Pa s (1993) 0.001-0.03 Pa s (1995a)
Femoral component.	r_1=19.5 mm (a-p) r_1'=38.4 mm (m-l)	Cylinder: radius 20 mm, 62 mm long
Tibial component.	r_2=-53.4 mm (a-p) r_2'=-50.0 mm (m-l)	Flat
Contact Area.	19.2 MPa 2 mm: 377 mm^2 19.2 MPa 3 mm: 483 mm^2 37. 9 MPa 2 mm: 245 mm^2 37. 9 MPa 3 mm: 357 mm^2	20 MPa 2.5 mm: 401 mm^2 20 MPa 5.0 mm: 497 mm^2 6 MPa 2.5 mm: 584 mm^2 6 MPa 5.0 mm: 756 mm^2
Theoretical lubricant film thickness.*	19.2 MPa 2 mm: 0.031 μm 19.2 MPa 3 mm: 0.036 μm 37. 9 MPa 2 mm: 0.023 μm 37.9 MPa 3 mm: 0.029 μm	20 MPa 2.5 mm: 0.047 μm 20 MPa 5.0 mm: 0.053 μm 6 MPa 2.5 mm: 0.065 μm 6 MPa 5.0 mm: 0.077 μm

Table 4.9. A comparison of test conditions used to assess compliant layer knees in this study, with those used by Auger *et al.* (1993a, 1995a).(* when η=0.001 Pa s).

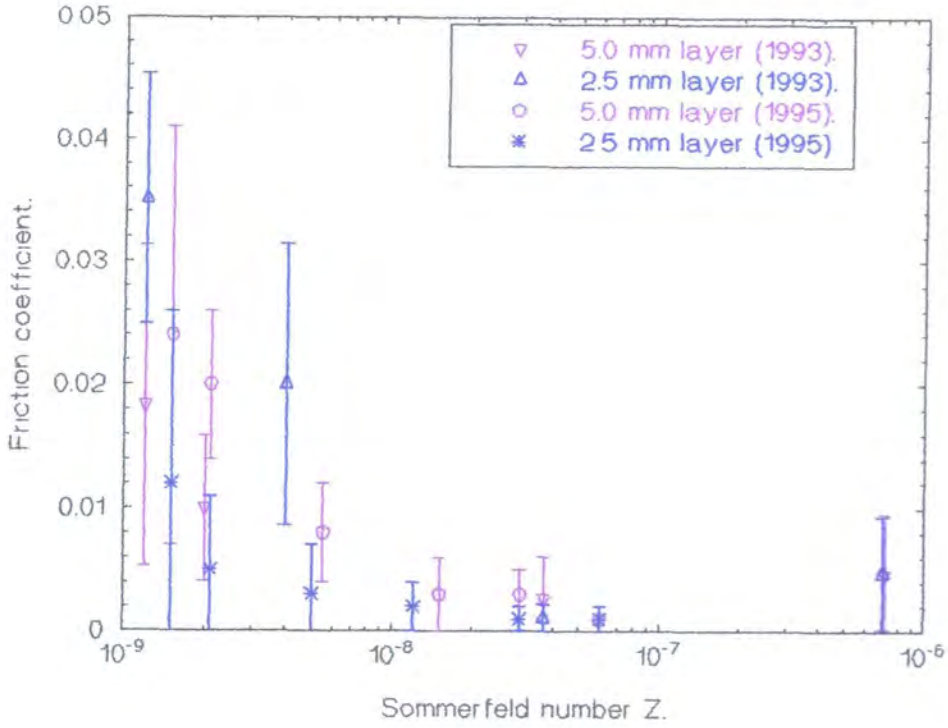

Figure 4.40 Stribeck analysis for Tecoflex 20 MPa compliant layer line contact bearing, after Auger *et al.* (1993a, 1995a).

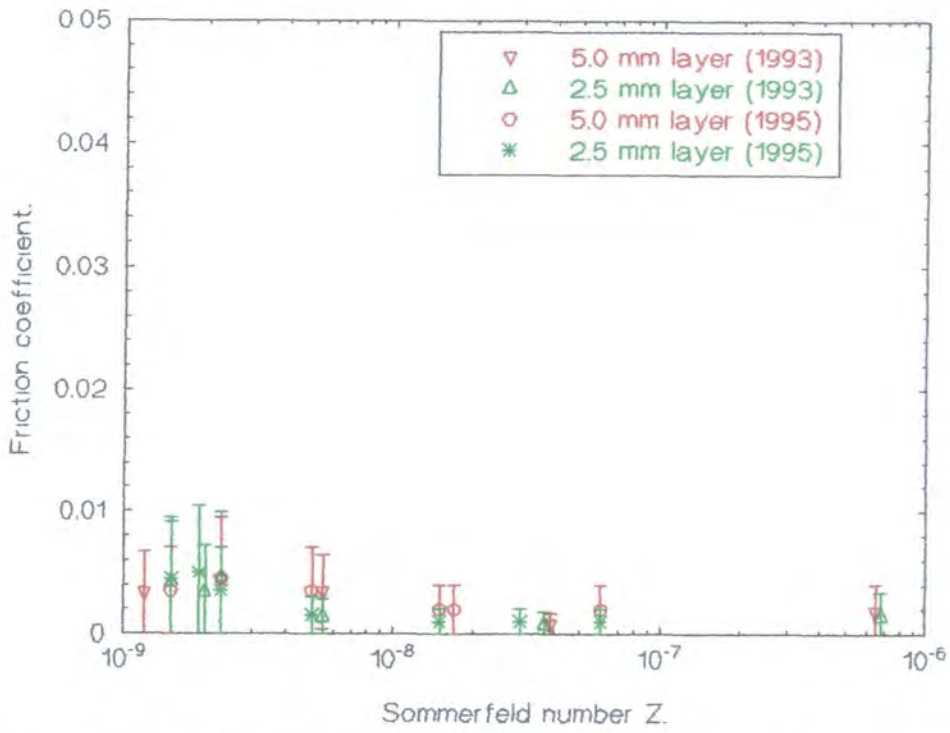

Figure 4.41 Stribeck analysis for Tecoflex 6 MPa compliant layer line contact bearing, after Auger *et al.* (1993a, 1995a).

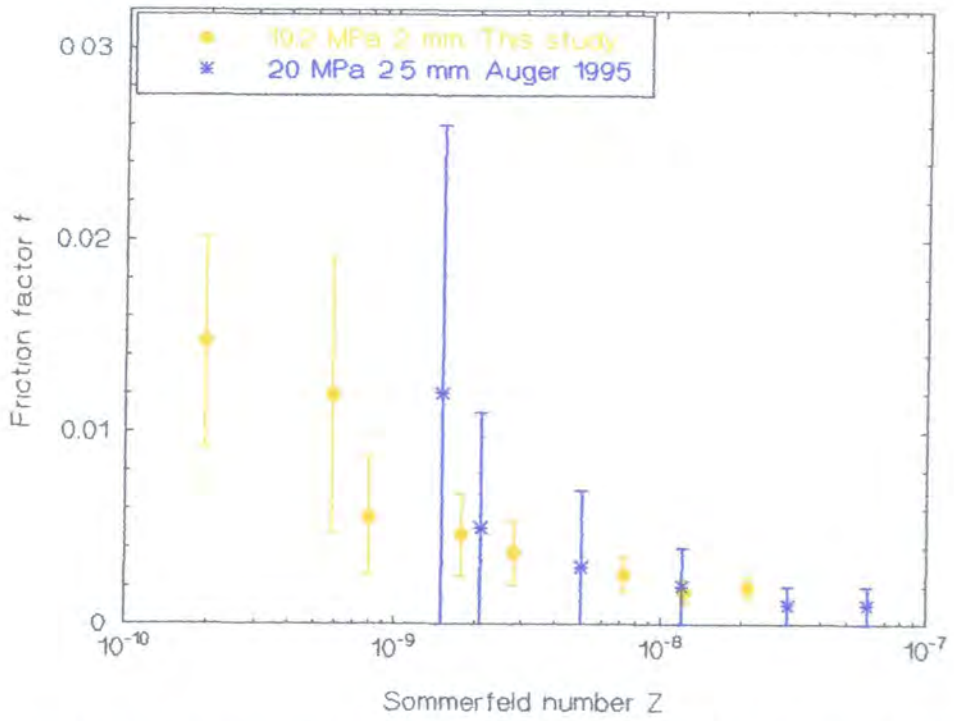

Figure 4.42 Comparison between Corethane 80A 2 mm results, with Auger's Tecoflex 20 MPa 2.5 mm results.

Knee friction measurement could be significantly enhanced. The main problem so far has been mounting a standard femoral prosthesis which has a variable centre of rotation, on the friction simulator which has a fixed centre of rotation. As a result, only the posterior condyles were used with an unrealistically small amplitude of motion. A special femoral component with a profile which reproduces the same contact regime as between a normal femoral and tibial components at 0°-15° flexion (stance phase), but with a fixed centre of rotation, would enable larger amplitudes of swing and hence higher more realistic velocities to be used. In addition the tibial component needs to be mounted to distribute the load evenly between the two condyles. During this experiment slight misalignments when mounting the tibial components may have resulted in an uneven and variable distribution of load between the condyles. However, despite these draw backs in experimental method, further investigations are recommended, especially in conjunction with durability and wear studies using the knee simulator discussed in Part B.

Chapter 5. Adhesion and Mechanical Properties: Results and Discussion.

5.0 Introduction.

Although it was demonstrated in the last chapter that compliant bearings operate with very low friction if designed correctly, it is also necessary to design and manufacture the bearing to withstand the cyclic loads applied *in vivo*. The main aspect of the mechanical performance addressed here is the adhesion of the compliant layer to its rigid backing; a problem which has previously received little attention. The bond between the elastomeric layer and rigid backing was assessed using peel and blister tests; and the influence of materials selection, surface treatments and manufacturing techniques were evaluated. The long term durability of the new bonding technology was subsequently assessed by dynamic loading of acetabular cups using a fatigue testing machine. The objective was to develop a strong bond between the layer and backing which would not fail over the extended life of the prostheses.

The mechanical properties of the materials used have also been examined. The effect of sterilising using irradiation, and of ageing in aqueous environments, has been evaluated by measuring indentation hardness and tensile properties. In addition, acetabular cups have been dynamically loaded and the effect of creep on the bearing dimensions measured over 7.2 million cycles. The overall objective of these experiments was to support the project with materials data, and to increase confidence in the durability of the prostheses.

Throughout the experiments reported here, Student's t-test has been used to compare different data sets. The P statistic is given, and considered significant if $P<0.05$.

5.1 Evaluation of adhesion

Results of compliant layer adhesion tests are presented in three sections. Initially methods of improving the bond strength between UHMWPE and PU were evaluated using the peel test (experiments designated PE#). Next, the adhesion between a rigid PU and a compliant PU was evaluated, again using the peel test (PU#). PU/PU adhesion in acetabular cups were assessed using the blister test (BL#), and finally a servo hydraulic fatigue test machine was used to assess the adhesion performance under dynamic loading.

5.1.1 Evaluation of UHMWPE/PU adhesion using the peel test.

There are several advantages in using UHMWPE as the rigid backing of a compliant layer TJR. UHMWPE has suitable mechanical properties and, in bulk, exhibits good biocompatibility. It is currently widely used for acetabular and tibial bearing designs, and these often incorporate a metal backing. UHMWPE backed compliant bearings could be easily substituted for the all UHMWPE component in these designs. In addition, should the compliant layer fail then a normal UHMWPE bearing surface would be exposed. Although polyolefins such as UHMWPE are difficult to bond due to low surface energy and low reactivity, it would be commercially attractive to develop a patentable process which solved the problem of adhesion between a compliant PU layer and UHMWPE backing.

Peel tests were used to assess the adhesion between UHMWPE and PU[1] using the protocol described in Section 3.3.1, except that a cross head separation rate of only 20 mm/min was used during these early experiments when the interfacial adhesion was relatively poor, instead of 200 mm/min. In addition only maximum peel force $\mathbf{F_{max}}$ was reported, and was used to calculate $\mathbf{G_c}$ values. The results are given in Table 5.1.

The adhesion between PU and untreated UHMWPE was very low, PE#1, and only able to sustain an $\mathbf{F_{max}}$ of 3.2N, equating to a $\mathbf{G_c}$ value of 0.03 kJm^{-2}. As a benchmark, this level of bond strength can be easily peeled by hand with minimal effort. As a result several methods were examined to modify the surface and improve adhesion, and these are reported here. (The chemistry and surface characterisation was conducted by Dr S Edge[2], and the mechanical testing conducted by the author). By promoting a chemical reaction between a more reactive organic molecule and the UHMWPE surface, the characteristics of the surface can be changed without affecting the bulk material properties. This can be achieved in several ways, including photo initiated chemical grafting. This involves the polymerisation of vinyl monomers onto the surface using photochemically activated benzophenone molecules. This technique was used to graft poly(2-hyroxyethylmethacrylate) (HEMA) and poly(acrylic acid) (AA) on to the UHWMPE surface.

[1]Tecoflex 93A was used during these early experiments since Corethane 80A was not available.
[2]Interdisciplinary Research Centre in Polymer Science and Technology, University of Durham.

Test ID	Materials	Details	Results		
			n	F_{max}/N (s.d.)	G_c/kJm^{-2}
PE#1	T93A/UHMWPE	No surface treatment.	10	3.2 (1.4)	0.03
PE#2	T93A/UHMWPE	HEMA grafted	10	12.4 (7.2)	0.11
PE#3	T93A/UHMWPE	No surface treatment	6	1.3 (0.3)	0.01
PE#4	T93A/UHMWPE	HEMA grafted	12	2.8 (1.2)	0.03
PE#5	T93A/UHMWPE	AA grafted.	10	2.6 (1.3)	0.02
PE#6	T93A/UHMWPE	Rough mach'd surface	9	3.0 (1.3)	0.03
PE#7	T93A/UHMWPE	Thick HEMA grafted	11	49.7 (33.7)	0.59
PE#8	T93A/UHMWPE	HEMA/X-linked PU	8	0.9 (1.7)	0.01
PE#9	T93A/UHMWPE	HEMA/linear PU	4	2.3 (0.7)	0.02
PE#10	T93A/UHMWPE	HEMA/isocyanate	8	15.2 (5.6)	0.14
PE#11	C80A/UHMWPE	NH_3 Plasma II	6	18.8 (8.6)	0.18
PE#12	C80A/UHMWPE	O_2 Plasma coating I	6	52.6 (38.8)	0.63
PE#13	C80A/UHMWPE	O_2 Plasma coating II	6	90.4 (65.6)	1.26
PE#14	C80A/UHMWPE	Allylamine Plasma I	6	23.3 (2.7)	0.23

Table 5.1. Peel test results. Evaluation of UHMWPE/PU adhesion, using different methods to improve bond strength.

The effectiveness of the grafting procedure was investigated by conducting two sets of comparative experiments, at different times. In the first set, PE#1 and PE#2, grafting showed a significant increase in $\mathbf{F_{max}}$ from 3.2 N for untreated samples to 12.4 N for HEMA surface modified samples (P=0.003). In the second set, PE#3 to PE#5, again grafting showed a significant increase in $\mathbf{F_{max}}$ from 1.3 N for untreated samples to 2.8 N for HEMA surface modified samples (P=0.001), and to 2.6 N for AA surface modified samples (P=0.011). Contact angle and attenuated total reflectance infrared spectroscopy (ATRIR) showed the presence of the grafting groups on the surface. The reactive HEMA

alcohol and ester groups, and AA acid groups interacted with the urethane moieties to form specific sites for adsorption, thus increasing $\mathbf{F_{max}}$. However, a comparison of the results from the two sets of experiments showed that, although they exhibited the same trend, the second set gave generally lower peel forces than the first, calling into question the consistency of the injection moulding or grafting process.

The effect of a qualitative increase in the surface roughness of the UHMWPE backing was also investigated. Roughly machined untreated UHMWPE blocks were used to manufacture peel test samples, PE#7. This resulted in $\mathbf{F_{max}}$ of 3.0 N, which was not significantly different (P=0.75) from the typical $\mathbf{F_{max}}$ of qualitatively smoother untreated samples, PE#1.

Contact angle and ATRIR measurements suggested that the UHMWPE was not covered with a homogeneous layer of poly(HEMA) by the normal grafting technique. In order to give an insight into the maximum $\mathbf{F_{max}}$ obtainable for the UHMWPE/HEMA/PU interface, a thick (≈1 mm) layer of poly(HEMA) was grafted onto the surface, PE#7. This resulted in a significant (P=0.004) increase in $\mathbf{F_{max}}$ from typically 12.4 N for normally grafted samples to 49.7 N for thick layer HEMA grafted samples, which failed at the PU/HEMA interface. Considering $\mathbf{G_c}$, this resulted in an increase from 0.11 kJm^{-2} for normally grafted samples to 0.59 kJm^{-2} for thick layer HEMA grafted samples.

Having established that the UHMWPE/HEMA bond was stronger than the HEMA/PU bond, methods of improving the weaker HEMA/PU interface were investigated. The possibility of utilising the grafted layer to produce surface bound PU capable of increased interaction with the bulk PU layer was investigated. HEMA grafted UHMWPE was

reacted with a diisocyanate and a macrodiol. Small amounts of X-linked PU (PE#8), linear PU (PE#9), and free isocyanate (PE#10) were identified on the HEMA surface using ATRIR. Neither the X-linked nor linear PU modified surfaces resulted in an increase in peel force when compared with untreated samples (PE#1). However, despite relatively low concentrations, the free surface isocyanate resulted in a significant increase in $\mathbf{F_{max}}$ (P=0.0004) through an increased interaction with the bulk PU layer.

Plasma treatment is often used (Kinloch, 1987) to promote adhesion of polyolefins, e.g. the adhesion of print to low density polyethylene bags. In order to establish the magnitude of possible increases in UHMWPE/PU[3] bond force due to plasma treatment, four sets of UHMWPE blocks were subjected to a proprietary plasma treatment by Advanced Surface Technologies (MA. US). The samples were treated in NH_3 plasma II (PE#11), O_2 plasma plus coating I (PE#12), O_2 plasma plus coating II (PE#13), and allylamine plasma I (PE#14). All showed significant increases (P=0.0001) in $\mathbf{F_{max}}$ when compared with untreated samples (PE#1). The plasma treated surfaces were characterised using X-ray photoelectron spectroscopy (XPS), and the proportion of reactive surface bound amines in total surface nitrogen and carbon were reported (Sheu, 1994) and plotted against $\mathbf{F_{max}}$ (Figure 5.1). Although no clear relationship existed, the general trend was that increases in surface bound amines resulted in improved adhesion, presumably through increased absorption bonding. This approach resulted in the highest peel forces for the UHMWPE/PU system, equating to a $\mathbf{G_c}$ value for PE#13 of 1.26 kJm^{-2}. As a benchmark, the bond strength has been increased to a level which can be peeled by hand, but with some effort.

[3]Corethane 80A became available at this point in the project. It was identified as the preferred material, as discussed in Section 2.3, as so was used for these and most subsequent experiments.

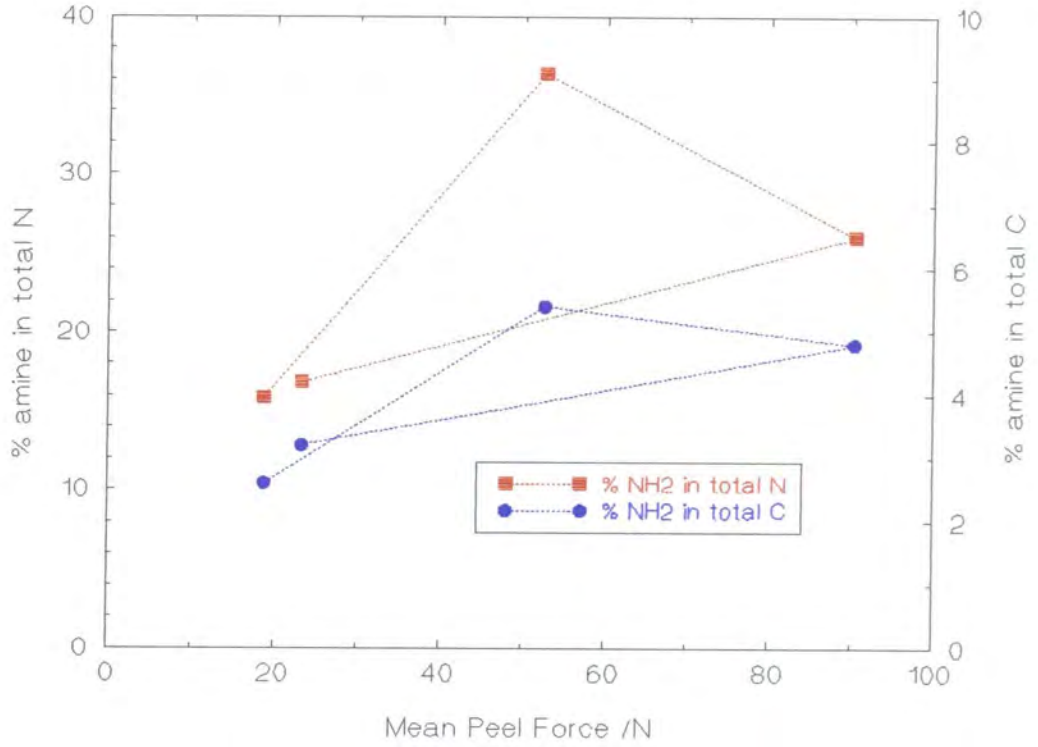

Figure 5.1 Effect of surface bound amines on the UHMWPE/PU bond.

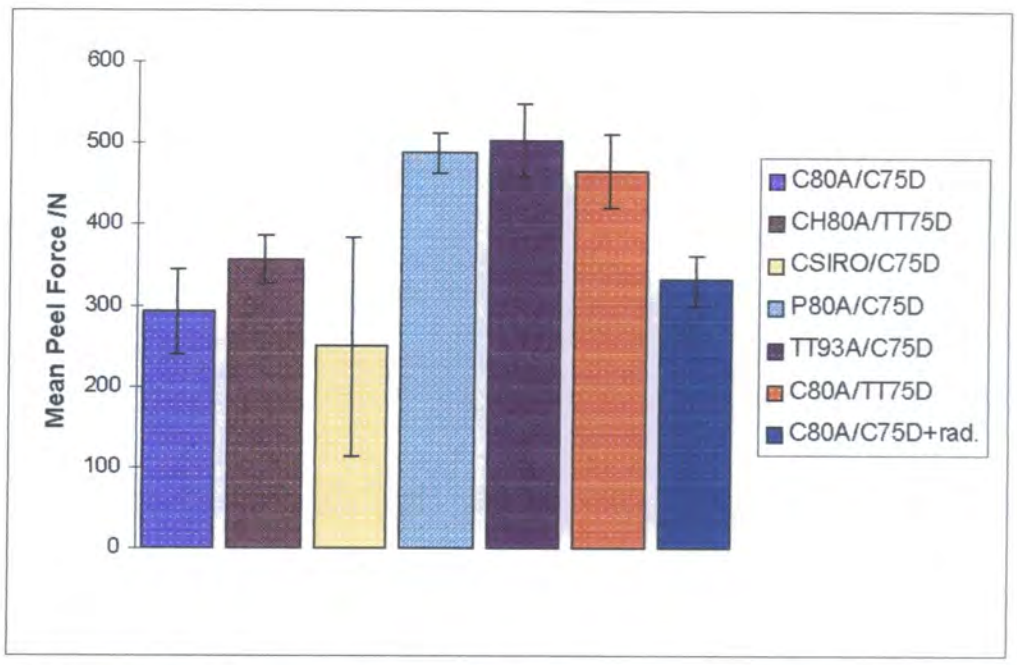

Figure 5.2. Variation of mean peel force with material system and irradiation. Results from tests PU#1 to PU#7.

5.1.2 Evaluation of PU/PU adhesion using the peel test.

The results presented in the previous section clearly illustrated the difficulty in promoting good adhesion between PU and UHMWPE. However an excellent bond between the layer and backing is a prerequisite to the success of compliant bearing technology, and so other backing materials were considered. In addition to the compliant PU grades available, several manufactures also produced a harder grade with an increased hard segment ratio. These materials possessed mechanical properties not dissimilar to UHMWPE, with the added advantages of thermoplastic properties, similar surface chemistry to the softer PU grades, and miscibility with the softer PU grades. Thus, a series of experiments were conducted to investigate the possibility of promoting a bond between soft and hard grades of PU, using injection moulding techniques. By injecting molten PU under pressure onto a preformed PU surface it was expected that sufficient wetting would occur, and that the high thermal energy would result in strong diffusion bonds.

Preliminary adhesion tests suggested that excellent PU/PU adhesion was possible, and as a result the peel test protocol was changed slightly to reflect the increased peel strength. The cross head separation rate was increased from 20 to 200 mm/min, and both the maximum and mean peel forces $\mathbf{F_{max}}$ and $\mathbf{F_{mean}}$ were recorded, as discussed in Section 3.3.1. As a benchmark, and in contrast to the UHMWPE/PU system, none of the PU/PU peel test specimens considered here could be peeled by hand.

5.1.2.1 The effect of material grade and sterilisation on bond strength.

The first set of experiments, PU#1 to PU#7, were conducted to assess the magnitude of bond strength between soft and hard PU grades. The effect that the use of different soft

PU grades had on the bond strength was assessed, as was the effect of gamma irradiation (Table 5.2, Figure 5.2). The results were very exciting, with typically two orders of magnitude increase in $\mathbf{F_{max}}$ compared with the untreated UHMWPE/PU system, and at least a five fold increase compared with the best results for surface modified UHMWPE/PU.

ID.	Materials	Sterilisation: Moulding conditions:	Results			
			n	F_{max}/N (s.d.)	F_{mean}/N (s.d.)	G_c/kJm^{-2} (s.d.)
PU#1	C80A/C75D	-none -normal	10	350 (55)	291 (53)	9.5 (3.6)
PU#2	CH80A/TT75D	-none -normal	10	403 (39)	357 (30)	36.6 (6.4)
PU#3	CSIRO/C75D	-none -normal	10	315 (127)	248 (136)	5.3 (4.3)
PU#4	P80A/C75D	-none -normal	10	542 (22)	488 (24)	44.4 (4.3)
PU#5	TT93A/C75D	-none -normal	10	561 (49)	502 (45)	23.2 (4.5)
PU#6	C80A/TT75D	-none -normal	8	533 (54)	466 (45)	47.1 (8.8)
PU#7	C80A/C75D	-γ rad 2.5Mrads -normal	10	369 (34)	330 (31)	18.7 (3.6)

Table 5.2 Peel test results: Effect of material and sterilisation on PU/PU bond strength.

The results seem to indicate that the preferred C80A/C75D material system does not represent the best materials combination for maximising $\mathbf{G_c}$. Comparing $\mathbf{F_{mean}}$ for the C80A/C75D material system with the other material systems; CSIRO/C75D showed no significant difference ($P=0.37$), while the other systems had a significantly larger $\mathbf{F_{mean}}$ ($P<0.004$). The injection moulding conditions were varied to suit the rheological

characteristics of the different materials used, and this may account for some of the observed variation in results. Sterilisation, using γ irradiation (PE#7), resulted in no significant change in $\mathbf{F_{mean}}$ (P=0.062).

5.1.2.2 The effect of ageing in Ringers solution on bond strength.

Thermoplastic PUs absorb moisture, and are potentially susceptible to degradation when implanted in the body. These degradation mechanisms are complex and depend on a large number of factors, including stress level and environment, and are extremely difficult to replicate *in vitro* (Stokes, 1987). In order to assess the susceptibility of the PU/PU bond to hydration, peel test samples were subjected to treatment in Ringers solution, which was used to simulate a simple bio-environment. Five sets of 5 or 6 C80A/C75D peel test samples were moulded, and irradiated at 2.5 MRads. Four sets were immersed in Ringers solution at 37°C, and removed and tested at 4, 12, 26, and 52 weeks. One set was stored dry and tested at 52 weeks.

ID.	Materials	Time immersed	Results			
			n	F_{max}/N (s.d.)	F_{mean}/N (s.d.)	G_c/kJm^{-2} (s.d.)
PU#8	C80A/C75D	4 weeks	5	432 (129)	352 (102)	14.3 (6.5)
PU#9	C80A/C75D	12 weeks	5	427 (114)	372 (117)	29.9 (16.7)
PU#10	C80A/C75D	26 weeks	5	428 (124)	345 (137)	21.5 (12.0)
PU#11	C80A/C75D	52 weeks	6	362 (220)	313 (214)	14.9 (12.6)
PU#12	C80A/C75D	52 weeks -dry control	5	429 (213)	395 (201)	17.1 (11.1)

Table 5.3 Peel test results: effect of immersion in Ringers at 37°C for up to one year.

The results (Table 5.3) show no significant reduction in peel force over the duration of the test, either through wet or dry ageing. There was no significant reduction in $\mathbf{F_{mean}}$ (P=0.70) between the samples immersed for 4 weeks and those immersed for 52 weeks. In addition, there was no significant reduction in $\mathbf{F_{mean}}$ (P=0.526) between the samples stored dry for 52 weeks and those immersed for 52 weeks. On closer examination, the peel strength seemed to depend on sample ID number; samples with the lower ID numbers giving high results, and samples with higher ID numbers giving low results, Figure 5.3. This correlation between peel strength and processing ID number, rather than time immersed in Ringers solution, suggests a possible change in manufacturing conditions towards the end of the production run. Product quality, particularly layer adhesion, will be of paramount importance if clinical failures are to be avoided, so the effect of moulding conditions on bond strength were assessed.

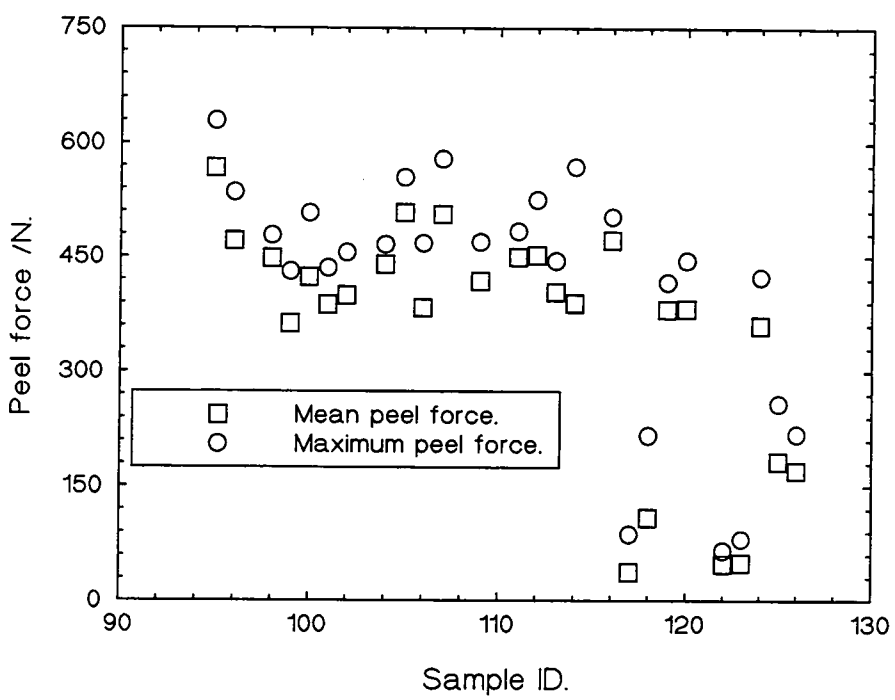

Figure 5.3. Variation of peel force with sample ID number for tests PU#8 to PU#12.

5.1.2.3 The effect of injection moulding conditions on bond strength.

Clearly a good bond is developed between compliant and rigid PU's using an injection moulding manufacturing route. Results from previously reported experiments seems to suggest that bond strength may be affected by injection moulding conditions. The adhesion mechanism is likely to result predominantly from diffusion bonding, which in turn will be dependent upon thermal energy and chain mobility. As a result, injection moulding conditions such as moulding temperature, moulding pressure, ram speed and holding time were judged to have the potential to affect the bond strength. Standard moulding conditions were set by reference to the materials manufacturer's data and from experience gained through moulding previous peel test samples, thus the effect of changing these standard conditions was assessed.

Peel test samples PU#13 were manufactured from C80A/C75D, using a variety of processing conditions (Table 5.4). Peel testing was conducted by an undergraduate student, under the authors supervision. For each of temperature, pressure and ram time[4], a comparison was made between the standard setting, and the lower and higher settings. For each of these parameters, the mean value of the individual $\mathbf{F_{max}}$, $\mathbf{F_{mean}}$, and $\mathbf{G_c}$ results were determined using all samples manufactured at that particular condition, irrespective of the values of the other parameters not being considered. For example, considering the set of samples manufactured at a temperature of 205°C, pressures of 40, 50 and 60 bar and speeds of 3, 4 and 5 s would have been used.

[4]The ram time (s) used here was specific to the injection moulding machine used in this trial, and reflects the speed at which the ram travels.

Injection moulding conditions.	Low setting	Standard setting	High setting
Temperature /°C	205	215	225
Injection pressure /bar	40	50	60
Ram Time (speed) /s	3	4	5
Time to fill /s	2.6, 2.7, and 3.8 plus 1 or 10s hold		

Table 5.4. Variation of C80A injection moulding conditions for experiment PU#13.

The effect of changing the processing conditions from the standard settings is illustrated in Figures 5.4, 5.5, and 5.6, where the difference in $\mathbf{F_{mean}}$ and significance of the results are shown. The following conclusions can be drawn from these results. A reduction in temperature from 215°C to 205°C significantly ($P<0.0001$) reduced $\mathbf{F_{mean}}$, whereas an increase in temperature from 215°C to 225°C resulted in a significant ($P=0.0079$) but smaller increase in $\mathbf{F_{mean}}$. A decrease in ram time from 4 to 3 s showed an almost significant ($P=0.0647$) increase in $\mathbf{F_{mean}}$, whereas an increase in ram time from 4 to 5 s showed no significant difference. A decrease in pressure from 50 to 40 bar significantly ($P=0.023$) reduced $\mathbf{F_{mean}}$, where as an increase in pressure from 50 to 60 bar resulted in no significant difference. Similar results were obtained if $\mathbf{F_{max}}$ or $\mathbf{G_c}$ were considered.

For a subset of the PU#13 samples, the time taken to fill the mould and the additional time for which pressure was maintained was measured. The time taken to fill the mould was a function of the temperature used, and so no correlation to the peel force was undertaken. Considering the additional hold time there was no significant difference in $\mathbf{F_{mean}}$ for a 1 s and 10 s pressure hold, as shown in Figure 5.7. The mass of the C80A soft layer was measured for each peel test sample. A significant correlation was found

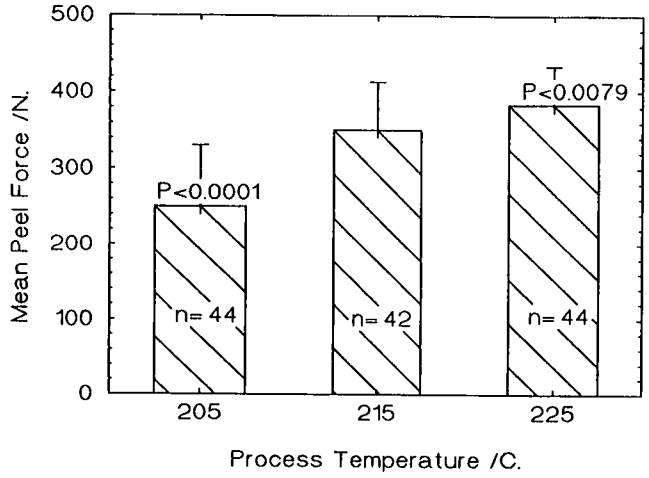

Figure 5.4. Effect of processing conditions; Barrel Temperature.

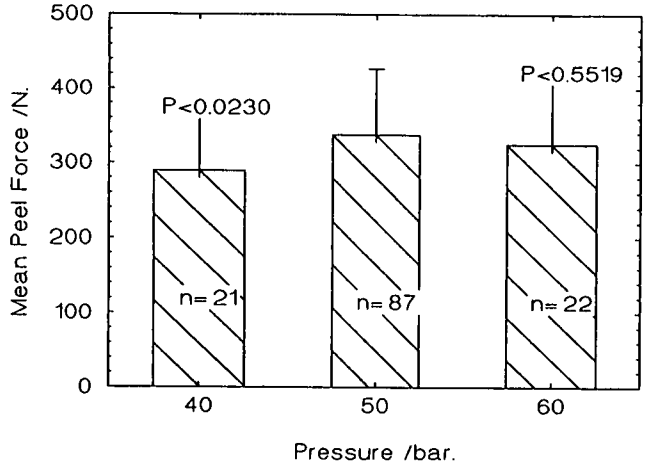

Figure 5.5. Effect of processing conditions; Injection Pressure.

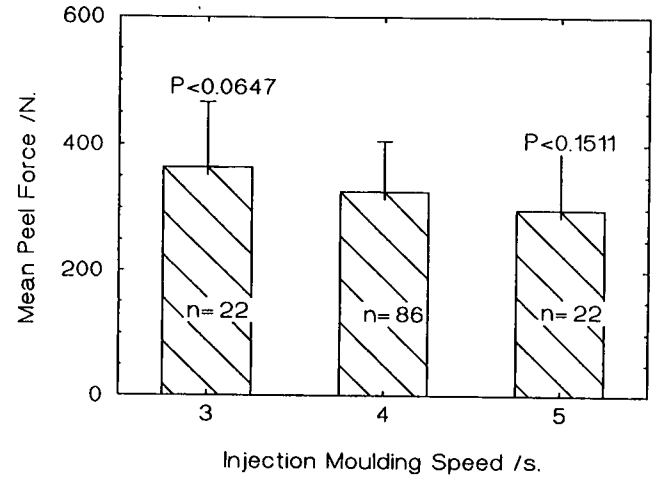

Figure 5.6. Effect of processing conditions; Injection Speed.

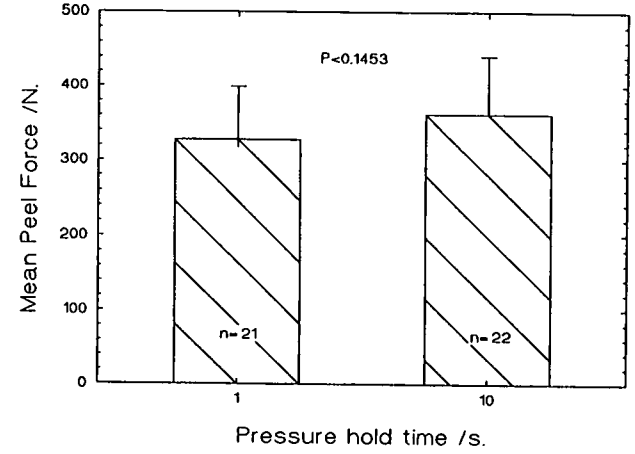

Figure 5.7. Effect of 1s and 10s pressure hold after mould fill.

with both $\mathbf{F_{mean}}$ (R^2=0.05, P=0.008) and $\mathbf{F_{max}}$ (R^2=0.07, P=0.003). Although the correlation was significant, less than 7% of the variation in peel force could be explained by measuring the mass of the soft layer, and hence it would be a poor predictor of bond strength.

In order to establish the relative importance of the various processing parameters, linear regression analysis was conducted (Computing Resource Centre, 1992). The following linear model of the results was proposed:

$$F_{mean} = K + (A \times \text{temperature}) + (B \times \text{ram time}) + (C \times \text{pressure})$$

The coefficients K, A, B and C were found to be -1076, 6.6, -29.8 and 1.9 respectively. Considering the significance of the results, temperature was most significant (P<0.0001), injection speed less significant (P=0.003) and pressure almost significant (P=0.056). In addition R^2=0.4635, indicating that only 46.35% of the variation in $\mathbf{F_{mean}}$ could be explained by this linear model. In other words, over 50% of the variation in peel force could not be explained by this linear processing conditions relationship.

The evaluation of moulding parameters demonstrated the importance of moulding temperature with respect to bond strength, with higher temperatures resulting in higher peel strengths. Hence, in order to increase the bond strength, the effect of increasing the processing temperature above 225°C was investigated, PE#14 to PE#17 (Table 5.5).

Caution must be exercised when examining these results, because of the large number of samples which tore at some point during the test, making statistical comparisons difficult. Tearing occurred when the adhesive bond strength exceeded the tear strength of the

flexible adherend. Considering PU#14 to PU#16, the number of samples tearing and not peeling indicated that increasing moulding temperature improves the bond strength. This conclusion was also reinforced by comparing the $\mathbf{F_{max}}$ and $\mathbf{F_{mean}}$ results.

ID.	Moulding conditions: C80A/C75D (No γ irradiation)	% samples tearing	Results			
			n	F_{max}/N (s.d.)	F_{mean}/N (s.d.)	G_c/kJm^{-2} (s.d.)
PU#14	mould at 230°C	none	10	480 (31)	439 (30)	25.3 (3.7)
PU#15	mould at 240°C	40%	10	540 (40)	471 (19)	25.7 (2.9)
PU#16	mould at 250°C	100%	8	586 (63)	-	-
PU#17	mould at 230°C, pre-heat C75D to ≈55°C	70%	10	528 (54)	425 (24)	23.5 (3.0)
PU#18	inverse moulding	100%	3	862 (3)	-	-

Table 5.5 Peel test results: Effect of increasing moulding temperature. (NB. $\mathbf{F_{max}}$ results include all samples, whereas $\mathbf{F_{mean}}$ and $\mathbf{G_c}$ results include only samples which peeled and did not tear.)

In order to increase the available thermal energy, but minimise the C80A moulding temperature, samples were moulded at 230°C over C75D blocks which were preheated to ≈55°C, PU#17. The ratio of torn to peeled samples, and $\mathbf{F_{max}}$, showed an advantage in preheating the C75D blocks, when compared with moulding at 230°C without preheating (PE#14). Since the samples which actually peeled did so with generally lower forces, the mean peel force does not confirm this conclusion. In addition, increasing moulding temperature above the recommended 210-220°C (Corvita product literature) resulted in a

noticeable decrease in sample quality, and will also tend to degrade the C80A which may compromise its biostability.

Up to this point all samples were manufactured by moulding the soft PU over a preformed hard PU block (Figure 3.2). The specific heat capacity of C75D was qualitatively greater than C80A, and so in order to increase the thermal energy available to the bonding process the moulding method was reversed, designated 'inverse moulding'. For inverse moulding, the C75D was injected onto the surface of a preformed C80A layer. Although the moulding temperatures for individual materials were the same, the molten C75D imparted more thermal energy to the interface resulting in an improved bond which could not be peeled apart, PU#18. In addition, the C80A component of samples PU#18 was moulded at the lower temperature of 215°C; and a comparison with the PU#16 results indicated that the tear strength of the material was improved.

5.1.3 Evaluation of PU/PU adhesion in acetabular cups using the blister test.

Having successfully demonstrated a good bond between soft and hard PU grades using peel test specimens, an attempt was made to assess the bond between the compliant layer and backing in an acetabular cup. It was considered important to develop a test method applicable to acetabular cups to ensure that good adhesion was developed under similar moulding conditions to the peel test specimens. It was hoped that a technique could be developed which could be used as a quality control tool as the project progressed towards clinical trials.

The test requires only a circular debonded area which when pressurised with a fluid, forms a blister. It was chosen as the best method to assess the adhesion in acetabular cups, however two problems were identified: the geometry was hemispherical and not flat; and no naturally debonded area existed and a crack starter would be difficult to incorporate within the injection moulding process.

Only flat test geometries have been considered in the literature. Considering a blister in a sample with a hemispherical geometry, clearly as the blister radius increases the strain energy density will decrease rapidly, and the work required to increase **a** will also decrease rapidly. Thus the ratio $\mathbf{a/R_1}$ was minimised so as the analysis approached the flat case. To enable comparisons to be made between samples **a** was also kept constant. Samples which leaked at the mount or burst, rather than blistered, were not included in the results (Table 5.6).

The first set of experiments used a debonded area machined at the pole of the cup, as detailed in Section 3.3.2. Initially the holes were machined manually. In order to assess the experimental method and compare the results with those from the peel test, five experiments were conducted; two using C80A/C75D and two using Chronoflex/C75D cups manufactured using the same conditions but at different times BL#1 to BL#4; and one using CSIRO cups, BL#5. The first point of note is that the $\mathbf{G_c}$ results are the same order of magnitude as those reported for the PU/PU peel test experiments. There was a significant difference (P=0.027) between $\mathbf{P_{cr}}$ for the C80A/C75D tests BL#1 and BL#2, indicating either variable adhesion or experimental technique. However, the $\mathbf{G_c}$ results from set BL#1 were comparable with those for C80A/C75D peel test PE#1 manufactured under similar (non-optimum) conditions. There was no significant

ID	Materials: (Moulding conditions)	Testing details:	Results		
			n	P_{cr}/MPa (s.d.)	G_c/kJm^{-2} (s.d.)
BL#1	C80A/C75D (normal)	manually machined hole test rate 500 units/s	5	5.1 (0.8)	14.0 (4.5)
BL#2	C80A/C75D (normal)	manually machined hole test rate 500 units/s	6	2.2 (2.4)	5.7 (8.12)
BL#3	Chronoflex/C75D (normal)	manually machined hole test rate 500 units/s	11	3.6 (1.2)	13.6 (10.8)
BL#4	Chronoflex/C75D (normal)	manually machined hole test rate 500 units/s	6	4.6 (1.2)	21.6 (10.2)
BL#5	CSIRO/C75D (normal)	manually machined hole test rate 500 units/s	8	3.4 (1.8)	4.0 (3.1)
BL#6	CSIRO/C75D (normal)	CNC lathe machined hole test rate 500 units/s	11	3.7 (2.4)	5.0 (6.2)
BL#7	C80A/C75D (optimum)	CNC lathe machined hole test rate 300 units/s	5	9.2 (3.1)	49.3 (34.7)
BL#8	C80A/C75D (moulded at 195°C)	CNC lathe machined hole test rate 300 units/s	7	8.5 (0.5)	38.5 (4.7)
BL#9	C80A/C75D (moulded at 225°C)	CNC lathe machined hole test rate 300 units/s	23	7.8 (0.8)	32.8 (6.8)
BL#10	C80A/C75D (moulded at 225°C)	Metal crack starter test rate 300 units/s	3	4.9 (0.9)	13.2 (5.0)
BL#11	C80A/C75D (moulded at 225°C)	UHMWPE crack starter test rate 300 units/s	5	3.9 (0.6)	8.3 (2.4)

Table 5.6. Blister test results: PU/PU acetabular cups.

difference (P=0.13) between $\mathbf{P_{cr}}$ for the Chronoflex/C75D tests BL#3 and BL#4, but the $\mathbf{G_c}$ results were lower than those from the Chronoflex/C75D peel test PE#2. Although the CSIRO/C75D system BL#5 gave comparable critical pressure results to other PU/PU

systems, this resulted in a lower G_c due to the higher elastic modulus of CSIRO. The results from BL#5 compare well with the results from the peel test PU#3, and confirmed that G_c for the CSIRO/C75D system is lower than the other PU/PU systems considered.

Although the results were encouraging, they exhibited large deviations in P_{cr}. The nature of the crack tip will have a large effect on the critical pressure needed to initiate crack propagation, and thus the deviations were thought to be due to variations in the manual machining method used to create the debonded area. In order to improve the sample preparation method, the mounting hole was machined using a computer numerically controlled (CNC) lathe, where the depth of tool penetration was controlled to ±0.05 mm, and hence the debonded area extended to the interface with repeatable precision. For the first set of samples using CNC lathe preparation BL#6, the critical pressure varied from 0.65 MPa to 8.70 MPa, representing the largest and almost the smallest values measured throughout the total series of blister tests conducted to date! On reflection, the CSIRO/C75D was not a good combination to use to assess the repeatability of the experiment, since peel test results tended to be low and somewhat variable, PU#3.

Five C80A/C75D cups were prepared using the CNC machining technique, and tested using a 40% reduction in fluid flow in an attempt to assess the rate dependence of the failure mechanism, BL#7. This small sample gave a significant (P=0.035) increase in P_{cr} compared with BL#1, which may have been due to the use of more 'optimum' moulding conditions, or as a result of the rate dependency of the failure mechanism. So, in order improve confidence in the blister test, an attempt was made to replicate the peel test results concerning moulding temperature. Cups were produced at 195°C and 225°C, BL#8 and BL#9. The scatter of results for these tests has clearly decreased when

compared with earlier studies, which suggests an improvement in either the test protocol or the manufacturing technique. The results showed a significant reduction (P=0.012) in $\mathbf{P_{cr}}$ of 8% when the moulding temperature was increased. This is at odds with the results reported in the previous section, which showed that increasing the moulding temperature tended to increase $\mathbf{G_c}$.

The main criticism of the machined debonded area is that it is not natural, and hence will be variable and blunt. So, in order to develop a more appropriate flaw the soft layer was moulded over an insert which was subsequently removed prior to testing. A threaded hole was made in the pole of the C75D shells in to which either a metal or UHMWPE insert was assembled. The centre of the insert had a hole running through it so that the C80A layer could be moulded in the normal way. After moulding the layer the insert was removed and the cups were tested, BL#10 and BL#11. The $\mathbf{P_{cr}}$ results using either of the insert types were significantly lower ($p<0.013$) than those using CNC lathe machined flaws produced under similar conditions, BL#9. This could be a result of sharper more natural flaws which may propagate at lower energies. The $\mathbf{P_{cr}}$ results using the inserts were remarkably consistent, however there was no significant (P=0.16) difference between the results using the different types of inserts.

5.1.4 Adhesion performance under fatigue conditions.

Although the peel and blister test results illustrate considerable progress in developing a good bond between the PU layer and backing materials, one must still consider whether the bond is adequate to last several decades *in vivo*. Also, it was not possible to compare the maximum shear stress at the interface derived by Yao (1994) with the $\mathbf{G_c}$ values

obtained from the tests. Hence a practical evaluation of the long term performance of PU/PU acetabular cups, with particular reference to the bond, was undertaken.

A 50 kN servo hydraulic fatigue testing machine (Dartec, UK) was used. Three non-irradiated C80A/C75D acetabular cups, with a nominal internal diameter of 32.2 mm, were mounted in bone cement and arranged so that they were loaded in the pole by a femoral head. They were equally subjected to a sinusoidal cyclic load of 0.1 to 4 kN, at 1 Hz. The exact moulding conditions used to manufacture these cups was unknown. The cups were immersed in Ringers solution at 37°C. Stainless steel ball bearings, with a nominal diameter of 32.0 mm, were used for the first 3.4 million cycles, and CoCrMo modular heads, also with a nominal diameter of 32.0 mm, were used subsequently. The cups were examined every 1 million cycles, and in addition the test was automatically stopped if the displacement of the head exceed a user defined limit, which would indicate possible debonding of the layer.

The three cups completed 14.4 million cycles (before the test was stopped due to a machine breakdown), with no visible deterioration of the bond, or of either of the PU materials. This is in contrast to the work of Blamey (1992) who used a similar test and reported layer debonding after 2 to 3 million cycles when he considered different PUs and backing arrangements.

5.1.5 Discussion.

The overall aim of this work was to develop a system with a good bond between the compliant layer and backing, which was also easily manufactured and did not

compromise the biocompatibility of the component materials. Initially a PU/UHMWPE system was considered. With hindsight, and given the difficulty experienced throughout industry when bonding anything to a polyolefin, one may have expected that promoting good adhesion would be a considerable challenge. The inherent adhesion of the basic system was extremely low, and although up to an order of magnitude increase in peel strength was achieved though a series of surface treatments, the adhesion was still fairly poor. Although the methodology used during this phase of the project was very similar to a patented method (Nguyen *et al.*, 1991) developed to improve the adhesion of an UHMWPE fibre to a (PU) resin, the level of adhesion achieved is unlikely to be sufficient for this application. Thus at this point the PU/PU system was considered.

Initially injection moulding one PU onto the surface of another resulted in a two order of magnitude improvement in peel strength compared with the basic PU/UHMWPE system. The pressure under which the molten PU is injected ensures intimate contact between the two components. Once intimate contact is achieved, two adhesion mechanisms may contribute; diffusion and adsorption bonding. Adsorption bonds may develop, since the organic groups which make up polyurethane are relatively charged and reactive (unlike ethylene groups). However, evidence suggests that diffusion bonding is the major mechanism contributing to the high bond strengths observed.

The C80A/C75D interface was examined using a transmission fourier transform infrared (FTIR) microscope. The work was conducted by Dr D Finch[5] and is discussed here briefly to illustrate the nature of the bond. Specimens were taken from the peel test samples and prepared using cryo ultramicrotomy, resulting in specimen thicknesses in the range of 2

[5] Dept. Materials Technology, Brunel University.

to 3 μm. FTIR spectra were recorded, using a slit size of 12.5 μm × 2 mm placed parallel to the interface. The specimens were moved across the slit in 12.5 μm increments, thus enabling the relative quanties of chemical groups to be determined when passing from bulk C80A through the interface to bulk C75D. The spectra were analysed across the interface for changes in free to bonded carbonyl, bonded carbonyl to bonded N-H and hard to soft segment ratios.

The ratio of bonded to unbonded carbonyl for a sample moulded at 230°C (Figure 5.8) clearly shows a diffuse interface, with a gradually increasing ratio passing from bulk C75D to bulk C80A. The width of the diffuse region is estimated to be 64 μm. Similar analyses on samples moulded at 218°C and 220°C indicate diffuse regions of 38 μm and 41 μm respectively, indicating a possible linear relationship between interfacial width and processing temperature. Similar results were obtained from the bonded carbonyl to bonded N-H and hard to soft segment ratios, confirming that the interface is a diffuse composite of the two polymers.

The FTIR results confirmed those from the adhesion tests; that processing parameters (particularly temperature) effect the nature of the interface. When C80A is moulded onto a solid C75D surface in the normal way, the peel test results showed that the significance of the processing parameters are temperature > ram time > pressure. By optimising the process conditions the peel strength and adhesive fracture energy is increased above the values initially measured for the C75D/C80A system. In particular, increasing the amount of thermal energy available to the diffusion process by using higher moulding temperatures seems critical; this is confirmed by the increase in bond strength, and thicker diffusion zones at higher process temperature. However, increasing the

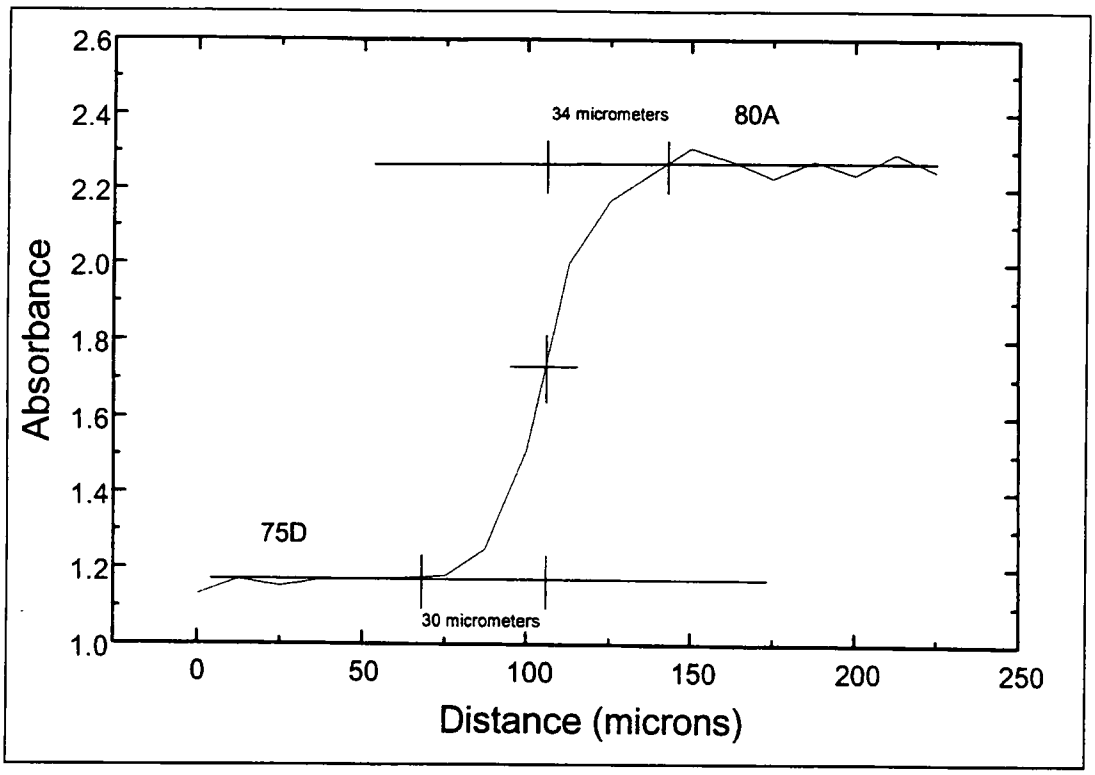

Figure 5.8 Free to bonded carbonyl ratio across a C75D/C80A peel test sample interface. Sample manufactured at 230°C. (After D Finch).

processing temperature of the C80A component runs the risk of thermal degradation which may compromise its biostability. By inverse moulding the C75D/C80A system higher thermal energy is available for the diffusion process, while moulding both components at lower temperatures. This results in bond strengths and fracture energies greater than can be measured using the current peel test arrangement. The only disadvantage is that inverse moulding C75D on to flexible C80A is more difficult, and can result in poorer component quality. These milestones in the development of a strong bond between a PU compliant layer and a rigid backing are summarised in Figures 5.9 and 5.10.

The experimental results also indicated that the bond strength was maintained during sterilisation using γ irradiation, and after prolonged exposure to Ringers solution at

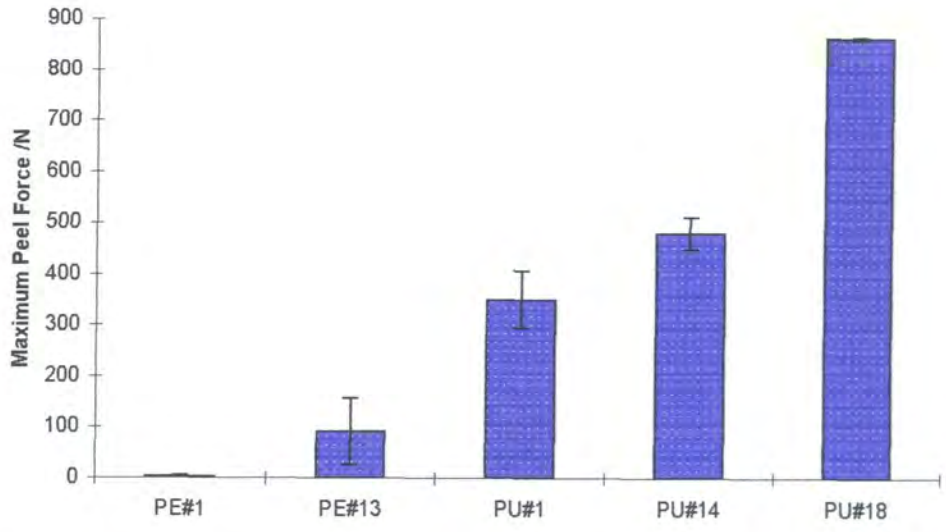

Figure 5.9 Summary of the improvements in peel strength F_{max} made over the duration of the project. (Error bars represent one s.d. PE#1- base UHMWPE/PU; PE#13- best UHMWPE/PU; PU#1- base C80A/C75D; PU#14- improved moulding C80A/C75D; PU#18- inverse moulding C75D/C80A. Note that for PU#18 since samples tore and did not peel, hence F_{max} may be larger than the value given).

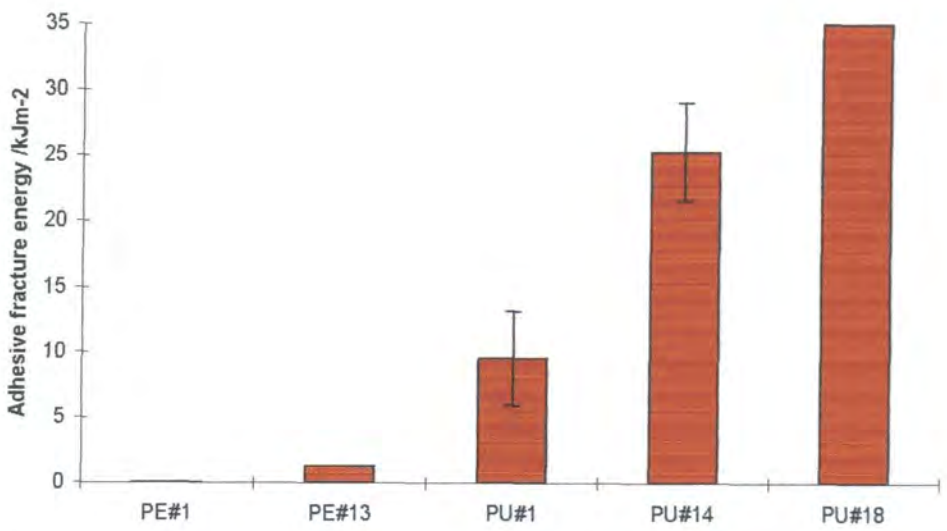

Figure 5.10 Summary of the improvements in adhesive fracture energy G_c made over the duration of the project. Notes as for Figure 5.9. No error bars were determined for PE#1, PE#13 and PU#18.

37°C. Although the blister test protocol was not greatly successful (and can not be recommended as a quality control tool due to the difficulty in obtaining a sharp natural flaw) it did confirm that the acetabular cups could be manufactured with the same high level of adhesion between layer and backing as measured in peel test samples. In addition, the performance of the cups, when loaded dynamically to 4 kN for 14.4 million cycles without any visible deterioration of the bond, further illustrates that the system may be capable of performing over several decades. In any case, these results give the confidence required to proceed to simulator, and subsequently, animal studies.

5.2 Material characterisation.

Some simple material characterisation and testing has been conducted for two reasons; to determine elastic modulus data for use in the lubrication analyses, and to investigate the effects of irradiation and immersion in aqueous solutions on the mechanical properties of the PUs used. A Lloyd R6000 universal materials testing machine was used for these tests.

5.2.1 Polyurethane Hardness Testing.

The ball indentation hardness was determined, according to BS 2782: Part 3: Method 365D: 1991 (ISO 2039-1: 1987). This method was used to assess the effect of irradiation on a range of PUs, and the effect of immersion in aqueous solutions on C80A and C75D only.

Material	Non-Irradiated		Irradiated (2.5 MRads)		% hardness increase (Significance)
	Hardness Nmm^{-2} (s.d)	E_2 MPa	Hardness Nmm^{-2} (s.d)	E_2 MPa	
Tecoflex EG 93A	4.468 (0.050)	13.7	4.782 (0.067)	14.9	7.0% (P<0.0001)
Tecothane 1080A	5.191 (0.041)	17.9	5.112 (0.047)	17.3	-1.5% (P=0.0008)
Chronoflex AL 80A	3.977 (0.030)	11.0	3.952 (0.043)	11.0	-0.6% (P=0.1489)
Corethane 80A	5.380 (0.146)	19.2	5.561 (0.200)	20.6	3.4% (P=0.0329)
CSIRO 85A	7.894 (0.147)	37.9	8.068 (0.127)	39.6	2.2% (P=0.0110)
Corethane 75D *	89.40 (2.31)	-	96.18 (5.79)	-	7.6% (P=0.0029)

Table 5.7. PU hardness and elastic modulus before and after irradiation. Elastic modulus calculated according to Waters (1965). (10 tests per sample were conducted, and a load of 49 N was used in all cases, except * where a load of 358 N was used.)

Effect of irradiation.

The effect of 2.5 MRads irradiation on a range of PUs (Table 5.7) was typically to increase the hardness by a small but significant amount. Although this was a useful comparison between materials, it did not give exact quantitative values of hardness since the thickness of the samples were only 2.3 mm, whereas the recommended specimen thickness in the standard is 4 mm. This limited the indentation of the ball due to the effect of the test table and resulted in higher hardness values. Waters (1965) studied the effect of finite sheet thickness on the indentation depth when using this method. His analysis and experimental results related indentation depth (and hence hardness) to elastic modulus, taking in to account the finite thickness of the sheet tested. Hence his method

was used to derive the elastic modulus data (Table 5.7) from the hardness results, which were subsequently used in the lubrication analysis (Chapter 4).

The effect of immersion in aqueous solutions.

Hardness tests were carried out on 3 mm thick dumbbell specimens conditioned dry at room temperature, and also on samples conditioned in Ringers solution at 37°C for 96 hours. Three different process temperatures were used to mould the materials. Only the preferred materials C80A and C75D were assessed (Table 5.8).

Conditioning the C80A material in Ringers solution decreased its hardness by approximately 11%. Higher moulding temperature resulted in both lower hardness and a smaller reduction in the hardness after conditioning. During preliminary tests of C75D, a considerable variation between the ends of the dumbbell specimens was noted. Hence, two hardness tests were conducted for this material, one at each end of the sample. This was done to determine whether the material properties changed with distance from the injection end. Before conditioning in Ringers, a considerable difference in hardness can be observed between the two ends of the dumbbell samples. The hardness of the material is higher away from injection end by between 58 - 87%. After conditioning in Ringers, the hardness of the material decreases by between 49 and 65%. After conditioning, the above noted difference in hardness from end to end is not so obvious but does, however, still exist.

Material: Moulding Temperature (specimen end)	Hardness /Nmm^{-2} (s.d)		% hardness decrease (Significance)
	conditioned dry at 20°C.	Ringers at 37°C for 96 hours.	
C80A: 205°C	6.502 (0.083) *	5.743 (0.214)	11.6% (P<0.0001)
C80A: 215°C	6.419 (0.112) *	5.611 (0.102)	12.6% (P<0.0001)
C80A: 225°C	6.201 (0.100) *	5.566 (0.089)	10.2% (P<0.0001)
C75D: 219°C (end1)	69.26 (9.27)	28.87 (3.28)	58.3% (P<0.0001)
C75D: 219°C (end0)	129.6 (23.7)	49.19 (1.54)	62.0% (P<0.0001)
C75D: 230°C (end1)	83.31 (20.68)	38.80 (9.05)	53.4% (P<0.0001)
C75D: 230°C (end0)	132.6 (13.1)	47.80 (1.39)	64.0% (P<0.0001)
C75D: 240°C (end1)	84.45 (5.57)	43.09 (1.96)	49.0% (P<0.0001)
C75D: 240°C (end0)	133.4 (12.0)	46.40 (0.77)	65.2% (P<0.0001)

Table 5.8. Effect of immersion in Ringers solutions on Hardness: Corethane 80A and Corethane 75D. (10 measurements were conducted, except * where 20 were used. Note that end1 is the injection end, end0 is the end furthest from the injection point)

5.2.2 Polyurethane Tensile Testing.

The effect of immersion in aqueous solutions on tensile properties of C80A and C75D was assessed by conducting tests as outlined in BS 2782: Part 3: Method 320A: 1976. The test specimens were dumbbell shaped and injection moulded such that the thickness of each specimen was approximately 3 mm, the width of the narrow parallel portion approximately 6 mm and the length of the narrow parallel portion approximately 28 mm. A cross head separation rate of 200 mm/min was used. For C80A the ultimate tensile strength (UTS), the maximum elongation, and the secant modulus (at an extension of 100% and 300%) were calculated. For C75D the yield stress and the elongation at yield were calculated. These tests were performed on samples conditioned dry at room temperature, and samples conditioned in Ringers solution at 37°C for 96 hours.

Corethane 80A. A typical force-displacement curve for C80A is given in Figure 5.11, which illustrates the highly elastomeric nature of the material. The C80A results (Table 5.9) confirmed that conditioning softened the material which resulted in a reduction in UTS and maximum elongation. In addition, the results indicated that increased moulding temperature led to an increase in UTS, maximum elongation, but a slight reduction in secant modulus.

Moulding temperature.	UTS Nmm^{-2} (s.d)	Max. Elong. % (s.d)	Secant Mod /Nmm^{-2}	
			100%	300%
C80A conditioned dry at room temperature				
205°C	25.84 (0.61)	628.8 (5.8)	5.86	4.07
215°C	26.83 (2.38)	746.5 (60)	5.60	3.52
225°C	37.65 (4.82)	971.1 (60.8)	5.46	3.22
C80A conditioned in Ringers solution at 37°C for 96 hours.				
205°C	20.35 (1.10)	565.0 (17.6)	5.40	3.75
215°C	19.28 (1.85)	653.4 (56.4)	5.12	3.21
225°C	27.92 (3.28)	922.4 (70.7)	4.96	2.88

Table 5.9. Corethane 80A tensile test results (5 samples per result).

Corethane 75D. Typical force-displacement curves for C75D dumbbell samples are given in Figure 5.12. Before conditioning in Ringers solution at 37°C for 96 hours the material possesses a distinct yield point, but conditioning results in the loss of this yield point, a reduction in yield stress, and a softening of the material (Table 5.10). Processing temperature has little effect of the tensile properties of C75D.

These results indicated that an aqueous solution considerably softened C75D, however the extent of the process, that is the time taken to reach a minimum reduction in

mechanical properties, was still unknown. Thus the hardness and yield stress of irradiated C75D dumbbell samples were assessed after 0, 24, 48, 96, 192, and 384 hours in Ringers solution at 37°C (Figures 5.12 and 5.13). Both the yield strength and hardness decrease with ageing, but only slight reductions occurred after 96 hours. As the material ages a distinct yield point is quickly lost (for comparison purposes a pseudo yield point was estimated at the point of inflection of the force displacement curve).

Moulding temperature.	Yield Stress. Nmm^{-2} (s.d)	Elongation at yield. % (s.d)
C75D conditioned dry at room temperature		
219°C	44.33 (1.59)	21.14 (1.51)
230°C	43.73 (3.21)	21.92 (2.22)
240°C	44.11 (1.35)	20.90 (0.30)
C75D conditioned in Ringers solution at 37°C for 96 hours.		
219°C	21.89 (0.53)	22.02 (0.67)
230°C	21.15 (0.63)	22.23 (0.94)
240°C	21.26 (0.51)	21.51 (0.54)

Table 5.10. Corethane 75D tensile test results (5 samples per result).

5.2.3 Discussion.

Processing temperature had little effect on the hardness or tensile properties of either Corethane 80A or 75D. However the distance from the injection moulding point resulted in large differences in hardness between the ends of dumbbell specimens made from C75D. Hydration (in Ringers solution at 37°C) reduced both the hardness and tensile properties of C75D, and to a lesser extent C80A. Irradiation typically increases hardness by a small but significant amount.

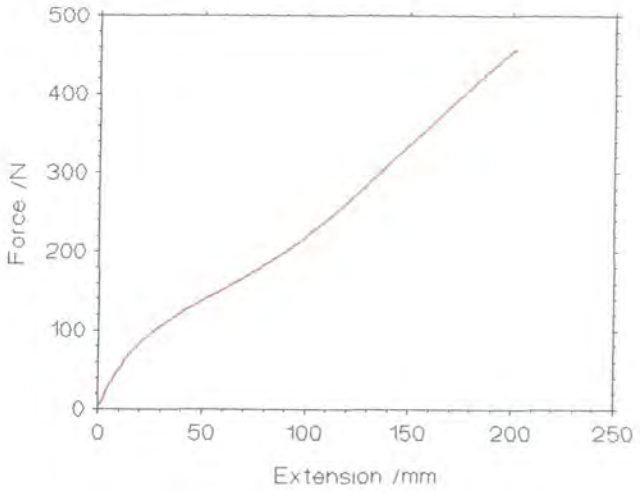

Figure 5.11 Typical force-extension curve for C80A dumbbell specimen.

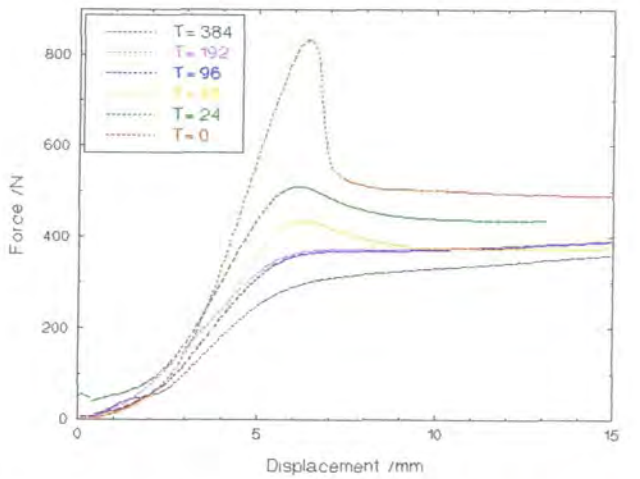

Figure 5.12 Typical force-extension curves for C75D dumbbell specimens, aged in Ringers solution at 37°C for T hours. Note the loss of the distinct yield point.

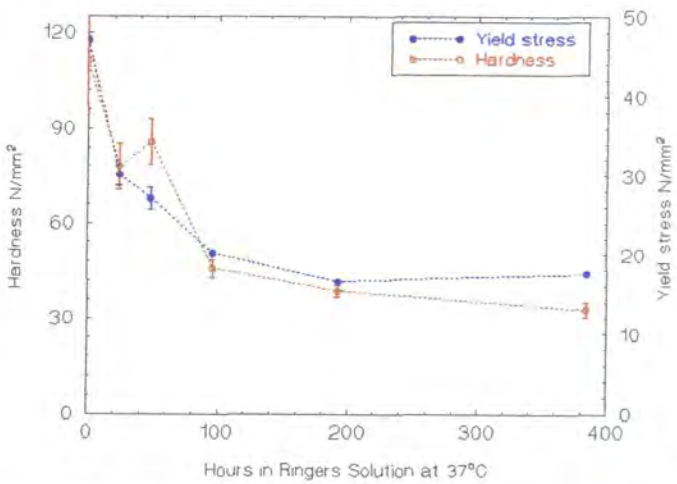

Figure 5.13 Reduction in hardness and yield strength for C75D samples after conditioning in Ringers solution at 37°C.

Clearly the action of water and heat will plasticize these materials. Zdrahala *et al.* (1986) suggested that this is due to saturation of both inter- and intra-molecular hydrogen bonding, and increased chain mobility. From tests conducted on similar polyether urethanes Zdrahala concluded that the softening depends primarily on the interface layer between the hard and soft segment domains, with soft segment molecular weight an important factor. In some circumstances the hard segment concentration was also shown to be important. These softening effects were shown to decrease with time due to the an "annealing" effect, with a typical softening effect of 67% reduced to 40% over 2 years.

The reduction in strength and stiffness of the C75D backing material after hydration may be a cause for concern, and warrants further investigation. However, comparing, the mechanical properties of C75D with Hoechst UHMWPE GUR 412 shows that C75D has a higher yield point than GUR 412 before hydration (typically 44 Nmm^{-2} *cf.* 20 Nmm^{-2}), but after conditioning they become broadly comparable (approximately 20 Nmm^{-2}). This suggests that, with careful design, softening of C75D may be accommodated. Both the tensile test and the hardness test results illustrate the importance of conducting product performance tests in a representative environment. In addition, design analysis should be conducted using the mechanical properties of the hydrated material.

5.3 Creep: Results and Discussion.

Design equations suggest that conformity is one of the most important factors which affects the lubrication regime, and that increasing conformity (decreasing clearance)

increases film thickness. However experimental evidence has suggested that, although the lubrication regime is fairly insensitive to conformity, if the clearance is too small contact may occur and mixed lubrication will prevail. The PU layer would be expected to creep and change the bearing surface dimensions during service and so the objective of this experiment was to assess changes in bearing form during loading.

Cups were loaded using a fatigue testing machine as described in Section 5.1.4, except six cups were used (three on top of three). The dimensions of the cups were assessed periodically by two methods; direct CMM measurement at the National Gear Metrology Centre, and CMM measurement of replicas at Howmedica, using the protocol described in Section 3.5.

Two sets of cups were tested; BB 66, 67, 68 which were made on a 32.424 mm diameter core; and BB 94, 95, 96 which were made on a 32.696 mm diameter core. The 6 cups, plus a dry and wet control (DC and WC), were measured as received, after conditioning in Ringers at 37°C for more than 96 hours, and after 0.95, 2.27 and 7.2[6] million cycles. Since the replicas were taken within 10 minutes after removal of the load, any material recovery was minimised. On the other hand, the direct CMM measurement of the cups took place some 24 to 48 hours after the removal of the load and so some recovery may have occurred. The hope was that by comparing one measurement method with the other, the degree of recovery may be established. However, the comparison between the two

[6]At approximately 5 million cycles some cracks appeared in the bone cement used to mount the cups. The cracks only occurred in samples BB67, BB94 and BB95, and ran through the reference hole C. These cracks may have occurred as a result of fatigue, or application of a single high load due to malfunction of the machine. In either case, the cups then became poorly supported and able to flex on loading, which lead to fretting between head and cup resulting in some surface damage at the edge of the contact area. These factors may have resulted in spurious CMM results for both the cracked and uncracked samples at 7.2 million cycles.

protocols revealed opposing trends. The Howmedica data (Figure 5.14) suggested that overall the bearings increase their spherical diameters during dynamic loading; whereas the Newcastle data (Figure 5.15) indicated a decrease in the diameter of the pole of the cup under the same conditions.

Considering the Howmedica data in more detail, the changes in the diameter of the unloaded wet control (WC) cup indicate that some portion of the diameter increase is due to moisture absorption. In addition, reference to Figure 5.16 shows that as the cups creep a ridge forms at the edge of the contact area which will result in differences in bearing form between the pole and sides of the cup. One can easily envisage the ten data points used in the Howmedica protocol falling both above and below the ridge, making interpretation of the changes in bearing form difficult.

Considering the Newcastle data, the consistency of the DC and WC data gives confidence in the accuracy of the measurement protocol. The diameter of sphere 1 initially decreases with increasing cycles, probably as the cup gradually conforms to the femoral head (Figure 5.15). This process seems to steady off after 1 million cycles, with possibly slight recovery by 7 million cycles. The femoral head penetrates into the pole of the cup as the layer creeps under load (Figure 5.17) which will effectively decrease the layer thickness by between 0.55 and 0.85 mm. This process slows after 1 million cycles, and appears to steady off and even recover slightly by 7 million cycles. Neither the Howmedica or the Newcastle data illustrate any great differences in performance between the different clearance cups.

The creep characteristics of soft layered components are important. Creep may lead to a change in bearing performance over time. For example, a change in conformity may affect both the lubrication regime and the applied stress, as may thinning of the compliant layer. Also, any out of roundness in the bearing may disappear during the creep process. It is unclear in practise whether creep will work to improve the performance of compliant bearings or not. Although acetabular cup dimensions did seem to stabilise after several million cycles the effect on the long term performance requires further investigation. Potentially, a cup manufactured with a small clearance, but which performs well during friction measurement, may creep and close up over time resulting in grabbing of the head, contact between bearing surfaces, and thus failure through wear. On the other hand, for a cup manufactured with a large clearance and some out of roundness, creep may improve the lubrication and reduce contact stress. Although important for hips, creep will become critical when compliant layers are applied to knee joints. Long term joint simulator studies may shed more light on the role of creep, and would be of particular interest at this stage of development of these TJRs.

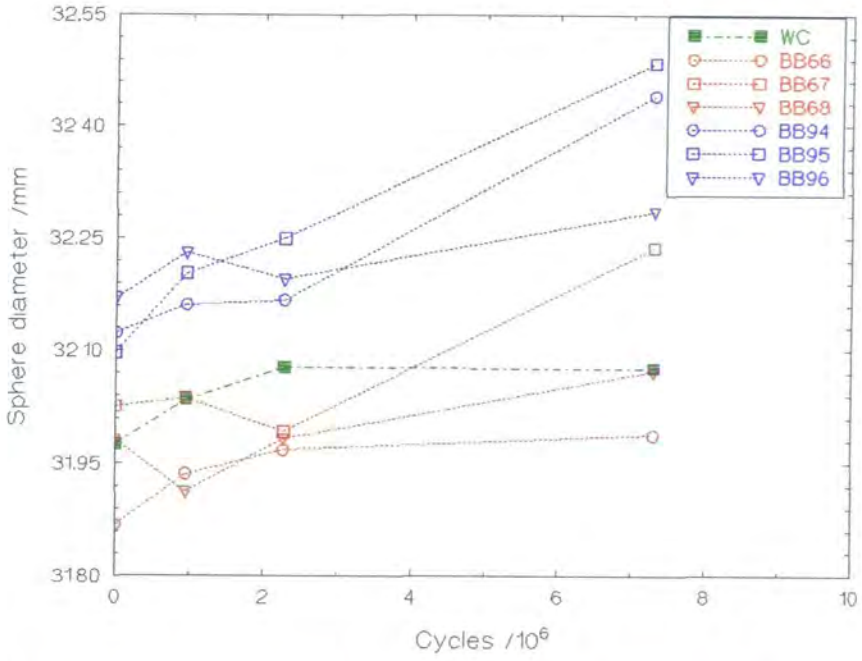

Figure 5.14 Change in dimensions due to creep after dynamic loading. (Howmedica CMM data). Zero cycles corresponds to the as manufactured and conditioned cups. WC- wet control cup.

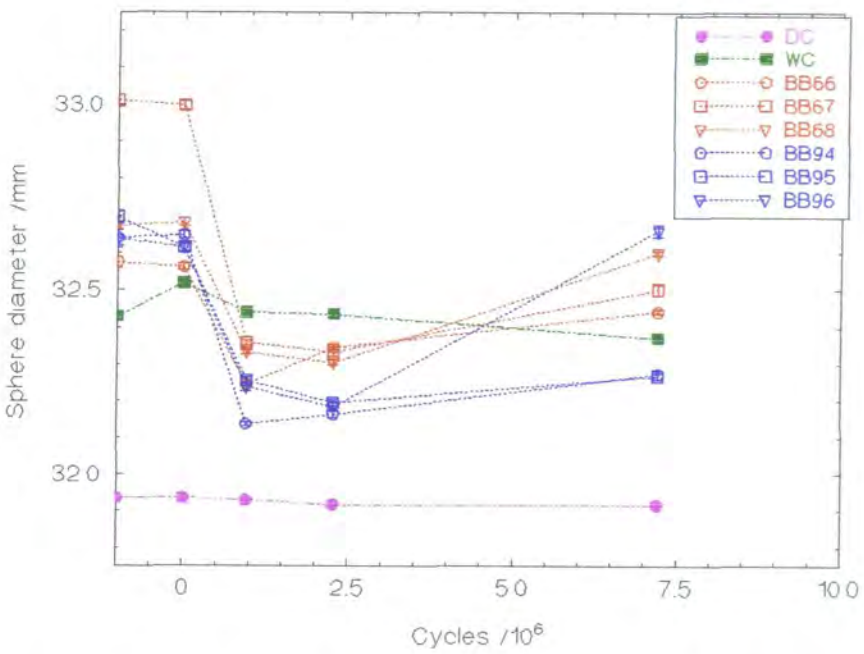

Figure 5.15 Change in dimensions due to creep after dynamic loading; Sphere 1 (see Figure 3.20b). (Newcastle CMM data). -1 million cycles corresponds to as manufactured cups, and zero cycles to as manufactured and conditioned. DC- dry control; WC wet control.

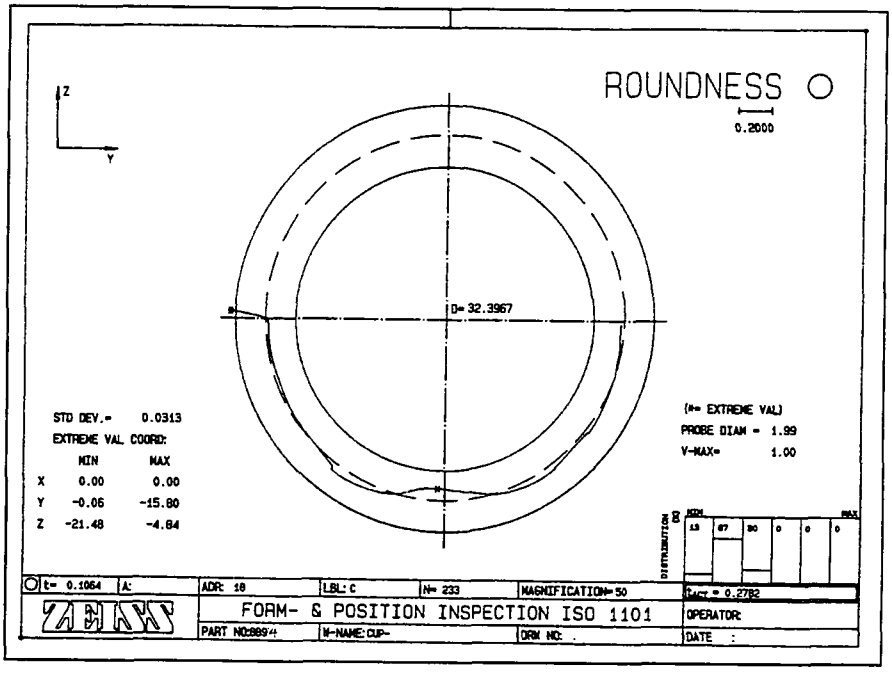

Figure 5.16a Section C through cup BB94 before dynamic loading (see Figure 3.20b). Note that the cup is essentially spherical, apart from the slight disruption at the injection moulding point in the pole of the cup.

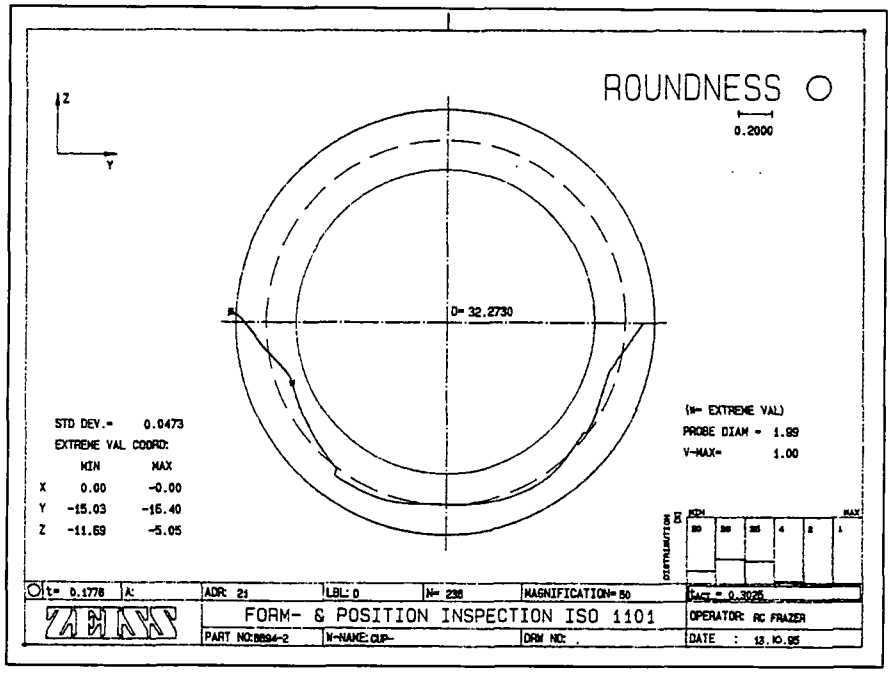

Figure 5.16b Section C through cup BB94 after 2.3 million cycles. Note that the cup is no longer spherical, and that ridges appear at the edge of the contact region.

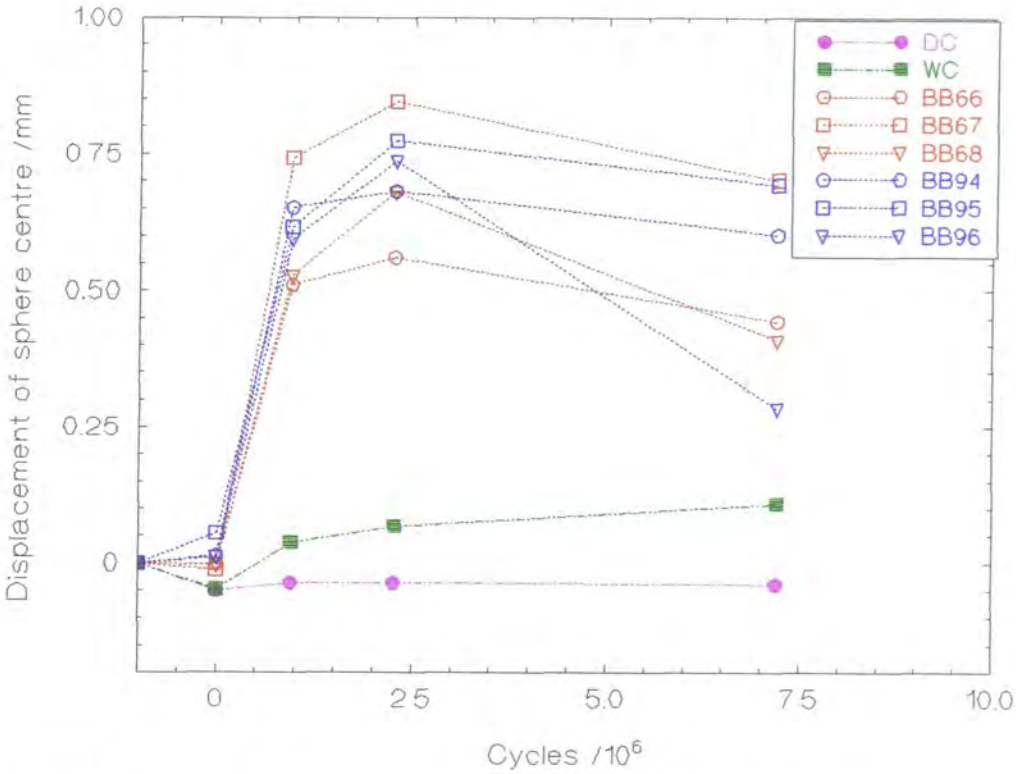

Figure 5.17 Change in dimensions due to creep after dynamic loading; penetration of sphere 1 into the cup along the Z axis (see Figure 3.20b). (Newcastle CMM data.) -1 million cycles corresponds to as manufactured cups, and zero cycles to as manufactured and conditioned. DC- dry control; WC wet control.

Chapter 6. Knee simulator: Literature review.

6.0 Introduction.

The objective was to design a knee simulator that could predict the realistic wear performance of prosthetic joints. In particular, the machine was commissioned in order to support the development of compliant bearing knees. It was anticipated that, as a result of the unconforming nature of the bearing surfaces, development of compliant bearing knees would be quite a challenge and hence long term simulator testing would be an important part of the research.

In order to build such a machine it was important to review and understand the biomechanics of the natural and artificial knee. A few knee wear simulators already exist, and the features of these machines have also been reviewed. There was much literature available concerning the wear performance of TKRs *in vivo*, which was important as it defined the resulting wear expected from testing a prosthesis on the proposed simulator, and would form the basis of any simulator validation exercise. Having reviewed the literature, the aim was to draw up a comprehensive specification for a new design of knee wear simulator.

6.1 Biomechanics of the natural and artificial knee.

6.1.1 The natural knee.

The natural knee is an example of a synovial or diarthrodial joint (Adams, 1993) which typically comprises articular surfaces enclosed within a capsule and lubricated with synovial fluid. The biomechanics of the natural knee are complex and have been widely examined and reviewed by many, including Seedhom (1981); whereas those of the prosthetic knee have not been analysed in such detail. Thus, in order to establish design criteria for the simulator, data for the natural knee have been considered. Seedhom pointed out that the knee is one of the most heavily taxed joints in the human body, and that its function is dependent on a range of unique anatomical features which account for the large range of motion and high load carrying capacity.

6.1.1.1 Range of motion, geometry and kinematics.

The natural knee has an unconforming articular surface geometry, which results in a large range of motion of up to 160° of flexion. This allows activities such as deep knee bends and squatting on the haunches. Seedhom *et al.* (1972) showed that the femoral condyles in the sagittal plane are approximately spiral in shape, with radii decreasing posteriorally. The medial tibial plateau is mildly concave in both sagittal and coronal planes, where as the lateral tibial plateau is convex in the sagittal plane and almost flat in the coronal plane. This particularly incongruent geometry allows for the large natural range of motion.

O'Connor and Zavatsky (1990) have likened the cruciate ligaments to a four bar linkage, and an analysis of this mechanism shows how the complex geometry of the articular

surfaces are defined, and illustrates the complex rolling and sliding between the femur and tibia. They believe that the cruciate ligaments are responsible for the translation of the instant centre of rotation, about which the bones move relative to each other. This results in the point of contact between the femur and tibia moving posteriorly during flexion, and anteriorly during extension. Although the four bar linkage model may not be universally accepted (the ligaments may become slack for example), the roll back action of the point of contact during flexion is easily demonstrated.

Thus together, the surface geometry and the action of the cruciate ligaments both help to define the kinematic conditions of the knee. Since walking will account for the majority of lower limb activity, it is important to appreciate the kinematics of normal gait. Perry (1993) discusses aspects of gait in general. For the natural knee, the range of motion during normal gait has been assessed by many workers, including Lafortune *et al.* (1992), who reviewed experimental techniques and the results of previous studies. Lafortune's main criticism of previous work was that the use of exoskeletal markers or linkages would lead to errors due to skin and soft tissue movements, which in turn would result in inaccuracies in determining more subtle movement such as internal-external rotation, and abduction-adduction. Lafortune used intra-cortical traction pins to fix the target markers, and published motion profiles for the six degrees of freedom (rotations of flexion-extension, internal-external and abduction-adduction; and linear displacements of medial-lateral shift, anterior-posterior drawer, and compression-distraction).

6.1.1.2 Knee joint reaction forces and load bearing mechanisms.

The forces acting on the natural knee are the joint reaction forces, the muscle forces and the forces in the ligaments and joint capsule. Many workers have presented

biomechanical analyses of the reaction forces across joints in the lower limb. Paul (1967) and Morrison (1968, 1970) used a simplified geometry of anatomical features, photographic measurement of the three-dimensional configuration of the leg segments during walking, force plate measurements of the ground to foot forces and electromyographic assessment of which muscles were acting during each part of the walking cycle, to analyse the joint reaction forces transmitted by the knee. Both reported similar variations in joint reaction force with time. Paul (1967) reported maximum joint reaction forces of typically 3.4 times body weight (BW), and Morrison (1968, 1970) reported maximum joint reaction forces of between 2.0 and 4.0×BW. Seireg and Arvikar (1975) used a more complete model of muscle forces, but a simplified ground reaction force, and a criterion of minimising the sum of muscle and ligament forces to solve the statically indeterminate system of equilibrium equations. They reported a different variation force with time compared with Paul and Morrison, and a maximum joint reaction force of 7.1×BW. Seireg and Arvikar assumed some antagonistic muscle activity (whereas Paul and Morrison did not) and a different criterion for reducing the large set of equations to a solvable system, which they believed accounted for the difference in results. Rohrle *et al.* (1984) showed that maximum joint reaction forces also depended on gait velocity; increasing the velocity resulted in increased joint reaction force. Also, considerable increases in maximum joint reaction forces could be expected during activities such as ascending stairs and jumping (Seedhom, 1981).

Clearly the contact stresses acting on the unconforming articular surfaces of the knee joint would be large if some mechanism of load transmission were not present. This is the most important of the functions performed by the menisci, which have a wedge shaped cross section and act to increase the conformity and hence reduce the stresses

between the articular surfaces. The functions of the menisci, including load transmission, shock absorption and improving lubrication, have been reviewed by Kelly *et al.* (1990).

6.1.2 The Prosthetic Knee.

The objective of the prosthetic knee is to restore pain free function to the patient. Rand and Ilstrup (1992) identified nine general types of implants, although these fall into two groups: the constrained hinge type which fixes the knee with a constant centre of rotation, and the unconstrained condylar resurfacing type. The hinge type arthroplasty was generally unsuccessful as no internal-external rotation was allowed, resulting in failure of the hinge or the fixation, and patellar pain. The resurfacing type allows rotations and rolling sliding motions, similar to those of the natural knee. There are many different design philosophies within this group and this has led to a huge range of TKR available to the surgeon. The initial resurfacing designs were moderately conforming with UHMWPE tibial components without a metal backing. Subsequently, most designs used a metal backed tibial component to improve fixation and evenly distribute the stresses to the bone. Cementless fixation has been developed to reduce the rate of loosening of metal backed components when used in younger patients (Rand, 1991). Unicondylar devices, often fairly unconforming in design, have been developed for the treatment of unicompartmental osteoarthrosis. Stabilised prostheses are also used, which generally have a tibial peg which locates into the femoral component, and allows for the sacrifice of both cruciate ligaments while maintaining stability and allowing rotation and rolling sliding motions during flexion. The conformity of the bearing surfaces varies considerably between designs, and a compromise exists between conforming designs which reduce contact stresses, and nonconforming designs which give larger ranges of

motion. The meniscal bearing designs allow a conforming bearing to translate on the metal backing to increase the range of motion, in a similar way to the mobile menisci of the natural knee (Argenson and O'Connor, 1992).

The designs predominantly used today are the unconstrained condylar resurfacing prostheses (typically with retention of the posterior cruciate ligament) and any design of knee simulator will clearly need to accommodate these designs. These designs restore the joint kinematics so that they are similar to those of the natural knee. A knee wear simulator needs to be able to accommodate these condylar resurfacing designs in a manner which reflects the different kinematic and loading conditions resulting from the many different prosthetic designs, surgical techniques and patient activity levels. However, there is a lack of kinematic and loading data for the wide range of TKRs available.

6.2 Review of existing knee simulators.

A machine to assess joint wear may be a simple screening device, an anatomically accurate joint simulator, or fall between these two extremes. Screening devices include 'pin on plate' or 'pin on disc' wear test machines (i.e. ASTM F732) which typically feature simple geometry, static loads and either constant velocity or simple harmonic motion. Anatomically accurate simulators will simulate natural dynamic forces and joint motion, typically along several axes. There is an obvious need to compromise between physiologically realistic simulators which are complex and expensive to develop and run, and the simple wear machines which can provide economic screening and ranking of the

wear of materials, but no design specific data. The success of a wear simulator will be judged on its ability to simulate the wear patterns observed *ex vivo*, not on the accuracy of the load and motion simulation.

Several knee simulators have been built and are reported in the literature. These fall in to three broad categories; those with constrained femoral components which move about a fixed centre of rotation, those with an instantaneous centre of rotation usually based around a four bar linkage mechanism, and those which are more unconstrained with actuators which represent anatomical muscle groups (particularly the quadriceps).

6.2.1 Fixed centre of rotation simulators.

Swanson *et al.* (1973) used a single station device which applied simple flexion-extension only (±45°), with a simple sinusoidally varying load (890N). Few design details were given, but many short term wear results (typically<1.8×10^6cycles) were included. Wear was assessed by measuring the number of metallic ions in solution or the number of particles. Pappas and Buechel (1979) developed a single station device which applied flexion-extension about a fixed centre of rotation, anterior-posterior translation, and internal-external rotation of the tibia using a mechanical cam and follower system. Dynamic tibio-femoral and quadriceps loading were applied using cam controlled hydraulic systems. No indication of the loads or motions applied was given. Wear results comparing a typical incongruent type of knee prosthesis with a meniscal bearing type of knee prosthesis were presented; the former loosened after only 0.1×10^6cycles and the latter completed 2×10^6cycles. Dowson *et al.* (1977) built a single station device which applied flexion-extension (0-75°) using a cam, rack and pinion. Dynamic loads were

applied both vertically (1780N) and in the anterior posterior direction (-66 to 220N) using hydraulic actuators. A creep station was also incorporated. Wear data for several different designs of prostheses were reported (Dowson *et al.*, 1985 and 1990). Treharne *et al.* (1981) developed a single station machine which utilised computer controlled servo hydraulic actuators for control of a dynamic load (5500N) and flexion-extension motion (0-60°). Experimental protocols for measuring wear rates were given, along with useful wear rate data for a range of knees tested over several, one million cycle, tests.

6.2.2 Instantaneous centre of rotation simulators.

Paul *et al.* (1977) developed a complex simulator which utilised an adjustable four bar linkage mechanism to give a range of flexion-extension about an instantaneous centre of rotation. Internal-external rotation and a joint reaction force were applied using servo hydraulic actuators. Bosma *et al.* (1979) also developed a complex simulator based around a four bar linkage mechanism. Both flexion-extension and internal-external rotation were applied using lever and cam mechanisms. The load was applied pneumatically.

6.2.3 Less constrained simulators, with anatomical muscle group actuators.

The simulator developed by Shaw and Murry (1973) used a hydraulically operated quadriceps action to provide the normal flexion-extension motion and muscle forces. The motion was controlled using micro-switches and logic relays. On-off dynamic loading of the joint occurred during the stance-swing phase. Zachman *et al.* (1978) used four servo hydraulic actuators to control flexion-extension (135°), abduction-adduction (±20°),

internal-external rotation (±20°) and applied forces. Joint reaction forces were due to the action of vertical and quadriceps forces. Szklar and Ahmed (1987) developed an unconstrained single station simulator which was suitable only for kinematic evaluation of cadavers or prostheses. Open loop servo-hydraulic actuators were used to represent the muscle groups, which applied the loads and resultant flexion-extension motion. A maximum flexion of 40° and a maximum frequency of only 0.5 Hz were possible.

By reviewing this broad range of simulators developed over the past 30 years, several factors stand out. All the authors have concluded that it is desirable to have a dynamically applied joint reaction force synchronised to a physiologically representative flexion-extension motion of *ca.* 0 to 60°, to simulate the stance and swing phase of the normal gait cycle. Notably, no multi-station knee simulators have been reported in the literature.

The simulators with a fixed centre of rotation are simpler in concept than the others and, if published results are used as a measure of usefulness, then these seem to have been most successful. However, only machines with anterior-posterior motion produce something approaching the correct kinematic conditions of rolling and sliding. Machines based on a four bar linkage have an added degree of complexity so as to produce the characteristic rolling sliding motion. The kinematic conditions of a particular knee joint will depend both on the geometrical design, and on the outcome of the surgical procedure which will include alignment and laxity. The problem of defining the true joint kinematics applies to all simulator designs, but is particularly critical when designing a four bar linkage. The added complexity will extend the time taken to develop the simulator, and potentially reduce its reliability. Less constrained simulators, with muscle group actuators probably represent the most anatomically correct devices. If a flexible

system is designed, which is easily constrained in certain directions, and has load and motion patterns which are easily modified, the simulator will provide a useful tool in assessing function of natural and artificial knees. However this category of knee simulator is not suitable for long term wear studies, as it is inherently less robust in design and a lubricant bath is difficult to accommodate.

6.3 Wear in total knee arthroplasty.

In order to design and validate a machine which simulates the wear of the tibio-femoral bearing of TKRs, the patterns and wear modes found *ex vivo* must be characterised, and the factors affecting them understood. Not all revision procedures are undertaken specifically due to tibial wear, but many are as a result of the wear process *e.g.* component subluxation and loss of function, pain, and component loosening due to severe osteolysis.

Prosthetic wear can be assessed by examining components explanted during revision surgery. Apart from limited autopsy retrievals, or arthroscopic evaluation (Mintz *et al.*, 1991), this is the only method of studying the wear of 'used' prostheses, with the obvious disadvantage that all samples are failures for some reason. Whereas the wear of acetabular cups has been assessed quantitatively by several groups (Kabo *et al.*, 1993, and Hall *et al.*, 1995) in terms of a number of parameters, the quantification of tibial wear is more difficult due to the component's complex geometry. Plante-Bordeneuve and Freeman (1993), Argenson and O'Connor (1992) and Hailey *et al.* (1994) have reported penetration rates of the femoral into the tibial component, however quantitative

measurement of penetration rates is only useful for simple geometries which still have unworn reference surfaces intact. Most studies use a wear score system (Hood *et al.*, 1983). Such systems allow for distinction between different wear modes in different areas of the bearing surface, but are somewhat subjective.

6.3.1 Characteristics of tibial wear.

Several modes of UHMWPE degradation and wear have been identified, and are described by Hood *et al.* (1983). These are surface deformation, pitting, embedded particles, scratching, burnishing, abrasion and delamination. Surface deformation includes plastic deformation and creep (cold flow) of the UHMWPE. Pitting describes depressions in the articulating surface typically 2 mm across and 1 mm deep. Embedded debris typically consists of bone cement particles. Scratching describes linear indentations, usually in the anterior-posterior direction. Burnishing refers to highly polished areas, whereas abrasion describes areas of shredded or tufted UHMWPE due to contact with bone or bone cement. Delamination is a result of a subsurface failure mechanism occurring parallel to the articulating surface, and describes the detachment of large (many mm^2) sheets of UHMWPE.

Wear occurs in different locations of the tibial surface. Wasieleski *et al.* (1994) identified that wear could occur in different proportions in the medial or lateral compartments, depending on the alignment of the knee, with a predominance in the medial compartment associated with a varus or normally aligned knee. They also reported that wear occurred with various degrees of anterior posterior bias, with a predominantly posterior wear track being more common, presumably due to the restoration of the normal roll back condition

found in the natural knee. Rotational wear patterns have been observed by Wasieleski *et al.* (1994) and Lewis *et al.* (1993). External rotation was predominant, with wear posteriorly located in the medial compartment and more anteriorly in the lateral compartment, although internal rotation was also identified. Clearly there is no one distinct wear pattern that is representative of *ex vivo* knee wear, with surgical alignment being an important influence.

6.3.2 Factors affecting tibial wear.

The literature suggests that a range of factors are responsible for the wear of current UHMWPE tibial components, including patient characteristics and the length of time of implantation, surgical practice, material properties and manufacturing process, bearing conformity, bearing thickness, and overall prosthesis design.

Patient characteristics and length of time of implantation.

Hood *et al.* (1983) showed a significant positive correlation between wear damage score, patient weight and implantation time. This was confirmed by Tsao *et al.* (1993), who showed that increased weight and decreased age were significant predictors of increased risk of failure.

Surgical practise.

Wasielewski *et al.* (1993) demonstrated that surgical factors such a component size and position, knee alignment and ligament balance all affected the severity of tibial wear patterns. Blunn *et al.* (1991) demonstrated experimentally that anterior-posterior sliding, associated with high ligamentous laxity in a low conformity component, led to severe

wear. Thus the influence of surgery on the kinematics of the prosthesis will affect tibial wear.

Material properties and manufacturing process.

The *in vivo* wear of the UHMWPE tibial component has been shown to depend on the integrity of the bulk material. Defects in the bulk material have been identified and shown to increase the surface wear (Wrona *et al.,* 1993). These defects were specific to certain designs of prosthesis (Blunn *et al.,* 1992), and were also identified in some new unused UHMWPE stock, indicating that they were a result of the manufacturing process rather than developed *in vivo*. Such defects were thought to be a result of incomplete fusion of UHMWPE particles during the extrusion or compression moulding manufacturing process. They were typically 150 μm in size (Blunn *et al.*. 1992), and thought to act to initiate sub-surface cracks due to cyclic stresses, resulting in a fatigue failure and delamination of the material. Other material properties, such as crystallinity and molecular weight, also affect the severity of wear (Blunn *et al.,* 1992).

Once the UHMWPE stock has been manufactured it must be subsequently processed in to the desired shape. Most tibial components are machined, but a post machining hot pressing process used to create a smooth bearing surface on one particular tibial design (PCA, Howmedica) was shown by Bloebaum *et al.* (1990) and others to affect the structural integrity of the material and result in severe delamination wear.

Bearing conformity.

The contact stress between the femoral and tibial components will be dependent on the bearing geometry (Bartel *et al.*, 1986), with a decrease in bearing conformity resulting in an increase in contact stress. Collier *et al.* (1991) showed that for a widely used range of metal backed tibial components, the contact stress often exceeded the uniaxial yield stress of UHMWPE, particularly for the less conforming designs. Furthermore he showed a positive correlation between the severity of tibial wear and the level of contact stress, with non congruent designs having greater wear than fully congruent geometries. However, Blunn *et al.* (1992) concluded that "low conformity *per se* didn't necessarily lead to an excessive amount of wear", only that it contributed to the multifactorial problem.

Bearing thickness.

Wear, and in particular surface damage such as pitting, is associated with large contact stresses. Bartel *et al.* (1985, 1986) used both finite element and elasticity solutions to investigate the effect of conformity and material thickness on these stresses, for a range of metal backed components. In addition to showing that increased conformity of the contact led to reduced stresses, they also showed that increasing the thickness of the underlying UHMWPE material had a critical influence in reducing stress. As a result they recommended a minimum material thickness of 8 mm for the tibial component. This observation was confirmed clinically by Engh *et al.* (1992), who examined a range of retrieved metal backed tibial components, and reported that severe wear was generally associated with the thinner tibial components.

Overall Prosthesis Design.

Given that all these features will affect the severity of tibial wear, a design which has several of these features would be expected to show a significant increase in wear related failure, compared with a design which exhibited only a few or none of these detrimental factors. The Porous Coated Anatomic (PCA) total and unicondylar knee prosthesis (Howmedica, NJ, US) has many of these detrimental features including thin non-conforming tibial condyles, manufactured using a hot pressing process. The catastrophic wear and subsequent failure of a high proportion of these devices is widely reported in the literature (Bloebaum *et al.,* 1990, Kilgus *et al.,* 1991, Jones *et al.,* 1992, Tsao *et al.,* 1993). Other authors report similar cases of particular design features resulting in high tibial wear and subsequent failure (Feng *et al.,* 1993, Bartley *et al.,* 1994). In contrast, Windsor *et al.,* (1989) reports only a 1.7% failure rate in a series of 1430 cemented primary Total Condylar TKRs over a fifteen year period, for which technical error and infection were cited as the major causes. This design has none of the implicated design features which result in severe wear.

This review of the literature suggests that no single wear mode or pattern is representative of tibial *in vivo* wear. A knee wear simulator would need to demonstrate the characteristic wear for a particular design type. In order to validate the simulator, a particular design should be tested retrospectively, with the aim of producing wear characteristics similar to those reported in the literature. This will require a simulator in which a whole range of factors, such as joint kinematics, surgical alignment and prosthetic design can be varied and their effect on tibial wear monitored.

Chapter 7. Knee simulator: Design and development.

7.0 Introduction.

In order to build a machine which simulates *in vivo* wear of the tibio-femoral joint, a design specification was required. Then several design concepts were considered, and the most promising taken on to the detailed design stage. The design process naturally consisted of several loops, as the design was further refined. However, only the final optimum design is discussed here. The performance of the simulator depended primarily on the design of the hydraulic systems, and so detailed design calculations are presented for this portion of the work. The overall objective here is to outline the design rationale, and chart the development of a six station knee simulator.

7.1 Design specification for a knee wear simulator.

When drawing up the specification for the knee wear simulator it was important to consider the applied loads and motions, the test environment, and the method of load and motion actuation. A method of assessing the performance of the test prostheses, the flexibility (the ease of changing prostheses type, and load or motion profile), and reliability of the simulator were also important.

7.1.1 Applied loads and motions.

A dynamic tibio-femoral load and a flexion-extension motion which are linked to give the basic stance and swing phase of normal gait are fundamental requirements which distinguish a 'simulator' from a wear screening device. All the knee simulators reviewed in the literature had some form of dynamic load. The loads calculated by Seireg and Arvikar (1975) were the most severe reported in the literature, and hence represented the maximum design case. Medial-lateral and anterior-posterior joint reaction forces are significantly smaller than the vertical joint reaction force, and it is difficult to determine the proportion of these forces which are resisted by the soft tissues and ligamentous structures. For these reasons, only a vertical force of up to 5.0 kN of the form reported by Seireg and Arvikar (1975) was specified (Figure 7.1). Having decided on a tibio-femoral load synchronised with a basic flexion-extension motion (Figure 7.2) to simulate normal gait, some consideration as to which other rotations or translations to apply was required. To build a simulator which was able to duplicate all 6 degrees of freedom of motion (Table 7.1) would be complex and costly, and hence a compromise was required.

First the three linear translations were considered. The control of anterior-posterior translation (Figure 7.3) is important, as it will influence the instantaneous centre of rotation of the femoral component, and result in the correct rolling-sliding ratios of the joint surfaces. This is desirable since they have been shown to influence the wear of conventional prostheses (Blunn *et al.*, 1991). The sliding distance is also important, as it will directly affect the number of surface interactions which result in wear particles. The entraining velocity between the two components has been shown to be one of the most important factors in the lubrication of the joint (Dowson *et al.*, 1991). Flexion-extension has the major effect, with anterior-posterior translation the next most influential motion

when considering kinematics, sliding distance and entraining velocity. Hence a simulator with a fixed centre of rotation, synchronised with anterior-posterior translation was specified negating the need for a four bar linkage. Medial-lateral shift is small and would have little effect on the sliding distance or entraining velocity. Compression-distraction would be controlled by the application of the vertical tibio-femoral load and therefore need not require further consideration.

Next, the two rotations of the knee in addition to flexion-extension were considered. Abduction-adduction and internal-external rotation are considerably smaller in magnitude than flexion-extension, and occur at lower velocities. These will not greatly affect the overall sliding distance or velocity. However, it is important not to constrain the joint in

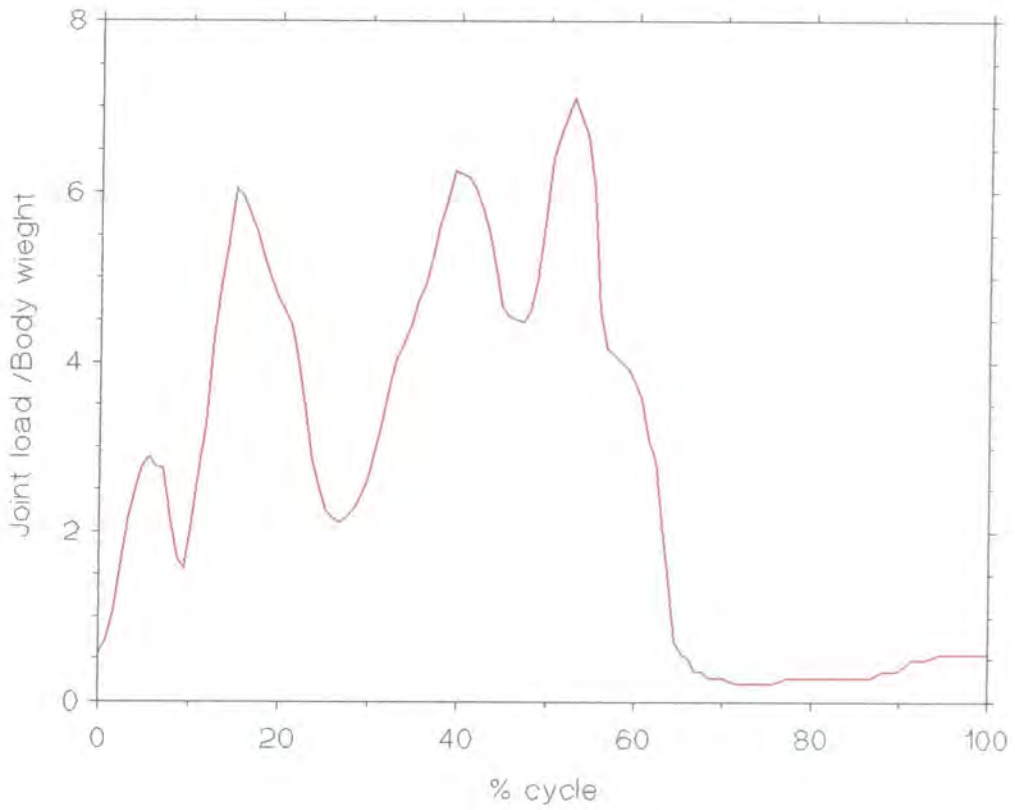

Figure 7.1. The applied tibio-femoral load profile. After Seireg and Arvikar (1975).

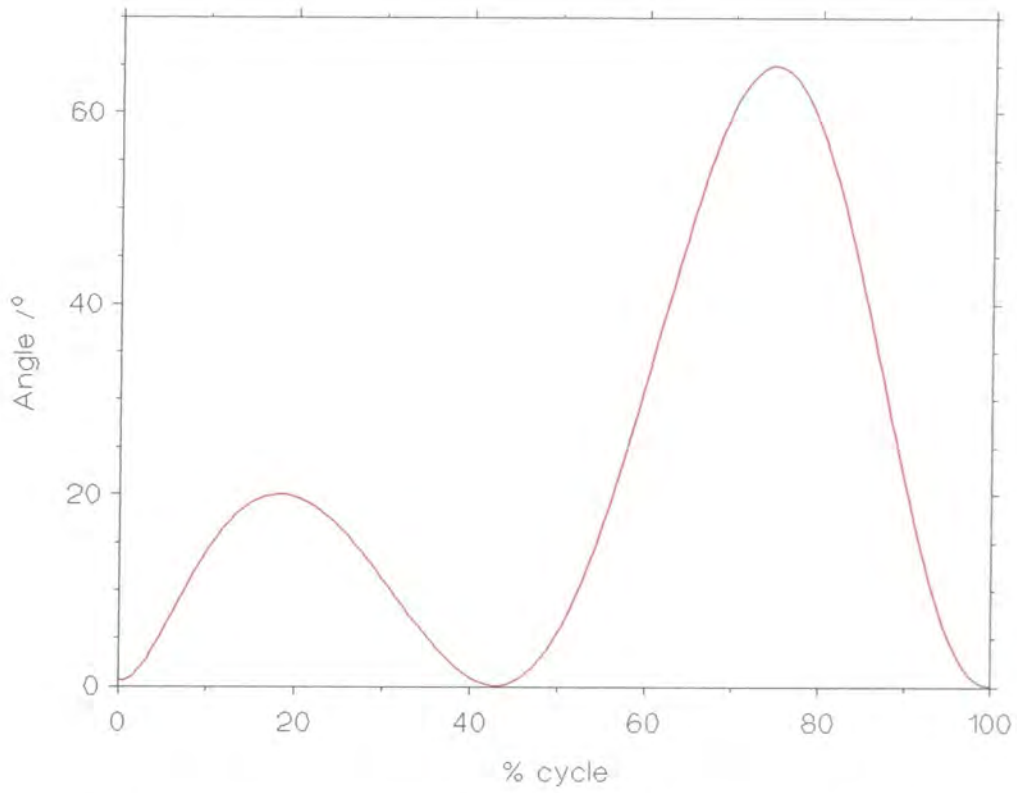

Figure 7.2. The flexion-extension motion profile. After Lafortune *et al.* (1992).

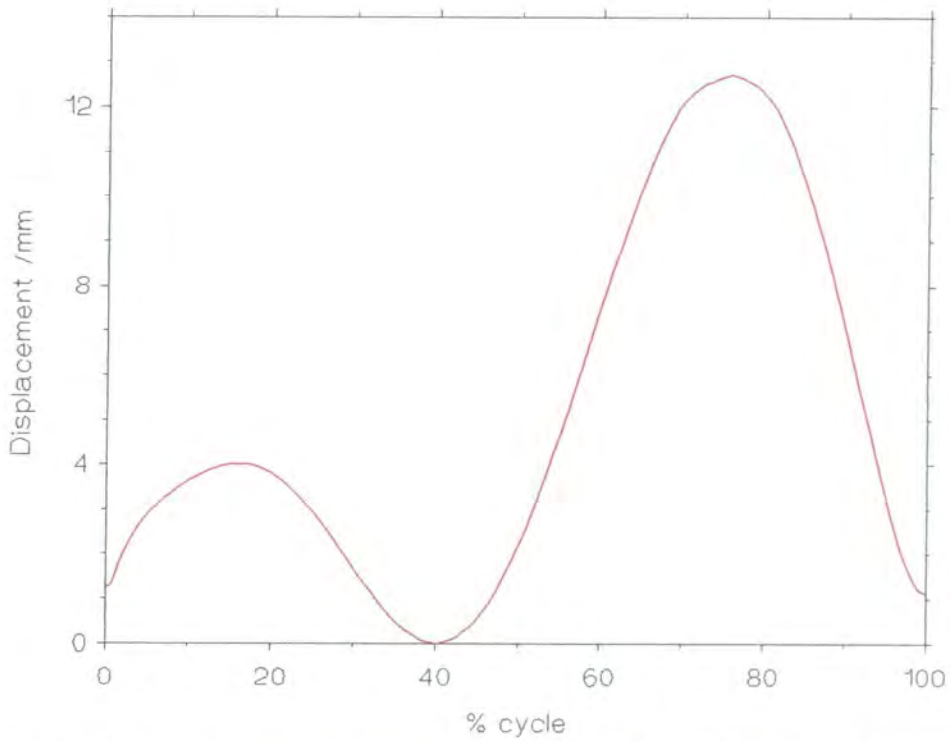

Figure 7.3. The anterior-posterior translation profile. After Lafortune *et al.* (1992).

abduction-adduction and internal-external rotation or unrealistically high localised contact stresses could develop in the joint itself. The loads which produce these small movements would normally be accommodated by the soft tissues *in vivo*. Hence passive abduction-adduction and internal-external rotation were specified. The load and anterior-posterior translation were individually controlled for each station, whereas the flexion-extension was common to all six stations. This represented a good compromise between simplicity and totally realistic motion. A gait frequency of 1 Hz is typical (Lafortune *et al.*, 1992). The basic design specification is summarised in Table 7.1.

Motion	**Range of natural joint***	**Simulator specification.**
Flexion-extension	65° - 0°	Motion control to Figure 7.2.
Abduction-adduction	1.2° - 6.4	Unconstrained passive rotation of the tibia about the anterior-posterior axis.
Internal-external rotation	±5°	Unconstrained passive rotation of the tibia about the vertical axis.
Anterior-posterior translation	15.6 mm	Motion control to Figure 7.3.
Lateral-medial shift	5.6 mm	Fixed, no motion.
Compression-distraction	7.0 mm	Load control to Figure 7.1.

Table 7.1. Summary of load and motion specification. *After Lafortune *et al.* (1992).

7.1.2 Test environment.

Many workers have considered the question of test environment. Distilled water is often used as it is convenient, and inherently consistent. However, it does not contain the high

molecular weight proteins of synovial fluid, and often produces gross transfer films of UHMWPE on metallic counter-faces during *in vitro* wear testing, whereas such transfer films are not observed *in vivo*. For these reasons, bovine serum is now commonly used (McKellop and Rostlund, 1990) as a convenient substitute lubricant in simulator studies. This required a chamber that was inert, corrosion resistant and easily removed for cleaning. Since such fluids may be difficult and expensive to obtain in large quantities the chamber volume was minimised. Although there is no evidence which confirms the importance of testing at 37°C, it was still considered a desirable feature.

7.1.3 Methods of applying loads and motions.

There are three main methods of load and motion actuation; electromechanical, pneumatic, and hydraulic. All these methods have been used previously to some extent in knee and hip simulators.

Mechanical application of near sinusoidal motion is easily done using an electric motor and a crank (Saikko *et al.*, 1992). More complex motions require the use of specially shaped cams and followers. This method has been used successfully by Dowson *et al.* (1977) for the flexion-extension motion in a knee simulator, and also by O'Kelley *et al.* (1977) for compressing a simple hydraulic system for load application in a hip simulator. This method is cost effective but changes in load or motion profile require a new cam to be made. DC stepper motors can also be used, with the advantage that motion profiles can be changed easily by reprogramming, although they are prone to generate large amounts of electrical noise and are susceptible to inertia effects.

Pneumatics are commonly used in many engineering applications for applying load and motions, and sophisticated proportional control valves are readily available. Saikko *et al.* (1992) used pneumatically applied forces in his five station hip simulator, which completed 35 million cycles in one particular study (Saikko, 1993), illustrating the potential reliability of such a system. Although moderately priced, especially since a compressed air supply is routinely available in most research laboratories, it has inferior response times compared with hydraulic actuation. It is best suited to on-off control, as subtle load and motion profiles are more difficult to achieve.

The near incompressibility of oil makes the response and fine control of hydraulics superior to mechanical or pneumatic systems. The oil flow is best controlled using a servo valve. Originally developed for the aerospace industry these valves are reliable and allow control of large hydraulic forces using control signals in the range of mV. Although open loop servo hydraulics can be used (Blunn *et al.*, 1991), closed loop feed back control allows complex motion and load profiles to be applied with high accuracy over many cycles. This method has been used in many hip and knee simulator designs (*e.g.* Treharne *et al.*, 1981). Although hydraulic control offers superior performance, actuators, valves, and a power supply are more costly compared with the other methods discussed. Within the cost constraints of the project, closed loop servo hydraulic control was chosen for all applied load and motion actuators, due to the superior performance of such a system.

7.1.4 Other considerations.

The measurement of wear has been widely discussed, and a review of various methods used has been given by Dumbleton (1981). The important factor in the design of the

simulator is that the components under test can easily be removed for wear assessment, by which ever method used, and subsequently replaced in exactly the same position for the test to continue. In addition, the fixation needs to be compatible with a wide range of TKR designs, and reflect methods used in clinical practice. For these reasons it was proposed that both components were mounted on design specific mounts using bone cement, while allowing the mount assembly to be easily removed and relocated in the simulator throughout the experiment. Where possible, advantage would be taken of snap fit designs, which are fairly typical in current TKRs, to remove the tibial bearing from the metal base plate.

The use of servo hydraulics goes hand in hand with computer control. The reliability and flexibility of the system was the most important consideration in the design of computer hardware and software. The system requirements were control of 13 servo hydraulic systems, monitoring the performance of each system in hardware and software, and stopping the test if an error condition occurred. It was also required to display and record the performance of each servo system. A method of calibrating each hydraulic system was required, as was easy reprogramming of the load and motion profiles. Apart from the PC, all hardware and software was built and supported in house, and was an extension of the system successfully used to control the two Durham friction simulators (see Section 3.2.1.4).

7.2 Design concept.

The design concept is shown in Figure 7.4. All applied loads and motions use servo hydraulic actuators. The knee components are mounted in an anatomical position. The concept allows flexion of the femoral component about a fixed axis using a rotary actuator, coupled with anterior-posterior translation of the tibial component using a linear actuator, to allow the characteristic rolling and sliding kinematics associated with the natural and artificial knee. The tibia is mounted on the top mobile face of a small die set to which a dynamic load is applied by a linear actuator. The die set serves to protect the load actuator from bending moments which would severely reduce its service life. The tibial mount allows passive rotation about both the vertical and anterior-posterior axes. The design rationale was to use off-the-shelf components where possible so as to minimise the build time. Initially a single test station machine was commissioned (Burgess *et al.*, 1995). Once this was shown to be satisfactory, another five stations were added.

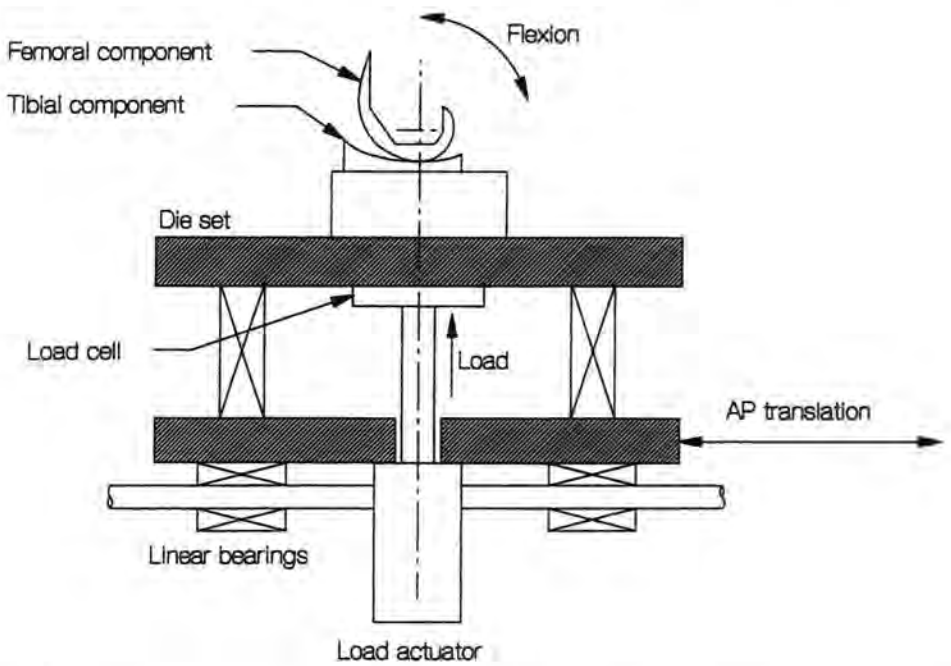

Figure 7.4. The design concept. An anterior-posterior section through the wear station.

7.3 Detail design.

The detailed design has been split into three sections. One of the primary objectives of the mechanical design (Section 7.3.1) was the requirement for simple 'in house' manufacture. The design uses complex load and motion profiles, which required careful specification of the servo hydraulic components (Section 7.3.2), for which computer simulation was used as a design tool. The design of the software and hardware used to control the simulator (Section 7.3.3) was important to ensure reliable and optimal control of the servo hydraulic systems. An general view of the six station simulator is shown in Figure 7.5.

7.3.1 Mechanical design.

The tibial component was mounted on a stainless steel mount assembly using bone cement. The design allowed passive abduction-adduction and internal-external rotation, using DX (Glacier, UK) bearings. These gave fairly low friction (μ=0.01 to 0.1) at low sliding speeds, and had good corrosion resistance and a long service life (50×10^6 cycles) at the design load used. Stainless steel was used in areas near or contacting the lubricating environment to enable a range of fluids to be considered. The top part of the mount assembly could be easily removed and replaced in the same position. A polyethylene bath was screwed on to the top of the mount assembly. The tibial mount assembly was itself mounted on the upper face of a die set. The load was applied using an actuator via a load cell which transferred the load to the upper face of the die set. The die set was translated with anterior-posterior motion on two shafts, again using DX bearings, by a linear actuator. The flexion-extension was provided by a rotary actuator. The femoral

component was mounted on a stainless steel yoke using bone cement. The mechanism was supported on a keyed steel shaft running in pillow bearings. The actuators and mechanisms were mounted on a frame manufactured from steel tube and ground flat plate. This formed a stiff heavy frame which was easy to manufacture and dampened vibrations. A test station is shown in detail in Figure 7.6. The anterior-posterior and flexion-extension mechanisms and actuators are shown in Figure 7.7.

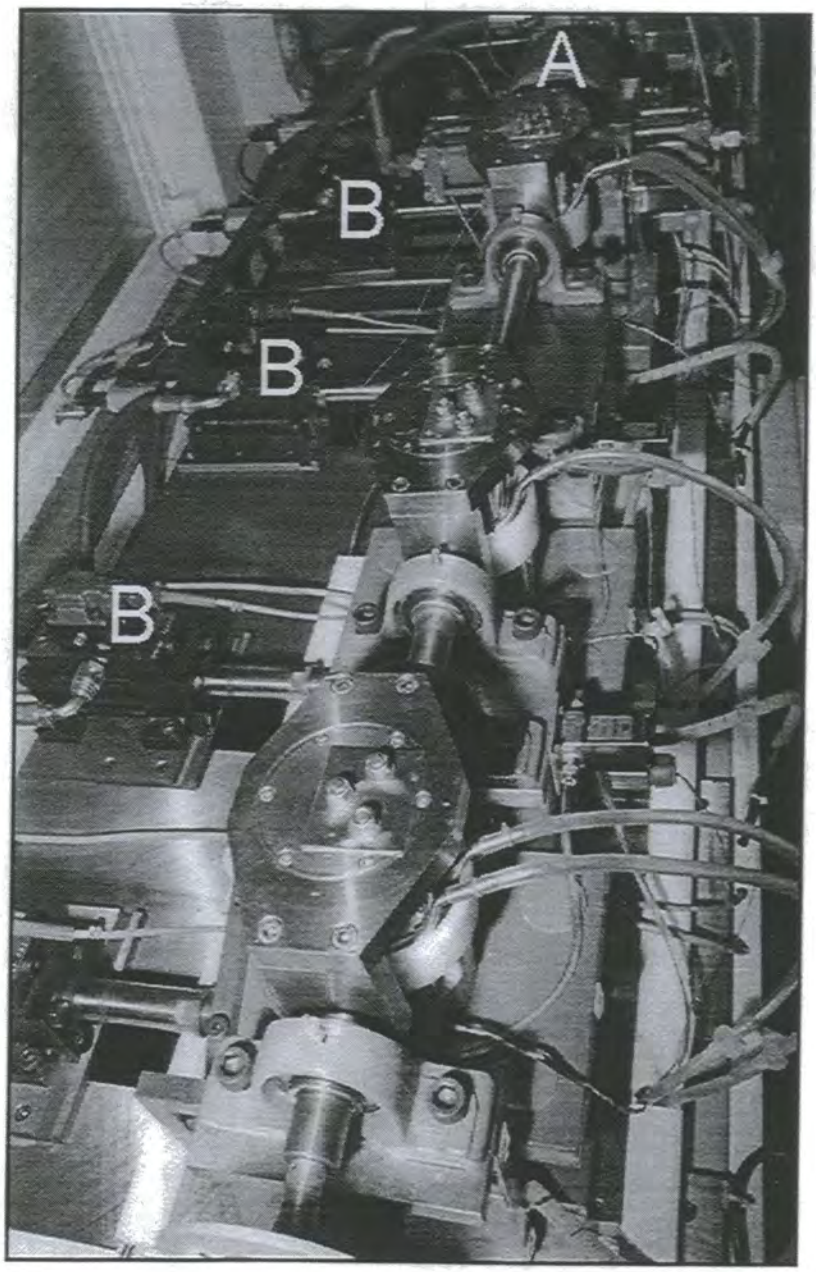

Figure 7.7 A view of the six station simulator looking from above, showing **A** Flexion-extension mechanism and actuator, **B** Anterior-posterior mechanisms and actuators.

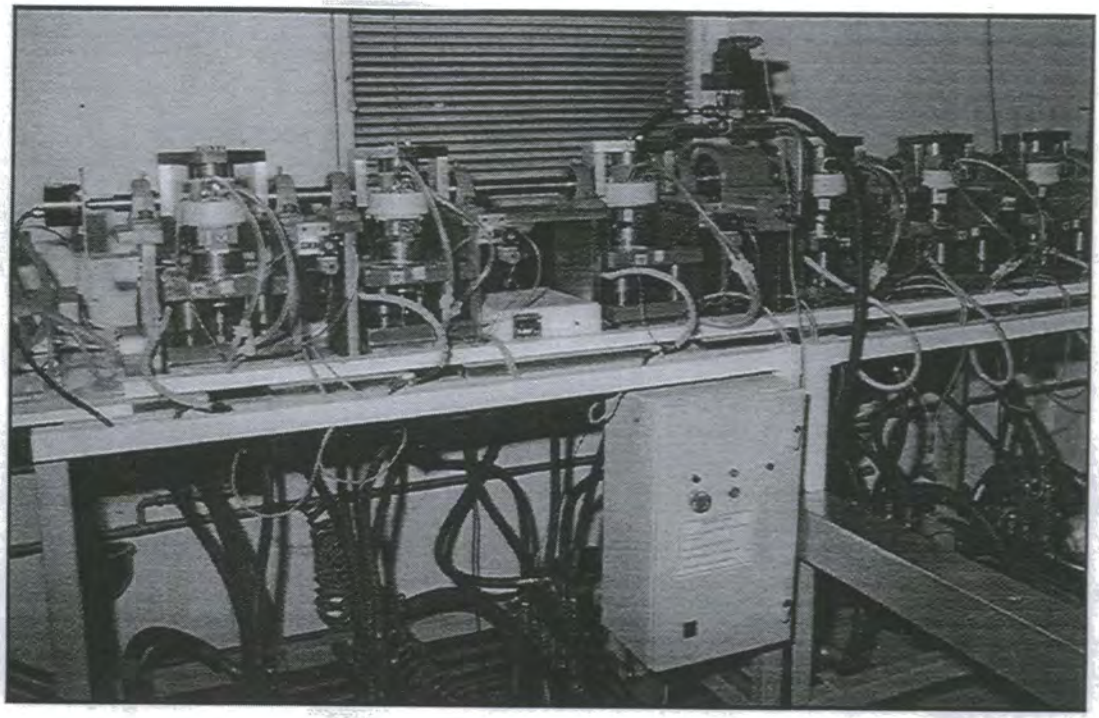

Figure 7.5. A general view of the six station knee wear simulator (covers removed for clarity).

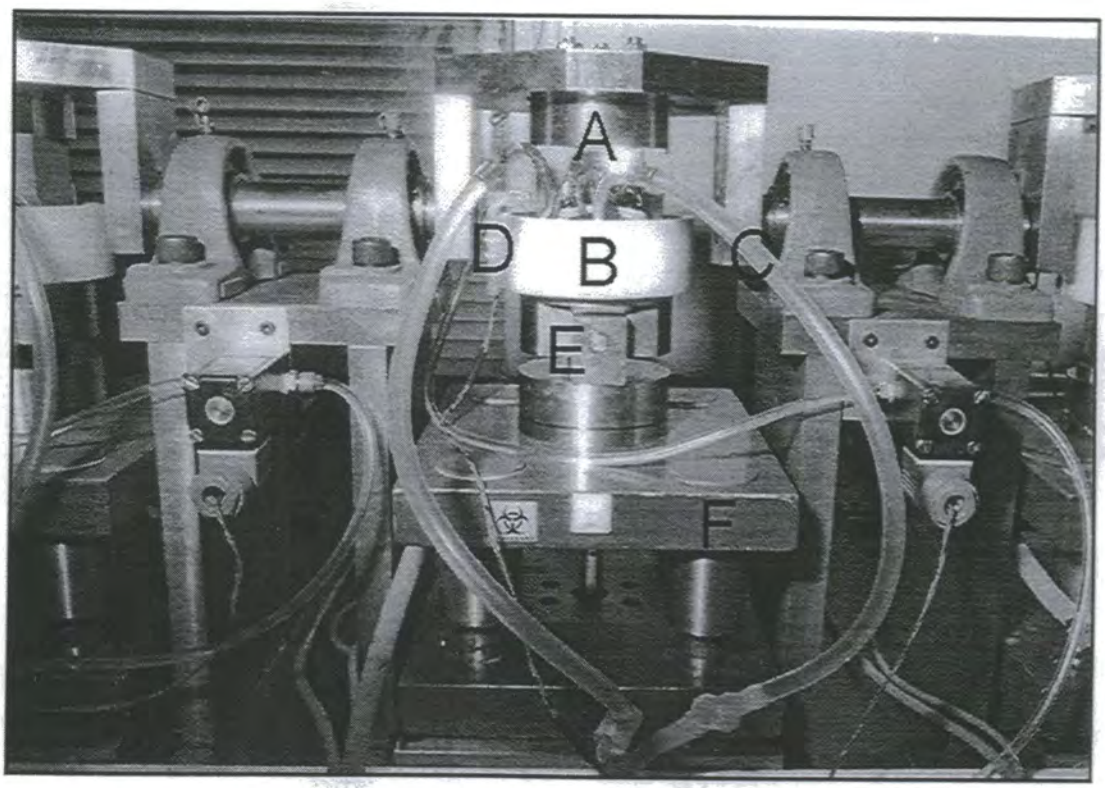

Figure 7.6. One of the six testing stations in the medial-lateral plane, with the cover removed for clarity. **A** Femoral component; **B** Lubricant bath containing the mounted tibial component; **C** Lubricant heating system; **D** Lubricant top-up sensor; **E** Tibial mount assembly; **F** Die set mounted on linear bearings.

7.3.2 Servo hydraulic design, using computer simulation.

Servo hydraulic systems offer superior power control characteristics, compared with pneumatic or electromechanical methods. As a result of commissioning and maintaining the two Durham friction simulators considerable experienced has been gained within the Centre for Biomedical Engineering regarding the design and use of these control systems. However, due to the complex multi-station multi-actuator nature of this machine, a new approach was required when designing the servo hydraulic system.

To aid design, a computer simulation technique was used. Initially a computer simulation of the servo valve was conducted, and the characteristics of the model compared with the performance data given in the manufacturers technical literature. The actuator and mechanical system were then added to the model of the valve, and a full computer simulation of each hydraulic system conducted. This enabled actuator sizes, valve sizes, and oil flow rates to be assessed, and their effect on performance and pump size to be determined. The simulation program was designed to solve a set of linear and initial value ordinary differential equations using the Runge-Kutta fourth order method (Bajpai *et al.*, 1977). The simulation language is discussed in Appendix D.

7.3.2.1 Servo valve model.

A review of the literature showed that modelling and dynamic computer simulation of a servo valve has been undertaken previously, and that different workers advocated different degrees of model complexity. However the analysis of Merritt (1967) formed the basis of a majority of the analyses. Although modelling the discrete components of the servo valve improved the model accuracy (Arafa and Rizk, 1987a and 1987b, Lin and Akers, 1989 and 1991), for simulation based design of the knee wear simulator a model

which displayed the basic non-linear characteristics of a servo valve was considered sufficient. Successful simulation based design of servo hydraulic applications has been employed by several authors (Foster and Hooker, 1983, Vukobratovic *et al.*, 1987). It was clear from the literature that realistic models of the actuator and mechanical system were as important as that of the valve.

The operation of a servo hydraulic valve was described in detail by Merrit (1967). They are considered to have two stages and act as power amplifiers. The first stage takes a low power current and converts it into a mechanical torque of the flapper spring, which in turn controls the hydraulic power used to control the second stage. The second stage is a spool, the position of which controls the flow of the high power supply fluid. Typically the spools are manufactured or lapped so as to give a small leakage flow at the central or null position. These features result in two important characteristics. Firstly, the fluid flow is proportional to the input current, at a constant supply pressure (Figure 7.8). Secondly, in a region of typically ±1.5% of the maximum control current, the pressure difference between the two output ports varies between ± supply pressure (Figure 7.9). Any servo valve model has to be capable of demonstrating these characteristics.

The servo valve model was built up in the following way. The spool or second stage of a servo valve could be represented by the diagram shown in Figure 7.10. The flow of fluid through the valve was determined by considering the flow across each of the spool surfaces A to D. The position of the spool and hence the size of the opening was proportional to the control current. When the port was open, the flow was proportional to the square root of the pressure difference and the size of the opening, the well known equation for flow through an orifice. At the null position, a small leakage flow still

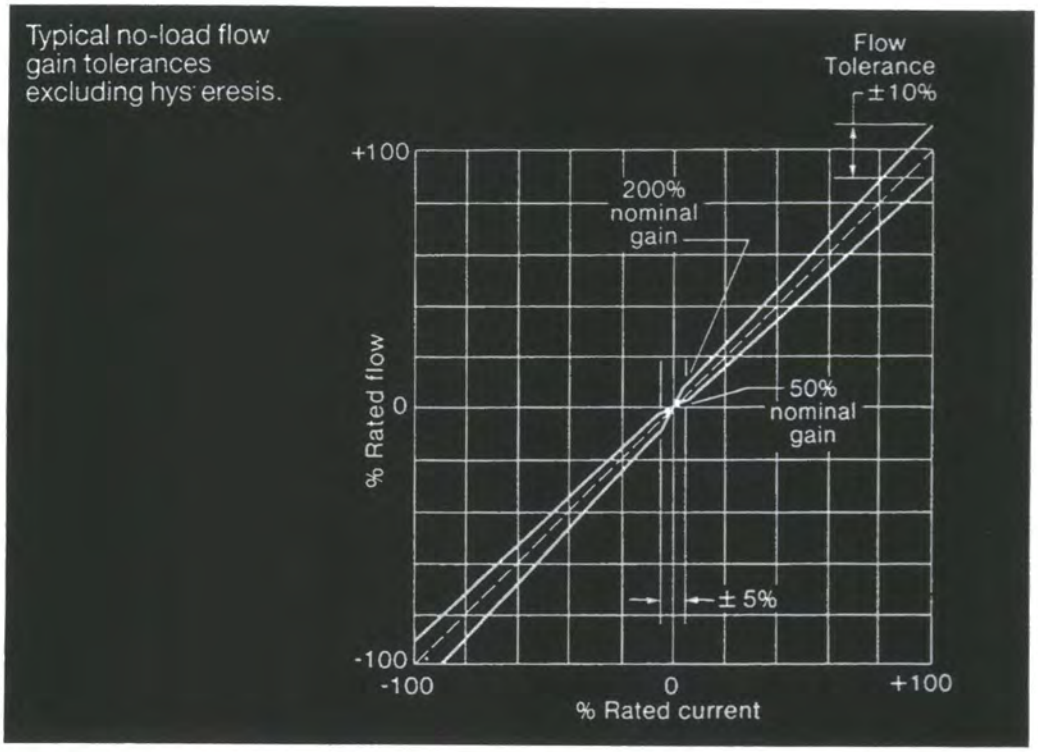

Figure 7.8. Proportional flow characteristics. (Vickers SM4 servo trade literature).

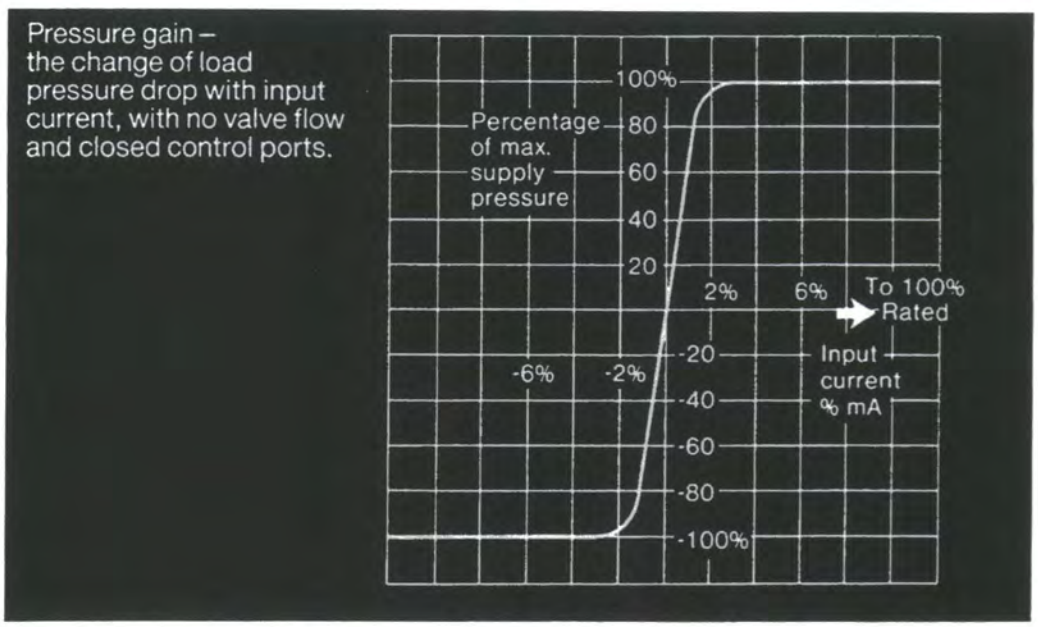

Figure 7.9. No-flow gain characteristics. (Vickers SM4 servo trade literature).

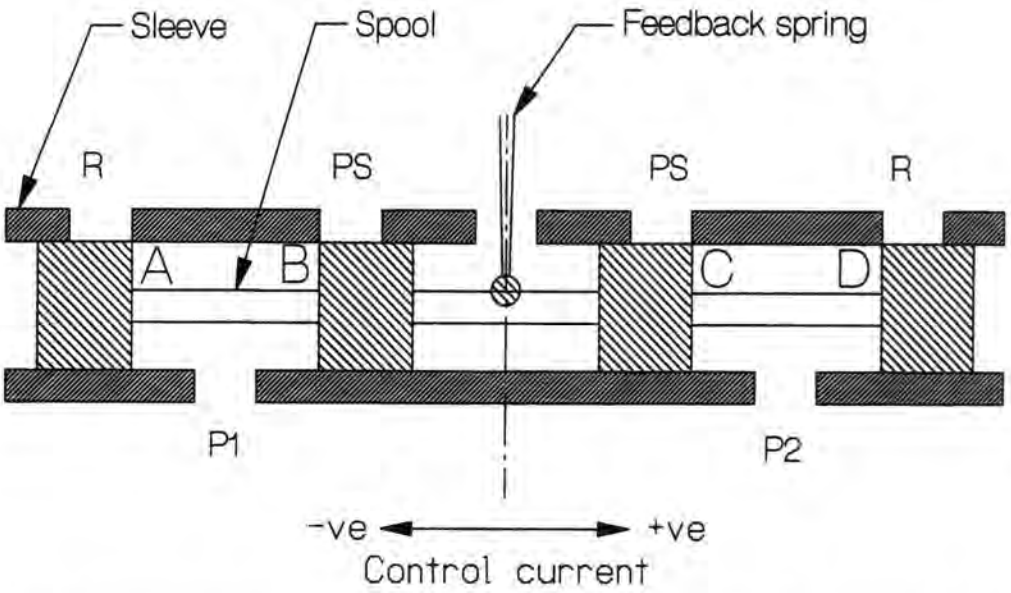

Figure 7.10. Representation of the second stage of a servo valve (PS -fluid supply, R - fluid return, P1 and P2 -pressure at output ports).

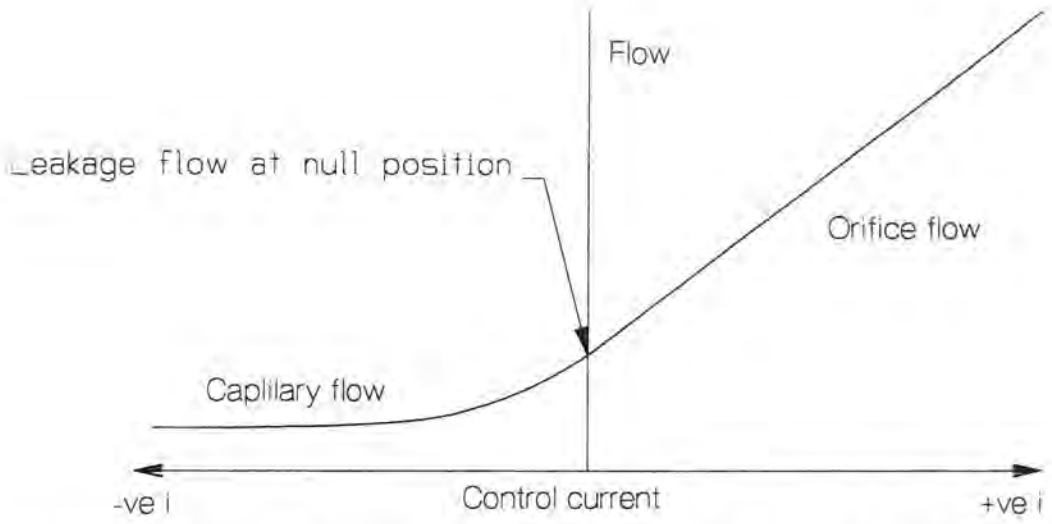

Figure 7.11. Variation of flow with spool position, for spool surface B or D, for simulation valve model.

occurred. As a port opened from the null point to maximum supply current the fluid flow was given by

$$Q = K_o i(\Delta P)^{0.5} + K_c \Delta P \qquad 7.1$$

When the port was closed a small leakage flow occurred which was proportional to the pressure difference and the reciprocal of the size of the overlap between the spool and body. This was the equation for capillary flow. However, to maintain continuity when the valve was just closed, an exponential function was considered to be a better approximation of flow across the closed port. Hence the flow was given by

$$Q = K_c \Delta P \exp\{-K_d i\} \qquad 7.2$$

The flow through the range of spool positions is shown in Figure 7.11. The decay constant K_d will determine the null band width. An estimate of K_d was made with reference to the performance, as illustrated shortly.

The constants K_o and K_c were determined from the valve specification data, which for the servo valve model used (Vickers SM4, UK) is given in Table 7.2. Considering both the flow at the null point (i=0) and when the valve was fully open ($i=i_r$), the constants K_c and K_o were found from Equations 7.2 and 7.1 respectively. Approximately one third of the leakage flow is through the valve and two thirds through the control jet at the null position, hence

$$K_c = \frac{Q_l}{3P_l} \qquad 7.3$$

$$K_o = \frac{Q_v}{i_r (\Delta P_v)^{0.5}} \qquad 7.4$$

Valve type (Vickers)	SM4-10/3.8	SM4-10/9	SM4-10/38
Nominal Size / l/min	3.8	9.0	38
Q_V /$10^{-5}m^3s^{-1}$	6.333	15.00	63.33
P_V /$10^5m^3s^{-1}$	70	70	70
i_r /10^{-3}A	±40	±40	±40
Q_l /$10^{-5}m^3s^{-1}$	1.583	1.583	1.583
P_l /$10^5m^3s^{-1}$	210	210	210
τ /10^{-3}s rad^{-1}	2.274	2.274	3.183
Ω /ohms	80	80	80
K_d # /A^{-1}	2875	2000	300

Table 7.2. Servo valve data. (# determined from simulation model performance.)

By considering whether the spool position connected an output port to return (atmosphere) or supply, the pressure difference across each surface was calculated.

$$\Delta P_A = a - P_1 \qquad 7.5$$

$$\Delta P_B = P_s - P_1 \qquad 7.6$$

$$\Delta P_C = P_s - P_2 \qquad 7.7$$

$$\Delta P_D = a - P_2 \qquad 7.8$$

The flow through the valve was then found from Equations 7.1 to 7.8. For surfaces A and C, -ve input current resulted in an opening, whereas for surfaces B and C +ve input current resulted in an opening. Surface B is given as an example;

For surface B

$$\Delta P_B = P_s - P_1$$

if (i ≥0)

$$Q_B = K_o i (\Delta P_B)^{0.5} + K_c \Delta P_B$$

else

$$Q_B = K_c \Delta P_B \exp\{-K_d i\}$$

The total flow through each output port was the sum of the supply and exhaust flows over each surface.

$$Q_1 = Q_A + Q_B \qquad 7.9$$

$$Q_2 = Q_C + Q_D \qquad 7.10$$

Equations 7.1 to 7.10 relate the flow through the valve to the pressure difference across the connecting ports and the spool position, which is directly proportional to the input current. The typical flow characteristics were determined for a no-load configuration (atmospheric pressure at the output ports). The simple model simulation code combining equations 7.1 to 7.10 in a no-load configuration is given in Appendix D. The results for three servo valve sizes, given in Figure 7.12, show good agreement with the typical flow characteristics (Figure 7.8).

In order to assess the model's pressure gain characteristics around the null point, a no flow condition was imposed, that is the volume attached to each port was set as a very small constant value. The pressure at the output ports depended on the compressibility of the fluid in this volume. The bulk compressibility of a fluid is defined as the change in pressure divided by the relative change in volume.

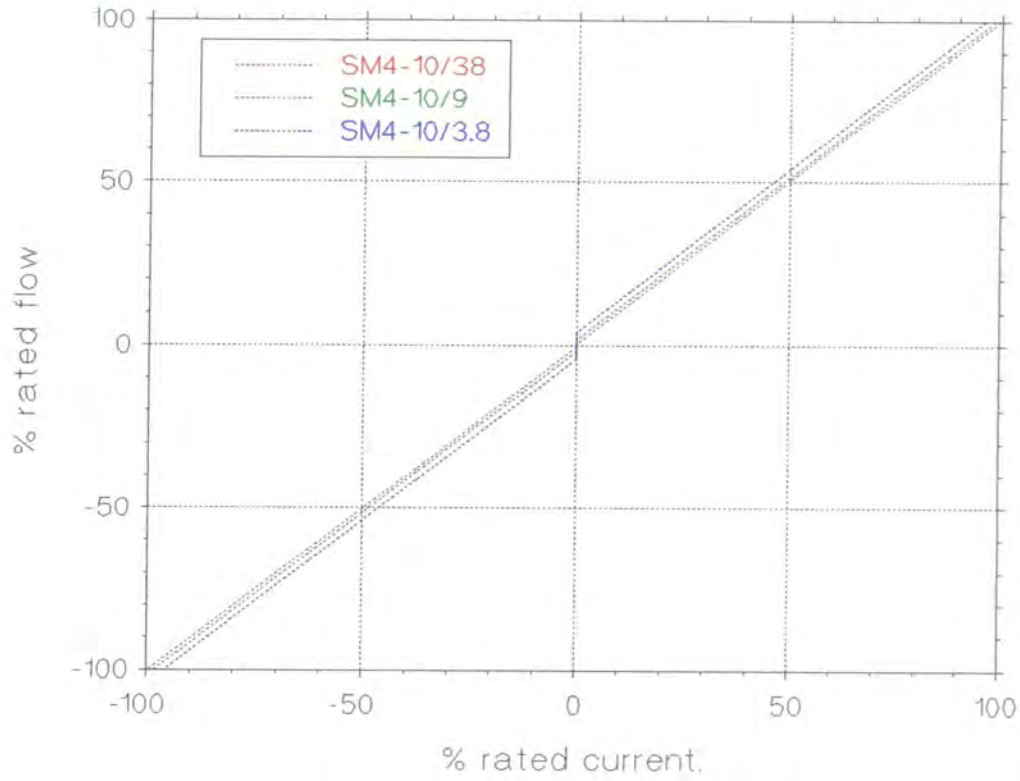

Figure 7.12. Simulation results: No-load proportional flow characteristics.

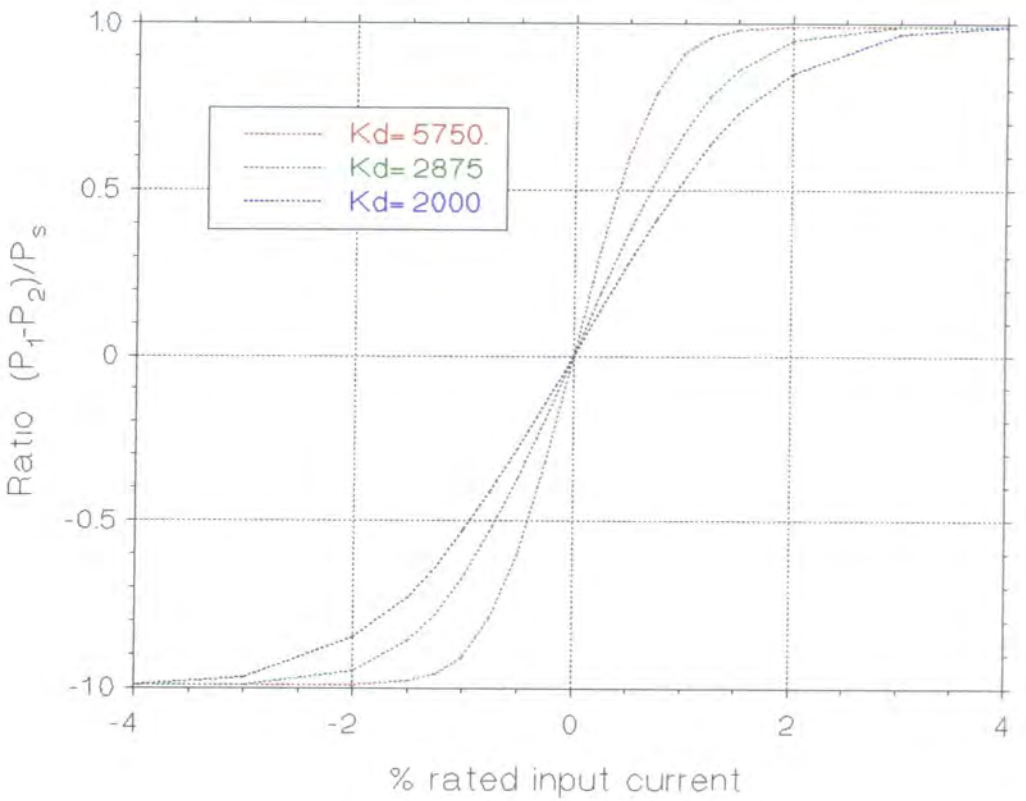

Figure 7.13. Simulation results: No-flow gain characteristics for SM4-10/3.8.

$$K = \frac{-\delta P}{\delta V / V} \quad \text{hence} \quad \delta V = \frac{-\delta P V}{K} \tag{7.11}$$

Hence the flow was given by

$$Q = \frac{\delta V}{\delta t} = \frac{V}{K}\frac{\delta P}{\delta t} \tag{7.12}$$

The pressure at each output port could then be found by integrating Equation 7.12

$$P = \int_0^t \frac{QK}{V}\,dt \tag{7.13}$$

The flow equations (7.1 to 7.10) were combined with the differential equations for each output port (7.13). The resulting simulation code is given in Appendix D. The value of K_d directly affected the size of the null band, as illustrated in Figure 7.13 for the SM4-10/3.8 valve. This model was used to estimate K_d so as to give acceptable pressure gain characteristics in the null region (compared with Figure 7.9) for all three servo valve sizes. The results are given in Table 7.2.

The results from the simulation show that the servo valve model demonstrates the required characteristics. The model was then combined with expressions representing an actuator, simple control electronics, and the mechanical system to build complete simulation models for each hydraulic system.

7.3.2.2 Simple valve and actuator model.

A simple generic valve actuator model is shown in Figure 7.14. The valve now controlled fluid flow to two variable volume cylinders on either side of the piston, denoted 1 and 2. The flow into each cylinder was related to its rate of volume change and the compressibility of the fluid, and could be written in terms of actuator dimensions, piston velocity and position.

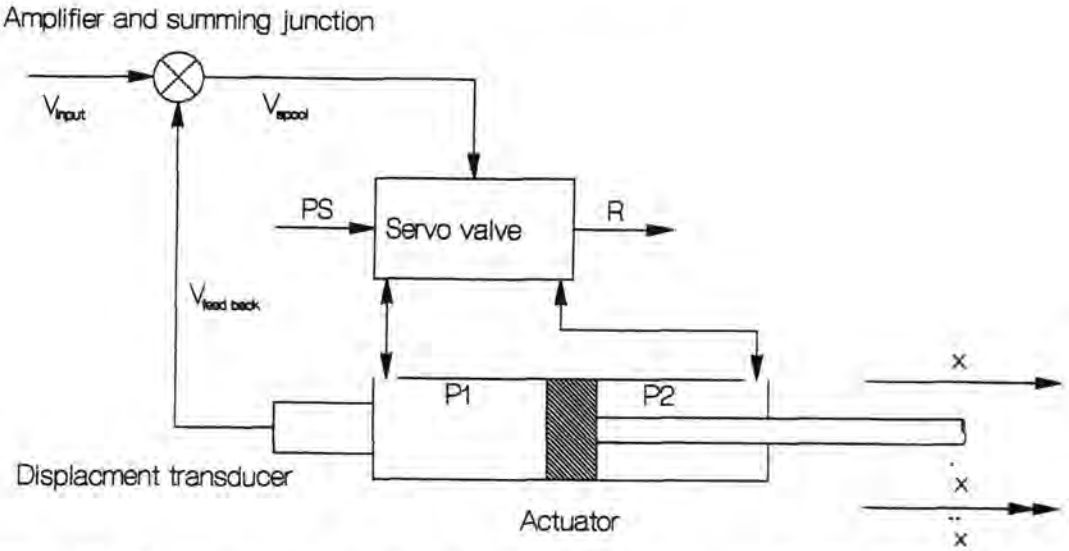

Figure 7.14. Representation of generic servo valve actuator model system, showing simple motion control feedback.

$$Q = \left(\frac{\delta V}{\delta t}\right)_{cylinder\ \ motion} + \left(\frac{\delta V}{\delta t}\right)_{compressibility}$$

$$Q = A\,\dot{x} + \frac{dP}{dt}\frac{Ax}{K} \qquad 7.14$$

rearranging and integrating Equation 7.14 gives

$$P = \int_0^t \frac{(Q - A\,\dot{x})K}{Ax}\,dt \qquad 7.15$$

When cylinder 1 increased in volume, cylinder 2 decreased and the pressure in each cylinder was determined from Equation 7.15.

$$P_1 = \int_0^t \frac{Q_1 - A_1\,\dot{x}}{A_1 x}\,dt,\quad P_2 = \int_0^t \frac{Q_2 + A_2\,\dot{x}}{A_2(L - x)}\,dt \qquad 7.16$$

The force accelerating the actuator piston mass resulted from the difference between the pressures in each cylinder.

$$F = P_1A_1 - P_2A_2 \qquad 7.17$$

The acceleration, and hence velocity and position of the cylinder, was expressed in the usual form of differential equations.

$$\ddot{x} = \frac{F}{M} \qquad 7.18$$

$$\dot{x} = \int_0^t \ddot{x}.\, dt \qquad 7.19$$

$$x = \int_0^t \dot{x}.\, dt \qquad 7.20$$

A 0-10V range was used for input voltage, feedback transducer voltage, and for summing amplifier limits. The input voltage was compared with the feed back voltage, and the error between them amplified by the summing amplifier in a normal feed back loop, Equation 7.21. The output from the summing amplifier, the spool voltage, resulted in a current in the valve armature. The spool current will not change instantaneously with the spool voltage applied to the armature, due to the inductance of the coil. Together with mechanical damping these features resulted in a frequency response curve. However the electrical damping was the dominant feature, and thus the frequency response dependency could be modelled by the usual form of differential equation for a current in an RL circuit, Equation 7.22.

$$v_{sp} = g\left(v - v_{fb}\right) \text{ where } \mathbf{g} \text{ is the gain} \qquad 7.21$$

$$i = \int_0^t \frac{v_{sp}/\Omega - i}{\tau} dt \qquad 7.22$$

The valve Equations 7.1 to 7.15, together with the actuator and mechanics Equations 7.16 to 7.20, and those describing a simple feedback loop 7.21 and 7.22 made up the simple valve and actuator model. This model formed the basis for the models specific to each of the anterior-posterior translation, flexion-extension and tibio-femoral load hydraulic systems.

7.3.2.3 Anterior-posterior translation model.

A single acting linear actuator (Hydroline, USA) moved the tibial component in anterior-posterior translation. An internal cylinder-mounted non-contacting position transducer (Balluff, USA) was used for 0-10V closed loop feedback control, as it was inherently robust and reliable. Due to the physical size of this transducer the minimum rod diameter was 35 mm. A 50 mm stroke was specified so as to allow for positioning of the tibial component. The profile reported by Lafortune *et al.*, (1992) Figure 7.3, was simulated by a 2 Hz sine wave of amplitude 6 mm. In addition to accelerating the mass of the tibial mount assembly and the die set, the frictional damping effect of the linear bearings and prostheses were also included in the model. The simulation code is given in Appendix D. The design parameters were varied so as to give the best response characteristics, and the results for the optimum design configuration are given in Figure 7.15a-d. The control signal was varied ±1.2 V to give a request amplitude of ±6 mm at 2 Hz (Figure 7.15a). The small variations in pressure and flow between different parts of the cycle (Figures 7.15c and d) were a result of the different frictional effects during the stance and swing phase. The effects of changing valve and actuator sizes on the resulting performance of the system (Figure 7.15b) was then established, and the limitations of the proposed design were investigated.

7.3.2.4 Flexion-extension model.

This actuator had to move all six femoral components in the reported flexion-extension angular motion given by Lafortune *et al.*, (1992) Figure 7.2, which was simulated by a 2 Hz sine wave of amplitude 32.5°. A method of producing hydraulically controlled rotary motion of the femoral component was required. A novel design of rotary actuator (Helac, USA) based on a piston moving within a helix (reported to avoid wear and

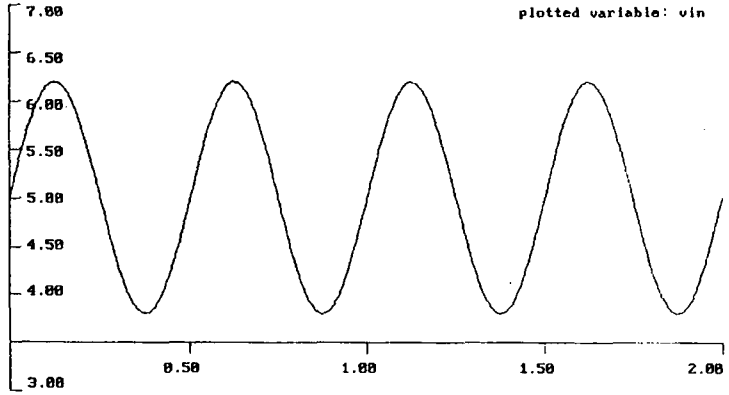

a. Control signal v_{in}.

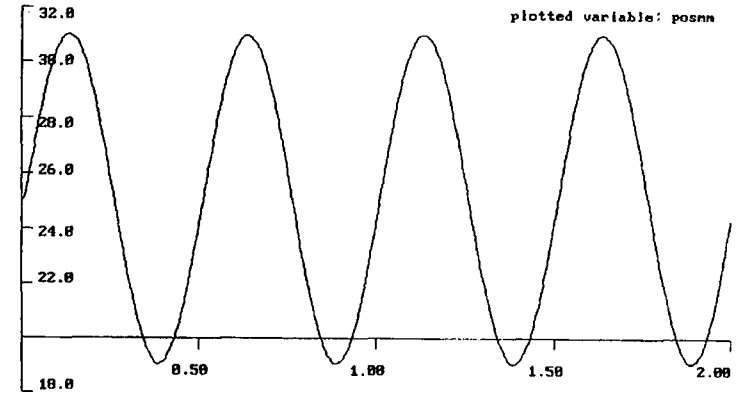

b. Resulting anterior posterior translation ±6mm at 2Hz.

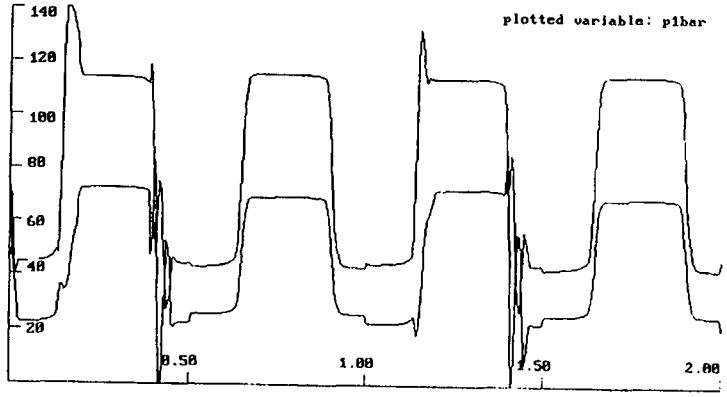

c. Pressure variation on each side of the actuator piston. Both P1 and P2 shown (bar).

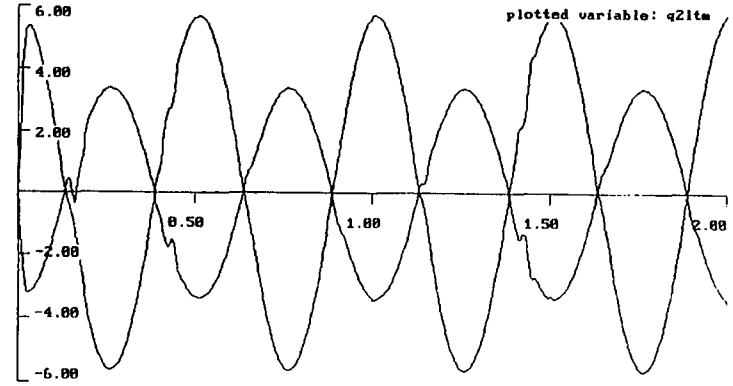

d. Flow variation for each side of the actuator piston. Both Q1 and Q2 shown (lts/min).

Figure 7.15. Simulation results for the anterior-posterior translation model.

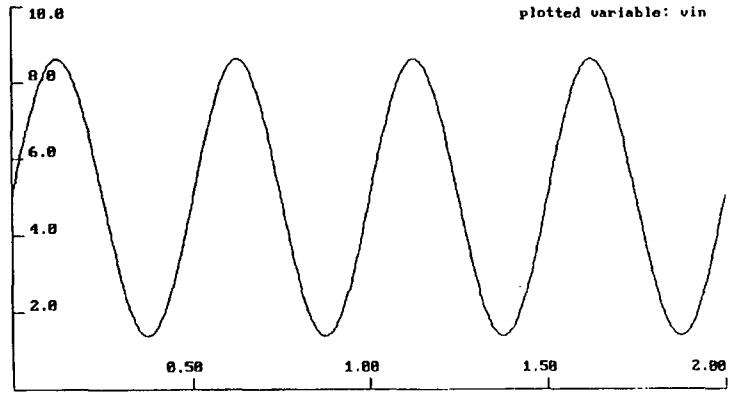

a. Control signal v_{in}.

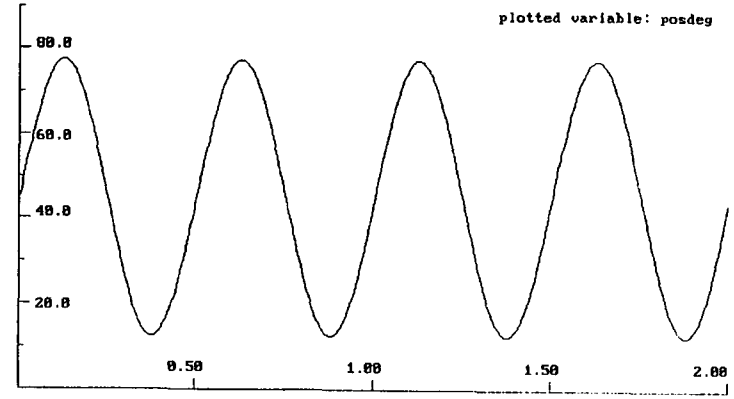

b. Resulting flexion extension rotation of ±32.5° at 2Hz.

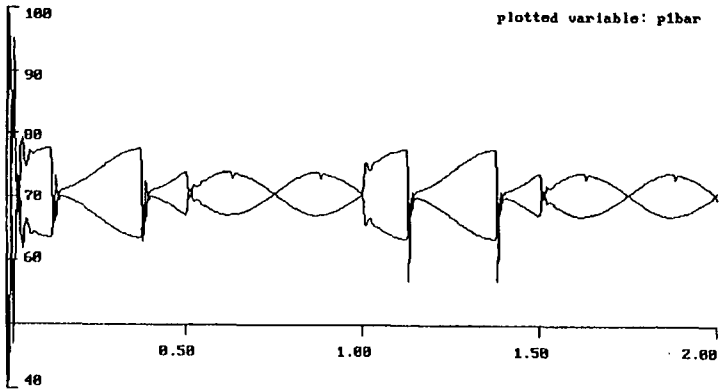

c. Pressure variation on each side of the actuator piston. Both P1 and P2 shown (bar).

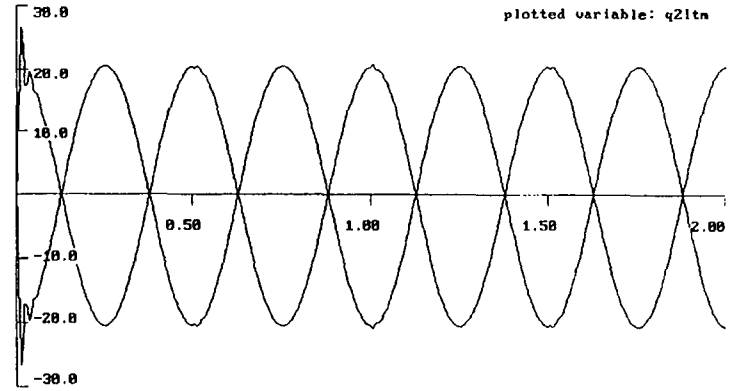

d. Flow variation for each side of the actuator piston. Both Q1 and Q2 shown (lts/min).

Figure 7.16. Simulation results for the flexion-extension model.

backlash problems), was discounted as it was found to be too costly and have a suspected short seal life. Other options included in-house manufacture of a rack and pinion driven by a standard linear actuator, or an integral double cylinder rotary actuator with rack and pinion (AID, UK). The last option was chosen since control of commercial machining tolerances minimised backlash to only 20'. A 90° motion range was sufficient for a normal walking cycle. A non-contacting incremental encoder (Homer, UK) was specified as the 0-10 V rotary feedback transducer, for reasons of long term reliability. The actuator torque, which induced angular acceleration on the mass of the femoral components, mounts and shaft, also had to overcome the frictional damping of the roller bearings and prostheses. The simulation code is given in Appendix D. The design parameters were varied so as to give the best response characteristics, in much the same way as the anterior-posterior translation system, and the results for the optimum design configuration are given in Figures 7.16a to d. This clearly showed how all the important variables changed during the cycle. This system required high peak flow rates of 20 l/min, the largest single requirement of hydraulic fluid flow in the system.

7.3.2.5 Tibio-femoral load model.

This actuator applied the dynamic load given by Seireg and Arvikar (1975), Figure 7.1, to the tibio-femoral joint, with a maximum load of 5 kN. The load system model is shown in Figure 7.17. The main difference between this system and the previous two models is that load control was used rather than position control. A 10 kN load cell (Model 41E, RDP, UK) was used to give the 0-10 V feedback signal. During load control a servo valve would operate around the null region, with the resulting pressure difference between the two cylinders controlling the applied load. Since the femoral components of current TKRs tend not have a constant centre of rotation, a small amount of vertical

motion of the tibia was required so as to maintain contact. Thus a conflict resulted, since load control requires spool currents in the ±1.5% i_r null region, whereas motion requires fluid flow and spool currents greater than ±1.5% i_r. For this reason the design of the load system was the most complex, and thus the computer simulation offered a significant improvement over discrete point in time analysis.

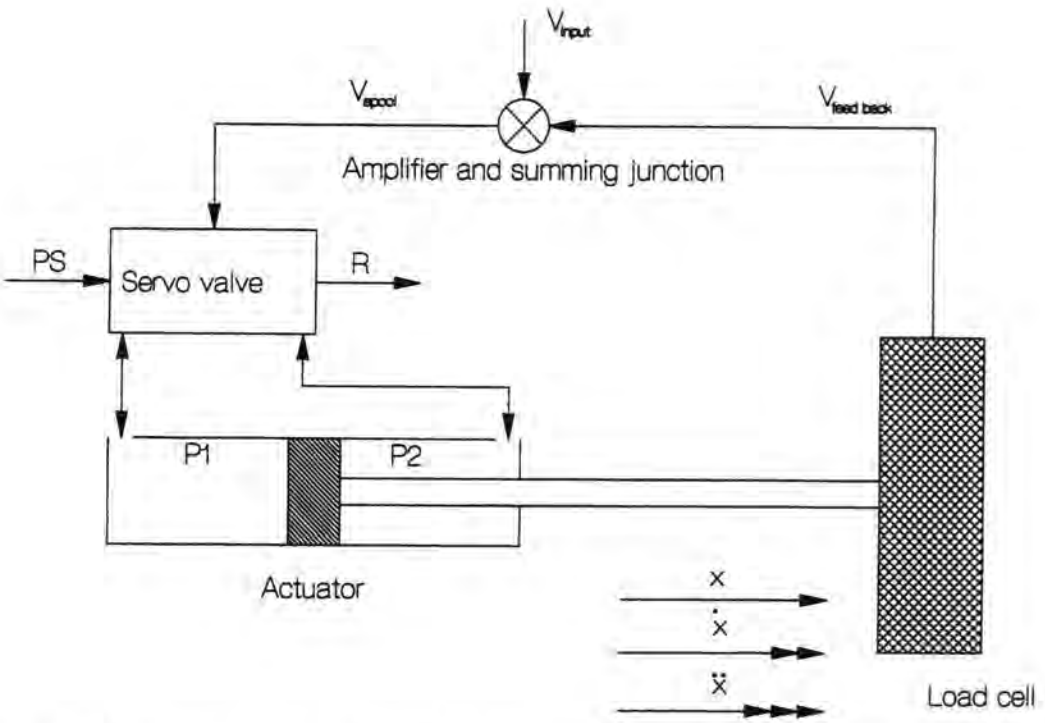

Figure 7.17. Representation of servo valve actuator model system, with simple load control feedback.

A standard linear actuator (Hydroline, USA) was used, with a manifold mounted servo valve for fast response characteristics. The actuator force applied the tibio-femoral load, accelerated the tibia mount mass to maintain contact with the femoral component, compressed both the load cell and the prosthesis (especially if a compliant layer prosthesis was under test), and overcame frictional and viscous damping. These features were all built into the simulation code, which is given in Appendix D. The design parameters were varied so as to give the best response characteristics, and the results for

the optimum design configuration are given in Figure 7.18a-h. The limitations of the proposed design were also investigated.

The control signal was varied between 0.2 and 5 V to give a simplified stance and swing phase loading cycle of 0.2 to 5 kN, of the form shown in Figure 7.18a. In addition to the load cycle, contact had to be maintained with the femoral component which was modelled with sinusoidal vertical displacement of ±2 mm at 2 Hz (Figure 7.18b). The model indicated that although the small servo valve (SM4-10/3.8) initially specified for the load system was capable of controlling the applied load, as soon as an additional requirement of the vertical displacement was imposed on the system it became unstable. This was because the fluid flow was insufficient to maintain contact while still controlling load. However the simulation did illustrate that a slightly larger servo valve (SM4-10/9) would allow contact between the joint surfaces while still maintaining good load control. Note from Figure 7.18c that the SM4-10/9 valve operates around its null point throughout the cycle. The loads measured by the load cell and those applied at the bearing surface (Figures 7.18e and f) were near identical, illustrating the negligible effect of the die-set top inertia. The variation of cylinder pressure and fluid flow was determined from Figures 7.18g and h, illustrating a maximum pressure of 140 bar, and peak flow rates of about 1 l/min.

7.3.2.6 Final design of the hydraulic system.

Using the results from the computer simulation, a specification and detail design of the hydraulic system was drawn up. This is summarised in Table 7.3. A total maximum flow of 62.1 l/min was required when the cylinder velocity was greatest, which occurred at the same point in the gait cycle for each servo hydraulic system, *i.e.* during the early and late

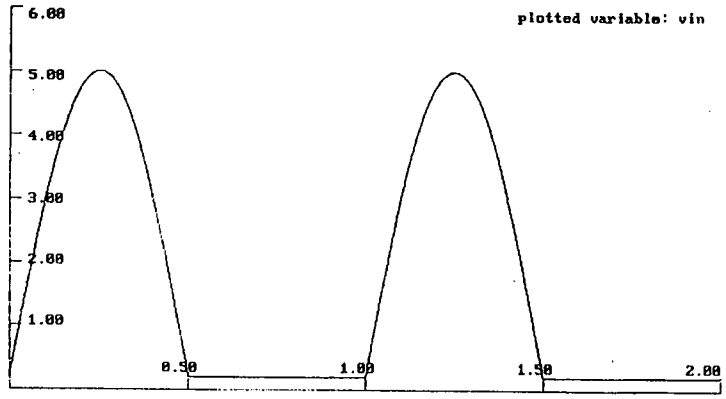

a. Control signal v_{in}, representing a stance load of 5000N and a swing load of 200N.

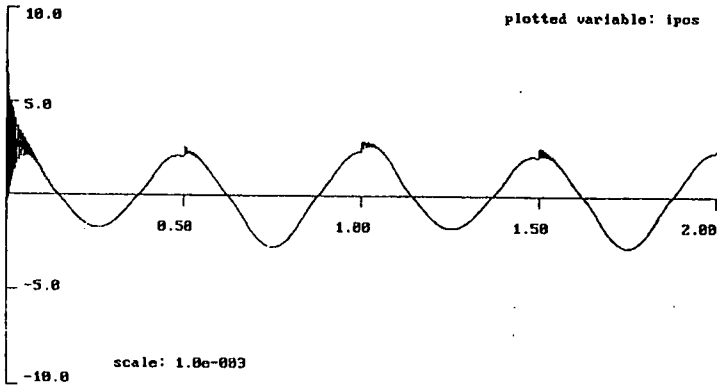

c. Resulting control current (A). Note that the valve is operating mainly around it's null point.

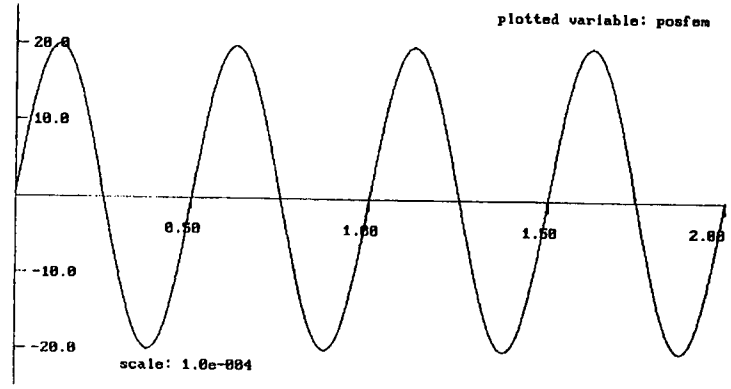

b. Vertical displacement of the femoral component due to the flexion extension motion (m).

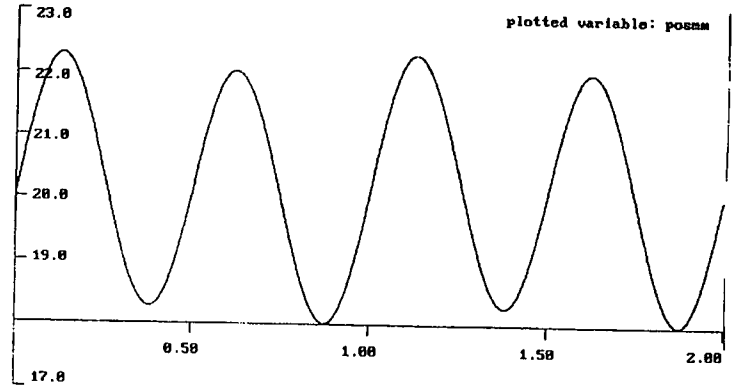

d. Piston position (mm). Note the smaller displacements observed during the low load swing phase.

Figure 7.18. Simulation results for the load model.

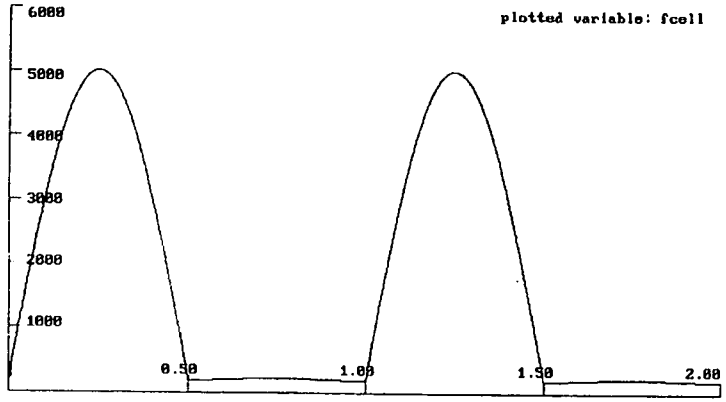

e. Resulting load applied to the load cell (N).

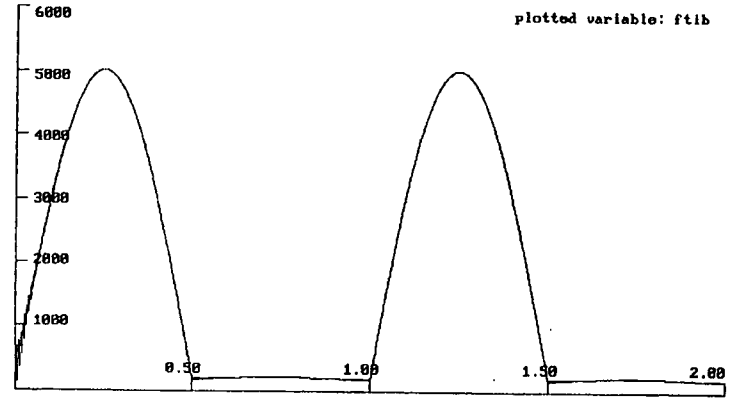

f. Resulting load applied to the tibial component (N).

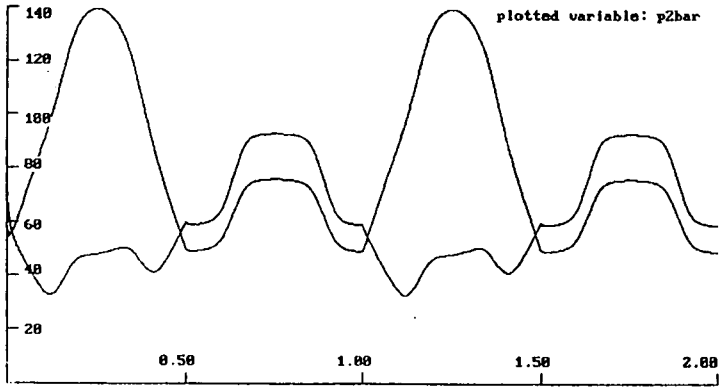

g. Pressure variation on each side of the actuator piston. Both P1 and P2 shown (bar).

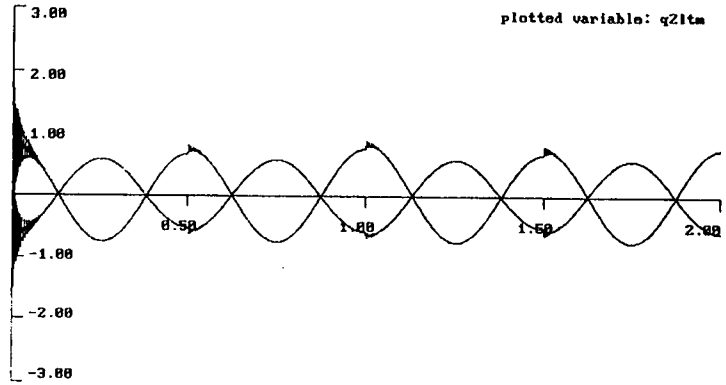

h. Flow variation for each side of the actuator piston. Both Q1 and Q2 shown (lts/min).

Figure 7.18 (cont.). Simulation results for the load model.

parts of the swing phase. The fluid was required at a pressure of 140 bar. Thus the maximum fluid power required was 14.5 kW.

System	Actuator specification*.	Valve specification.	No. off	Maximum fluid flow #	Feed back device.
Anterior posterior drawer	N5 cylinder. 50x39x50 mm (Hydroline, US)	SM4-10/9 (Vickers, UK)	6	35.4 l/min	Magnetostriction LDT, BT series. (Balluff, US.)
Flexion extension actuator	Rotary single rack. TR15. 90° (AID, UK)	SM4-10/38 (Vickers, UK)	1	20.7 l/min	Encoder. CSWKD23A (Homer, UK)
Load actuator	R5 cylinder. 25x12.5x40 mm (Hydroline, US)	SM4-10/9 (Vickers, UK)	6	6.0 l/min	Load cell 41E 10 kN (RDP, UK.)

Table 7.3. Summary of hydraulic system design specification. (*actuator dimensions; borexrodxstroke. # total maximum fluid flow for six station machine, including the control jet leakage).

Allowing for transmission losses, an 18.5 kW motor driving a variable displacement hydraulic pump (Vickers, UK) was specified, and supplied with a 400 l fluid reservoir which gave a suitable circulation time for the oil (Quick Hydraulics, Newcastle). The pump unit was situated in a pump room due to its size and operating noise.

7.3.3 Computer control.

The design of the hardware and software was an extension of the basic system used to control the single servo hydraulic systems in the two Durham friction simulators. The basic arrangement of the current system is shown in Figure 7.19. The PC acted as a terminal for the Motorola 68020 microprocessor, displayed the output from each

feedback transducer, and saved the data. The Motorola 68020 microprocessor controlled the operation of the 13 servo hydraulic systems; it updated the DAC and read the ADC 128 times per cycle. Also as a safety feature, it compared the feedback signal to the request signal, and if differences of more than a user defined amount were detected the test was stopped. For each of the six stations, a PCB containing ADC, DAC, summing amplifier and comparitor for both the load and anterior-posterior translation systems was designed and built. A similar PCB was designed and built to control the flexion-extension actuator. As an additional safety feature, hardware limits were set to trip the hydraulic pump if the output from any of the feedback transducers exceeded a user defined value. The software was written, and the detailed hardware design conducted by Mr M Kolar[1].

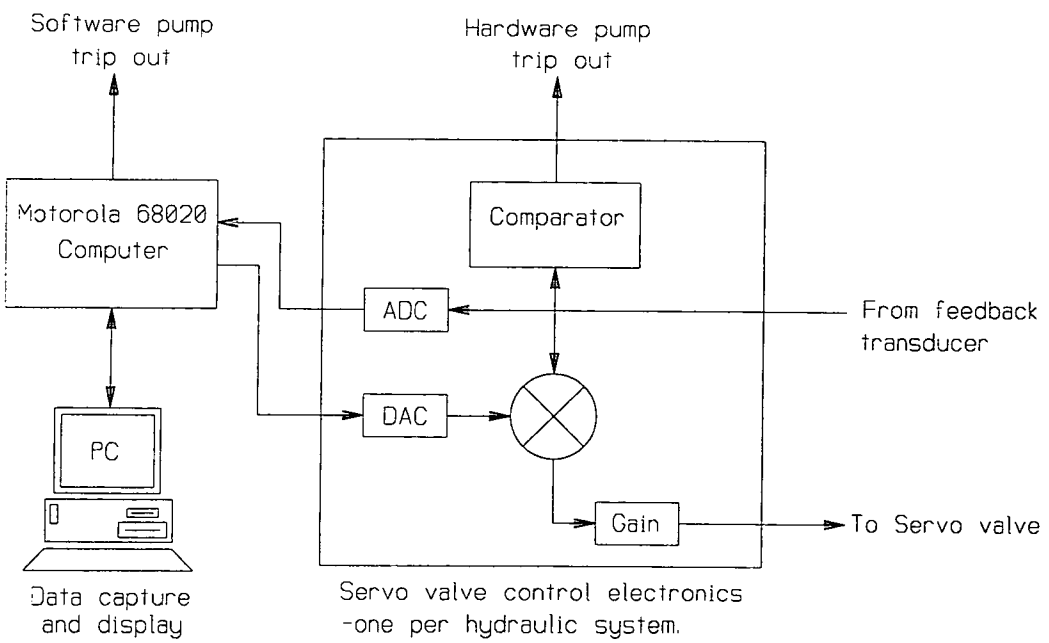

Figure 7.19. Representation of the computer control system.

[1]Microprocessor centre, School of Engineering, University of Durham.

7.4 Commissioning.

Initially a single station prototype knee wear simulator, incorporating three servo hydraulic systems, was built and commissioned. Commissioning the servo hydraulic systems was similar in all three cases. Having established that all the electronic control circuitry was functioning, the servo valve was first driven by a DC power supply, then open loop from the computer driven DAC, and finally using closed loop feedback control. The control function used progressed from sinusoidal, to triangular, and finally to a stepped function. The gain was progressively adjusted to give a fairly fast response with a small overshoot, while still maintaining stability. Finally the load and motion profiles (Figures 7.1, 7.2 and 7.3) were digitised and used to control the respective systems. In order to validate the single station prototype simulator, and confirm that it met the objectives outlined in the previous chapter, a preliminary long term wear test (8 million cycles) was conducted. The overall performance of the simulator and the wear results are discussed in the next chapter.

Next, the simulator was extended to six stations. Slight modifications were made to the analogue control PCB's, and commissioning progressed in a similar way to the single station prototype, except that now thirteen servo hydraulic systems had to be correctly adjusted! Finally a long term validation wear test (5.6 million cycles) for the six station machine was conducted, which is also discussed in the next chapter.

Chapter 8. Knee simulator: Wear results and discussion.

8.0 Introduction.

The wear experiments described here were conducted primarily to validate the machine and the method of wear assessment. The objective was to compare *in vitro* wear rates with results published in the literature, and hopefully to demonstrate similar wear patterns compared with *ex vivo* studies. This was an important developmental step, since it showed whether the simulator was a valid tool for assessing the performance of new designs of knee prostheses. Two validation tests were conducted; an 8.0 million cycle test using the single station prototype machine, and a 5.6 million cycles test using the completed six station machine. The materials and methods used in each test were essentially the same, and where differences existed these are highlighted in the relevant results section. These results are then discussed with reference to the *in vitro* and *ex vivo* studies in the literature. Finally, since the reason for developing the simulator was to support the development of compliant bearing knee prostheses, the results from two half million cycle tests using early prototype compliant bearing knees are presented.

8.1 Materials and methods.

Each femoral component was mounted with the centre of rotation of the posterior condyles co-incident with the centre of rotation of the simulator. This minimised the

vertical translation of the bearing surface during flexion. The UHMWPE tibial components were located on a metallic base plate using a snap fit. The UHMWPE components were all conditioned in Ringers solution at 37°C for more than thirty days before the start of a test.

The experiments were conducted in 30% bovine serum with 0.2% sodium azide added to retard degradation. The serum degraded over several days and needed replacing regularly. The lubricant was made up using bovine serum filtered using a 1 μm filter (GF/B, Whatman, UK). To maintain the lubricant at 37°C, heated water was pumped through a stainless steel coil immersed in the lubricant bath. The temperature of this water was controlled using a PID controller (CAL 9900, UK), three 40W 12V heating elements in a water reservoir, and a feedback thermocouple situated in one of the lubricant baths. This method was chosen, rather than a recirculating lubricant system, since it would have been too costly to replace large volumes of bovine serum regularly. As the level of the lubricant dropped due to evaporation, a sensor activated a valve which allowed distilled water to flow in to the lubricant bath and maintain the correct level.

A gravimetric or weight loss method was chosen as the method of wear assessment. This method is accurate so long as the component can be easily removed and replaced for assessment, and account is taken of any moisture absorption over the duration of the experiment. For this reason soak control UHMWPE bearings were used, which were immersed in bovine serum and placed in the heated water reservoir at 37°C, but not subjected to any loading. The tests generally ran 24 hours per day, 7 days per week. The lubricant was changed approximately every 150,000 cycles (generally every Monday, Wednesday and Friday), and the wear and control samples weighed. To ensure accurate

and reproducible results a specified cleaning and weighing protocol was strictly adhered to (Table 8.1). This was similar to that recommended in ASTM F04.0302.12 (1992), ASTM F04.2.5.23 (1991), and BS 7251: Part8: 1990.

1. The tibial and femoral mounts were removed from the machine, and the used lubricant decanted and frozen.
2. The wear sample was removed by prising apart the snap fit. (Previous experiments showed that this did not affect the mass of the specimen.)
3. The wear and control specimens were rinsed with tap water to remove the bulk of the contaminants.
4. The specimens were washed in a 1% solution of Neutracon (Decon, UK) in an ultrasonic bath for 30 minutes at 40°C, to remove other contaminants.
5. The specimens were rinsed under tap water, and then under a stream of distilled water.
6. The specimens were then rinsed in acetone for 60s to remove water from the surface.
7. The specimens were allowed to dry in air for 30 minutes before weighing.

Table 8.1. Cleaning protocol for the tibial components during the two validation tests.

The weight loss or gain of the samples was measured using a Mettler AE200 balance, with an accuracy 0.1 mg, taking an average of three readings. The effect of moisture absorption was eliminated using the method detailed in BS 7251: Part8: 1990. To clean the bath and femoral component, they were immersed in a warm 1% solution of Neutracon for 20 minutes, and then rinsed under tap and distilled water.

8.2 Results.

In order to validate the machine and the method of wear assessment two validation tests were conducted; an 8.0 million cycle test using the single station prototype machine, and a 5.6 million cycles test using the completed six station machine. Conventional TKRs were used in each. The quantitative results are presented in three forms; weight loss per million cycles, volume loss per million cycles, and wear factor (defined for example by Dowson *et al.* 1990). The gradient of the straight line least squares fit to the true weight loss data gave the weight loss per million cycles. This was converted to volume loss per million cycles by dividing the weight loss by the density of UHMWPE (0.93 g mm^{-3}). The wear factor is given by Equation 8.1.

$$V = k\int L.\,dx \qquad 8.1$$

$\int L\delta x$ is derived from the load and motion profiles (Figure 8.1). The advantage of using a wear factor is that it takes account of the load and sliding distance and hence makes comparisons between different experimental conditions easier.

8.2.1 Single station validation test results.

A medium Kinemax TKR (Howmedica Europe, Staines) with an 8 mm thick tibial component was tested in the initial single station simulator, using a maximum load of 3 kN, extension-flexion of 0-65°, and anterior-posterior translation of 12 mm. UK adult bovine serum (Medical and Veterinary Supplies Ltd, Bucks, UK) was used. It was made up to the correct concentration in bulk and frozen until required. The wear rates were determined from Figure 8.2. The mass loss was 2.66 mg/10^6 cycles (95% confidence

interval 2.74 to 2.58 mg/10^6 cycles), volume loss 2.86 $mm^3/10^6$ cycles, and wear factor 0.05 $mm^3/Nm/10^6$.

The simulator met the design specification in most respects and performed reliably over the duration of the 8.0 million cycle test, with two exceptions. The lubricant heating system functioned erratically during the first 3.5 million cycles as a result of a sticking relay, with occasional variation in temperatures from ambient to 47°C. This resulted in erratic moisture absorption, but this occurred equally in both the wear and control samples, and hence the overall wear rate was not affected (see Figure 8.2). The simulator performed satisfactorily at a test frequency of 1 Hz, but an electrical noise problem was encountered which caused the Motorola 68020 control computer to crash, typically once every 24 hours. However, a test frequency of 0.8 Hz did not give such a problem, and hence the majority of the test was conducted with the simulator operating continuously at 0.8 Hz.

8.2.2 Six station validation test results.

Three medium Kinemax TKRs and three medium Kinematic TKRs were tested (Howmedica Europe, Staines), all with an 8 mm thick tibial component. A maximum load of 3 kN and extension-flexion of 0-65° was used for each station. New Zealand calf bovine serum (Medical and Veterinary Supplies Ltd, Bucks, UK) was used throughout the test, and was made up to the correct concentration on the day of use.

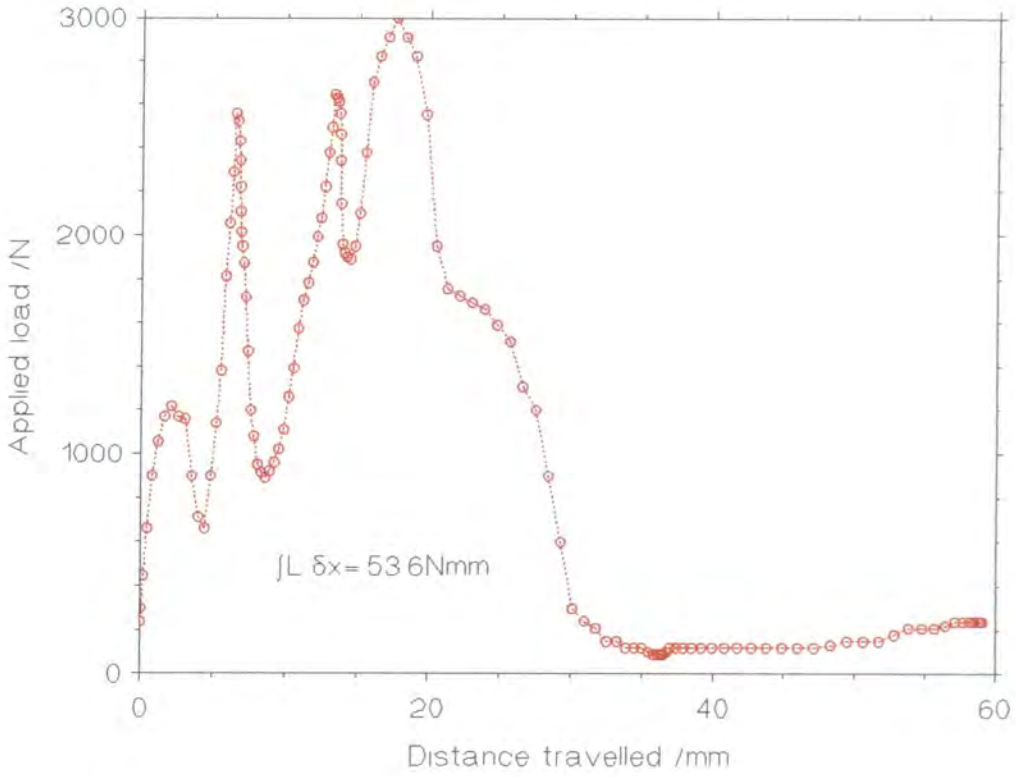

Figure 8.1. Function ∫Lδx over one complete cycle.

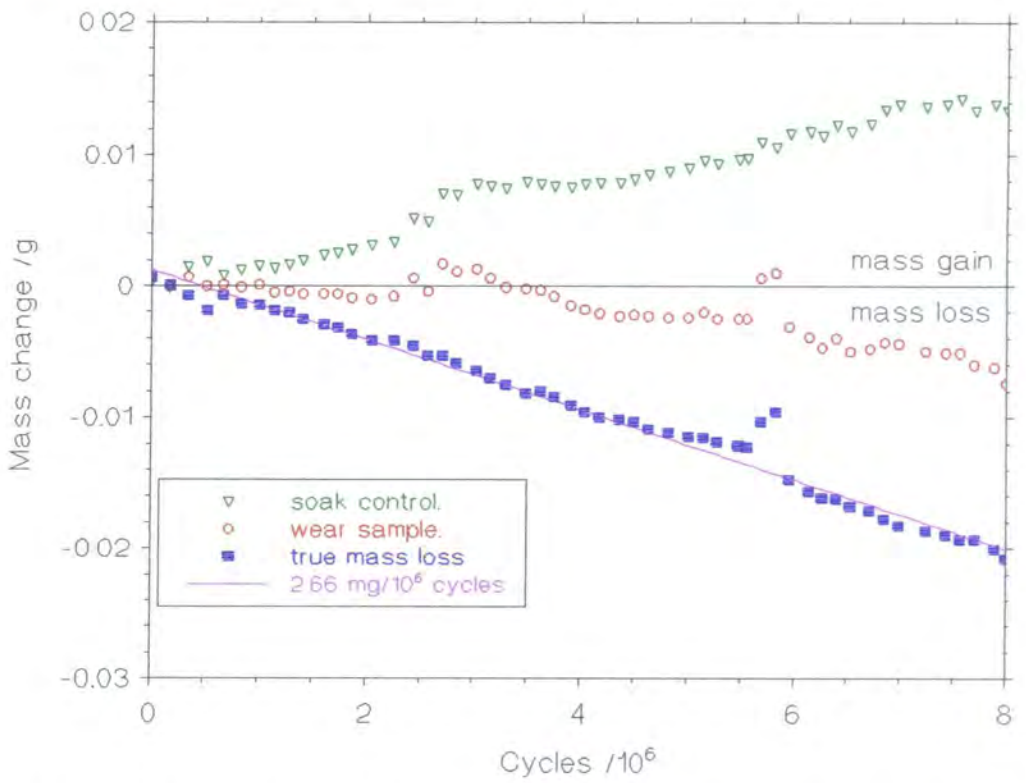

Figure 8.2 Wear results: Kinemax tested on the single station prototype machine. (Note that the two rogue data points just before 6 million cycles were discarded during regression analysis. They were due to a lump of precipitate lodged under a cut out).

The anterior-posterior translation was changed to suit the different designs of prostheses, as indicated in Table 8.2. The decision regarding the amount of anterior-posterior translation applied to a particular design of prostheses is probably critical, but was made using a combination of range of motion observations, and intuition. The anterior-posterior translation profile (Figure 7.3) was scaled to give the desired amplitude of motion, based on the conformity of the bearing and the contact regime at the extremes of flexion. For example, the Kinematic TKRs were less conforming than the Kinemax TKRs, and so simple observation of the contact regime indicated that larger translations were more suitable for the less conforming Kinematic design. Sensible transition limits were derived by observing the point of contact while moving both the flexion-extension and anterior-posterior actuators discretely, and applying a load across the bearing.

In addition, internal-external rotation was added to two stations (stations 1 and 6) using a simple mechanical lever mechanism which linked rotation of the tibial component to the anterior-posterior translation motion. The lever arm lengths were adjusted to give ±5° of rotation in both cases. The other four stations retained uncontrolled passive internal-external rotation, as specified in the original design specification.

The load and kinematic conditions applied to each of the test prostheses are outlined in Table 8.2. Clearly stations 2 and 3, and stations 4 and 5 were programmed using nominally the same conditions. Hence, in order to investigate any inter-station variability, the test prostheses were swapped between these two pairs of stations and any differences in wear rates recorded. Linear regression analysis was performed on each set of true weight loss data (taking account of any moisture absorption using suitable soak control samples). The analysis was carried out on the complete data sets, and also on data before

and after swapping test prostheses between stations (if relevant). A summary of all the wear data is given in Table 8.3, and illustrated graphically in Figures 8.3 to 8.8.

Test prosthesis.	#1	#2	#3	#4	#5	#6
Prosthesis type.	Medium Kinematic LH. 8 mm bearings.			Medium Kinemax 8 mm bearings		
Load.	3 kN.					
Flexion.	0-65°.					
A-P translation.	7.0 mm	8.5 mm		5.5 mm		4.5 mm
Int-Ext rotation.	±5°	Passive		Passive		±5°
Soak control.	Kinematic #7			Kinemax #8		
Test station.	1	2 (3)*	3 (2)*	4 (5)+	5 (4)+	6

Table 8.2. Test conditions applied during the six station validation test. (*stations swapped after 1.5 million cycles, +stations swapped after 3.5 million cycles).

Test prostheses	Cycles /10^6	Wear rate (95% confidence interval) mg/10^6 cycles		
		First station	Second station	All data
#1	1.8	-	-	4.72 (5.26-4.20)
#2	5.6	1.00 (1.46-0.54)*	1.19 (1.29-1.10)*	1.33 (1.40-1.26)
#3	5.6	4.97 (5.49-4.44)*	1.89 (2.07-1.71)*	2.96 (3.29-2.64)
#4	5.6	6.45 (7.07-5.83)+	2.72 (3.11-2.32)+	4.74 (5.21-4.26)
#5	5.6	1.42 (1.57-1.28)+	2.69 (3.36-2.03)+	1.70 (1.83-1.58)
#6	5.6	-	-	4.89 (5.12-4.66)

Table 8.3. A summary of wear rate data from the six station validation test. (*stations swapped after 1.5 million cycles, +stations swapped after 3.5 million cycles).

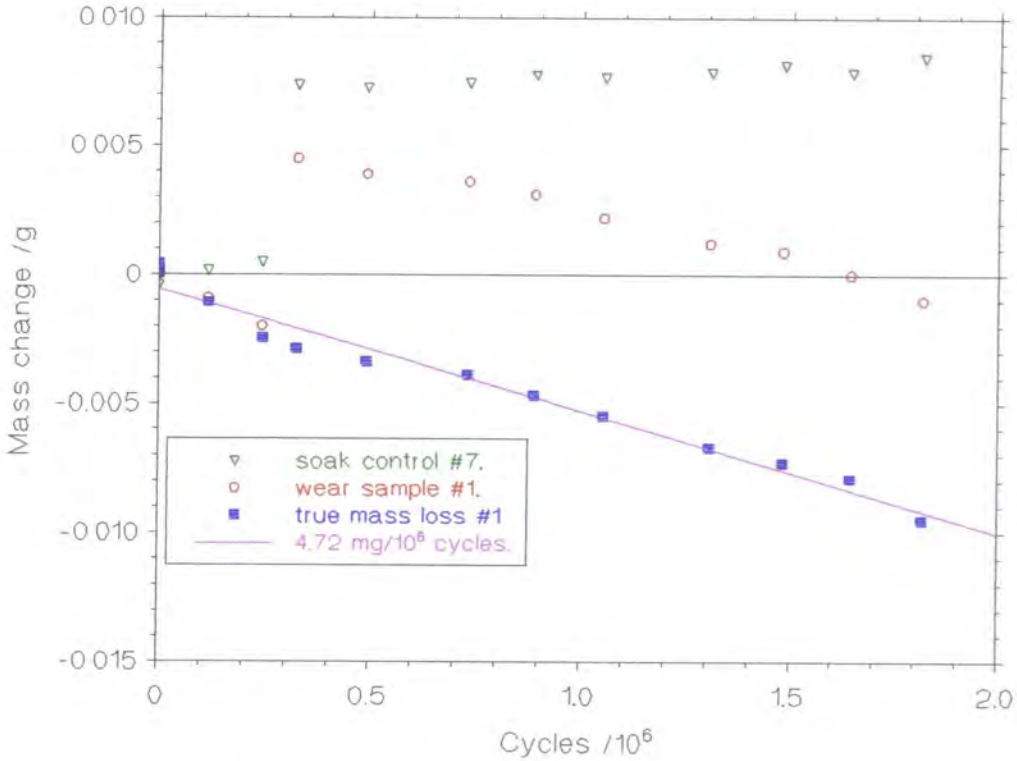

Figure 8.3 Wear results: Kinematic #1 with rotation. The load valve developed a fault after 0.2 million cycles. During the repair period the wear and soak control samples (kept under the same conditions) absorbed moisture, hence the step in the data in this figure.

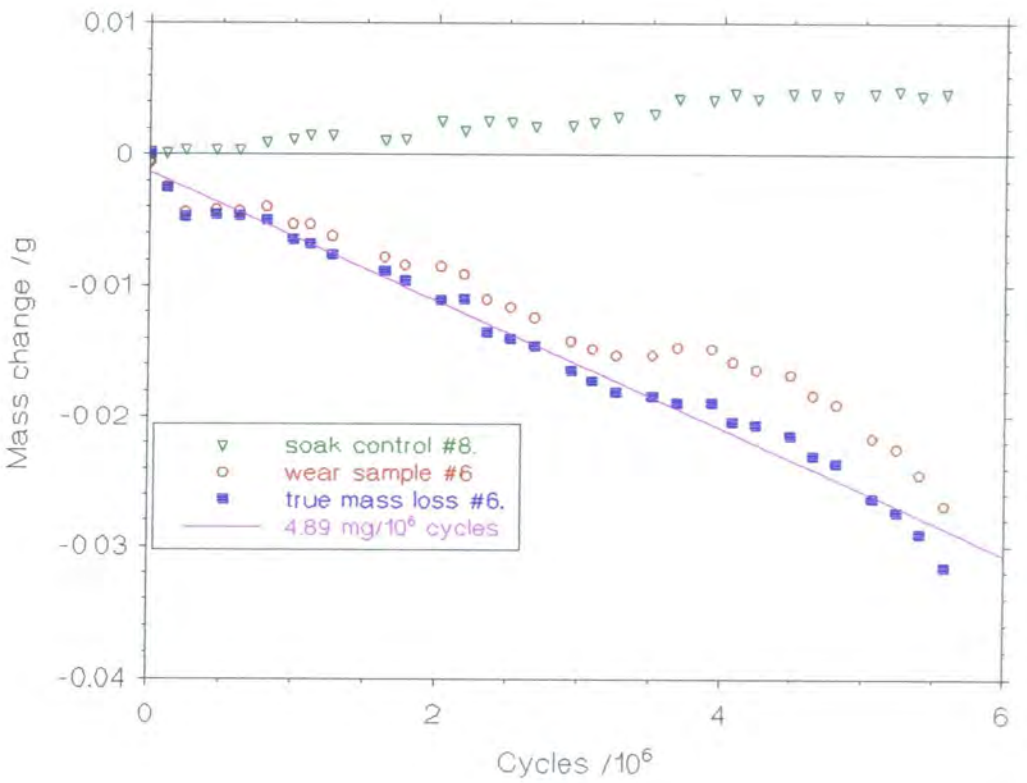

Figure 8.4 Wear results: Kinemax #6 with rotation.

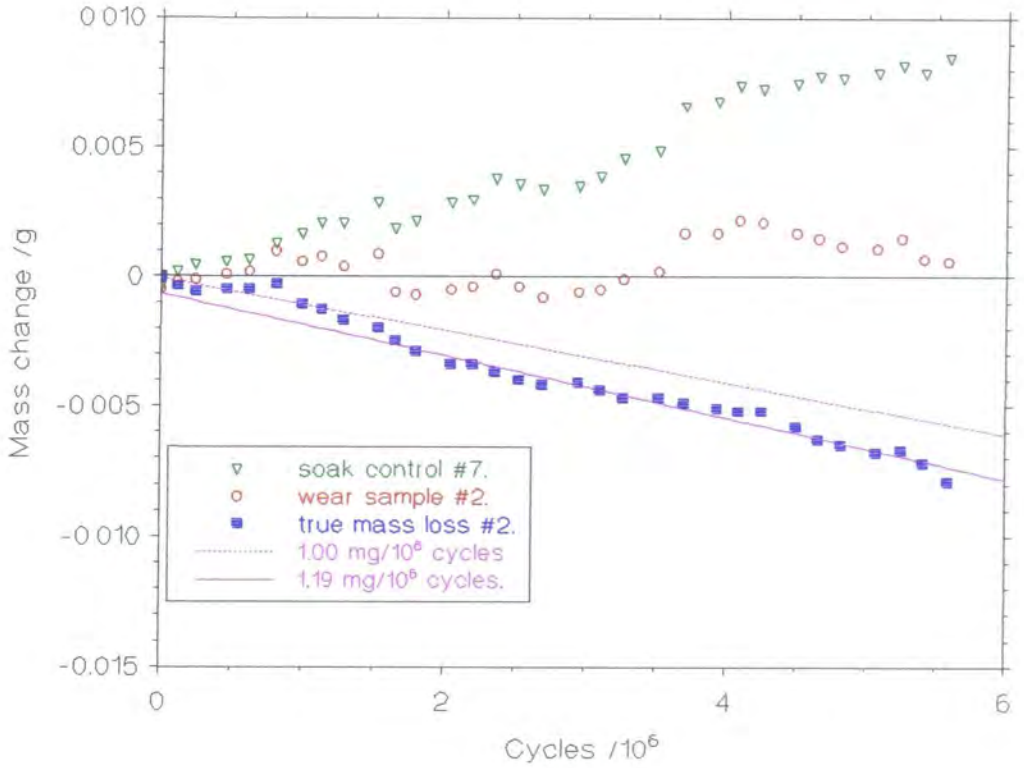

Figure 8.5. Wear results: Kinematic #2. This sample was swapped from station 2 to 3 at 1.5 million cycles. (---station 2 regression analysis; — station 3 regression analysis).

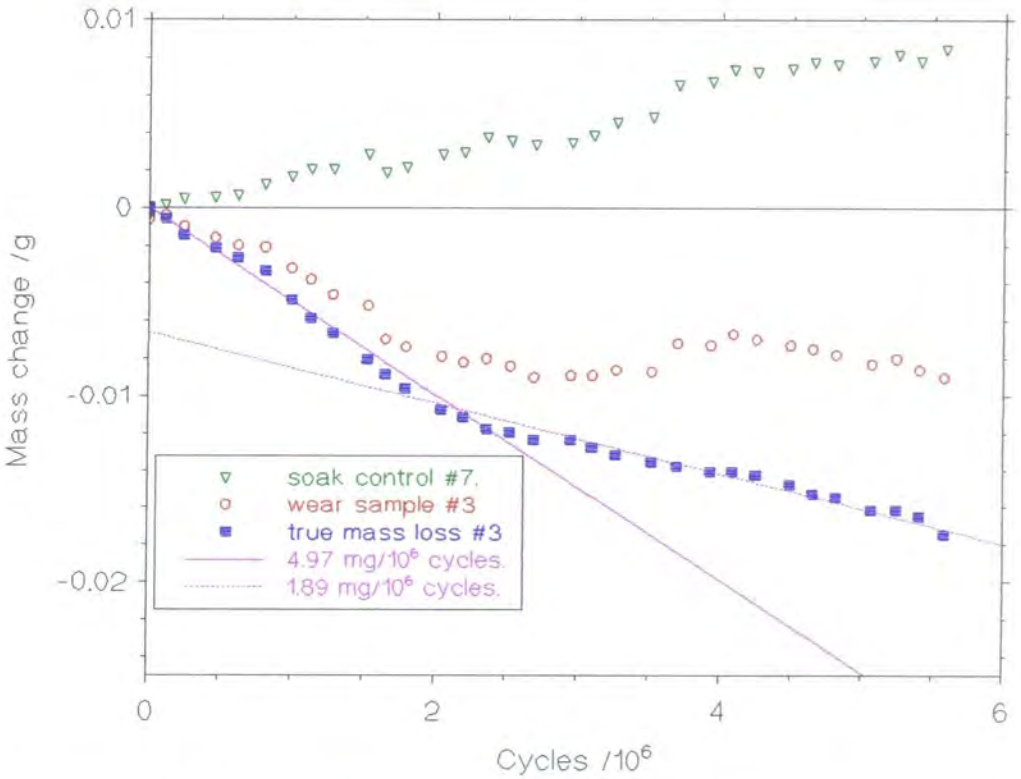

Figure 8.6. Wear results: Kinematic #3. This sample was swapped from station 3 to 2 at 1.5 million cycles. (---station 2 regression analysis; — station 3 regression analysis).

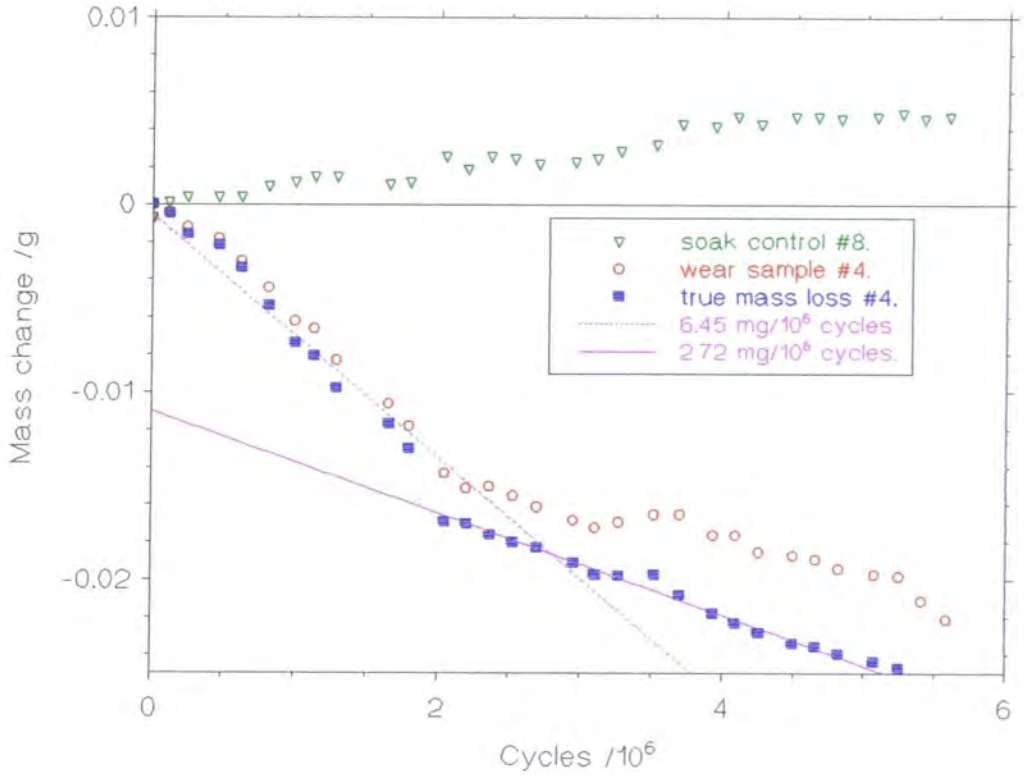

Figure 8.7. Wear results: Kinemax #4. This sample was swapped from station 4 to 5 at 3.5 million cycles. (---station 4 regression analysis; —station 5 regression analysis).

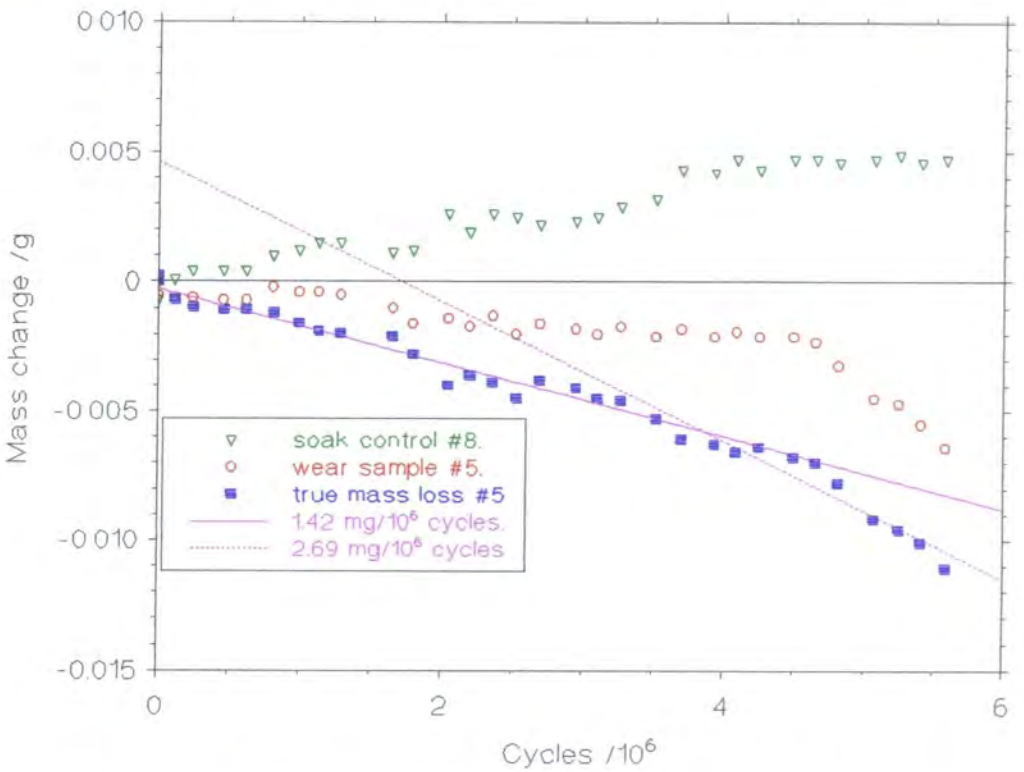

Figure 8.8. Wear results: Kinemax #5. This sample was swapped from station 5 to 4 at 3.5 million cycles. (---station 4 regression analysis; —station 5 regression analysis).

Once again the simulator performed reliably over the duration of the 5.6 million cycle test, with one exception. The servo valve controlling the load actuator in station 1 developed a fault after only 0.2 million cycles, and was returned to Vickers for repair. (The fault was found to be trapped wire in the coil). Hence station 1 completed only 1.8 million cycles. The electrical noise problem which caused the Motorola 68020 control computer to crash when the test was run at 1 Hz during the single station test was over come by improved earthing of all the components, hence this test was conducted with the simulator operating continuously at 1 Hz.

8.3 Discussion.

8.3.1 Simulator performance.

Apart from the issues of reliability discussed in the previous two sections, the simulator performance was also assessed from the accuracy of the applied load and motion profiles. During each test, the data from each measurement transducer was saved to a file every two hours. This was used to monitor the performance of the simulator. Analysis of the data suggested that the applied profiles were both very accurate and consistent. In order to demonstrate this, 20 files were selected randomly from the thousand or so of these data files saved during the 5.6 million cycle six station wear test. The mean and range were calculated for each of the 128 data points in each cycle for each actuator. These results confirmed that each of the six load actuators, each of the six anterior-posterior translation actuators and the flexion-extension actuator all performed with excellent and reliable control throughout the test (Figures 8.9 to 11).

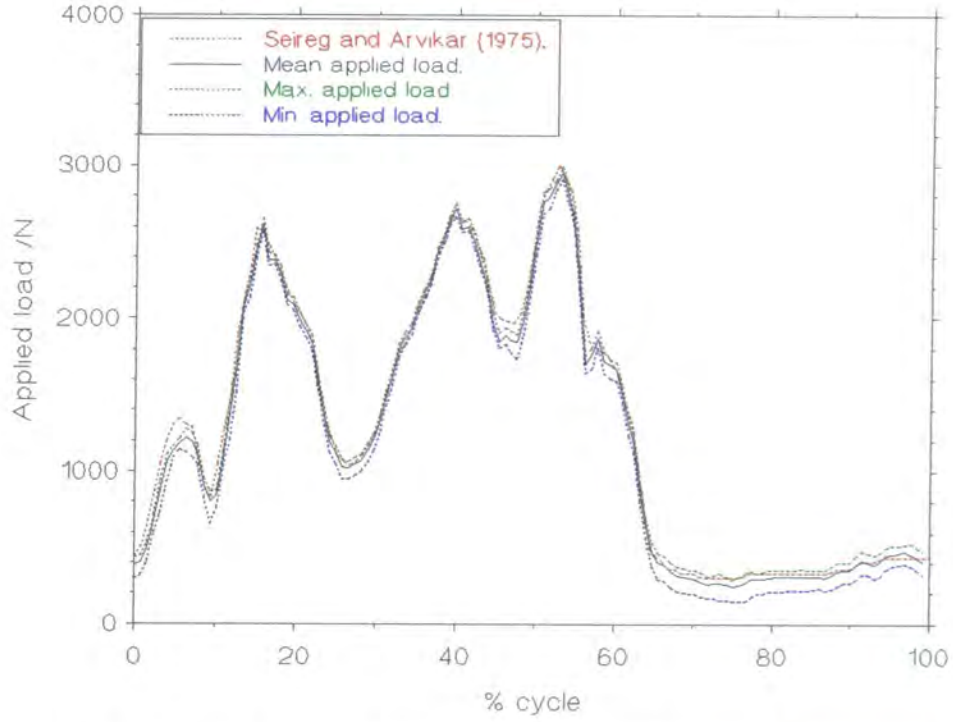

Figure 8.9. Performance of the load system. The mean and range of the measured applied load compared with the requested profile. (20 randomly selected data files throughout the 5.6 million cycle six station test, combining all six load systems, *i.e.* 120 data sets).

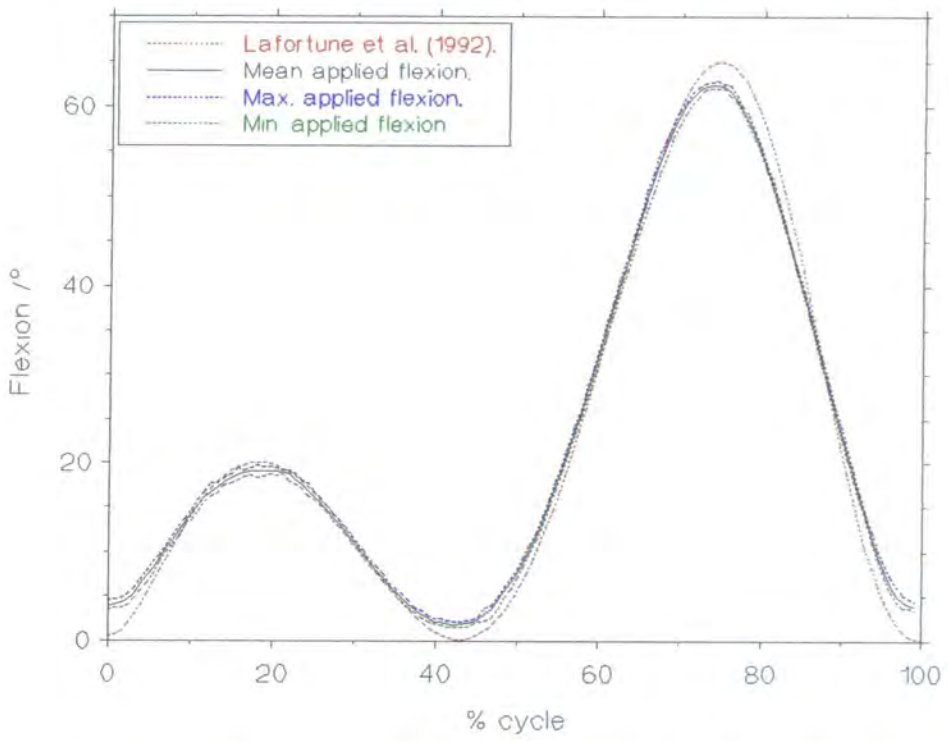

Figure 8.10. Performance of the flexion-extension system. The mean and range of the measured flexion compared with the requested profile. (20 randomly selected data files throughout the 5.6 million cycle six station test, *i.e.* 20 data sets).

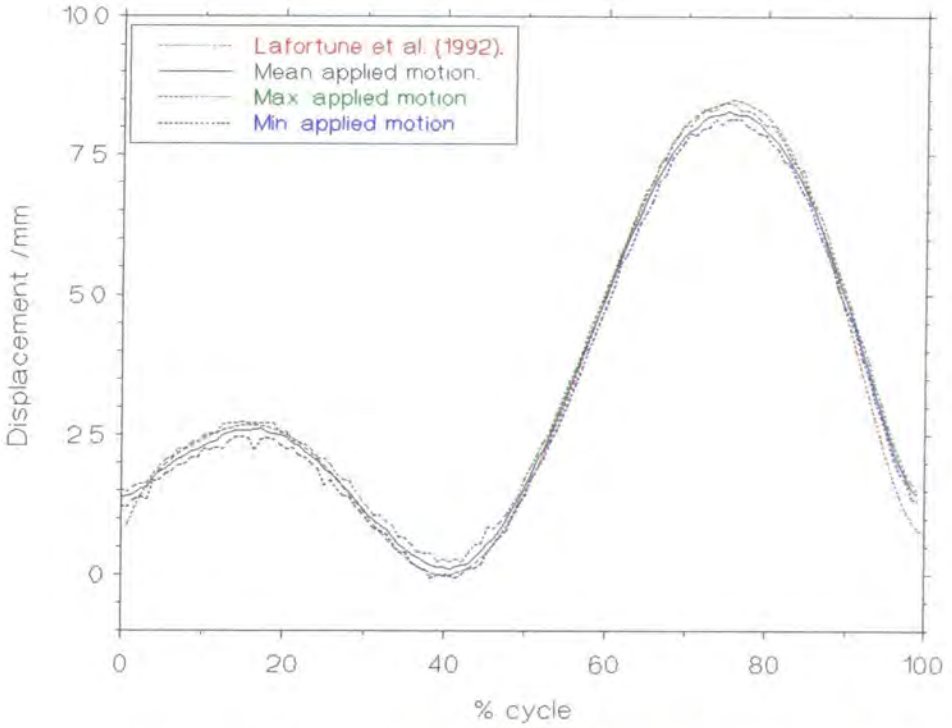

Figure 8.11. Performance of station 3 anterior-posterior translation system. The mean and range of the measured motion compared with the requested profile. This performance is typical, but since each station was programmed to perform with different amplitudes the data from all six stations could not be amalgamated. (20 randomly selected data files throughout the 5.6 million cycle six station test, *i.e.* 20 data sets).

The addition of forced internal-external rotation on stations 1 and 6 further improved the kinematics of the bearing surfaces. In the medial condyle the anterior-posterior translation acted in the opposite way to the translation of the point of contact due to the instantaneous centre of rotation. This resulted in a sliding point contact which was almost stationary and located to the posterior of the bearing. In contrast, in the lateral condyle the two translation effects were additive which resulted in a long sweeping point of contact extending more anteriorly with a larger proportion of rolling. The result was a wear pattern which more closely resembled the predominant rotational wear pattern identified by Wasieleski *et al.* (1994).

8.3.2 Comparison of results with other *in vitro* wear studies.

There have been many *in vitro* studies of prosthetic hip joints, using different designs of hip simulators. However, there are far fewer *in vitro* studies of the wear of TKRs. Only two extensive studies are presented in the literature. Treharne *et al.* (1981) conducted their experiments using calf serum at 37°C, a maximum load of 5.5 kN, and no applied anterior-posterior translation or load. They used a weight loss method to assess the resulting wear. Dowson *et al.* (1985, 1990) conducted their experiments using distilled water at 37°C, a maximum load of 1.78 kN, and an applied anterior-posterior load of 200 N. They used an optical method to measure the wear volume directly. A comparison of these testing parameters with those used in the current study shows that there is no overall consensus, and this therefore makes direct comparison of the results difficult. To aid comparison, the wear data reported in the literature are expressed in three forms (Table 8.4).

The experimental protocol used by Treharne *et al.* (1981) was broadly similar to that used in this study, and they showed that lower conformity designs resulted in higher wear rates. The higher applied loads used compared with this study may explain the higher wear rates which they measured.

The considerably higher wear rates reported by Dowson *et al.* (1985, 1990) can be explained by differences in experimental protocol. The main difference in protocol was the use of distilled water as the lubricant, while Treharne *et al.* (1981) and this study used serum. McKellop (1981) conducted experiments on UHMWPE using a wear screening device. He reported that the "wear was as much as four times higher with distilled water than serum", and in addition, "heavy transfer layers of polymer formed on

Author	Duration 10^6 cycles.	Knee tested.	Wear rates / factors		
			$mg/10^6$	$mm^3/10^6$	$mm^3/Nm/10^o$
Treharne	1.0	RMC	**1.48**	*1.59*	(a)
et al.	1.0	Total Condylar.	**3.45**	*3.71*	
(1981)	1.0	Townley	**12.85**	*13.8*	
	1.0	Anametric	**12.93**	*13.9*	
	1.0	UCI type	**30.3**	*32.6*	
Dowson	1.0	Leeds	*51.5* (b)	*55.5* (b)	**0.83** (b)
et al.	1.0	Freeman-Swanson	*44.0* (b)	*47.3* (b)	**0.99** (b)
(1985)		(Original)			
Dowson	2.0	Geomedic	*72.5*	*78.0*	**1.8**
et al.	1.5	Freeman-Swanson	*73.9*	*79.5*	**1.7**
(1990)		(Modified)			
	1.0	Polycentric	*72.0*	*77.4*	**1.5**
This	8.0	Kinemax. (c)	**2.66**	**2.86**	**0.05**
study.	1.8	Kinematic #1. (d)	**4.73**	**5.08**	**0.09**
	5.6	Kinematic #2.	**1.33**	**1.43**	**0.03**
	5.6	Kinematic #3.	**2.96**	**3.18**	**0.06**
	5.6	Kinemax #4	**4.74**	**5.10**	**0.10**
	5.6	Kinemax #5.	**1.70**	**1.83**	**0.03**
	5.6	Kinemax #6. (d)	**4.89**	**5.26**	**0.10**

Table 8.4. Comparison of wear rates and factors. (**bold**-reported data. *italics*-reported data converted to different form. a-insufficient data to calculate wear factors. b-volume measurement includes creep component. c-data from single station prototype. d-forced internal-external rotation).

the metal counterface in distilled water which were not formed when using serum". The long chain serum proteins are thought to act as boundary lubricants in a similar manner to those found in synovial fluid. Since transfer films have not been observed on explanted

prosthetic joints, distilled water seems to induce a wear mechanism not observed *in vivo*. This, together with the fact that third body abrasion due to acrylic bone cement particles was noted, may account for the significantly higher wear rates reported.

Optical methods of assessing wear volumes, such as dual-index and fringe projection holography as used by Dowson *et al.* (1985, 1990), are very attractive as they allow comparison of volumes of complex shapes such as tibial components (although no indication of measurement errors or accuracy was given). Such methods would be particularly useful in measuring the wear volumes in specimens where moisture uptake was very large and hence the weight loss method becomes inaccurate, *i.e.* compliant bearings. However, the method requires a correction for creep to give true rates of material loss, necessitating the use of a simulator creep station.

The wear rate data obtained in this study did not distinguish between the two designs tested. The less conforming Kinematic bearing may have been expected to wear more than the more conforming Kinemax (Treharne *et al.*, 1981 and Collier *et al.*, 1991). Although different wear tracks were observed the experimental wear rates did not distinguish between the two designs. The wear rate was found to be station dependent in some cases (Table 8.3), notably samples #3, #4 and #5. Since variability in the applied load and motion between stations was found to be practically non-existent (Section 8.3.1) slight differences (<0.5 mm) in the alignment of the femoral and tibial components when mounted on different stations were thought to be responsible. Surgical alignment has been identified as critically influencing the wear of tibal components (Wasieleski *et al.*, 1994), however it was disappointing that, in this experiment at least, alignment seemed to influence wear to a greater extent than component design.

8.3.3 Comparison of results with retrieved *ex vivo* studies.

Ex vivo wear can be assessed by examining components explanted during revision surgery. In contrast to hips, far less data exists in the literature regarding TKR retrieval studies, and none is currently available for Kinemax or Kinematic TKRs. The wear patterns were observed, and a wear score system (Hood *et al.*, 1983) applied to each of the seven tibial components tested on the simulator.

The simulator specimens subjected to passive internal-external rotation all had equal wear on the medial and lateral condyles, with a posterior bias and no rotational wear patterns. This would be expected, since the applied load was distributed equally between the medial and lateral compartments, anterior-posterior translation caused the bearing contact to move posteriorly during flexion, and no enforced internal-external rotation was applied. The Kinematic design operated with a line contact and hence swept out a rectangular wear area. In contrast, the Kinemax design developed a point contact and so created a tear drop shaped wear area (Figure 8.12).

In the samples where internal-external rotation was applied, wear was posteriorly located in the medial compartment and more anterior in the lateral compartment; a pattern which more closely resembled rotational wear (Wasieleski *et al.*, 1994), although this was more marked in the Kinematic design. Wasieleski *et al.* identified wear in the medial compartment, a posterior wear track and external rotation as predominant, although they concluded that no one distinct wear pattern was representative of *ex vivo* knee wear.

The worn surfaces of all seven tibial components were shiny which is indicative of burnishing, with slight unidirectional scratching in the anterior-posterior direction. Some

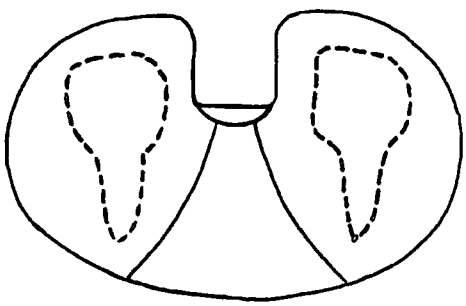

Kinemax, single station 8 million cycle test.

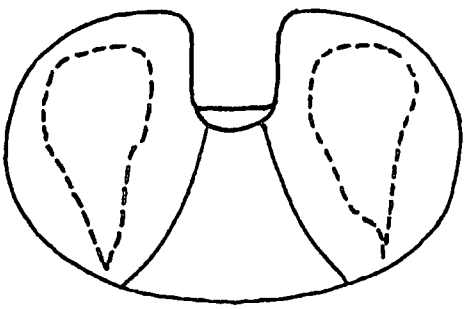

Kinemax #4.

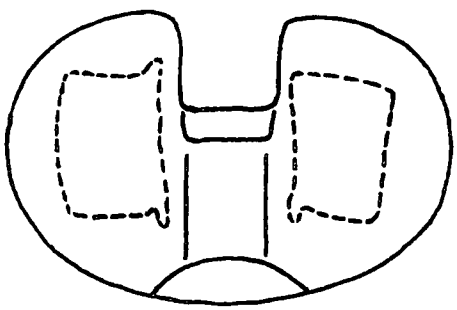

Kinematic #3.

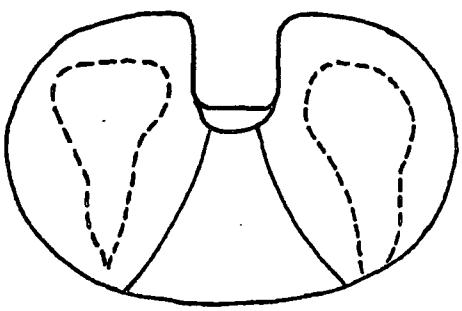

Kinemax #5.

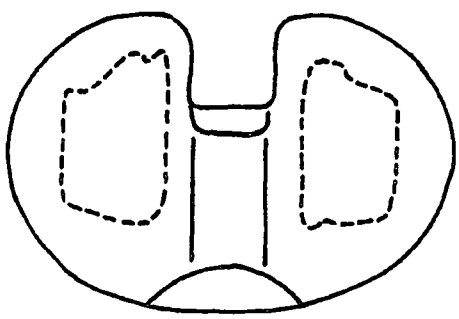

Kinematic #2.

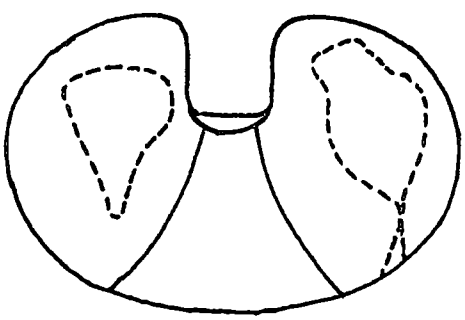

Kinemax #6 with rotation.

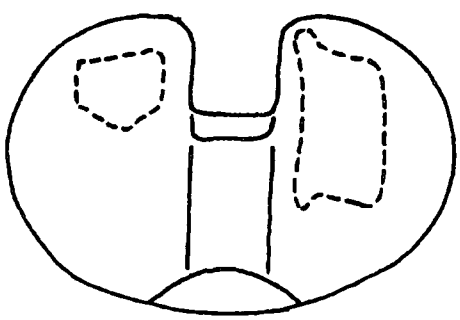

Kinematic #1 with rotation.

Figure 8.12. Sketches of the worn areas from components tested in both the single station 8.0 million cycle test and the six station 5.6 million cycle test, samples #1 to #6. (Photographs were unable to highlight the worn areas.)

slight surface deformation may have occurred, but no pitting, embedded particles, abrasion or delamination were observed. Burnishing is indicative of predominantly adhesive wear, with the scratching indicative of slight abrasive wear. In addition, the back of the tibial component had worn directly under the load bearing area, where small pits were observed.

All seven tibial components scored between 21 and 24 points which compares with a median wear score of 21.5 for a range of 48 explanted Total Condylar tibial components (Hood *et al.*, 1983). This highlighted a significant draw back with the score system; that it did not distinguish between the severity of different wear types. For example, both severe burnishing and severe delamination both score a 3 if they extend over more than 50% of a particular area, although clearly delamination is far more detrimental than burnishing. The similarity of the wear scores only indicate that the system is weighted for wear area and not wear type, and so few conclusions could be drawn.

The literature suggests that wear of UHMWPE tibial components is a multi-factorial problem. Patient characteristics, length of implant, surgical practice, material properties, manufacturing process, bearing conformity and bearing thickness are all cited as important parameters. Given that all these features will affect the severity of tibial wear, a design which has several of these features would be expected to show a significant increase in wear related failure, compared with a design which exhibited only few or none of these detrimental factors. The design of either the Kinematic or Kinemax TKRs tested here have few if any of these features, and hence severe wear and catastrophic failure may not be expected over a 5.6 or 8.0 million cycle test period. The Kinematic TKR is similar to the Kinemax in all these factors except that it was less conforming and

therefore may be expected to have worn more. However the simulator wear test could not distinguish between the two designs. In order to complete the validation process, retrospective testing of a TKR design with many of these detrimental features known to be susceptible to delamination and catastrophic failure would be of particular interest, *e.g.* a PCA (Howmedica, NJ, USA).

8.4 Compliant bearing knees: preliminary wear results and discussion.

Several Interax (Howmedica, Staines) based prototype 3 mm compliant bearings were tested on the knee wear simulator. As detailed in Section 3.1.3, these bearings were manufactured using the trial stabilised component mould (see Figure 3.5). The stabilising post was removed and the cavities underneath the component filled with bone cement. The component was fixed to the base plate using a central screw. The bearings were tested with flexion of 0-65°, using load and anterior-posterior translation detailed in Table 8.5, and conditioned for at least 72 hours in Ringers solution at 37°C before testing. The tests were conducted in water at 37°C. The aim of this set of preliminary experiments was to examine the mechanical and tribological performance of early compliant bearing knees.

The failure mechanism was invariably debonding of the layer from the backing. Failure of the C80A/Acrylic #1 component was expected, since the peel force between PU and Acrylic was found to be only 10% of the PU/PU value. Two C80A/C75D components were tested, one with and one without anterior-posterior translation. After 0.5 million cycles the bearing subjected to anterior-posterior translation started to debond mainly in

Prostheses type: (Loading and AP translation conditions)	Test stopped /10^6 cycles.	Details:
C80A /Acrylic #1. (5 kN, 6 mm)	0.080	Total delamination of the C80A layer on both condyles. Slight scratching of bearing surfaces.
C80A/C75D #2. (3 kN, 6 mm)	0.500	Delamination of the C80A layer (mainly the posterior edge of both condyles. No scratching of the bearing surfaces. Some creep. (Fig 8.13)
C80A/C75D #3. (3 kN, none)	0.500	No delamination of the C80A layer. No scratching of the bearing surfaces. Some creep. (Figure 8.13)

Table 8.5. Test conditions and results for compliant bearing knees. (Based on the Interax stabilised bearing, consisting of C80A on either Acrylic or C75D backing materials.)

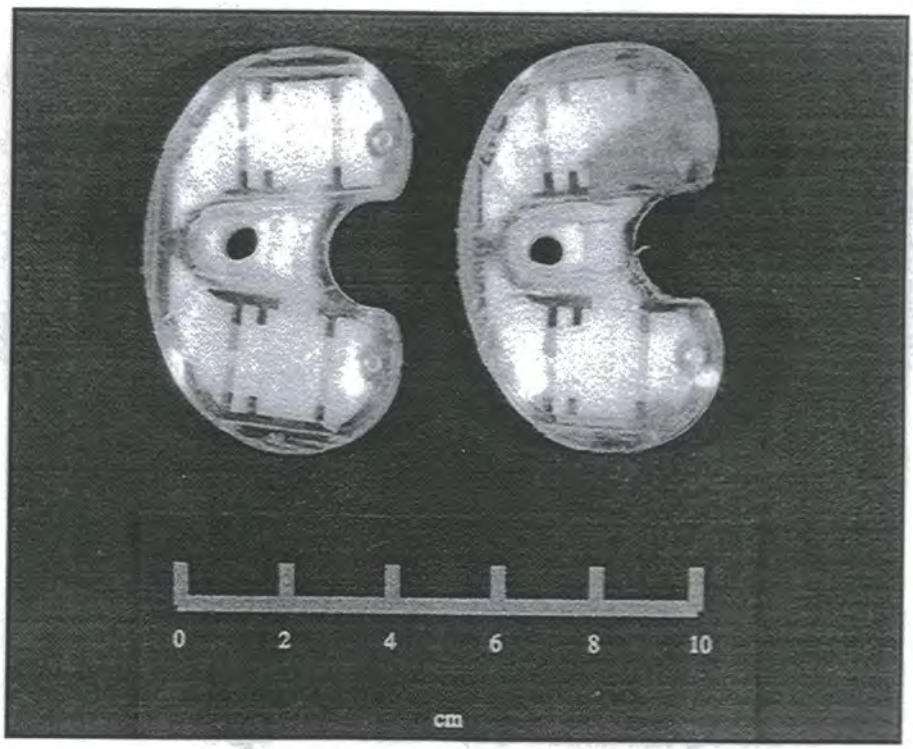

Figure 8.13. Prototype compliant bearings #2 (Right hand side) and #3 (Left hand side) after 0.5 million cycles. Debonding in the posterior area of bearing #2 was highlighted by colouring the exposed interface with ink.

the posterior condyle area; whereas the bearing with out anterior-posterior translation was visually perfect after 0.5 million cycles (Figure 8.13). The test illustrates that the higher contact stresses experienced in the knee may lead to debonding in a PU/PU system. Failure may occur sooner if the point of contact moves over the bearing surface near to the edge of the component, as occurred with the test incorporating anterior-posterior translation. The results have highlighted the need for good layer adhesion, and also the need to reduce the stress at the edge of the bearing. This could be achieved either by using meniscal type bearings, or designing the bearing so that the edge of the C80A/C75D interface occurred in an area of low stress. Although only 0.5 million cycles were conducted, it was encouraging that no bearing surface damage was observed in the C80A/C75D bearings, indicating the predominance of fluid film lubrication.

Chapter 9. Conclusions.

9.0 Introduction.

The objective of this research was to contribute to the design and development of new joint prostheses, which would last longer than the TJRs currently available to the orthopaedic surgeon. The approach used to achieve this end was to incorporate a compliant or soft bearing surface, like the cartilage of a natural joint, which would encourage fluid film lubrication and result in minimal wear. One of the main reasons that TJRs fail is through the body's reaction to wear debris which leads to osteolysis and loosening of the prosthesis. Thus reducing wear is a sound method of increasing the life of joint prostheses. Specifically, the objectives were to

- contribute to the understanding of how these compliant layer joints are lubricated, and hence which design parameters it is important to control.
- develop the technology to ensure excellent adhesion between the compliant layer and the rigid backing.
- commission a knee simulator which could be used to assess the long term performance of compliant layer knee joints.

The joints were manufactured using medical grade polyurethanes (PUs). In the past PUs have been known to degrade *in vivo* by several different mechanisms; with the insulation on pacing leads being a well known example. However, new PUs with enhanced biostability are now available, and have been use in the majority of this research.

9.1 Compliant bearing tribology.

These new TJRs are required to operate in the fluid film lubrication regime. In order to establish which design parameters were important both experimental and theoretical research has been published previously. Notably Auger *et al.* (1993b) tried to demonstrate an agreement between theory and experiment, but only demonstrated limited agreement for the single design case chosen. No research had been done to demonstrate a correlation between theory and experiment over a wide range of design parameters, and so this work was the subject of part of this thesis.

A simulator, which applied realistic dynamic loads and motions and measured friction at the articulating surfaces, was used to evaluate the lubrication regime of a wide range of designs of compliant layer acetabular cups and tibial components. However, when the experimental results were then compared with theory, little or no correlation was found. This was in part due to the increasing relative error associated with measuring increasingly smaller values of frictional torque by the apparatus. However these experiments still demonstrated that the design is insensitive to many design parameters, which the theory suggests are important. From the experimental results the following conclusions were drawn regarding the design of compliant layer acetabular cups.

- Clearance between the head and cup is not critical, so long as it isn't too small such that significant contact occurs, due either to grabbing of the head by the cup or an inability to tolerate out of roundness of the bearing surface. A radial clearance of between 0.10 and 0.25 mm is recommended.
- Head size may not be critical. Both 32 mm and 22 mm cups perform with very low friction (although 28 mm cups give unexplained high friction results). This has

implications for animal based clinical trials, since larger head sizes may not be applicable to animal models.

- Surface topography will affect the lubrication regime. A bearing surface with a σ_2 value below 0.25 μm is recommended.
- Layer modulus is important, although theory suggests it is one of the least important parameters. An optimum elastic modulus for the layer has not been identified, since most experiments have been conducted using 20 MPa modulus material, which performs well. Significantly, a harder material with an elastic modulus of almost 40 MPa also performed well under certain circumstances.

Extremely high values of start-up friction were measured by Caravia *et al.* (1993a) using a simple pin on plate rig and plane compliant layer contacts, which led them to suggest that surface contact and wear at the onset of motion may lead to failure of compliant bearing TJRs. So, in addition to assessing friction and lubrication during normal gait, the simulator was also used to assess the friction at the onset of motion. By developing a new experimental protocol to measure start-up friction in real prostheses, the scale of the problem was more accurately assessed. Lower levels of start-up friction were measured during this research, compared with those reported by Caravia, and were found to reduce rapidly as motion began. These results indicate that start-up friction may not be such a problem as originally envisaged. In this research, the combination of a head coated with diamond like coating (DLC) and a cup soaked in Ringers solution at 37°C showed quite low start-up friction, and demonstrated that using the simulator in this way gives an ability to investigate different coatings and treatments to reduce start-up friction.

9.2 Compliant layer adhesion and mechanical properties.

A good bond between the compliant layer and rigid backing is very important if the joint is to last several decades and withstand many millions of loading cycles *in vivo*, although this aspect of compliant bearing technology has received little attention in the past. Most of the arrangements used by previous researchers to investigate the tribology of these designs were not suitable as long term implants. Initially the bond between medical grade PU and UHMWPE was considered, and several methods of enhancing the interface to promote a good bond were investigated. Although the attraction of UHMWPE was that its biostability and mechanical performance is well known to the orthopaedic community, bonding anything to a polyolefin is difficult, and although significant improvements in adhesion were measured, the bond was not considered suitable for this demanding application. Hence other material combinations were examined. Next, the adhesion between low modulus and high modulus PU was investigated. Both PU grades were suitable for injection moulding, and an excellent diffusion bond between them was created by moulding one to the other.

The nature of the PU/PU bond was investigated using a peel test arrangement. The moulding process was optimised to give the maximum bond strengths, and was found to be most dependent on moulding temperature, with higher temperatures giving higher bond strengths. (Material degradation and poor component quality at high temperatures were the limiting factors.) The stability of the bond when immersed in Ringers solution at 37°C for up to 52 weeks was confirmed. An attempt to measure the adhesion between layer and backing in acetabular cups using a blister test confirmed the same high adhesion as found in the peel test samples, although the method proved unable to discern

differences between samples due to difficulties in creating a sharp and consistent starting crack. Finally, cups were subjected to 14 million 4 kN sinusoidal loading cycles, with no deterioration of the bond or materials. Overall, this part of the research enabled PU/PU components with an excellent bond between the compliant layer and rigid backing to be produced, and contributed to the filing of a European Patent (Smith *et al.*, 1996).

Although not discussed before in the context of compliant layer TJRs, the creep characteristics of the layer are important. This was demonstrated by a test in which six cups were subjected to 7 million 4 kN sinusoidal loading cycles, and changes in bearing form were monitored using a co-ordinate measuring machine. Both the form and the thickness of the compliant layer were found to change. A change in conformity may affect the lubrication regime and the applied stress, and may also eliminate out of roundness and surface roughness. It is still unclear whether creep will work to improve the bearing's performance or not.

9.4 Development of a six station knee simulator.

In order to evaluate the long term performance of compliant layer knee joints, a simulator which subjected the bearing to loads and motions representative of normal gait was required. A simulator was designed and commsioned which applied a dynamic tibio-femoral load of up to 5 kN, flexion-extension of 0-65°, and anterior-posterior translation of up to 12 mm. Thirteen servo hydraulic systems were used to apply the loads and motions, and computer based modelling was found to be a valuable tool in the design of each of these systems. Initially a single station simulator was built, and the design

assessed during an 8 million cycle wear test using a conventional UHMWPE knee. Then the simulator was extended to six stations, and a 5.6 million cycle wear test was conducted, again using conventional UHMWPE knees. Finally, two short (0.5 million cycles) tests on prototype compliant tibial components were conducted.

The tests on compliant tibial components were interesting as they illustrated that the high contact stresses experienced in the knee may lead to debonding in a PU/PU system, especially if the point of contact moves over the bearing surface near to the edge of the component. Although only 0.5 million cycles were conducted, it was encouraging that no bearing surface damage was observed in the PU/PU bearings, indicating the predominance of fluid film lubrication.

The majority of testing was conducted on conventional TKRs, in order to validate the simulator. Two types of UHMWPE TKRs were tested, the Kinemax and the Kinematic. (Howmedica Europe, Staines, UK). Both are broadly similar in design apart from the contact geometry. The Kinematic has a less conforming line contact, and the Kinemax a more conforming point contact. Given that tibial wear is a multi-factorial problem, with retrieval studies indicating that conformity is an important factor, the less conforming design might be expected to wear more. This was not the case in this study, as similar wear rates of 1.2 to 6.5 mg/10^6 cycles were measured for the Kinemax, compared with 1.0 to 5.0 mg/10^6 cycles for the Kinematic. Although some explanted components of both these designs do show delamination, only burnishing and no pitting or delamination was observed during these tests. Wear rates were found to be more sensitive to the station on which they were tested, rather than TKR design. An analysis of load and motion data revealed variations of <5% between stations over the duration of the test. The only

variation between stations which was considered important was the alignment of the components, with variations of less than 0.5 mm measured. The implication for product testing on simulators is that alignment is critical if real differences between designs are to be established. In addition, longer test durations must be used in order to give a chance of delamination, a wear mode which has not yet been reported in this or any other knee simulator study on a production quality component.

9.5 Recommendations for future work.

It is widely accepted that the lubrication of natural joints relies on an effective boundary lubricant (in addition to fluid film lubrication mechanisms) to ensure a long service life. Compliant layer joint prosthesis are also likely to require an effective boundary lubricant. Thus research into treatments and coatings designed to reduce start-up friction are recommended, using the start-up friction protocol developed here. Only limited research has been conducted, either here or elsewhere, on the tribology of compliant bearing knees using a realistic model. Further research and improvements to the model along the lines outlined in Section 4.6 are therefore recommended.

The research presented in this thesis has developed compliant bearing technology up to a point where long term simulator studies can begin. Simulator studies are expensive and time consuming to undertake, but are necessary to investigate both the tribological and mechanical performance of these types of joints over many millions of cycles. Long term knee simulator studies can now be conducted at Durham using the simulator developed here, whereas the hip simulator testing may have to be conducted else where. Simulator

testing of compliant layer joints will require extra consideration over and above testing of conventional joints. For example, the gravimetric method for calculating weight loss may be unable to measure the very small wear rates expected for PU joints, as they absorb high proportions of moisture. Also creep will be an important factor, and must be assessed throughout the test. Finally since start-up friction could potentially lead to premature failure of these joints, a simulator cycle which includes stopping and re-starting of the motion under load would be beneficial. Indeed, there may be a need to move away from normal walking cycles to a 'day in the life' type cycle, which includes a whole range of typical activities.

One must recognise that given the fairly radical design of this type of joint, and the increasingly litigious environment particularly in the USA, any manufacturer who wishes to exploit this technology will have to have conducted an extremely extensive range of product tests. The biostability of the new medical grade PUs under high cyclic stress conditions found in this application are still unproven. Hence it is inevitable that animal studies will be required to test the performance of both the prostheses and the material *in vivo*, before human based clinical trials can begin.

References.

Adams LM, (1993) The anatomy of joints related to function. Chapter 2 In: *Mechanics of human joints*. Eds. V Wright and E Radin. Marcel Dekker, New York.

Anderson GBJ, Freeman MAR, Swanson SAV, (1972) Loosening of the cemented acetabular cup in total hip replacement. *JBJS.* **54B**, 590.

Anderson GP, DeVries KL, Williams ML, (1974) The influence of loading direction upon the character of adhesive debonding. *J. Colloid and Interface Sci.*, **47** ,3 ,600-609

Anderson GP, Bennett SJ, DeVries KL, (1977) Analysis and testing of adhesive bonds. Academic Press. New York.

Andrews EH, Stevenson A, (1978) Fracture energy of epoxy resin under plane strain conditions. *J. Mat. Sci.*, **13**, 1680-1688.

Arafa HA, Rizk M, (1987) Identification and modelling of some electrohydraulic servo-valve non-linearities. *Proc. Inst. Mech. Engrs*, **201**, C2, 137-144.

Arafa HA, Rizk M, (1987) Spool hydraulic stiffness and flow force effects in electrohydraulic servo-valves. *Proc. Inst. Mech. Engrs*, **201**, C3, 193-199.

Argenson JN, O'Connor JJ, (1992) Polyethylene wear in meniscal knee replacement. *JBJS.*, **74-B**, 2, 228-232.

Aronhime M, Einstein K, Cohn D, (1994) Poly(ether urethane) oligomers as poly(HEMA) crosslinkers. *Clinical Mater.*, **15**, 161-167.

ASTM F04.2.5.23 (1991). Recommended method for the friction and wear evaluation of materials and prosthetic hip-design combinations in hip-simulator devices. Draft.

References.

ASTM F04.0302.12 (1992). Wear evaluation of materials and prosthetic knee-design combinations in knee-simulator devices. Draft.

Auger DD, Medley JB, Fisher J, Dowson D, (1990) A preliminary investigation of the 'cushion bearing' concept for joint replacement implants. In: *Mechanics of coatings*, 16th Leeds Lyon Symposium, Eds. D Dowson, CM Taylor, M Godet, Elsevier, Amsterdam, 251-260.

Auger DD, Dowson D, Fisher J, Jin Z-M, (1993a) Friction of cylindrical cushion form bearings for artificial joints- a comparison of theory and experiment. In: *Thin films in Tribology*, Tribology Series 22, Eds. D Dowson, CM Taylor, M Godet, Elsevier, Amsterdam, 683-692.

Auger DD, Dowson D, Fisher J, Jin Z-M, (1993b) Friction and lubrication in cushion form bearings for artificial hip joints. *Proc. Inst. Mech. Engrs.*, **H207**, 25-33.

Auger DD, Dowson D, Fisher J, (1995a) Cushion form bearings for total knee joint replacement. Part 1: design, friction and lubrication. *Proc. Inst. Mech. Engrs.*, **H209**, 73-81.

Auger DD, Dowson D, Fisher J, (1995b) Cushion form bearings for total knee joint replacement. Part 2: wear and durability. *Proc. Inst. Mech. Engrs.*, **H209**, 83-91.

Bajpai AC, Mustoe LR, Walker D, (1977) Advanced engineering mathematics, John Wiley and Sons, Chichester.

Bartel DL, Burstein AH, Toda MD, Edwards DL, (1985) The effect of conformity and plastic thickness on contact stresses in metal backed plastic implants. *J Biomech. Eng.*, **107**, 193-199.

Bartel DL, Bicknell VL, Ithaca MS, Wright TM, (1986) The effect of conformity, thickness, and material on stresses in UHMWPE components for total joint replacement. *JBJS*, **68-A**, 7, 1041-1051.

References.

Bartley RE, Stulberg SD, Robb WJ, Sweeney HJ, (1994) Polyethylene wear in unicompartmental knee arthroplasty. *Clin. Orth.*, **299**, 18-24.

Bassani R, Piccigallo B, (1992) Hyrostatic lubrication. Elsevier, Amsterdam.

Bennet SDJ, Devries KL, Williams ML, (1974) Adhesive fracture mechanics. *Int. J. of Fracture.*, **10**,1, 33-43.

Bevington PR, (1969) Data reduction and error analysis for the physical sciences. McGraw Hill, New York.

Blamey JM, Rajan S, Unsworth A, Dawber R, (1991) Soft layered prostheses for arthritic hip joints: a study of materials degradation. *J. Biomed. Eng.*, **13**, 180-184.

Blamey JM, (1993) Improved tribology and materials for a new generation of hip prosthesis. PhD thesis. University of Durham.

Blamey JM, Mullin PJ, Seaton J, Unsworth A, Parry TV, (1993) Bonding of soft layers to rigid backings. In: *Thin films in Tribology*, Tribology Series 22, Eds. D Dowson, CM Taylor, M Godet, Elsevier, Amsterdam, 693-703.

Bloebaum RD, Nelson K, Dorr LD, Hofmann AA, Lyman DJ, (1990), Investigation of early surface delamination observed in retrieved heat-pressed tibial inserts. *Clin. Orth.*, **269**, 120-127.

Blunn GW, Walker PS, Joshi AB, Hardinge K, (1991) The dominance of cyclic sliding in producing wear in TKRs. *Clin. Orth*, **273**, 253-260.

Blunn GW, Joshi AB, Lilley PA, Engelbrecht E, Ryd L, Lidgren L, Hardinge K, Nieder E and Walker PS, (1992) Polyethylene wear in unicondylar knee prostheses. *Acta Orthop Scand*, **63**, 3, 247-255.

References.

Bosma R, Moes H, Ligterink D, Miehlke R, (1979) The development of a knee joint simulator. *J. Eng. in Medicine*, **8**, 3, 177-180.

Briscoe BJ, Panesar SS, (1991) The application of the blister test to an elastomeric adhesive. *Proc. Roy. Soc. Lond. A*, **433**, 23-43.

Briscoe BJ, Panesar SS, (1992) The effect of surface-topography on the adhesion of poly(urethane) metal contacts. *J. Physics D*, **25**, 1A, A20-A27.

BS 2782 Part 3, (1991) Method 365D: Determination of hardness by the ball indentation method.

BS 5350 Part C9, (1990) Adhesives: Floating roller peel test.

BS 7251 Part 8, (1990) Orthopaedic joint prostheses: Guide to laboratory evaluation of change of form of bearing surfaces of hip joint prostheses.

Bulstrode CJK, Murray DW, Carr AJ, Pynsent PB, Carter SR (1993) Designer hips. *BMJ*, **306**, 732-733.

Burgess IC, Cunningham J, Unsworth A, (1995) Development of a knee wear simulator, and preliminary wear results. *JBJS*, **77-B:Supp III**, 324-325.

Caravia L, Dowson D, Fisher JF, (1993a) Start up and steady state friction of thin polyurethane layers. *Wear*, **160**, 191-197.

Caravia L, Dowson D, Fisher JF, Corkhill PH, Tighe BJ, (1993b) A comparison of friction in hydrogel and polyurethane materials for cushion-form joints. *J. Mat. Sci. Medicine*, **4**, 515-520.

References.

Caravia L, Dowson D, Fisher JF, Corkhill PH, Tighe BJ, (1995) Friction of hydrogel and polyurethane elastic layers when sliding against each other under a mixed lubrication regime. *Wear*, **181-183**, 236-240.

Cavanagh J, Mordue A, Fisher R (1992) Elective hip and knee joint replacement surgery- a study of health needs. Northern Regional Health Authority, Durham, UK.

Chang WV, Peng SH, (1992) Nonlinear elastic analysis of adhesive blister test. *Int. J. Fracture*, **53**, 1, 77-89.

Chu YZ, Durning CJ, (1992) Application of the blister test to the study of polymer polymer adhesion. *J. Applied Polymer Science*, **45**, 7, 1151-1164.

Collier JP, Mayor MB, McNamara JL, Suprenant VA, Jensen RE, (1991) Analysis of the failure of 122 polyethylene inserts from uncemented tibial knee components. *Clin. Orth*, **273**, 232-242.

Collins JJ, O'Connor JJ, (1991) Muscle-ligament interactions at the knee during walking. *Proc. Inst. Mech. Engrs*, **205H**, 11-18.

Cooke AF, Dowson D, Wright V, (1978) The rheological properties of synovial fluid and some potential synthetic lubricants for degenerate synovial joints. *Eng. in Medicine*, **7**, 2, 66-72.

Computing Resource Center (1992) Stata referance manual. Release 3. 5th Ed. Santa Monca, CA, USA.

Corkhill PH, Trevett AS, Tighe BJ, (1990) The potential of hydrogels as synthetic articular cartilage. *Proc. Inst. Mech. Engrs*, **H204**, 147-155.

Crocombe AD, Adams RD, (1981) Peel analysis using the finite element method. *J. Adhesion*, **12**, 127-139.

References.

Dowson D, Jobbins B, O'Kelly J, Wright V, (1977) A Knee Joint Simulator, Chapter 7 In: *Evaluation of Artificial Joints*. Biological Engineering Soc., London

Dowson D, (1981) Lubrication of Joints, Chapter 13 In: *An Introduction to the Bio-mechanics of Joint and Joint Replacement.* Eds D. Dowson and V. Wright. Mechanical Engineering Publications Ltd. London. 120-133.

Dowson D, Gillis BJ, Atkinson J, (1985) Penetration of metallic femoral components into polymeric tibial component observed in a knee joint simulator. American Chemical Society Symposium 287 *Polymer Wear and its Control*, 216-228.

Dowson D, Jin ZM, (1986) Micro-elastohydrodynamic lubrication of synovial joints. *Eng. in Medicine*, **15**, 2, 63-65.

Dowson D, (1989) Are our joint replacement materials adequate? Proc. Int. Conf. on: *The changing role of engineering in orthopaedics*, Mechanical Engineering Publications Ltd. London. 1-5.

Dowson D, (1990) Biotribology of natural and replacement synovial joints. Chapter 29 In: *Biomechanics of diarthrodial joints: Vol 2.* Eds Mow, Ratcliffe, Woo. Springer-Verlag, New York. 305-345.

Dowson D, Jin ZM, (1990) The influence of elastic deformation upon film thickness in lubricated bearings with low elastic modulus coatings. In: *Mechanics of coatings*, 16th Leeds Lyon Symposium, Eds. D Dowson, CM Taylor, M Godet, Elsevier, Amsterdam, 263-269.

Dowson D, Yao J, (1990) A full solution to the problem of film thickness prediction in natural synovial joints. In: *Mechanics of coatings*, 16th Leeds Lyon Symposium, Eds. D Dowson, CM Taylor, M Godet, Elsevier, Amsterdam, 91-101.

Dowson D, McCullagh PJJ, Wright V, (1990) An assessment of the relative importance of wear and creep in the overall performance of load bearing total replacement knee

joints. In: *UHMWPE as Biomaterial in Orthopaedic Surgery*. Eds Willert HG, Buchhorn GH, Eyerer P, 32-40.

Dowson D, Fisher J, Jin ZM, Auger DD, Jobbins B, (1991) Design considerations for cushion form bearings in artificial hip joints. *Proc. Inst. Mech. Engrs.*, **H205**, 59-68.

Dowson D, Jin ZM, (1992) A full numerical solution to the problem of microelastohydrodynamic lubrication of a stationary compliant wavy layered surface firmly bonded to a rigid substrate with particular reference to human synovial joints. *Proc. Inst. Mech. Engrs.*, **H206**, 185-193.

Dowson D, Yao J, (1994) Elastohydrodynamic lubrication of soft-layered solids at elliptical contacts. Part 2: film thickness analysis. *Proc. Inst. Mech. Engrs.*, **H208**, 43-52.

Dumbleton JH, (1981) The tribology of artificial and natural joints. Elsevier, Amsterdam.

Engh GA, Dwyer KA, Hanes CK, (1992) Polyethylene wear of metal backed tibial components in total and unicompartmental knee prostheses. *JBJS.*, **74-B**, 1, 9-17.

Feng EL, Stulberg SD, Wixson RL, (1993) Progressive subluxation and polyethylene wear in TKRs with flat articular surfaces. *Clin. Orth.*, **299**, 60-71.

Foster CG, Hooker RJ, (1983) Simulation based design of hydraulic servo-controlled apparatus for damping measurement. *Simulation*, **14**, 6, 229-238.

Gahde J, Friedrich JF, Gehrke R, Loeschcke I, Sachse J, (1992) Adhesion of polyurethane to surface-modified steel. *J. Adhesion Sci. Tech.*, **6**, 5, 569-586.

Gent AN, Hamed GR, (1975) Peel mechanics. *J.Adhesion*, **7**, 91-95.

Gent AN, Hamed GR, (1977a) Peel mechanics for an elastic-plastic adherend. *J. Applied Polymer Science*, **21**, 2817-2831.

References.

Gent AN, Hamed GR, (1977b) Peel mechanics of adhesive joints. *J Polymer Engineering and Science*, **17**, 7, 462-466.

Gent AN, Lai SM, (1994) Interfacial bonding, energy-dissipation, and adhesion. *J. Polymer Science Part B-Polymer Physics*, **32**, 8, 1543-1555.

Gent AN, Lewandowski LH, (1987) Blow -off pressures for adhering layers. *J. Applied Polymer Science*, 33, 1567-1577.

Gladstone JR, Medely JB, (1990) Comparison of theoretical and experimental values for friction of lubricated elastomeric surface layers under transient conditions. In: *Mechanics of coatings*, 16th Leeds Lyon Symposium, Eds. D Dowson, CM Taylor, M Godet, Elsevier, Amsterdam, 251-260.

Gore TA, Higginson GR, Kornberg RE, (1981) Some evidence of squeeze-film lubrication in hip prostheses. *Eng. in Medicine*, **10**, 2, 89-95.

Griffith AA, (1920) The phenomena of rupture and flow in solids. *Phil. Trans. Roy. Soc.*, **A221**, 163-198.

Gunatillake PA, Meijs GF, Rizzardo, Chatelier RC, McCarthy SJ, Brandwood A, Schindhelm K, (1992) Polyurethane elastomers based on novel polyether macrodiols and MDI: synthesis, mechanical properties, and resistance to hydrolysis and oxidation. *J. Applied Polymer Sci.*, **46**, 319-328.

Hailey JL, Fisher J, Dowson D, Sampath SA, Johnson R, Elloy M, (1994) A tribological study of a series of retrieved Accord knee explants. *J. Med. Eng. Phys.*, **16**, 223-228.

Hall RM, Unsworth A, Wroblewski BM, Burgess IC, (1994) Frictional characterisation of explanted Charnley hip prostheses. *Wear*, **175**, 159-166.

References.

Hall RM, Unsworth A, Craig PS, Hardaker C, Siney P, Wroblewski BM, (1995) Measurement of wear in retrieved acetabular sockets. *Proc. Inst. Mech. Engrs*, **H209**, 233-242.

Hayes WC, Keer LM, Herrmann G, Mockros LF, (1972) A mathematical analysis for indentation tests of articular cartilage. *J. Biomech.*, **5**, 541-551.

Hergenrother RW, Wabers HD, Cooper SL, (1993) Effect of hard segment chemistry and strain on the stability of polyurethanes: *in vivo* biostability. *Biomater.*, **14**, 6, 449-458.

Higginson GR, (1966) The theoretical effects of elastic deformation of the bearing liner on journal bearing performance. *Proc. Inst. Mech. Engrs*, **180**, 3B, 31-38.

Higginson GR, (1978) Elastohydrodynamic lubrication in human joints. *Eng. in Medicine*, **7**, 1, 35-41.

Higginson GR, Snaith JE, (1979) The mechanical stiffness of articular cartilage in confined oscillating compression. *Eng. in Medicine,* **8**, 1, 11-14.

Hirano F, Murakami T, (1975) Photoelastic study of elastohydrodynamic contact condition in reciprocating motion. Proc. of 7th International Conference on *Fluid Sealing*, BHRA, 51-70.

Hirata N, Matsumoto K-I, Inishita T, Takenaka Y, Suma Y, Shintani H, (1995) Gamma-ray irradiation, autoclave and ethylene oxide sterilisation to thermosetting polyurethane: sterilisation to polyurethane. *Radiation. Phys. Chem.*, **46**, 3, 377-381.

Hood RW, Wright TM, Burstein AH, (1983) Retrieval analysis of total knee prostheses: A method and it's application to 48 total condylar prostheses. *J. Biomed. Mat. Res.*, **17**, 829-842.

Hooke CJ, O'Donoghue JP, (1972) Elastohydrodynamic lubrication of soft highly deformed contacts. *J Mech. Eng. Sci.*, **14**, 1, 34-48.

References.

Howie DW, Haynes DR, Rogers SD, McGee MA, Pearcy MJ, (1993) The response to particulate debris. *Orthopaedic Clinics of North America.* **24**, 4, 571-581.

Ihara T, Shaw MC, Bhushan B, (1986) A finite element analysis of contact stress and strain in an elastic film on a rigid substrate. Part 1: Zero friction. Part 2: With friction. *Tans. ASME: J Tribology*, **108**, 527-539.

Ikeuchi K, Goto S, Isobe K, Oka M, (1993) An experimental study of contact condition and friction in hip prostheses. In: *Thin films in Tribology*, Tribology Series 22, Eds. D Dowson, CM Taylor, M Godet, Elsevier, Amsterdam, 521-527.

Irwin GR (1973) *Appl. Mater. Res.*, **3**, 65.

Jaffar MJ, (1988) A numerical solution for axisymmetric contact problems involving rigid indenters on an elastic layer. *J. Mech. Phys. Solids.*, **36**, 401-416.

Jensen HM, (1991) The blister test for interface toughness measurement. *Eng. Fracture Mechanics*, **40**, 3, 475-486.

Jin ZM, Dowson D, Fisher J, (1991) Stress analysis of cushion form bearings for total hip replacements. *Proc. Inst. Mech. Engrs.*, **H205**, 219-226.

Jin ZM, Dowson D, Fisher J, (1993a) Wear and friction of medical grade polyurethane sliding on smooth metal counterfaces. *Wear*, **162-164**, 627-630.

Jin ZM, Dowson D, Fisher J, (1993b) Minimum and central film thickness formulae for an elastic layer firmly bonded to a rigid cylindrical substrate under entraining motion. *Wear*, **170**, 281-284.

Jin ZM, Dowson D, Fisher J, (1993c) Fluid film lubrication of natural hip joints. In: *Thin films in Tribology*, Tribology Series 22, Eds. D Dowson, CM Taylor, M Godet, Elsevier, Amsterdam, 545-555.

References.

Jin ZM, Dowson D, Fisher J, Rimmer D, Wilkinson R, Jobbins B, (1994a) Measurement of lubricating film thickness in low elastic modulus lined bearings, with particular reference to models of cushion form bearings for total joint replacements. Part 1: steady state entraining motion. *Proc. Inst. Mech. Engrs.*, **J208**, 207-212.

Jin ZM, McClure G, Dowson D, Fisher J, Jobbins B, (1994b) Measurement of lubricating film thickness in low elastic modulus lined bearings, with particular reference to models of cushion form bearings for total joint replacements. Part 2: squeeze-film motion. *Proc. Inst. Mech. Engrs.*, **J208**, 213-217.

Johnson GR, Dowson D, Wright V (1975) A new approach to the determination of the elastic modulus of articular cartilage. *Anns. Rheum. Dis.*, **43**, Suppl. 116-117.

Johnson RC, Smidt GL (1969) Measurement of hip-joint motion during walking. *JBJS*, **51A**, 6, 1083-1094.

Jones SMG, Pinder IM, Morgan CG, Malcolm AJ, (1992) Polyethylene wear in uncemented knee replacements. *JBJS*, **74-B**, 1, 18-22.

Kabo JM, Gebhard JS, Loren G, Amstutz HC, (1993) In vivo wear of polyethylene acetabular components. *JBJS*, **75-B**, 2, 254-258.

Kaelble DH, (1960) Theory and analysis of peel adhesion: bond stresses and distributions. *Trans. Soc. Rheology*, **4**, 45-73.

Kavanagh BF, Wallrichs S, Dewitz M, Berry D, Currier B, Ilstrup D, Coventry M (1994) Charnley low friction arthroplasty of the hip. Twenty year results with cement. *J. Arthroplasty*, **9**, 3, 229-234.

Kelly MA, Fithian DC, Chern KY, Mow VC, (1990). Structure and function of the meniscus: basic and clinical implications. Chapter 7 In: *Biomechanics of diarthrodial joints: Vol 1.* Eds. Mow, Ratcliffe, Woo. Springer-Verlag, New York, 191-211.

References.

Kilgus DJ, Moreland JR, Fineramn GAM, Funahashi TT, Tipton JS, (1991) Catastrophic wear of tibial polyethylene inserts. *Clin. Orth.*, **273**, 223-231.

Kim KS, Kim J, (1988). Elasto-plastic analysis of the peel test for thin-film adhesion. *J. Engineering Materials and Technology, Trans. ASME*, **110**, 3, 266-273.

Kinloch AJ, (1987) Adhesion and Adhesives: Science and Technology. Chapman and Hall, London.

Kinloch AJ, Lau CC, Williams JG, (1994) The peeling of flexible laminates. *Int. J. of Fracture*, **66**, 1, 45-70.

Lafortune MA, Cavanagh PR, Sommer HJ, Kalenak A, (1992) Three dimensional kinematics of the human knee during walking, *J. Biomechanics*, **25**, 4, 347-357.

Lewis P, Rorabeck CH, Bourne RB, Devane P, (1993) Posteromedial tibial polyethylene failure in TKRs. *Clin. Orth.*, **299**, 11-17.

Lin SJ, Akers A, (1989) A dynamic model of the flapper-nozzle component of an electrohydraulic servo valve. *ASTM J. Dynamic systems, measurement, and control*, **111**, 105-109.

Lin SJ, Akers A, (1991) Dynamic analysis of a flapper-nozzle valve. *ASTM J. Dynamic systems, measurement, and control*, **113**, 163-167.

Lindley PB, (1971) Ozone attack at a rubber-metal bond. *J. Inst. Rubber Industries*, **5**, 243-248.

Linn FC, Radin EL, (1968) Lubrication in animal joints. III. The effect of certain chemical alterations of the cartilage and lubricant. *Arthritis Rheum.*, **11**, 674.

References.

Matthewson MJ, (1981) Axi-symmetric contact on thin compliant coatings. *J. Mech. Phys. Solids.*, **29**, 2, 89-113.

McCormick JA, (1978) A numerical solution for generalised elliptical contacts of layered elastic solids. Report no. 78TR52, Mechanical Technology Inc., Latham, New York.

McKellop H, (1981) Wear of artificial joint materials 2. Twelve-channel wear-screening device: correlation of experimental and clinical results. *Eng. in Medicine*, **10**, 3, 123-136.

McKellop HA, Rostlund TV, (1990) The wear behaviour of ion-implanted Ti-6Al-4V against UHMW polyethylene. *J. Biomedical Mat. Res.*, **24**, 1413-1425.

McMillin CR, (1994) Elastomers for biomedical applications. *Rubber Chemistry and Technology*, **67**, 417-446.

Medley JB, Pillar RM, Wong EW, Strong AB, (1980) Hydrophilic polyurethane elastomers for hemiarthroplasty: a preliminary *in vitro* wear study. *Eng. in Medicine*, **9**, 2, 59-65.

Medley JB, Dowson D, Wright V, (1984) Transient elastohydrodynamic lubrication models for the human ankle joint. *Eng. in Medicine*, **13**, 3, 137-151.

Meijers P, (1968) The contact problem of a rigid cylinder on an elastic layer. *Appl. Sci. Res.*, 18, 353-383.

Merritt HE, (1967) Hydraulic control systems, Wiley, New York.

Mintz L, Tsao AK, McCrae CR, Stulberg SD, Wright T, (1991) The arthroscopic evaluation and characteristics of severe polyethylene wear in total knee arthroplasty. *Clin. Orth.*, **273**, 215-221.

References.

Morris AEP, Shanahan MER, (1994) A preliminary study of polymer/sintered steel adhesion. *Inter. J. Adhesion Adhesives*, **14**, 2, 145-151.

Morrison JB, (1968) Bioengineering analysis of force actions transmitted by the knee joint. *J. Biomed. Eng.*, **3**, 164-170.

Morrison JB, (1970) The mechanics of the knee joint in relation to normal walking. *J. Biomech.*, **3**, 51-61.

Mow VC, Hou JS, Owens JM, Ratcliffe A, (1990) Biphasic and quasilinear viscoelastic theories for hydrated soft tissues. Chapter 8 In: *Biomechanics of diarthrodial joints: Vol 1*. Eds. Mow, Ratcliffe, Woo. Springer-Verlag, New York, 215-262.

Murakami T, Ohtsuki N, (1987) Lubricating film formation in knee prostheses under walking. In: *Fluid Film Lubrication -Osborne Reynolds Centienery*, 13th Leeds Lyon symposium, Eds. D Dowson, CM Taylor, M Godet, D Berthe, Elsevier, Amsterdam, 387-392.

Murakami T, Ohtsuki N, Higaki H, (1993) The adaptive multimode lubrication in knee prostheses with compliant layer during walking motion. In: *Thin films in Tribology*, Tribology Series 22, Eds. D Dowson, CM Taylor, M Godet, Elsevier, Amsterdam, 673-682.

Nguyen HX, Poursartip A, Riahi G, Bennett RC, Wood GM, (1991) treatment of ultra high molecular weight polyolefin to improve adhesion to a resin. US Patent 5039549.

Niesiolowski F, Aubrey DW, (1981) Stress distribution during peeling adhesive tapes. *J. Adhesion*, **13**, 87-98.

O'Kelly J, Unsworth A, Dowson D, Jobbins B, Wright V, (1977) Pendulum and simulator studies of friction in hip joints. Chapter 2 In: *Evaluation of artificial joints*. Biological Eng. Soc., London 19-29.

References.

O'Kelly J, Unsworth A, Dowson D, Wright V, (1979) An experimental study of friction and lubrication in hip prostheses. *Eng. in Medicine*, **8**, 3, 153-159.

O'Connor JJ, Zavatsky A, (1990) Kinematics and mechanics of the cruciate ligaments of the knee. Chapter 25 In: *Biomechanics of diarthrodial joints: Vol 2*. Eds. Mow, Ratcliffe, Woo. Springer-Verlag, New York. 197-241.

Packham DE, (1992) Peel Tests. In: Handbook of adhesion. Ed. D Packham. Longman, Harlow. 301-305.

Parry TV, Wronski AS, (1992) A technique for the measurement of adhesive fracture energy by the blister method. *J. Adhesion*, **37**, 4, 251-260.

Pappas M, Buechel F, (1979) New Jersey knee simulator. *Trans. 11th Intern. Biomaterials Symp.*, **3**, 101.

Paul I, Rose R, Simon S, Radin E, (1977) The MIT Knee Joint Simulator, Chapter 6 In: *Evaluation of artificial joints*. Biological Eng. Soc., London.

Paul JP, (1967) Forces transmitted by joints in the human body. *Proc. Inst. Mech. Engrs.*, **181**, 3J, 8-15.

Pearcy MJ (1988) A new generation of artificial hip joints. *Eng. in Medicine*, **17**, 4, 109-201.

Perry J, (1993) The mechanics of gait. Chapter 3 In: *Mechanics of human joints*. Eds. V Wright and E Radin. Marcel Dekker, New York.

Pinchuk L, (1994) A review of the biostability and carcinogenicity of polyurethanes in medicine and the new generation of 'biostable' polyurethanes. *J. Biomater. Sci. Polymer Edn.*, **6**, 3, 225-267.

References.

Plante-Bordeneuve P, Freeman MAR, (1993) Tibial high density polyethylene in conforming tibiofemoral prostheses. *JBJS*, **75-B**, 4, 630-636.

Rand JA, (1991) Cement or cementless fixation in total knee arthroplasty. *Clin. Orth.*, **273**, 52-62.

Rand JA, Ilstrup DM, (1991) Survivorship analysis of total knee arthroplasty. *JBJS*, **73-A**, 3, 397-409.

Rohrle H, Scholten R, Sigolotto C, Sollbach, Kellner H, (1984) Joint forces in the human pelvis-leg skeleton during walking. *J. Biomech.*, **17**, 6, 409-424.

Saikko V, Paavolainen P, Kleimola M, Slatis P, (1992) A five station hip joint simulator for wear rate studies. *Proc. Inst. Mech. Engrs.*, **H206**, 195-200.

Saikko V, (1992) A simulator study of friction in total replacement hip joints. *Proc. Inst. Mech. Engrs.*, **H206**, 201-211.

Saikko V, (1993) Wear of polyethylene acetabular cups against alumina femoral heads. *Acta Ortho. Scand.* **64**, 5, 507-512.

Sanchez-Adsuar MS, Pastor-Blas MM, Torregrosa-Macia R, Martin-Martinez JM, (1994) Relevance of polyurethane configuration on adhesion properties. *Inter. J. Adhesion Adhesives*, **14**, 3, 193-200.

Sayles RS, Thomas TR, Anderson J, Haslock I, Unsworth A, (1979) Measurement of the surface microgeometry of articular cartilage. *J. Biomech.* **12**, 257-267.

Seedhom BB, Dowson D, Wright V, Longton EB, (1972) A technique for the study of geometry and contact in normal and artificial knee joints. *Wear*, **20**, 189.

References.

Seedhom BB, (1981) Biomechanics of the lower limb: The knee. In: *An introduction to the biomechanics of joints and joint replacements.* Eds D Dowson and V Wright. Mechanical Engineering Publications Ltd. London. 73-81.

Seireg A, Arvikar RJ, (1975) The prediction of muscular load sharing and joint forces in the lower extremities during walking, *J. Biomechanics*, **8**, 89-102.

Shaw J, Murray D, (1973) Knee joint simulator. *Clin. Orth.*, **94**, 15-23.

Smith N, Doyle C, Jones E, (1996) Prosthesic bearing element and process for making such an element. European Patent EP 0698382A2.

Smith TJ, Medley JB, (1987) Development of transient elastohydrodynamic models for synovial joint lubrication. In: *Fluid Film Lubrication -Osborne Reynolds Centienery*, 13th Leeds Lyon symposium, Eds. D Dowson, CM Taylor, M Godet, D Berthe, Elsevier, Amsterdam, 369-374.

Spikes HA, (1996) Mixed lubrication -An overview. 10th International Colloquium on: *Tribology -solving friction and wear problems.* Esslingen, Germany. 1713-1735.

Stokes K, Urbanski P, Cobian K, (1987) New test methods in the evaluation of stress cracking and metal catalysed oxidation in implanted polymers. In *Polyurethanes in Biomedical Engineering II*, Eds. H Plack *et al.*, Elsevier, Amsterdam, 109.

Stokes K, (1987) Polyether polyurethanes: Biostable or not? *J. Biomat. Applications*, **3**, 228-259.

Stokes K, McVenes R, Anderson J, (1995) Polyurethane elastomer biostability. *J. Biomater. Applications*, **9**, 321-354.

Strozzi A, Unsworth A, (1994) Axisymmetric finite element analysis of hip replacement with an elastomeric layer: the effects of layer thickness. *Proc. Inst. Mech. Engrs.*, **H208**, 139-149.

References.

Swanson S, Freeman M, Heath J,(1973) Laboratory tests on total joint replacement prostheses. *JBJS*, **55B**, 4, 759-773.

Szklar O, Ahmed AM, (1987) A simple unconstrained dynamic knee simulator. *J. Biomech. Eng.*, **109**, 247-251.

Szycher M, (1987) Biostability of polyurethane elastomers. A critical review. *J. Biomat. Applications*, **3**, 297-402.

Tanzi MC, Mantero S, Freddi G, Motta A, Sada A, Peluso G, (1994) Cytocompatibility of two segmented biomedical polyurethanes. *J. Mater. Sci.: Mater. in Medicine*, **5**, 705-710.

Timoshenko SP, Goodier JN, (1970) Theory of Elasticity. McGraw Hill. Singapore.

Treharne RW, Young RW, Young SR, (1981) Simulation of the knee joint using a computer controlled system. *Eng. in Medicine*, **10**, 3, 137-142.

Tsao A, Mintz L, McCrae CR, Stulberg SD, Wright T, (1993) Failure of the PCA prosthesis in total knee arthroplasty due to severe polyethylene wear. *JBJS*, **75-A**, 1, 19-26.

Unsworth A, Dowson D, Wright V, (1974) The frictional behaviour of human synovial joints-Part 1: Natural joints. *Trans. ASME: J. Lub. Tech.*, **74-Lub-38**.

Unsworth A, (1978) The effects of lubrication in hip joint prostheses. *Phys. Med. Biol.*, **23**, 2, 253-268.

Unsworth A, Roberts BJ, Thompson JC, (1981) The application of soft layered lubrication to hip prostheses. *JBJS*, **63B**, 297.

References.

Unsworth A, Pearcy MJ, White EFT, White G, (1987) Soft layer lubrication of artificial hip joints. Proc. of Int'l Conference on *Tribology, friction, lubrication and wear, 50 years on*. Mechanical Engineering Publications Ltd, London, 715-724.

Unsworth A, Pearcy MJ, White EFT, White G, (1988) Frictional properties of artificial hip joints. *Eng. in Medicine*, **17**, 3, 101-104.

Unsworth A, (1993) The lubrication of human joints. In: *The bio-mechanics of human joints*, Eds V Wright and EL Radin, Marcel Dekker, New York.

Unsworth A, Hall RM, Burgess IC, Wroblewski BM, Streicher RM, Semlitsch M, (1995) Frictional resistance of new and explanted artifical hip joints. *Wear*, **190**, 226-231.

Voyutskii SS, (1963) Autohesion and adhesion of high polymers, Interscience, New York.

Vukobratovic M, Katic D, Potkonjak V, (1987) Computer assisted choice of electrohydraulic servo systems for manipulation robots using complete mathematical models. *Mech. Mach. Theory*, **22**, 5, 431-439.

Wasieleski RC, Galante JO, Leighty RM, Raghu NN, Rosenberg AG, (1994) Wear patterns on retrieved polyethylene tibial inserts and their relationship to technical considerations during total knee arthroplasty. *Clin. Orth.*, **299**, 31-43.

Waters NE, (1965) The indentation of thin rubber sheets by spherical indentors. *Brit. J. Appl. Phys.*, **16**, 557-563

Williams A, Statham A, (1993) Comparison of surface profile data obtained from two surface roughness instuments. Chapter 38 in: *Laser Metrology and Machine performance*, Computational Mechanics Pub., Southampton.

Williams MH, Frankel SJ, Nanchahal K, Coast J, Donovan J, (1992) Total knee replacement: Epidemiological based needs assessment. H.C.E.U., Univ. of Bristol.

References.

Williams MH, Newton JN, Frankel SJ, Braddon, Barclay E, Gray JAM (1994) Prevalence of total hip replacement: how much demand has been met? *J. Epidemiol. Community Health*, **48**, 188-191.

Williams ML, (1969) The continuum interpretation for fracture and adhesion. *J. App. Polymer Sci.*, **13**, 29-40.

Williams PF, Powel GL, Love B, Ishihara K, Nakabayashi N, Johnson R, LaBerge M (1995) Fabrication and charaterization of dipalmitoyl phosphatidylcholine (DPPC) attracting elastomeric material for joint replacements. *J. Biomaterials*, **16**, 15, 1169-1174.

Windsor RE, Scuderi GR, Moran MC, Install JN, (1989) Mechanisms of failure of the femoral and tibial components in total knee arthroplasty. *Clin. Orth.*, **248**, 15-20.

Wrona M, Mayor MB, Collier DE, Jensen RJ, (1993) The correlation between fusion defects and damage in tibial polyethylene bearings. *Clin. Orth.*, **299**, 92-103.

Yao JQ, Unsworth A, (1993) Asperity lubrication in human joints. *Proc. Inst. Mech. Engrs.*, **H207**, 245-254.

Yao JQ, (1994) Contact mechanics of soft layer artificial hip joints. Part 1: General solutions. *Proc. Inst. Mech. Engrs.*, **H208**, 195-205.

Yao JQ, Parry TV, Unsworth A, Cunningham JL, (1994) Contact mechanics of soft layer artifical hip joints Part 2: Application to joint design. *Proc. Inst. Mech. Engrs.* **H208**, 206-215.

Zachman NJ, Hillberry BM, Kettelkamp DB, (1978) Design of a load simulator for the dynamic evaluation of prosthetic knee joints. **ASME 78-DET-59.**

Zdrahala RJ, McGary CW, (1986) Thermoplastic polyurethanes softening in 37°C n-saline. *Materials. Research Soc. Symp. Proc.*, **55**, 407-413.

References.

Zhao Q, Casas-Bajar J, Urbanski P, Stokes K, (1995) Glass wool-$H_2O_2/CoCl_2$ test system for in vitro evaluation of biodegradative stress cracking in polyurethane elastomers. *J. Biomedical Mater. Research*, **29**, 467-475.

Appendix A. The Durham Friction simulator:

Assessment of friction in externally pressurised bearings.

Nomenclature.

A_e	Effective pad area.
A_L	Area of lands.
d_c	Capillary diameter.
h_F	Fluid film thickness.
h_0	Reference fluid film thickness
F	Applied simulator load.
l_c	Capillary length
P_s	Supply pressure 2.76MPa (400psi).
P_{r0}	Reference recess pressure
R_c	Hydraulic resistance of the capillary compensator where $R_c = \frac{128 l_c \eta}{\pi d_c^4}$.
R_0	Reference recess hydraulic resistance.
W	Load per pad.
W_0	Reference load per pad.
β	Reference pressure ratio P_{r0}/P_s.
η	Fluid viscosity, 0.07 $Nm^{-2}s$ at 25°C.
Ω	Maximum angular velocity, 2.138 rads/s.

Bearing dimensions	Value
Bearing Diameter (D) mm.	40.028
Bearing length (L) mm.	40.000
Clearance (C_0) mm.	00.039
Recess length (l) mm.	29.7
Angle extended by each pad.	50°
Angle between the pad centres (α).	45°

Table A.1. Hydrostatic journal bearing dimensions.

A.1 Theoretical Analysis.

The low friction journal bearings used on the second Durham friction simulator were designed by Blamey (1993). They are opposed cylindrical pocket hydrostatic bearings, and can be considered as twin pad rather than twin recess bearings, since on three sides of the pad oil flow is to atmosphere, and on only one side is there flow between the pads. An analysis of this bearing type is given by Bassani and Piccigallo (1992), who specify the ratio of film thickness under an applied load **F**, to the reference film thickness in Equation A.1.

Appendix A.

$$\frac{h_F}{h_0} = \sqrt[3]{\frac{R_0}{R_c}\frac{1-\beta W/W_0}{\beta W/W_0}} \qquad \text{A.1}$$

For cylindrical pad bearings the reference design configuration is when the film thickness $\mathbf{h_0}$ equals the bearing clearance $\mathbf{C_0}$. In this case the reference design load $\mathbf{W_0}$ is given by Equation A.2, and the recess reference pressure $\mathbf{P_{r0}}$ is found by equating the fluid flow through the capillary compensation device with that over the pad lands, and rearranging, Equation A.3.

$$W_0 = P_{r0} A_e \qquad \text{A.2}$$

$$P_{r0} = \frac{R_0 P_s}{(R_c + R_0)} \qquad \text{A.3}$$

The total load applied to the test prosthesis is shared across the four pads. The load supported by each pad is found by resolving vertically, Equation A.4

$$W = \frac{F}{2\cos\frac{\alpha}{2}} \qquad \text{A.4}$$

The coefficient of friction of the bearing is the ratio of the force required to shear the fluid of thickness $\mathbf{h_F}$ to the applied load, Equation A.5.

$$\mu = \frac{\eta A_L \Omega D/2}{h_F W} \qquad \text{A.5}$$

Assuming that the bearing operates with a film thickness similar to the journal clearance, and the displacement is small, the effective pad bearing area and the reference hydraulic resistance is given by Bassani and Piccigallo (1992) in Equations A.6 and A.7.

$$A_e = LD \sin\frac{\alpha}{2} A_e^* \qquad \text{A.6}$$

$$R_0 = \frac{\eta}{C_0^3} R^* \qquad \text{A.7}$$

where A_e^* is 0.82 and R^* is 0.25 for the pad dimensions of these bearings. The bearing dimensions are given in Table A.1. Solving Equations A.1 to A.7, the film thickness and coefficient of friction of these journal bearings were found, and the results given in Figure A.1.

Clearly the coefficient of friction of this bearing is very low at the joint reaction forces used during the simulator experiments, however reference to Bassani and Piccigallo (1992) shows that the bearing design is not optimum. The above analysis returns a reference load equivalent to a joint force of 5.2 kN, with a β value of 0.72. Design charts show that at loads below the reference load the film thickness is large but the bearing stiffness is low, and at loads above this reference value the bearing quickly collapses. The stiffness of the bearing could be improved by increasing the capillary resistance to the value of the pad reference resistance.

The above analysis has been conducted for oil at 25°C, typical of the hydrostatic bearing lubricant temperatures during the simulator experiments. As the temperature of the lubricant rises, its viscosity decreases. Bassani and Piccigallo (1992) point out that lubricant film thickness and bearing stiffness are independent of viscosity for compensated supply bearings, and the friction is directly proportional to viscosity. Thus, even though small rises in lubricant temperature result in large reductions in viscosity, the coefficient of friction actually reduces at the expense of increased flow and pumping power.

A.2 Experimental verification.

The friction carriage assembly originally designed by Blamey (1993) was replaced with a one piece carriage, in order to eliminate assembly misalignment and improve the carriage stiffness. In order to verify the correct operation of the hydrostatic bearings, a potential was applied between the journal and bearing housing. The potential across the bearing was continually monitored during a test, and contact between the two bearing surafces was indicated by a measured potential of zero volts, and no contact was indicated by a measured potential of supply volts. The results of this experiment showed that generally the bearings operated without contact. When contact was observed it occurred during transition between the swing and stance phase, or during the swing phase, probably due to low stiffness in the medial-lateral direction. No contact was observed during the loading phase of the cycle when the frictional torque was measured.

A.3 Conclusion.

By presenting these two short studies, the hydrostatic journal bearings were shown to operate with large fluid film thicknesses, and extremely low friction. Little or no contact between the bearing surfaces was observed experimentally. The method of frictional torque measurement relies fundamentally on the correct operation of these bearings, and hence these results give confidence that the simulator is functioning correctly.

Appendix A.

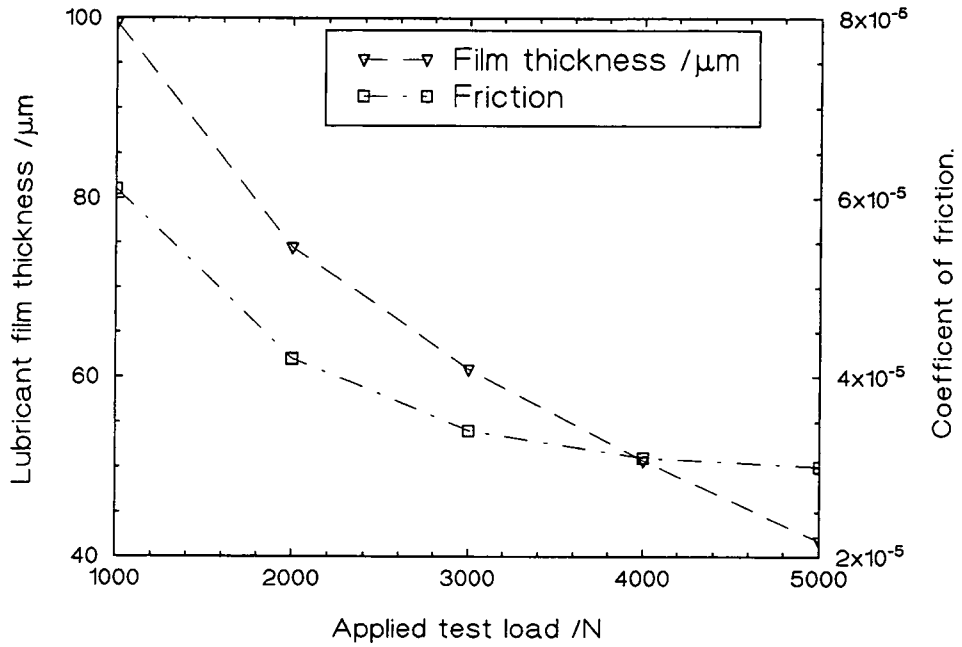

Figure A.1 Variation of lubricant film thickness and bearing friction with applied load for the Durham friction simulator hydrostatic journal bearings.

Appendix B. The Durham friction simulator:

An assessment of the repeatability and precision of the results.

B.1 Analysis of the measurement errors.

A measurement error signifies a deviation of the result from some 'true' value, and since this true value isn't known the error can only be estimated. An estimate of measurement error will enable the precision of the experiment to assessed, and has been made by examining the specification of the measurement transducers.

Examining the applied load measurement system first, reference to the main body of the text shows it consisted of four load cells each amplified by a strain gauge amplifier (SGA). The sum of the output from each SGA was then converted from an analogue to digital signal. The performance of the load cells, SGA and analogue to digital converter (ADC) are given in Table B.1. The maximum error ΔL was estimated by the expression

ΔL=*(ADC bit noise)+4*(cell nonlinearity + cell repeatability + SGA accuracy)*

For an applied load of 2 kN (each cell measured 500 N) the estimated maximum error was 55N.

Now considering the frictional torque measurement system, this consisted of the force transducer, charge amplifier, and ADC, the performance of which is also given in Table B.1. The maximum error ΔT was estimated by the expression

ΔT=*(ADC bit noise)+(transducer nonlinearity)+(charge amplifier inaccuracy)*

Although force transducer linearity of 1% full scale was specified by the manufacturer, experience has shown this to be a very conservative estimate as it's performance was found to be extremely linear and repeatable, and so a linearity of 0.1% was considered

more realistic. For a 32mm diameter femoral head, and an applied load of 2 kN, the frictional torque resulting in friction factors of 0.1, 0.01 and 0.001 were 3200 Nmm, 320 Nmm and 32 Nmm respectively. Applying the expression for $\Delta\mathbf{T}$, the estimated error in measure frictional torque was 53 Nmm, 25 Nmm and 22 Nmm respectively.

Finally considering the measurement of the femoral head, an error $\Delta\mathbf{R}$ of 0.01 mm in a radius of 16mm was considered reasonable.

The friction factor **f** was calculated from the experimental measurements using Equation B.1. Reference to Bevington (1969) showed that the propagation of the errors in the individual measuring systems leads to an estimated maximum error in the friction factor, which is given to a first approximation in Equation B.2.

$$f = \frac{T}{LR} \qquad \text{B.1}$$

$$\Delta f = f\sqrt{\frac{\Delta T^2}{T^2} + \frac{\Delta R^2}{R^2} + \frac{\Delta L^2}{L^2}} \qquad \text{B.2}$$

For the case of an applied load of 2 kN, a femoral head of radius of 16mm and friction factors values of 0.1, 0.01 and 0.001, the estimated maximum error in the friction factor resulting from a single test was 3.2%, 8.3% and 69% respectively. However, the true friction factor value was found by combining the results from two tests, and hence the relative estimated maximum error further increased by $\sqrt{2}$ to 4.5%, 12% and 98% respectively.

Although this was an estimate of the *maximum* error, these results were indicative of the trend in the relative precision of the machine. For friction factors between 0.1 to 0.01 (the

range of conventional joints) the experiment had an acceptable level of precision, better than ≈10%. However, for friction factor values below 0.01 (typical of compliant bearing joints) the precision decreases drastically. Although the simulator would demonstrate low friction factor values, discerning trends in this region would become more difficult as the results approach 0.001. The main cause of the relative imprecision at extremely low friction factor values was shown to be the ADC's, with an absolute accuracy of ±2bits, coupled with friction transducer linearity errors becoming significant at extremely low values of frictional torque.

Measurement	Device	Specification	Max error
Load	Load cells (FS=2 kN)	Non-linearity ±0.25%FS Non-repeatability 0.1%FS	5 N 2 N
Load	Strain Gauge Amp	Accuracy 1%	5 N
Load	ADC	±2 bits.	6.67 N
Frictional Torque	Force transducer (FS=17500Nmm)	Non-linearity ±0.1%FS (±1.0%FS max specified)	18 Nmm
Frictional Torque	Charge amplifier	Accuracy 1% (f=0.1, 0.01 and 0.001)	32 Nmm 3.2 Nmm 0.32 Nmm
Frictional Torque	ADC	±2 bits.	3.55 Nmm
Radius	Micrometer	0.01 mm	0.01 mm

Table B.1 Estimated maximum errors associated with the individual components of the measurement systems.

B.2 Repeatability of the results.

Another approach to the problem of assessing the performance of the simulator was to assess the repeatability of the results experimentally, which would give an indication of the precision of the experiment. A compliant layer hip joint was measured in the normal way under nominally consistent loading conditions, using water as the lubricant. The

friction factor was determined five or six times, and this was repeated three times during the course of a day. The results showed how the friction factor, Figure B.1, the temperature of the hydrostatic bearing oil, Figure B.2, and the applied minimum and maximum loads, Figure B.3, all varied over the duration of the experiment. Clearly, as the apparatus was used it warmed up. Specifically, the servo-hydraulic oil and hydrostatic bearing oil warmed up as work was done. Also the electronics and measuring transducers may have warmed up as a result of an increase in the ambient temperature or due to current flow. In order to assess which of the measurement and control systems were temperature dependant, each system was individually calibrated against an external standard, first when cold, then after a 400 cycle warm up, and then after a further 800 cycles of operation (equivalent to the cycles required for a typical Stribeck analysis).

The frictional torque and applied load measurement systems were found to operate independent of temperature, Figures B.4 and B.5, with the least squares fit of a straight line to the three sets of calibration data exhibiting no change in coefficients as the simulator warmed up. This was very encouraging, as these results showed that the friction and load measuring systems gave a consistent performance and precise results.

Calibration of the request load DAC signal against the applied load measured by an external standard, Figure B.6, showed that it exhibited temperature dependant characteristics. The least squares straight line fit to the three sets of calibration data had the same gradient but a decreasing intercept coefficient as the simulator warmed up. Figure 3.12 showed that one or more of three component groups could be responsible for the temperature dependence; the DAC and other electronic components, the servo-

hydraulic pump/valve/cylinder, or the load cells supplying the closed loop feedback signal. In addition the hydrostatic bearing oil was known to warm up during use.

In order to isolate which part of the simulator gave rise to these temperature dependent characteristics two more calibration experiments were conducted. Firstly the simulator was warmed up using *dummy* cycles, with both the servo-hydraulic power and hydrostatic bearing power turned off. Only the DAC and other electronics could warm up, and the results, Figure B.7, showed that they exhibited characteristics independent of the number of *dummy* warm up cycles. Secondly, the servo-hydraulic pump, oil and valve only were warmed up by requesting a constant load of 5kN applied first for 15 minutes, followed by a further 30 minutes. The hydrostatic bearing oil and the four feedback load cells both remained at ambient temperature throughout the calibration. The results, Figure B.8, indicated that it was the hydraulic system which exhibited characteristics dependent upon the simulator warming up, with the least squares straight line fit to the three sets of calibration data having equal gradients but with decreasing intercept coefficients. For a given requested DAC value, the actual applied load decreased by an amount independent of the magnitude of the requested load. Thus, as the simulator warmed up the actual applied load decreased by the same amount at both minimum and maximum loads, a result confirmed in Figure B.3.

Since the measurement systems were shown to be precise, it was concluded that a decrease in applied load had a direct effect on the lubrication regime which significantly affected the resulting frictional torque. The cause of the temperature dependence of the servo-hydraulic system remained unclear. Certainly as the valve warmed up, primarily as a result of the oil flow through the first stage jets, and the oil viscosity dropped and the

null characteristics of the valve would probably change. In addition, servo-hydraulic control of the very low forces required during the swing phase of the cycle is difficult. Control currents of only a few percent of the already tiny null region were required, resulting in inevitable variations in the applied load, and hence frictional torque.

B.3 Conclusions.

Theoretically, the simulator was estimated to perform with a precision of better than 10% for friction factor values greater than 0.01, but for values below 0.01 (typical of compliant bearing joints) the precision decreased drastically. Although discerning trends in the results as they approached 0.001 was judged to be difficult, the simulator could still demonstrate extremely low friction factors values.

Experimentally, the measuring systems were shown the be precise over the duration of a typical Stribeck test run. However, the servo-hydraulic system exhibited temperature dependent characteristics which resulted in decreases in both minimum and maximum load, of the same magnitude, over the duration of a test run. In turn, this resulted in a decrease in the measured friction factor, although it was postulated that this was due to changes in the lubrication regime, rather than a variation in parameter measurement. As a result of this study and reference to Figure B.1, the experimental protocol was modified to include a warm up period of 400 cycles, and the first result of each run was discarded. The temperature dependence of the applied load system was subsequently significantly reduced by modifications to the cooling system on the hydraulic pump unit.

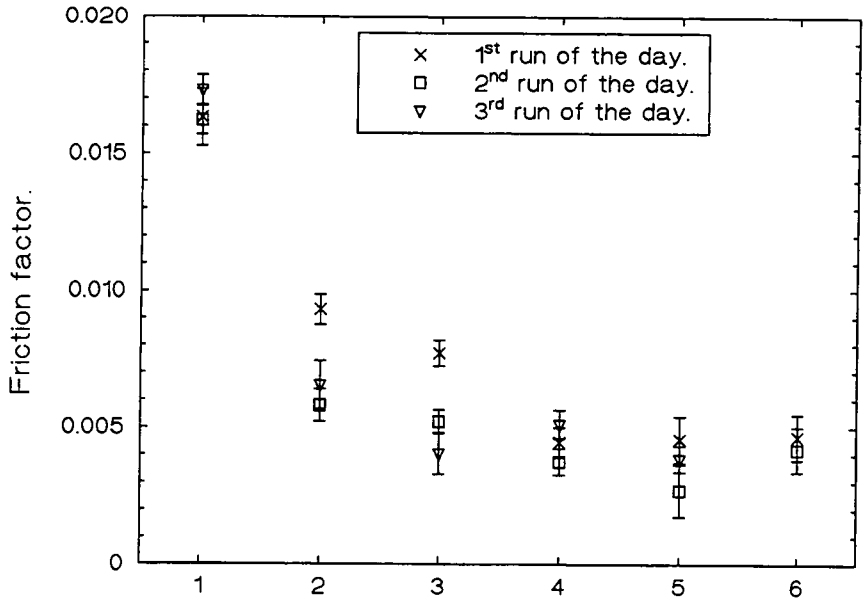

Figure B.1. The variation of friction factor measured throughout a day. The test was repeated five or six times each run, and three runs were completed during the course of a day. The compliant layer hip joint was tested under nominally similar conditions.

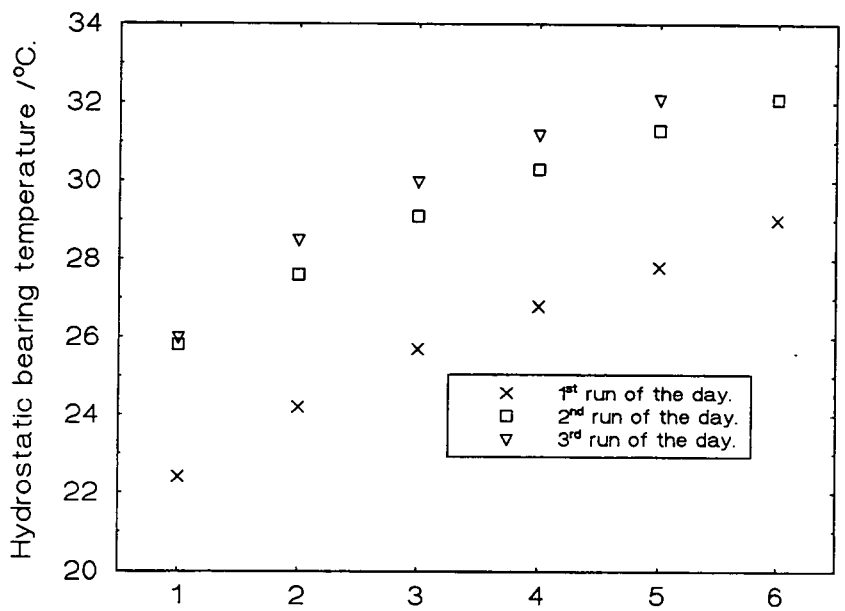

Figure B.2 The variation of hydrostatic bearing temperature measured throughout a day, as described in Figure B.1.

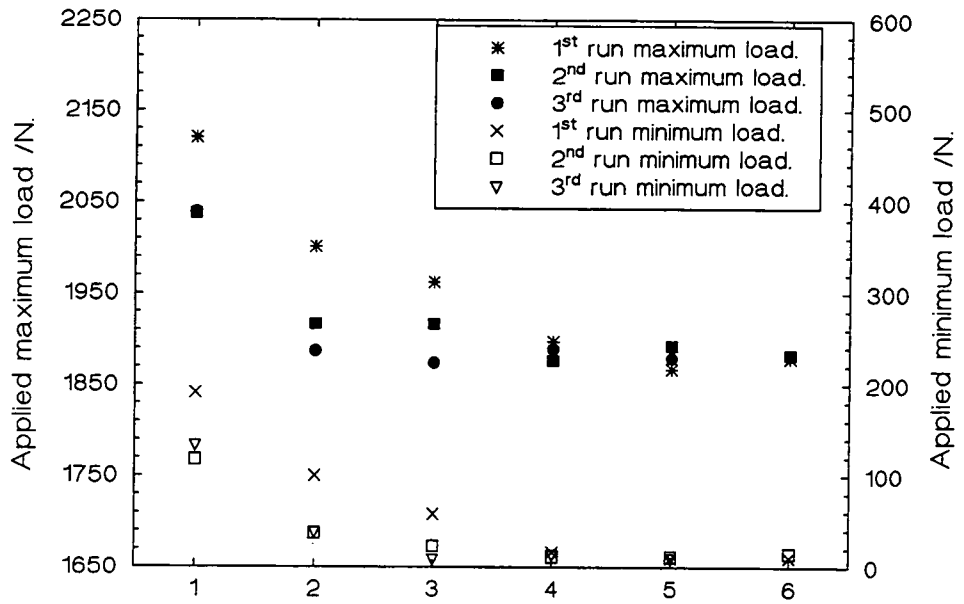

Figure B.3 The variation of applied minimum and maximum loads measured throughout a day, as described in Figure B.1.

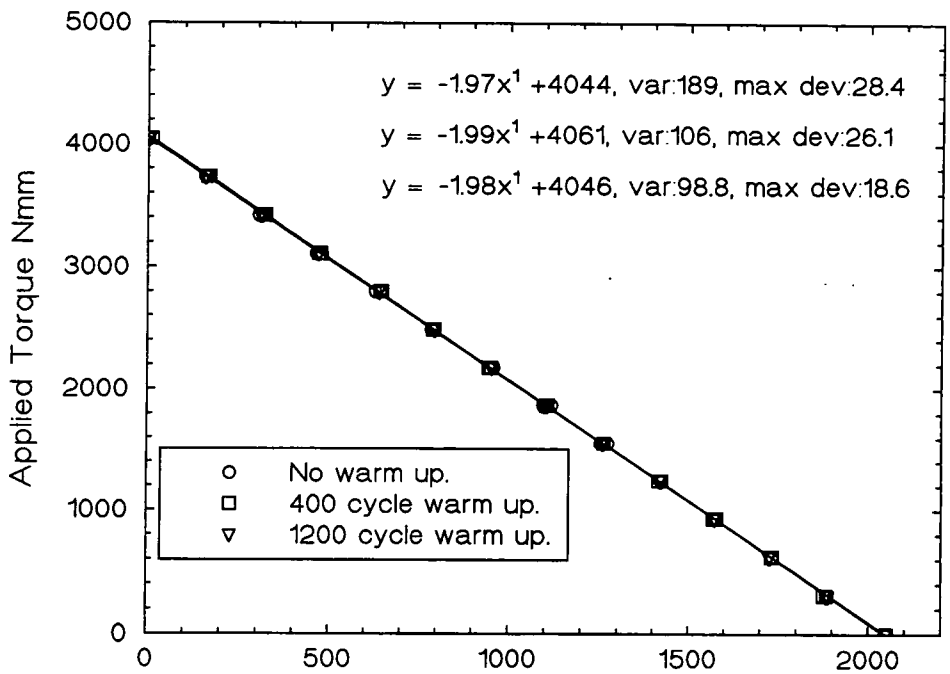

Figure B.4 Calibration of the frictional torque measuring system, illustrating no significant variation as the simulator warms up. The least squares fit of straight lines to the three sets of calibration data are shown, and exhibit no change in coefficients.

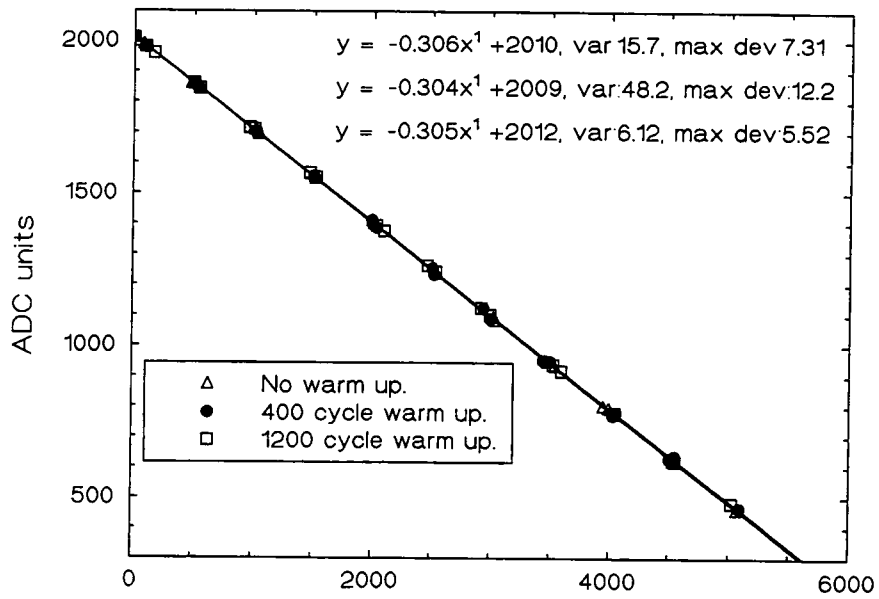

Figure B.5 Calibration of the applied load measuring system, illustrating no significant variation as the simulator warms up. The least squares fit of straight lines to the three sets of calibration data are shown, and exhibit no change in coefficients.

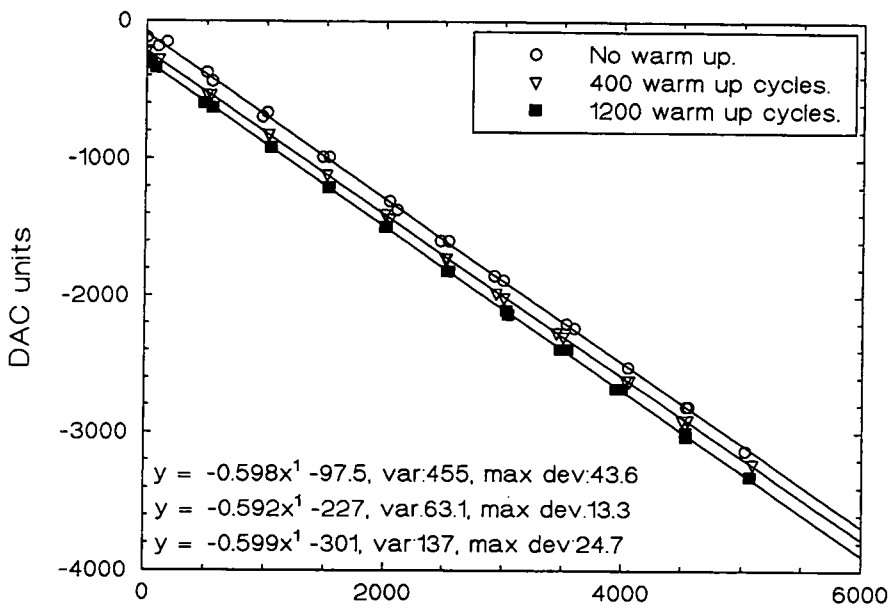

Figure B.6 Calibration of the request load system, showing temperature dependent characteristics. Coefficients of the least squares fit of straight lines to the three sets of calibration data are shown, and exhibit no change in the gradient but a decrease in the intercept.

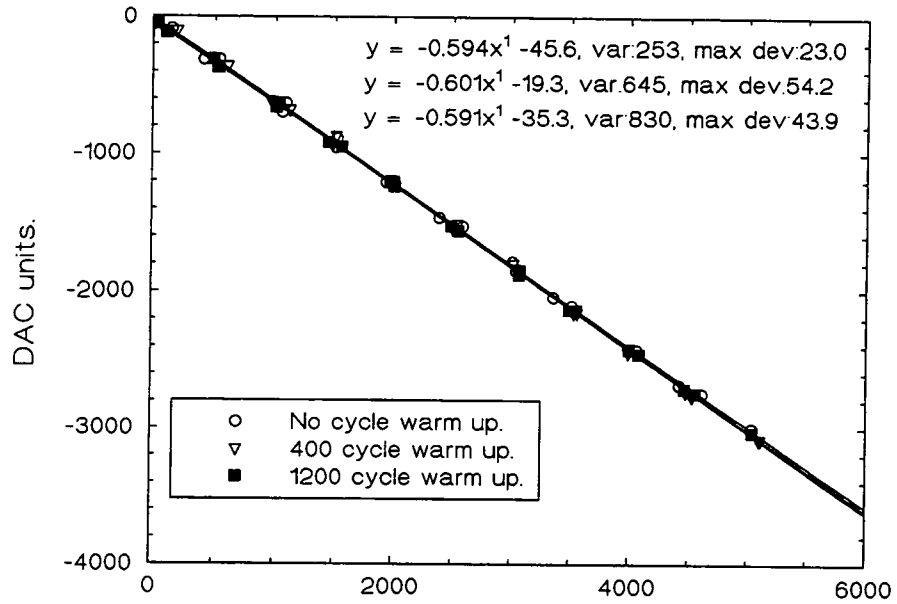

Figure B.7 Calibration of the DAC portion of the request load system, showing characteristics independent of the number of *dummy* warm up cycles.

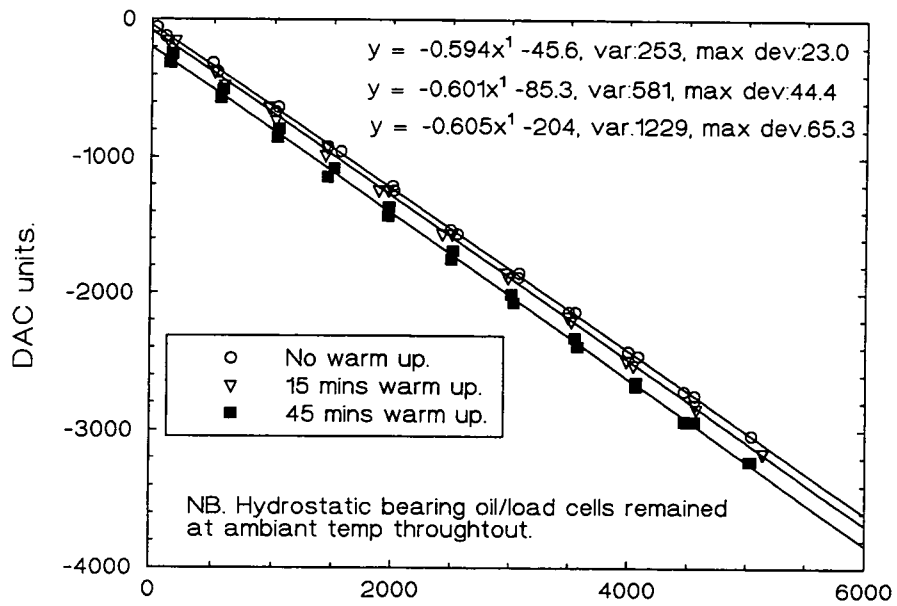

Figure B.8 Calibration of the request load system, showing that the temperature dependence can be isolated as a characteristic of the servo-hydraulic system.

Appendix C.

Non contacting optical profileometry.

C.1 Standard settings for the Micromap 512 NOP.

In order to evaluate the topography of the bearing surfaces, a Micromap 512 Non-contacting Optical Profiler (NOP) was used. To obtain the best results the samples were first cleaned in an ultrasonic bath in a 1% solution of Nutracon (Decon, UK) for 30 minutes, rinsed in distilled water and air dried for several hours. After a range of preliminary investigations a set of standard settings were used when taking measurements. These setting are detailed here, thus enabling comparable work to be carried out in the future.

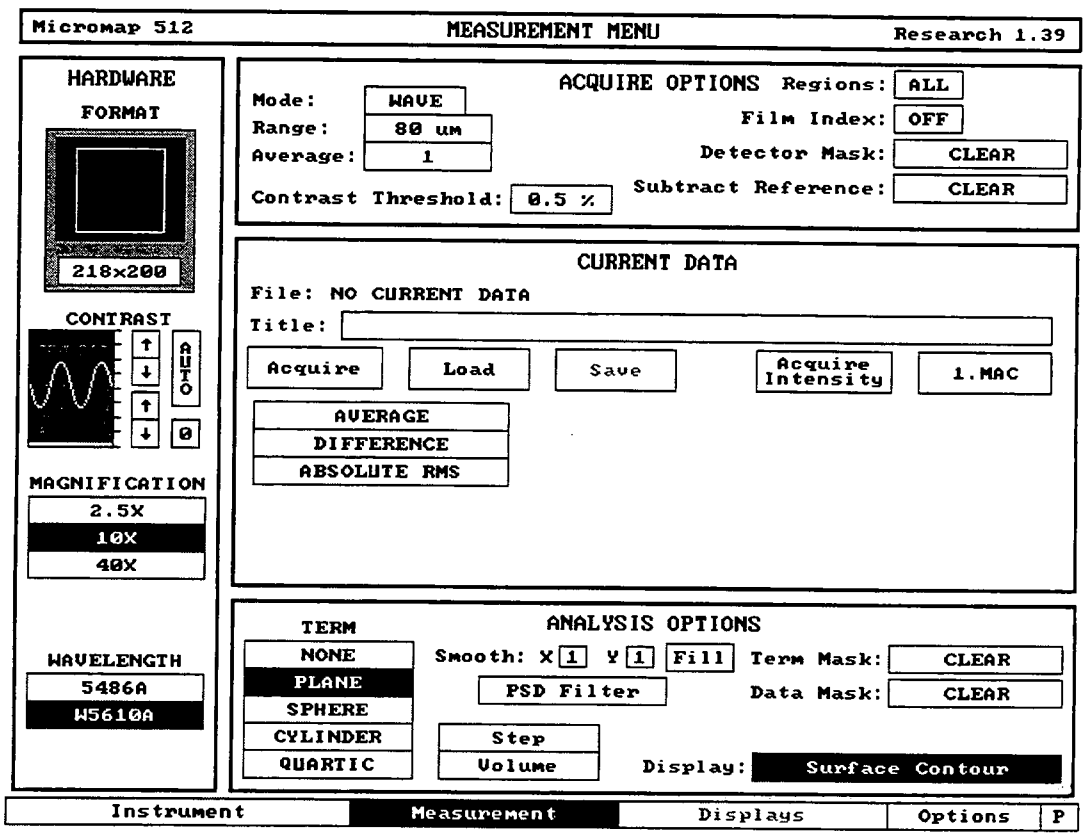

Figure C.1 Standard settings for the measurement of compliant layer bearings, with the exception of using a sphere term for acetabular cups, and a quartic term for tibial components.

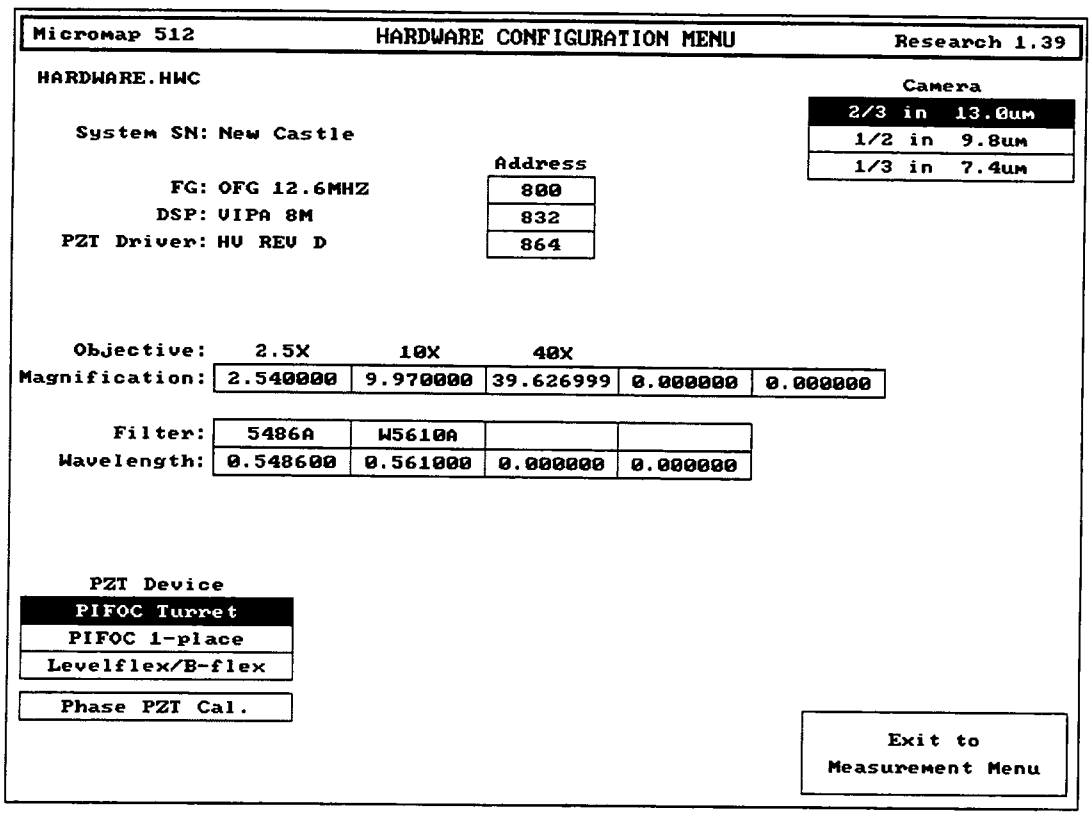

Figure C.2 Standard settings for the hardware configuration menu.

Appendix D. Computer simulation of the servo hydraulic systems.

Nomenclature.

Pressure (Nm^{-2}).

p1	pressure in cylinder 1.
p2	pressure in cylinder 2.
pd1e	pressure difference surface A, cylinder 1 exhaust.
pd1s	pressure difference surface B, cylinder 1 supply.
pd2s	pressure difference surface C, cylinder 2 supply.
pd2e	pressure difference surface D, cylinder 2 exhaust.
a	exhaust or atmospheric pressure (1×10^5).
ps	supply pressure (140×10^5).
stp1	initial pressure in cylinder 1.
stp2	initial pressure in cylinder 2.
p1bar	pressure in cylinder 1 (bar).
p2bar	pressure in cylinder 2 (bar).

Oil Flow (m^3s^{-1}).

qt	total oil flow supplied.
q1	net flow in to cylinder 1.
q2	net flow in to cylinder 2.
q1e	oil flow over surface A, cylinder 1 exhaust port.
q1eo	due to orifice flow.
q1ec	due to capilary flow.
	(similar notation for surfaces B, C, D)
q1lts	net flow in to cylinder 1 (lts/min).
q2lts	net flow in to cylinder 2 (lts/min).

Fluid flow constants.

vk	decay coefficient for capillary flow (A^{-1}).
fco	orifice flow constant ($m^3s^{-1}A^{-1}Pa^{-0.5}$).
fcc	capillary flow constant ($m^3s^{-1}Pa^{-1}$).
kbk	isentropic tangent bulk modulus for Shell tellus 37 oil at 140 bar ($1.7\times10^9Nm^{-2}$).

Servo valve data.

vsize	maximum flow capacity of valve at P_v (m^3s^{-1}).
psize	pressure at which valve size data is specified (Nm^{-2}).
irate	maximum valve current (A).
vleak	oil leakage at the null point at pressure P_l (m^3s^{-1}).
pleak	pressure at which valve leakage is specified (Nm^{-2}).
tor	frequency response characteristic (s^{-1}).
ohms	armature coil resistance (Ω).

Cylinder data.

vol	cylinder volume (m^3).
a1	area of piston in cylinder 1.
a2	area of piston in cylinder 2.
bore	bore diameter (m).
rod	rod diameter (m).
length	actuator stroke length (m).
pos	piston position (m).
vel	piston velocity (ms^{-1}).
acc	piston acceleration (ms^{-2}).
posmm	piston position (mm).
posdeg	piston position (°).

Mechanical system variables.

mass	load mass (kg).
fp	actuator force (N).
mofi	moment of interia
ff	friction force (N).
fn	normal force(N).
minl	minimum (swing phase) applied load (N).
maxl	maximum (stance phase) applied load (N).
u,u1,u2	coefficient of friction.

Control variables.

t	time (s).
ipos	armature or spool positioning current (A).
vin	input or request signal (V).
vlv	armature or spool positioning voltage (V).
gain	summing amplifier gain.
sti	spool current applied during band width test (A).
error	difference between input and feedback voltage (V).
amp	amplitude of the required system response (m or N).
freq	frequency of the required system response (Hz).

Appendix D.

D.1 The simulation program.

The simulation program was written by J Swift and P Baxendale[1]. The program takes a series of linear and ordinary differential equations and solves them using one of several iterative schemes. The Runge-Kutta fourth order method was used during this work. The user first creates a text file (i.e. **model.sim**) which defines the variables, governing equations and initial conditions of the model. The simulation program is then run which complies executable code specific to that model (i.e. **model.exe**). This code is then run to solve the governing equations over a user specified time frame and iteration interval. The constants and initial value of all the variables are initialised using a second text file (i.e. **model**). The simulation is then run and any variable can be monitored graphically over the specified time frame (see Figures 7.15, 16 and 18). Thus model specific executable code is generated for each application, but the values of the constants can be easily changed and the effect on the model evaluated. In order to use the simulation program the user need only create two simple text files; one containing the model equations and the other the initial variable values. The **model.sim** files takes the form

```
/[comments, model.sim]/

/[define constants]/
constant real A, B, C, D;

/[define variables]/
time var real E, F, G, H;

/[initialise some variables to their start point values]/
initial;
F=C/(1-D);

/[linear equations]/
G=A*F-B;
H=A*B*(D/H);
E=H-G;
.
```

[1]Microprocessor Centre, School of Engineering, University of Durham.

Appendix D.

In addition to all the normal C math operators, three additional operators were defined and used here; integral, select and limit.

Operator:	A=intgrl(B,C);	A=select(B,C,D);	A=limit(B,C,D);
Definition	$A = \int_{t=0}^{t} B.\,dt$ and A=C when t=0	if (B<0) A=C; else A=D;	if (B>D) A=D; else if (B<C) A=C; else A=B;

The **model** file takes the form

```
set A 0.0
set B 4.0
set C 0.0
set D 40.0
set E 0.0
set F 6.9
set G 0.0
set H 1.9
ftime 1.000000e-002          /[total simulation time]/
step 1.000000e-004           /[iteration step time]/
pval 1.000000e-003           /[plot point step]/
ymin -1.000000e+000          /[max y value on graph]/
ymax 1.000000e+000           /[min y value on graph]/
simtime 0.000000e+000/[start time]/
graph                        /[display graph]/
plot H                       /[variable plotted against time]/
rk4                          /[use Runge Kutta 4 method]/
axes
```

D.2 Simulation code for various models and systems.

In order to evaluate effects of valve and actuator size on the various designs of hydraulic systems several simulation programmes were complied from **model.sim** type files. These files are listed here.

Appendix D.

```
/[ servo valve model - proportional flow ]/
/[30.1.95 testflow.sim  no load flow charactoristics]/

/[ valve constants ]/
constant real fco , fcc , vsize , psize , irate , vleak , pleak , vk ;

/[system constants]/
constant real kbk , ps , a ;

timevar real qrat, q1, q2, q1s, q1e, q2e, q2s, pd1s, pd1e, pd2s, pd2e ;

timevar real ipos , q1eo, q1ec, q1so, q1sc, q2so, q2sc, q2eo, q2ec ;

/[start point constants]/
constant real  sti ;

initial ;

fco = vsize/(irate*sqrt(psize)) ;
fcc = 0.333*(vleak/(pleak)) ;


dynamic ;
/[..for surface A; cylinder 1 exhaust port ]/
pd1e = a-a ;
q1eo = fco*fabs( ipos )*sign( pd1e , sqrt( fabs( pd1e ) ) )+(fcc*pd1e) ;
q1ec = fcc*exp( ((-1)*fabs( ipos ))*vk )*pd1e ;
q1e = select( ipos, q1eo, q1ec) ;

/[..for surface B; cylinder 1 supply port ]/
pd1s = ps-a ;
q1so = fco*fabs( ipos )*sign( pd1s , sqrt( fabs( pd1s ) ) )+(fcc*pd1s) ;
q1sc = fcc*exp( ((-1)*fabs( ipos ))*vk )*pd1s ;
q1s = select( ipos, q1sc, q1so ) ;

/[..for surface C; cylinder 2 supply port ]/
pd2s = ps-a ;
q2so = fco*fabs( ipos )*sign( pd2s , sqrt( fabs( pd2s ) ) )+(fcc*pd2s) ;
q2sc = fcc*exp( ((-1)*fabs( ipos ))*vk )*pd2s ;
q2s = select( ipos, q2so, q2sc ) ;

/[..for surface D; cylinder 2 exhaust port ]/
pd2e = a-a ;
q2eo = fco*fabs( ipos )*sign( pd2e , sqrt( fabs( pd2e ) ) )+(fcc*pd2e) ;
q2ec = fcc*exp( ((-1)*fabs( ipos ))*vk )*pd2e ;
q2e = select( ipos, q2ec, q2eo) ;

/[ net flow into each cylinder will sum of 's' and 'e' flows]/
q1 = q1s ;
q2 = q2s ;

qrat = q1/(vsize*(sqrt(ps)/sqrt(psize))) ;

ipos = limit ( sti , -1*irate , irate ) ;
```

Appendix D.

```
/[ servo valve model -testnli.sim   null test ]/

/[ cylinder constants ]/
constant real vol ;

/[ valve constants ]/
constant real fco , fcc , vsize , psize , irate , vleak , pleak , vk ;

/[system constants]/
constant real kbk , ps , a ;

state real  p1 , p2 ;

timevar real qt, q1, q2, q1s, q1e, q2e, q2s, prat , pd1s, pd1e, pd2s, pd2e ;

timevar real ipos , q1eo, q1ec, q1so, q1sc, q2so, q2sc, q2eo, q2ec ;

/[start point constants]/
constant real stp1 , stp2 , sti ;

initial ;

fco = vsize/(irate*sqrt(psize)) ;
fcc = 0.333*(vleak/(pleak)) ;


dynamic ;
/[..for surface A; cylinder 1 exhaust port ]/
pd1e = a-p1 ;
q1eo = fco*fabs( ipos )*sign( pd1e , sqrt( fabs( pd1e ) ) )+(fcc*pd1e) ;
q1ec = fcc*exp( ((-1)*fabs( ipos ))*vk )*pd1e ;
q1e = select( ipos, q1eo, q1ec) ;

/[..for surface B; cylinder 1 supply port ]/
pd1s = ps-p1 ;
q1so = fco*fabs( ipos )*sign( pd1s , sqrt( fabs( pd1s ) ) )+(fcc*pd1s) ;
q1sc = fcc*exp( ((-1)*fabs( ipos ))*vk )*pd1s ;
q1s = select( ipos, q1sc, q1so ) ;

/[..for surface C; cylinder 2 supply port ]/
pd2s = ps-p2 ;
q2so = fco*fabs( ipos )*sign( pd2s , sqrt( fabs( pd2s ) ) )+(fcc*pd2s) ;
q2sc = fcc*exp( ((-1)*fabs( ipos ))*vk )*pd2s ;
q2s = select( ipos, q2so, q2sc ) ;

/[..for surface D; cylinder 2 exhaust port ]/
pd2e = a-p2 ;
q2eo = fco*fabs( ipos )*sign( pd2e , sqrt( fabs( pd2e ) ) )+(fcc*pd2e) ;
q2ec = fcc*exp( ((-1)*fabs( ipos ))*vk )*pd2e ;
q2e = select( ipos, q2ec, q2eo) ;

/[ net flow into each cylinder will sum of 's' and 'e' flows]/
q1 = q1s+q1e ;
q2 = q2s+q2e ;

qt = q1e+q2e ;

ipos = limit ( sti , -1*irate , irate ) ;

p1 = intgrl ( (q1*kbk)/(vol) , stp1 ) ;
p1 = select( p1 , 0 , p1 ) ;

p2 = intgrl ( (q2*kbk)/(vol) , stp2 ) ;
p2 = select( p2 , 0 , p2 ) ;

prat = (p1-p2)/ps ;
.
```

Appendix D.

```
/[anterior posterior model ]/
/[apnew.sim - all dimensions in SI units ]/

/[ cylinder constants ]/
constant real a1, a2, bore, rod, length ;

/[ valve constants ]/
constant real fco , fcc , vsize , psize , irate , vleak , pleak , vk, ohms, tor ;

/[ system constants ]/
constant real mass, gain, kbk, ps, a, pi ;

/[ frictional damping constants ]/
constant real u, maxl, minl;

/[ input voltage constants ]/
constant real amp, freq ;

/[ start point constants ]/
constant real stvel, stpos, stp1, stp2, stipos ;

/[integral variables ]/
state real  vel, pos, p1 , p2, ipos ;

/[time variables ]/
timevar real q1, q2, q1s, q1e, q2e, q2s, pd1s, pd1e, pd2s, pd2e ;

timevar real q1eo, q1ec, q1so, q1sc, q2so, q2sc, q2eo, q2ec ;

timevar real vin, error, vlv ;

timevar real fp, ff, fn, acc, posmm, q1ltm, q2ltm, p1bar, p2bar ;


initial ;

fco = vsize/(irate*sqrt(psize)) ;
fcc = 0.333*(vleak/(pleak)) ;
a1 = (bore/2)*(bore/2)*3.14159 ;
a2 = ((bore/2)*(bore/2)-(rod/2)*(rod/2))*3.14159 ;
pos = stpos ;
vel = stvel ;
ipos = stipos ;
p1 = stp1 ;
p2 = stp2 ;
pi = 3.142;

dynamic ;

/[..for surface A; cylinder 1 exhaust port ]/
pd1e = a-p1 ;
q1eo = fco*fabs( ipos )*sign( pd1e , sqrt( fabs( pd1e ) ) )+(fcc*pd1e) ;
q1ec = fcc*exp( ((-1)*fabs( ipos ))*vk )*pd1e ;
q1e = select( ipos, q1eo, q1ec) ;

/[..for surface B; cylinder 1 supply port ]/
pd1s = ps-p1 ;
q1so = fco*fabs( ipos )*sign( pd1s , sqrt( fabs( pd1s ) ) )+(fcc*pd1s) ;
q1sc = fcc*exp( ((-1)*fabs( ipos ))*vk )*pd1s ;
q1s = select( ipos, q1sc, q1so ) ;

/[..for surface C; cylinder 2 supply port ]/
pd2s = ps-p2 ;
q2so = fco*fabs( ipos )*sign( pd2s , sqrt( fabs( pd2s ) ) )+(fcc*pd2s) ;
q2sc = fcc*exp( ((-1)*fabs( ipos ))*vk )*pd2s ;
q2s = select( ipos, q2so, q2sc ) ;

/[..for surface D; cylinder 2 exhaust port ]/
pd2e = a-p2 ;
q2eo = fco*fabs( ipos )*sign( pd2e , sqrt( fabs( pd2e ) ) )+(fcc*pd2e) ;
q2ec = fcc*exp( ((-1)*fabs( ipos ))*vk )*pd2e ;
q2e = select( ipos, q2ec, q2eo) ;

/[ net flow into each cylinder will sum of 's' and 'e' flows]/
q1 = q1s+q1e ;
```

Appendix D.

```
q2 = q2s+q2e ;

/[cylinder pressures ]/
p1 = intgrl ( ((q1-(a1*vel))*kbk)/(a1*pos) , stp1 ) ;
p1 = select( p1 , 0 , p1 ) ;

p2 = intgrl ( ((q2+(a2*vel))*kbk)/(a2*(length-pos)) , stp2 ) ;
p2 = select( p2 , 0 , p2 ) ;

/[piston force ]/
fp = p1*a1-p2*a2 ;

/[friction damping ]/
fn = select( sin( 2*pi*time ) , minl , maxl+minl) ;
ff = select( vel , u*fn ,-1*u*fn ) ;

/[acceleration, velocity and position ]/
acc = (fp-ff)/mass ;
vel = intgrl( acc , stvel ) ;
pos = intgrl( vel , stpos ) ;

/[control signal ]/
vin = (10/length)*(amp*sin( 2*pi*freq*time )+stpos) ;

/[feedback loop ]/
error = vin-(10/length)*pos ;
vlv = limit( error*gain , -10 , 10 ) ;
ipos = intgrl( (((vlv/ohms)-ipos)/tor ), stipos ) ;
ipos = limit ( ipos , -1*irate , irate ) ;

/[convert to other more readable units ]/
/[ position in mm; flow in lts/min; pressure in bar ]/
posmm = pos*1000 ;
q1ltm = q1*60000 ;
q2ltm = q2*60000 ;
p1bar = p1/100000 ;
p2bar = p2/100000 ;
```

Appendix D.

```
/[flexion extension model ]/
/[11.02.95 ]/
/[flexnew.sim - all dimensions in SI units, and angular pos, vel, and acc ]/

/[ cylinder constants ]/
constant real area, vol, range, maxtorq ;

/[ valve constants ]/
constant real fco , fcc , vsize , psize , irate , vleak , pleak , vk, ohms, tor ;

/[ system constants ]/
constant real mofi, gain, kbk, ps, a, pi;

/[ frictional damping constants ]/
constant real u1,u2,rad1,rad2, maxl, minl;

/[ input voltage constants ]/
constant real amp, freq ;

/[ start point constants ]/
constant real stvel, stpos, stp1, stp2, stipos ;

/[integral variables ]/
state real  vel, pos, p1 , p2, ipos ;

/[time variables ]/
timevar real q1, q2, q1s, q1e, q2e, q2s, pd1s, pd1e, pd2s, pd2e ;

timevar real q1eo, q1ec, q1so, q1sc, q2so, q2sc, q2eo, q2ec ;

timevar real vin, error, vlv ;

timevar real torq, ftorq, fn, acc, posdeg, q1ltm, q2ltm, p1bar, p2bar ;


initial ;

fco = vsize/(irate*sqrt(psize)) ;
fcc = 0.333*(vleak/(pleak)) ;
area = vol/range/2 ;
pos = stpos ;
vel = stvel ;
ipos = stipos ;
p1 = stp1 ;
p2 = stp2 ;
pi = 3.142;

dynamic ;

/[..for surface A; cylinder 1 exhaust port ]/
pd1e = a-p1 ;
q1eo = fco*fabs( ipos )*sign( pd1e , sqrt( fabs( pd1e ) ) )+(fcc*pd1e) ;
q1ec = fcc*exp( ((-1)*fabs( ipos ))*vk )*pd1e ;
q1e = select( ipos, q1eo, q1ec) ;

/[..for surface B; cylinder 1 supply port ]/
pd1s = ps-p1 ;
q1so = fco*fabs( ipos )*sign( pd1s , sqrt( fabs( pd1s ) ) )+(fcc*pd1s) ;
q1sc = fcc*exp( ((-1)*fabs( ipos ))*vk )*pd1s ;
q1s = select( ipos, q1sc, q1so ) ;

/[..for surface C; cylinder 2 supply port ]/
pd2s = ps-p2 ;
q2so = fco*fabs( ipos )*sign( pd2s , sqrt( fabs( pd2s ) ) )+(fcc*pd2s) ;
q2sc = fcc*exp( ((-1)*fabs( ipos ))*vk )*pd2s ;
q2s = select( ipos, q2so, q2sc ) ;

/[..for surface D; cylinder 2 exhaust port ]/
pd2e = a-p2 ;
q2eo = fco*fabs( ipos )*sign( pd2e , sqrt( fabs( pd2e ) ) )+(fcc*pd2e) ;
q2ec = fcc*exp( ((-1)*fabs( ipos ))*vk )*pd2e ;
q2e = select( ipos, q2ec, q2eo) ;

/[ net flow into each cylinder will sum of 's' and 'e' flows]/
q1 = q1s+q1e ;
```

Appendix D.

```
q2 = q2s+q2e ;

/[cylinder pressures ]/
p1 = intgrl ( ((q1-(area*vel))*kbk)/(area*pos) , stp1 ) ;
p1 = select( p1 , 0 , p1 ) ;

p2 = intgrl ( ((q2+(area*vel))*kbk)/(area*(range-pos)) , stp2 ) ;
p2 = select( p2 , 0 , p2 ) ;

/[cylinder torque]/
torq = (p1-p2)*maxtorq/21000000 ;

/[friction damping ]/
fn = select( sin( 2*pi*time ) , minl , maxl+minl ) ;
ftorq = 6*select( vel , fn*((2*rad1*u1)+(rad2*u2)), -1*fn*((2*rad1*u1)+(rad2*u2)) ) ;

/[acceleration, velocity and position ]/
acc = (torq-ftorq)/mofi ;
vel = intgrl( acc , stvel ) ;
pos = intgrl( vel , stpos ) ;

/[control signal ]/
vin = (10/range)*(amp*sin( 2*pi*freq*time )+stpos) ;

/[feedback loop ]/
error = vin-(10/range)*pos ;
vlv = limit( error*gain , -10 , 10  ) ;
ipos = intgrl( (((vlv/ohms)-ipos)/tor) , stipos ) ;
ipos = limit ( ipos , -1*irate , irate ) ;

/[convert to other more readable units ]/
/[ position in deg; flow in lts/min; pressure in bar ]/
posdeg = pos*57.2958 ;
q1ltm = q1*60000 ;
q2ltm = q2*60000 ;
p1bar = p1/100000 ;
p2bar = p2/100000 ;
```

Appendix D.

```
/[load model ]/
/[11.02.95 ]/
/[loadnew.sim - all dimensions in SI units ]/

/[ cylinder constants ]/
constant real a1, a2, bore, rod, length, masscyl ;

/[ valve constants ]/
constant real fco , fcc , vsize , psize , irate , vleak , pleak , vk, ohms, tor ;

/[ system constants ]/
constant real massmnt, gain, kbk, ps, a, pi ;

/[ viscos damping and spring constants ]/
constant real ccyl, cmnt, kcell, ktib, ht, e, atib;

/[ input voltage, and femoral motion constants ]/
constant real cellrate, minl, maxl, amp, freq ;

/[ start point constants ]/
constant real stvel, stpos, stvelmnt, stposmnt, stp1, stp2, stvli ;

/[integral variables ]/
state real  vel, pos, velmnt, posmnt, p1 , p2, vli ;

/[time variables ]/
timevar real q1, q2, q1s, q1e, q2e, q2s, pd1s, pd1e, pd2s, pd2e ;

timevar real q1eo, q1ec, q1so, q1sc, q2so, q2sc, q2eo, q2ec ;

timevar real vin, error, vlv, ipos;

timevar real posfem, fp, fcell, ftib, fdamp, fdampmnt, acc, accmnt ;

timevar real posmm, q1ltm, q2ltm, p1bar, p2bar ;


initial ;

fco = vsize/(irate*sqrt(psize)) ;
fcc = 0.333*(vleak/(pleak)) ;
a1 = (bore/2)*(bore/2)*3.14159 ;
a2 = ((bore/2)*(bore/2)-(rod/2)*(rod/2))*3.14159 ;
vli = stvli ;
pos = stpos ;
vel = stvel ;
posmnt = stposmnt ;
velmnt = stvelmnt ;
p1 = stp1 ;
p2 = stp2 ;
pi = 3.142;
ktib= e*atib/ht;

dynamic ;

/[..for surface A; cylinder 1 exhaust port ]/
pd1e = a-p1 ;
q1eo = fco*fabs( ipos )*sign( pd1e , sqrt( fabs( pd1e ) ) )+(fcc*pd1e) ;
q1ec = fcc*exp( ((-1)*fabs( ipos ))*vk )*pd1e ;
q1e = select( ipos, q1eo, q1ec) ;

/[..for surface B; cylinder 1 supply port ]/
pd1s = ps-p1 ;
q1so = fco*fabs( ipos )*sign( pd1s , sqrt( fabs( pd1s ) ) )+(fcc*pd1s) ;
q1sc = fcc*exp( ((-1)*fabs( ipos ))*vk )*pd1s ;
q1s = select( ipos, q1sc, q1so ) ;

/[..for surface C; cylinder 2 supply port ]/
pd2s = ps-p2 ;
q2so = fco*fabs( ipos )*sign( pd2s , sqrt( fabs( pd2s ) ) )+(fcc*pd2s) ;
q2sc = fcc*exp( ((-1)*fabs( ipos ))*vk )*pd2s ;
q2s = select( ipos, q2so, q2sc ) ;

/[..for surface D; cylinder 2 exhaust port ]/
pd2e = a-p2 ;
```

Appendix D.

```
q2eo = fco*fabs( ipos )*sign( pd2e , sqrt( fabs( pd2e ) ) )+(fcc*pd2e) ;
q2ec = fcc*exp( ((-1)*fabs( ipos ))*vk )*pd2e ;
q2e = select( ipos, q2ec, q2eo) ;

/[ net flow into each cylinder will sum of 's' and 'e' flows]/
q1 = q1s+q1e ;
q2 = q2s+q2e ;

/[cylinder pressures ]/
p1 = intgrl ( ((q1-(a1*vel))*kbk)/(a1*pos) , stp1 ) ;
p1 = select( p1 , 0 , p1 ) ;

p2 = intgrl ( ((q2+(a2*vel))*kbk)/(a2*(length-pos)) , stp2 ) ;
p2 = select( p2 , 0 , p2 ) ;

/[piston force ]/
fp = p1*a1-p2*a2 ;

/[load cell force ]/
fcell=kcell*(pos-stpos-posmnt);

/[force in tibia ]/
ftib=ktib*(posmnt-stposmnt-posfem);
ftib=select(posmnt-stposmnt-posfem, 0, ftib);

/[cylider damping]/
fdamp=ccyl*vel;

/[ damping]/
fdampmnt=cmnt*velmnt;

/[acceleration, velocity and position of cylinder ]/
acc = (fp-fcell-fdamp)/masscyl ;
vel = intgrl( acc , stvel ) ;
pos = intgrl( vel , stpos ) ;

/[acceleration, velocity and position of mntia ]/
accmnt = (fcell-ftib-fdampmnt)/massmnt ;
velmnt = intgrl( accmnt , stvelmnt ) ;
posmnt = intgrl( velmnt , stposmnt ) ;

/[motion of femoral ]/
posfem=amp*sin(2*pi*time*freq) ;

/[control signal ]/
vin = (10/cellrate)*select( sin(2*pi*time) , minl , maxl*sin(2*pi*time )+minl ) ;

/[feedback loop ]/
error = vin-(10/cellrate)*fcell ;
vlv = limit( error*gain , -10 , 10 ) ;
vli = intgrl( (vlv-vli)/tor , stvli ) ;
ipos = limit( vli/ohms , -1*irate , irate );

/[convert to other more readable units ]/
/[ position in mm; flow in lts/min; pressure in bar ]/
posmm = pos*1000 ;
q1ltm = q1*60000 ;
q2ltm = q2*60000 ;
p1bar = p1/100000 ;
p2bar = p2/100000 ;
```

.